Investigation of Marangoni condensation of binary mixtures

A thesis submitted by

Saqib Raza Jivani

in part fulfilment of the requirements for the degree of

Doctor of Philosophy

in the

School of Engineering and Materials Science

Queen Mary, University of London

Mile End Road

London, E1 4NS

UK

(2017)

Abstract

It is a well-known phenomenon that during Marangoni condensation of binary mixtures, a small concentration of more volatile constituent with smaller surface tension gives significant heat transfer enhancements. This is due to surface tension gradients causing instability in condensate film, resulting in a pseudo-dropwise mode of condensation which resembles closely to dropwise condensation of pure fluid on the hydrophobic surface, consequently, the film gets thinner with lower thermal resistance across the condensate film and thus higher heat transfer coefficient is achieved. Marangoni condensation of steam-ethanol mixtures has been widely investigated in the past. However, Marangoni condensation of self-rewetting fluids e.g. steam-butanol is yet to be investigated where the constituent in a small concentration is a less volatile component.

Marangoni condensation of steam-ethanol, steam-butanol and steam-propanol mixtures has been investigated on a horizontal smooth tube at an atmospheric pressure. For all experiments, concentrations by mass in the boiler feed when cold prior to start of the experiment were 0.001%, 0.005%, 0.01%, 0.025%, 0.05%, 0.1%, 0.5% and 1.0%. The coolant temperature rise was measured accurately with a ten-junction thermopile. Tube wall temperature was measured using four thermocouples embedded in the test tube wall. Effects of pressure and vapour velocity over a wide range of vapour-to-surface temperature difference have been investigated. Care was taken to avoid error due to the presence of air in the vapour.

Marangoni condensation of steam-butanol and steam propanol mixtures show significant heat transfer enhancements compared with that of steam-ethanol mixtures. Higher Heat flux and heat-transfer coefficients were observed. For the steam-ethanol mixtures, enhancement ratio (heat flux or heat-transfer coefficient divided by the corresponding value for pure steam condensation on a horizontal smooth tube for the same vapour-to-surface temperature difference and vapour velocity) of 5.5 was found at an ethanol concentration of 0.01%. For steam-butanol mixtures, the maximum enhancement ratio was found to be 11 at a concentration of 0.005% and 0.01%. For steam-propanol mixtures, the maximum enhancement ratio of 8.5 was found at the same mass concentrations as steam-butanol mixtures. Enhancement ratio was generally higher at lower ethanol concentrations, increases at first with increasing vapour-to-surface

temperature difference and subsequently decreases at high vapour-to-surface temperature difference.

Finally, a semi-empirical model was proposed to predict the Marangoni condensation of steam-ethanol mixtures based on the vapour phase diffusion theory of Sparrow and Marchall (1969) and pure steam dropwise theory of Rose (2002).

Acknowledgement

First and foremost, I would like to express my deepest gratitude to Dr Hua Sheng Wang for his supervision, detailed guidance, helpful advice and extravagant encouragement during the experimental, theoretical and writing up stages of my work. I appreciate and value his trust in me and giving me the opportunity to study at the Queen Mary University of London. At times of low and stress, Dr Wang reminded me of my capabilities and shortcomings which enabled me to troubleshoot the problems.

I would also like to acknowledge the Sustainable Energy Lab technician Mr Roger Nelson for his constant support in re-assembling and maintaining the single tube condensation apparatus. His expertise and out of box thinking made it possible to manufacture thermocouple embedded tubes. I would also like to thank June Ma, Danny neighbour and Dennis Ife for their help and support whenever needed.

I would like to take this opportunity to gratefully acknowledge the endless love, care and support of my Parents. I would like to extend my appreciation to My Wife for the constant struggle with me and motivation she provided throughout my course. I would also like to thank my brothers and sisters and my parents-in-law for their encouragement and confidence in my work.

Finally, I would like to thank all my colleagues at the School of Engineering and Material sciences at the Queen Mary University of London.

Table of content

List of figures

List of tables

Nomenclature

A_i	inside surface area of tube
A_o	outside surface area of tube
A_{ts}	cross-sectional area of test section
ã	constant
a_1, a_2	constants
b_1, b_2	constants
C_e	ethanol concentration
C_{iL}	concentration of ethanol (initial in liquid at room temperature)
C_p	specific isobaric heat capacity of test fluid
C_{pc}	specific isobaric heat capacity of coolant at mean coolant temperature
C_v	equilibrium concentration of ethanol in vapour
C_L	equilibrium concentration of ethanol in liquid
D	drop diameter
d	outside diameter of smooth test tube, fin root diameter of finned tube
d_i	inside diameter of test tube
d_o	diameter of test tube at fin tip
d_t	diameter of thermocouple position in test tubes
E	thermo e.m.f
E_{in}	e.m.f for coolant at inlet to test tube
E_m	mean thermo e.m.f calculated at mean temperature of coolant in the test tube
F	dimensionless parameter, $\rho g d h_{fg}/k U_{v2} \Delta T$
g	specific force of gravity
H_1, H_2, H_3	liquid levels in mercury manometer
h_{fg}	latent heat of vaporization
K_l	Heat loss coefficient
k	thermal conductivity of condensate

k_c	thermal conductivity of coolant
k_w	thermal conductivity of tube material
L	length of flat plane
L_T	length of condensing test tube
l	active heat transfer length of test tube i.e. exposed to vapour for heat transfer
m	local condensation mass flux
m_v	vapour mass flow rate
M	molecular mass
Nu_c	coolant Nusselt number, $_{ci}k/d_c\alpha$
Nu_d	Nusselt number based on outside diameter of tube, $k/d\alpha$
P	saturation pressure
P_{atm}	atmospheric pressure
P_B	barometric pressure reading
P_v	vapour pressure
Pr_c	coolant Prandlt number, $\mu_c C_{pc}/k_c$
Q	heat transfer rate to coolant
Q_B	total power dissipated in heaters
Q_L	heat loss from apparatus
q	heat flux
R_c	thermal resistance of coolant side
R_o	overall thermal resistance
R_v	thermal resistance of condensate film
R_w	thermal resistance of tube wall
Re_c	coolant Reynolds number, $\rho_c V_c d_i/\mu_c$
Re_{tp}	two phase Reynolds number, $\rho U_v d/\mu$
T	thermodynamic temperature
T_a	ambient temperature
T_{atm}	atmospheric temperature

T_B	ambient temperature
$T_{c,\,in}$	temperature of coolant at inlet of tube
T_{cr}	temperature of condensate returning to boilers
T_s	temperature of surface
T_{sat}	saturation temperature
T_{ref}	reference temperature
$T_{wi,\,k}$	inside surface temperature of tube wall at angular position corresponding to k_{th} wall thermocouple
T_{wo}	mean outside wall temperature of test tube
T_{wk}	temperature measured by k_{th} wall thermocouple
$T_{wo,\,k}$	outside surface temperature of tube wall at angular position corresponding to k_{th} wall thermocouple
T_v	vapour temperature
V_c	mean coolant velocity
U_o	overall heat-transfer coefficient
U_v	upstream vapour velocity based on maximum cross-sectional area of test section
x	vapour concentration
y	liquid concentration

Greek symbols

α	vapour-side, heat-transfer coefficient, $q/\Delta T$
α_c	coolant-side, heat-transfer coefficient
σ	surface tension
ε	heat-transfer enhancement ratio, defined in Eq. (6.3)
δ	condensate film thickness
ΔE	thermo e.m.f. rise due to condensation
$\Delta E_{friction}$	thermo e.m.f rise due to frictional dissipation
ΔT_c	coolant temperature rise due to condensation
ΔT v	vapour-to-surface temperature difference

γ_e	activity coefficient of ethanol
γ_w	activity coefficient of water
ρ_c	density of coolant at mean coolant temperature
ρ	density of saturated liquid
ρ_{Hg}	density of mercury
ρ_{TF}	density of test fluid
ρ_v	density of saturated vapour
μ	dynamic viscosity of condensate at saturation condition
μ_c	dynamic viscosity of coolant at mean coolant temperature
μ_w d	dynamic viscosity of coolant at inside wall temperature

Subscripts

b	bulk
e	ethanol
Nu	Nusselt
max	maximum
min	minimum
w	water

Chapter 1

1 Introduction

Condensers are a major component in many engineering applications and plays key role in air conditioning, electric power generation and refrigeration plants. The global market of the steam condenser is growing at an annual rate of 5.5% and was reported to be $1.9 billion (Global Data 2012). Most of the research has been done to reduce the capital and running cost of the condenser without impacting adversely on the efficiency of the condensers. Most of the cost of the condenser comes from the heat transfer area required to transfer the specific amount of heat. Many investigations on improving the heat transfer coefficient by increasing the condenser surface area without significantly increasing its overall size have been done. There is a large number of experimental studies on increasing surface area by means of two-dimensional integral-fins and three-dimensional pin fins tubes. Researchers have successfully reported optimum fin geometries i.e. fin shapes, fin heights and fin spacing. Theoretical investigations such as Rose (1994) and Briggs and Rose (1994) have also been successful in developing reliable and simple models for integral fin tubes. These models include a combined effect of surface tension and gravity and are readily applicable by design engineers. However, these geometrically enhanced tubes (integral-fins and pin-fins) are expensive to manufacture and have a high maintenance cost. If other means of increasing the heat transfer coefficient of condensers can be achieved, then condenser size and capital cost can be significantly reduced without any adverse effects on efficiency.

In general, Condensate appearance on a solid surface can be categorised into two modes: film-wise and Drop-wise. Dropwise mode of condensation has found to give vapour-side higher heat-transfer coefficients up to 20 times higher than this for film-wise. However, it requires “non-wetted” (hydrophobic) surfaces which is both costly and hard to maintain under industrial conditions. Such surfaces have only maintained and tested under laboratory conditions and that also only for high surface tension fluids such as water. Therefore, in the practical condensers film-wise condensation is adopted which naturally occurs on any surface having a temperature lower than the saturation temperature of the vapour. An extensive amount of experimental data and well-known theoretical theory of

Nusselt (1916) and Rose (1984) are the pioneering work in this mode of condensation. Film-wise condensation on smooth surfaces results in lower heat transfer coefficients compared to the geometrically enhanced tube.

Another mean of achieving higher vapour-side heat transfer coefficient for condensers is by adding a small amount of secondary fluid. Generally, the heat transfer coefficient of vapour mixtures is lower compared to that of single-constituent fluid. This degradation is due to the diffusion resistance in the vapour phase. Contrary to this, adding a small amount of ethanol to water have shown higher heat-transfer coefficients. This is because of ethanol being more volatile component has lower surface tension results in unstable condensate film leading to pseudo-dropwise condensation mode. This type of condensation is known as Marangoni condensation and occurs only in binary mixtures of steam and alcohols.

So far ample amount of data is available on Marangoni condensation of steam-ethanol mixtures. Hijikata et al (1996) successfully explained the phenomenon involved in the instability of condensate film. Since then significant enhancements have been reported from various sources of which most prominent are Utaka and co-workers (1995, 2004), Murase (2007) and Ali (2012). However, due to the complicated phenomenon of diffusion and film instability, there is no theoretical or empirical model available that can predict the heat-transfer characteristics of Marangoni condensation for a wide range of parameters. All of this research in Marangoni condensation has based on steam-ethanol mixtures and no data is available for the mixtures of steam-alcohols other than ethanol. Mixtures of water and alcohols, with carbon atom greater than or equal to four, are known as self-rewetting fluids (such as steam-butanol) in boiling investigations. Although these alcohols are a less volatile component with lower surface tension but have shown significant enhancements in boiling investigations compared to pure steam and steam-ethanol mixtures.

Therefore, the present investigation aims to study the effect of butanol and propanol concentrations on condensation heat-transfer on a horizontal smooth tube. In this thesis, an attempt has also been made to develop an empirical model, covering a wide range of parameters, for condensation of the steam-ethanol mixtures on a horizontal smooth tube. The details of the aims are laid out in chapter 2. Whereas, Chapter 3 highlights all

the previous research in the Marangoni condensation of smooth tubes including experimental and theoretical investigations. It will also shed light on recent boiling investigations on self-rewetting fluids (steam-butanol) which is the sole motivation of this research. Methodology, experimental procedure and data reduction process are discussed in chapter 4.

To investigate any problem, it is necessary to first repeat the experimental condition of previous research and validate your methodology. Therefore pure-steam condensation experiments were conducted and compared with Nusselt (1916) and Rose (1984) theoretical models in chapter 5. Later in the same chapter, new data for steam-ethanol mixtures is collected which will aid in developing an empirical model for a wide range of parameters. In chapter 6 and 7, new data for steam-butanol and steam-propanol mixtures is collected to investigate if all members of alcohol mixtures give higher heat transfer coefficients by producing pseudo dropwise mode of condensation. This is the novelty of this research. Lastly, a semi-empirical model is developed to predict heat transfer characteristics of steam ethanol mixture in chapter 9. The final chapter concludes the entire research process and results and also discusses future work.

Chapter 2

2 Aims and objectives

Boiling investigations have shown that binary mixture of steam-propanol and steam-butanol perform better than the steam-ethanol mixture. The main aim of the present work is to investigate and compare the effects of mass concentration and vapour velocity in Marangoni condensation on a horizontal smooth tube using three different types of binary mixtures; steam-ethanol, steam-butanol and steam-propanol mixtures. The secondary aim is to develop an empirical model that is applicable to a wide range of steam-ethanol mixtures. Detailed aims are listed below.

2.1 Marangoni condensation of steam-ethanol mixtures

Experimental investigation of steam ethanol mixtures has been previously done by Murase (2007) and Ali (2012). Murase (2007) conducted experiments at higher ethanol mass concentrations (0.05%, 0.1%, 0.5% and 1%) and lower velocities (0.2, 0.35, 0.56 and 0.75 m/s). Ali (2012) experimented for higher velocities (0.78, 1.6, 2.4, 3.2, 4.9 and 7.5 m/s) and wide range of ethanol mass concentrations (0.001%, 0.005%, 0.01%, 0.025%, 0.05%, 0.1%, 0.5% and 1%). Data for lower concentration and lower velocities are not available. Therefore, the present investigation will fill this gap in these earlier data.

The objectives of this part include:

(i) To obtain condensation heat transfer data of pure steam, for purpose of validating the experimental apparatus and procedure.

(ii) To provide new data for Marangoni condensation of steam-ethanol mixtures at atmospheric pressure for ethanol mass concentrations of 0.001%, 0.005%, 0.01% and 0.025% at vapour velocities of 0.2 m/s, 0.35 m/s, 0.46 m/s, 0.56 m/s and 0.75 m/s. The new data will help in understanding the transition region in detail.

2.2 Marangoni condensation of steam-butanol mixtures

No experimental data on Marangoni condensation of steam-butanol mixtures are available so far. Based on the literature review on the boiling investigation of self-

rewetting fluids, it is predicted that steam-butanol mixtures may give higher enhancements than steam-ethanol mixtures.

The objectives of this part include:

(i) To obtain data for Marangoni condensation of steam-butanol mixtures under atmospheric conditions with butanol mass concentration of 0.001%, 0.005%, 0.01%, 0.025%, 0.05%, 0.1% and 0.5% at vapour velocities of 0.2 m/s, 0.35 m/s, 0.46 m/s, 0.56 m/s and 0.75 m/s.

(ii) To compare the new experimental data with earlier experimental data of steam-ethanol and pure-steam.

2.3 Marangoni condensation of steam-propanol mixtures

No experimental data on Marangoni condensation of steam-propanol mixtures are available so far. If steam-butanol mixtures are expected to give higher heat transfer enhancement than under same circumstances steam-propanol mixtures is expected to give better performance than steam-ethanol mixtures but lower enhancements than steam-butanol mixtures.

The objectives of this part include:

(i) To obtain data for Marangoni condensation of steam-propanol mixtures under atmospheric conditions with propanol mass concentration of 0.001%, 0.005%, 0.01%, 0.025%, 0.05% and 0.1% at vapour velocities of 0.2 m/s, 0.35 m/s, 0.46 m/s, 0.56 m/s and 0.75 m/s.

(ii) To compare the new experimental data with experimental data of steam-butanol, steam-ethanol and pure steam.

2.4 Semi empirical modelling of Marangoni condensation

Theoretical modelling of Marangoni condensation has been very difficult due to its complex phenomenon of Condensate film instability. Attempts have been made to provide a model to predict the heat flux and heat transfer coefficients for Marangoni

condensation of steam-ethanol mixtures. These models are limited to certain velocities and mass concentrations.

The objectives of this part include:

(i) To theoretically model the diffusion part of Marangoni condensation of steam-ethanol mixtures.

(ii) To Provide an empirical model of Marangoni condensation of steam-ethanol mixtures based on Rose (2002) dropwise condensation theory.

Chapter 2

3 Literature review

The phenomenon of condensation heat-transfer has been researched for over a century now. In the beginning, the primary focus to increase heat-transfer was kept limited to the increase in surface area. Later, it was revealed that surface tension forces play a vital role in thinning the condensate layer which in turn increases heat-transfer. This chapter reviews the literature on binary mixture condensation. Firstly, it will briefly cover the fundamental theories of pure steam condensation. The second section will discuss experimental and theoretical research on Marangoni condensation up to date. Lastly, it will discuss the potential of self-rewetting fluids (Steam-butanol and steam propanol mixtures) in condensation and their already tested performances in the boiling investigations.

3.1 Condensation of pure fluid

Condensation of a vapour occurs in many engineering applications. During condensation, the liquid condensate is collected in one of two ways, depending on whether it wets the condensing surface or not. At film-wise condensation, the condensate liquid forms into a continuous film or layer and covers the condensing surface. At dropwise condensation, it forms into small discrete droplets of different size. The heat transfer coefficient for dropwise condensation can be one to two orders of magnitude greater than those for film-wise condensation. A lot of attention has been paid to dropwise condensation over 80 years. The conventional dropwise condensation usually takes place when the condensing surface is specifically coated or heat transfer additives are added to the vapour. However, the specifically prepared surface is easily damaged in the real industrial environment, and the heat transfer additives are always out of operation after a long time. Accordingly, the conventional dropwise condensation cannot be sustained for a long time in practice. All surface condensers today are designed to operate in the film-wise mode.

Nusselt (1916) proposed a well-established theory for Laminar film-wise condensation on smooth isothermal surfaces. The theory has been verified by numerous experimental works and has served as the reference model for all other condensation investigations.

Nusselt made a key assumption that inertia term in the conservation of momentum equation and the convection term in the conservation of energy equation is so small in the condensate film that they can be neglected. These assumptions are well verified now by many numerical theories. Nusselt then proposed an expression for the horizontal tube condenser as follows.

$$Nu = 0.728\left\{\frac{\rho(\rho-\rho_v)gh_{fg}d^3}{\mu k\Delta T}\right\}^{\frac{1}{4}} \quad (3.1)$$

where,

Nu is the average Nusselt number,

ρ and ρ_v are the densities of condensate and vapour respectively,

g is the specific force of gravity,

h_{fg} is the specific enthalpy of evaporation,

d is the outside diameter of the condenser tube,

μ is the viscosity of condensate,

k is the thermal conductivity of condensate and

ΔT is the vapour-to-surface temperature difference.

Late in 1966, Shekriladze and Gomelauri modified the Nusselt theory to take account of vapour velocity effect. They assumed infinite asymptotic condensation rate and inertia, convection and pressure drop were neglected in the condensate layer as they are too small to have any significant effect. They also assumed potential flow outside the vapour boundary layer due to high suction caused by condensation. This simplified the vapour boundary layer separation problem.

Interfacial shear stress was given as:

$$\tau_\delta = m(U_\varphi - U_\delta) \quad (3.2)$$

For horizontal tube condensation, when gravity was omitted, the average Nusselt number was expressed as:

$$Nu_d {Re_{tp}}^{1/2} = 0.9 \quad (3.3)$$

where,

Re_{tp} is the two-phase Reynolds number and is defined as:

$$Re_{tp} = \frac{U_\infty \rho d}{\mu} \tag{3.4}$$

U_∞ is the free-stream vapour velocity,

After taking gravity into consideration Shekriladze and Gomelauri came up with interpolation formula shown below:

$$Nu_d Re_{tp}^{-1/2} = 0.644\left\{1 + (1 + 1.69F)^{1/2}\right\}^{1/2} \tag{3.5}$$

where,

$$F = \frac{\mu g h_{fg} d}{\mu^2 k \Delta T} \tag{3.6}$$

This equation approximately satisfies the Nusselt equation (equation 3.1) at low vapour velocity and equation 3.3 at high vapour velocity. The maximum error, when compared with the numerical solution, was found to be 2%.

In 1984 Rose showed that error found in the numerical solution of Shekriladze and Gomelauri (1966) could further be reduced to 0.4% and proposed a more accurate expression which satisfies the zero and infinite velocity asymptotes.

$$Nu_d Re_{tp}^{-1/2} = \frac{0.9 + 0.728F^{1/2}}{(1 + 3.44F^{1/2} + F)^{1/4}} \tag{3.7}$$

In this thesis, Nusselt (1916) and Rose (1984) theoretical models will be used for the reference and comparison purpose for all the condensation experimental and theoretical work.

3.2 Marangoni condensation of binary mixtures

3.2.1 Introduction

Condensation of binary mixtures has been under investigations for many years. It was first observed by Mirkovich and Missen (1961) that for some binary mixtures such as steam-methanol, steam-ethanol and steam-ammonia pseudo-dropwise mode of condensation appears, known as Marangoni Condensation. Ford and Missen (1968) explained this mode of condensation, which appears similar to dropwise condensation of

pure steam, occurs in the condensation of vapour mixture where the more volatile component has smaller surface tension, such as steam ethanol mixtures. These mixtures are known as positive mixtures. Such is the complexity of the phenomenon that a complete theory of Marangoni condensation has not yet established. However, to understand the phenomenon it is necessary to understand the concept of phase equilibrium behaviour of binary mixtures at the liquid-vapour boundary layer and the effect of surface tension in the condensate film.

3.2.2 Phase equilibrium behaviour of binary mixtures

At vapour-liquid equilibrium, the liquid and the vapour phases coexist. Figure 3.1 explains the condensation process of the binary mixture under the isobaric condition, where liquid and vapour mass fraction of more volatile component is denoted by x and y, respectively. The curve at the top is the bubble point curve and the one at the bottom is the dew point curve. If the superheated state of the binary mixture, point A with temperature T_a, is cooled then it will follow a vertical line and reach dew point temperature at point B as overall mass composition x_a remains constant during the condensation. The first dew will appear at this stage and x_b and y_b will be the liquid and vapour concentrations corresponding to dew point and bubble point curves. As cooling continues it will dictate vapour concentration to follow path BC and liquid concentration to follow B′C′. Finally, the mixture will reach point C at temperature T_c with mass composition y_c. Further cooling will result in the subcooled liquid region at D where the composition of the condensate is equal to one in the vapour.

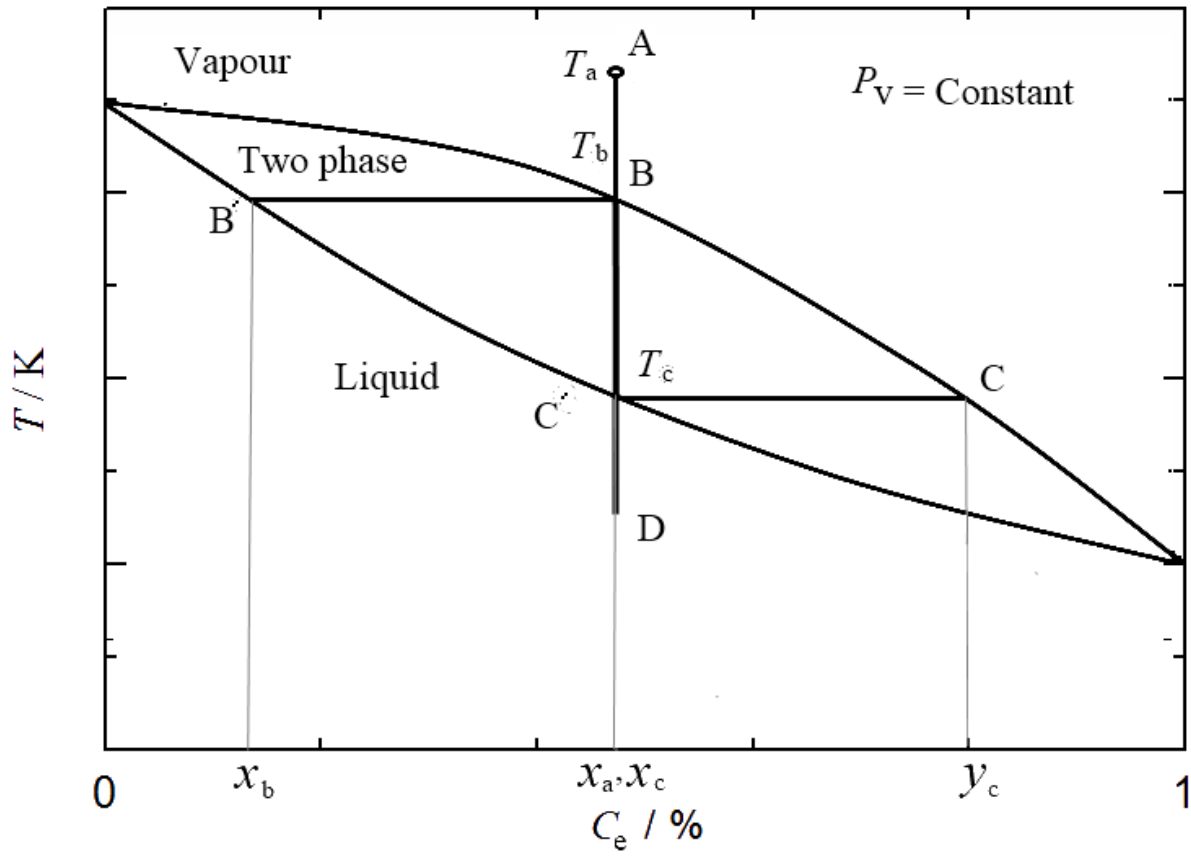

Figure 3-1: Phase equilibrium diagram of a binary mixture in a cooling process (Hassan (2012)).

3.2.3 Marangoni condensation and surface tension effect.

In 1865 Carlo Marangoni investigated the interface mass transfer between the two fluids with different surface tension. He found that in a mixture of two fluids with different surface tensions, liquid with higher surface tension tends to pull the liquid with lower surface tension. Eventually, the liquid will be drawn away from the lower surface tension area. In condensation of the steam-ethanol mixture, Hijikata et al. (1996) explained the Marangoni effect in detail. He figured that instability in the condensate film of the binary mixture could be the result of the difference in surface tensions of the two fluids. Figure 3.2 shows a schematic model of the growth development of drops from the instability of the condensate film. In case of any small irregularity in the condensate film, one would expect to have higher interface temperature at the crest where the film is thicker and lower interface temperature at the valley where the film is thinner. Correspondingly, according to the equilibrium phase diagram (Figure 3.3), the condensate will have lower ethanol concentration at crest and higher in the valley. Since ethanol has the lower surface tension than water the surface tension of the condensate film will be higher at

the crest and lower in the valley. The surface tension gradient from valley to crest increases resulting in further irregularity in the film and eventually the unstable film. Here, the surface tension gradient outweighs the effect of temperature and pressure gradient and marks the start of pseudo-dropwise condensation.

3.2.4 Diffusion in the vapour phase

Diffusion process in the condensation of binary mixtures is responsible for the mass transfer resistance and deterioration of the heat transfer. Figure 3.4 explains in detail the effect of diffusion on heat flux and heat-transfer coefficient in the context of phase equilibrium diagram. According to the phase equilibrium diagram, during condensation of binary vapour mixture, the less volatile component condenses more than the volatile component. Since the sum of mass concentration is kept constant in the vapour boundary layer the concentration of the volatile component increases in the vapour phase at the liquid-vapour interface. This phenomenon is accelerated by the constant supply of mass concentration from bulk to vapour-liquid interphase. On the other hand, convective mass transfer takes place to ensure the mass concentration at vapour-liquid interface approaches that in the bulk. These two mechanisms balance out to make the steady distribution of mass concentrations as shown in Figure 3.4 (a). Simultaneously, the vapour temperature decreases from bulk to interface and thus the heat transfer rate and condensation rate (Fujii (1991)). This effect can be minimised by high vapour velocities, enhance surfaces and high vapour-to-surface temperature difference (Stephan (1992)). However, this inevitable reduction in heat transfer is only applicable to binary mixture condensation where condensate is a film. In cases where condensate is pseudo-dropwise condensate thermal resistance is so low that it outnumbers the effect of diffusion resistance and significant enhancements at low vapour-to-surface temperature difference is obtained (Fujii et al. 1993).

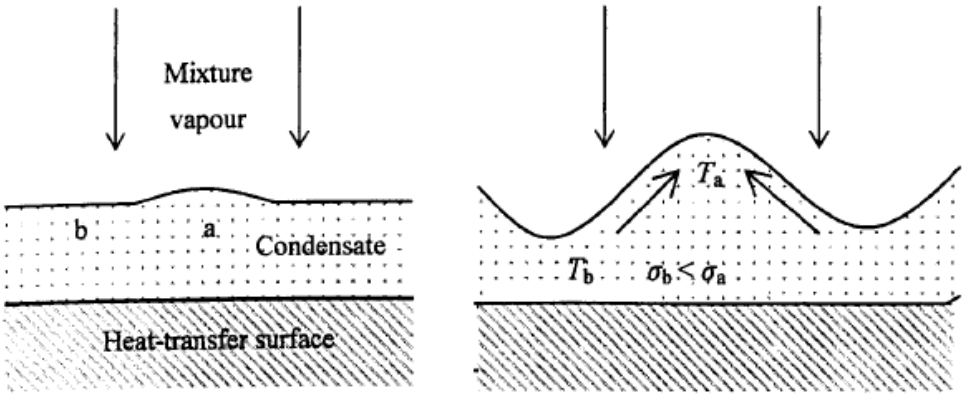

Figure 3-2: Development of pseudo-dropwise mode of condensation during Marangoni condensation of mixtures. σ denotes surface tension, a is the crest and b is the valley.

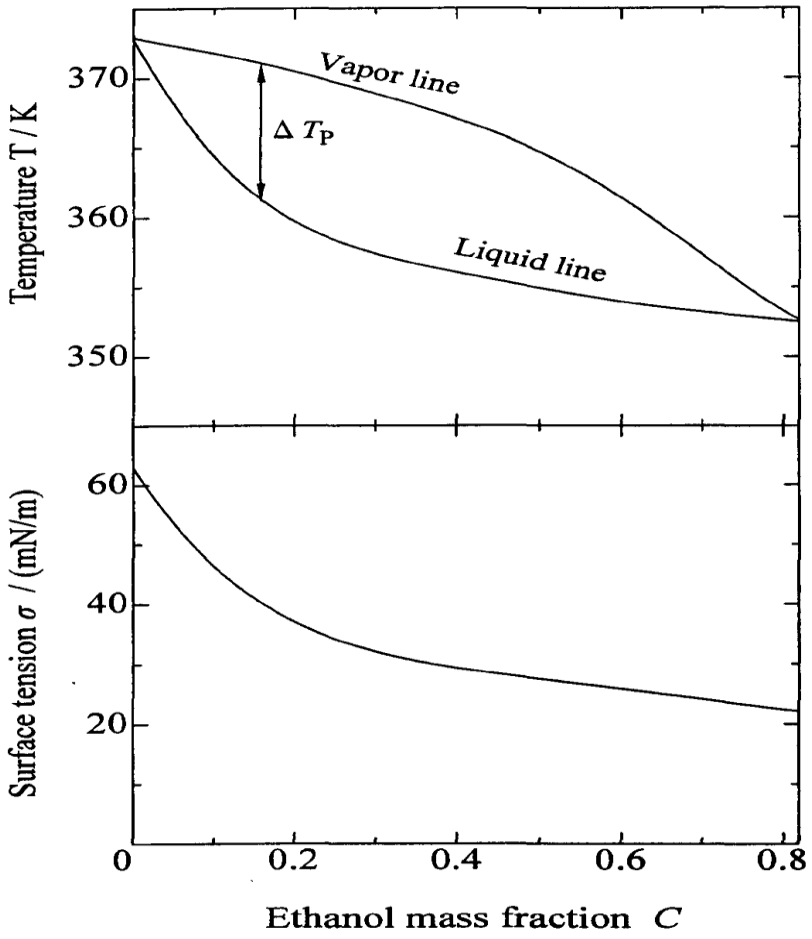

Figure 3-3: Phase equilibrium diagram of steam ethanol mixture and surface tension effect against ethanol mass concentration.

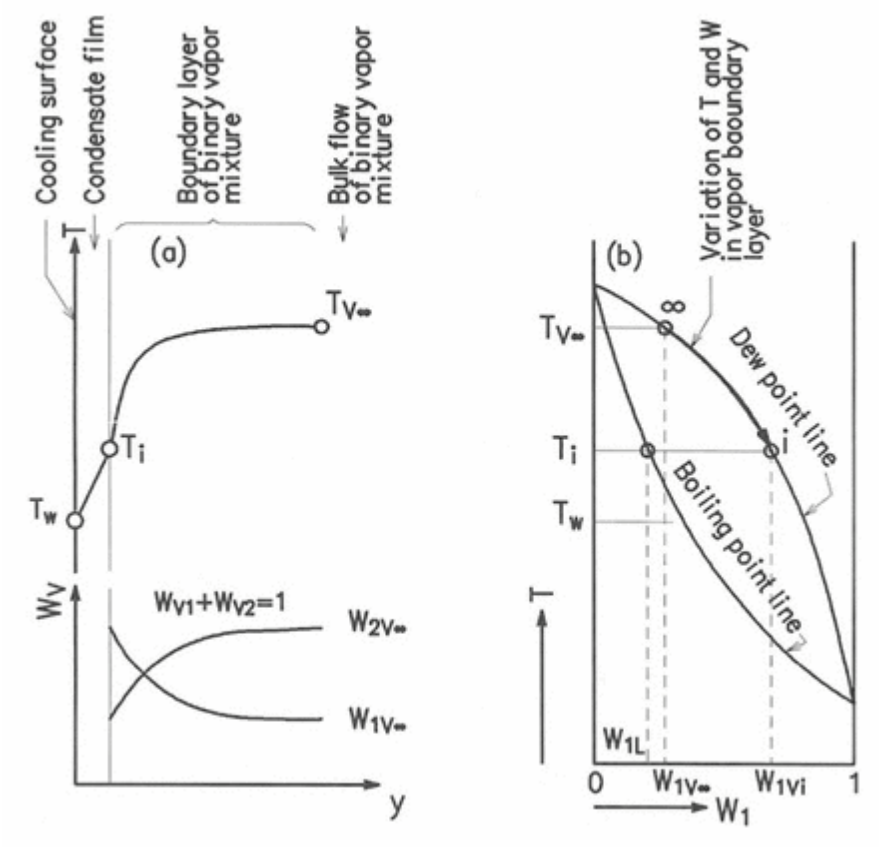

Figure 3-4: (a) distribution of Temperature (T) and mass concentration (W) in the condensate film and the vapour boundary layer. y is the normal distance from the surface. (b) Variation of "T" and "W" on a diagram of phase equilibrium. Subscripts: ∞ is bulk, i is vapour liquid interface, w is wall surface, 1 is a volatile component, 2 is a less volatile component, v is vapour and L is liquid (Fujii (1991)).

3.2.5 Experimental investigations

The very first experiments performed on the binary mixture condensation of steam ethanol mixture was by Wallace and Davison (1938). Experiments were conducted on the horizontal brass tube and contrary to the well-known established fact now, vapour side heat transfer coefficients for all concentration tested were found to be smaller than that of pure steam. No visual observations were made so no way of telling whether pseudo dropwise condensation mode was present.

Later, Mirkovch and Missen (1961) conducted experiments on a vertical tube of diameter 150 mm and length 40 mm using four different organic binary mixtures under atmospheric conditions. They made the visual observations and found that out of four mixtures; only pentane-methylene dichloride and pentane-methanol showed the non-film-wise mode of condensation while for the other two pairs of methylene dichloride-methanol and Pentane-Hexane condensation happen to appear in pure film-wise mode. They also investigated for enhancements in the heat transfer coefficient for the above mixtures in 1963. No significant heat transfer enhancements were found, however, in the case of the non-film-wise mode of condensation, a decrease in heat transfer coefficient was attributed to diffusion resistance in the vapour phase.

Ford and Missen (1968) reported the phenomenon of film instability and regarded its dependency on the surface tension of binary mixture and vapour to surface temperature difference. They observed that when a less volatile component of the binary mixture has high surface tension pseudo dropwise mode of condensation occurs for a range of vapour to surface temperature difference. they explained that condensate film thickness can be changed due to local variations of surface tension within the film. In other words, if a thin condensate film has low surface tension and comes in contact with the neighbouring thicker film having higher surface tension then this surface tension gradient will cause the liquid to be drawn from thinner film causing further instability in the film. If the former film has high surface tension and later low surface tension than the liquid will be drawn in other direction (from thicker film towards the thinner film) resulting in more stable condensate film. This brings ford and Missen to conclude that stability depends on the sign of the ratio of change in surface tension with a change in film thickness and they proposed the expression for film stability and instability.

The film is stable if:

$$\frac{\partial \sigma}{\partial \delta} < 0 \tag{3.8}$$

The film is unstable if:

$$\frac{\partial \sigma}{\partial \delta} > 0 \tag{3.9}$$

However, the former equation is a necessary and sufficient condition for stability and later equation is necessary but not the sufficient condition. This is backed by the visual observations in experimental investigations of steam-ethanol mixtures, where stable films are observed at higher vapour-to-surface temperature difference, higher condensation rate (thicker condensate film) or when compositions reach an azeotropic point (mixture behaves as a pure component).

In 1971 Ford and McAleer used high-speed cameras to photograph condensate appearances of six different mixtures. All mixtures showed the pseudo-dropwise mode of condensation which differs from the pure dropwise condensation. It was seen that the condensing surface was always covered with thin film. Initially, wavy films would develop and due to surface tension affect this wavy film turn into ridges. Ridges grows to form drop and when a drop is large enough it rolls off and the cycle repeats again. The table below shows the drop characteristics formed in six different combinations of mixtures used.

Table 3-1: Combination of mixtures used and their drops characteristics (ford and McAleer (1971))

Fluids	Mean droplet diameter (mm)	Average cycle time (s)
Methanol + n-pentane	0.84	0.008
Methanol + n-hexane	1.07	0.027
Methylene chloride+ n-pentane	1.04	0.013
Water + ethanol	1.76	0.012
Water + methanol	0.89	0.034
Water + acetone	1.40	0.052

Fujii et al. in 1989, conducted condensation experiments of binary mixtures on the horizontal smooth tube. The tube had a length of 385 mm and diameter of 18 mm. the

absolute pressure was between 3 to 20 kPa and vapour-to-surface temperature difference 2 to 20 K. Fluid mixtures used were steam-ethanol, steam-methanol and ethanol-methanol. They found the prediction of the smooth film by Ford and Missen (1968) to be true in the case of an ethanol-methanol mixture. In steam-ethanol case, for the mass fraction of 0.28 to 0.6, pseudo dropwise mode of condensation was observed and for the mass fraction of 0.73 to 0.83, streak wise mode of condensation. The heat-transfer enhancements were up to 2 to 3 times higher than pure steam filmwise condensation. In the steam-methanol case for a mass fraction of 0.08 to 0.85 dropwise mode of condensate appearance was observed, and 2 to 6 times higher heat-transfer coefficients were obtained. Figure 3.5 shows the experimental data of Fujii et al. (1989) plotted for heat flux against vapour-to-surface temperature difference. Table 3.2 shows the mode of condensation at different ethanol mass fraction (extracted from Fujii (1989)).

(a)

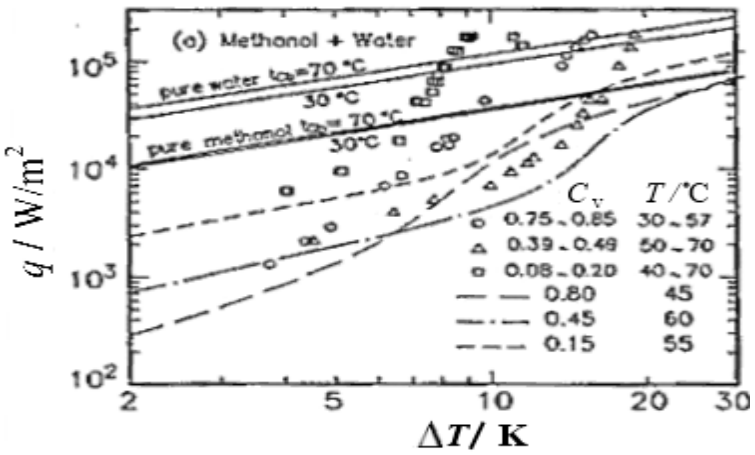

(b)

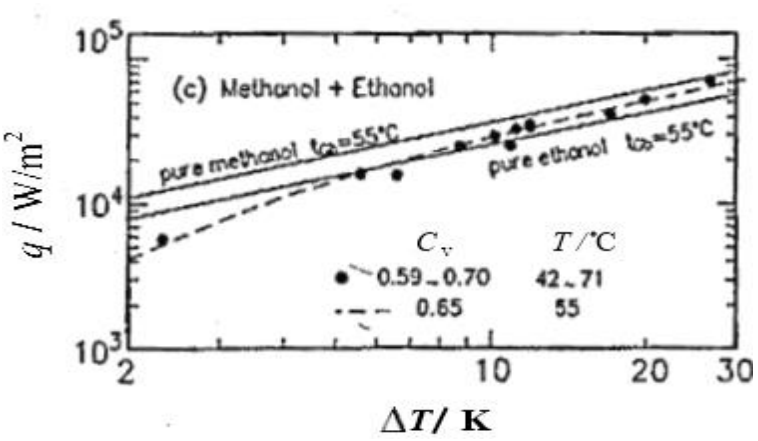

Figure 3-5: Heat flux versus vapour-to-surface temperature difference for different mixtures and their compositions (Fujii et al. (1989)). (a) methanol + water, (b) methanol + ethanol (Fujii et al. (1989)).

Table 3-2: Classification of condensation mode with respect to mass concentration (Fujii et al. (1989))

Ethanol vapour mass fraction range	Condensation mode
0	smooth-film
0.02 – 0.20	smooth-film
0.20 – 0.40	drop
0.52 – 0.65	drop and streak
0.75 – 0.78	ring
0.85	smooth-film
1	smooth-film

In 1993, Fujii et al. extended their previous work (Fujii et al. (1989)) using 9.8 and 18 mm outside diameter tubes. This time they experimented with steam-ethanol, steam-methanol, steam-ethanol, methanol ethanol, steam-n-propanol and methanol-n-propanol. All the mixtures of steam were observed to have non-film wise mode of condensation including drops, streak, ring, smooth film and wavy film. Figure 3.6 shows the photographic evidence for condensate appearance of steam-ethanol mixtures. Fujii found that condensation mode was strongly dependent on vapour pressure, vapour composition and heat flux. Heat-transfer coefficients for condensate appearances were significantly higher compared to Nusselt (1916) theory of pure steam. Drops had the highest enhancements up to 7 and while the wavy film has the lowest enhancements up to 2. Steam-methanol and steam-n-propanol also performed similarly to steam-ethanol. However, methanol-ethanol and methanol-n-propanol mixtures heat-transfer coefficient were in good agreement with Nusselt (1916) theory as their condensate appearance was a continuous film.

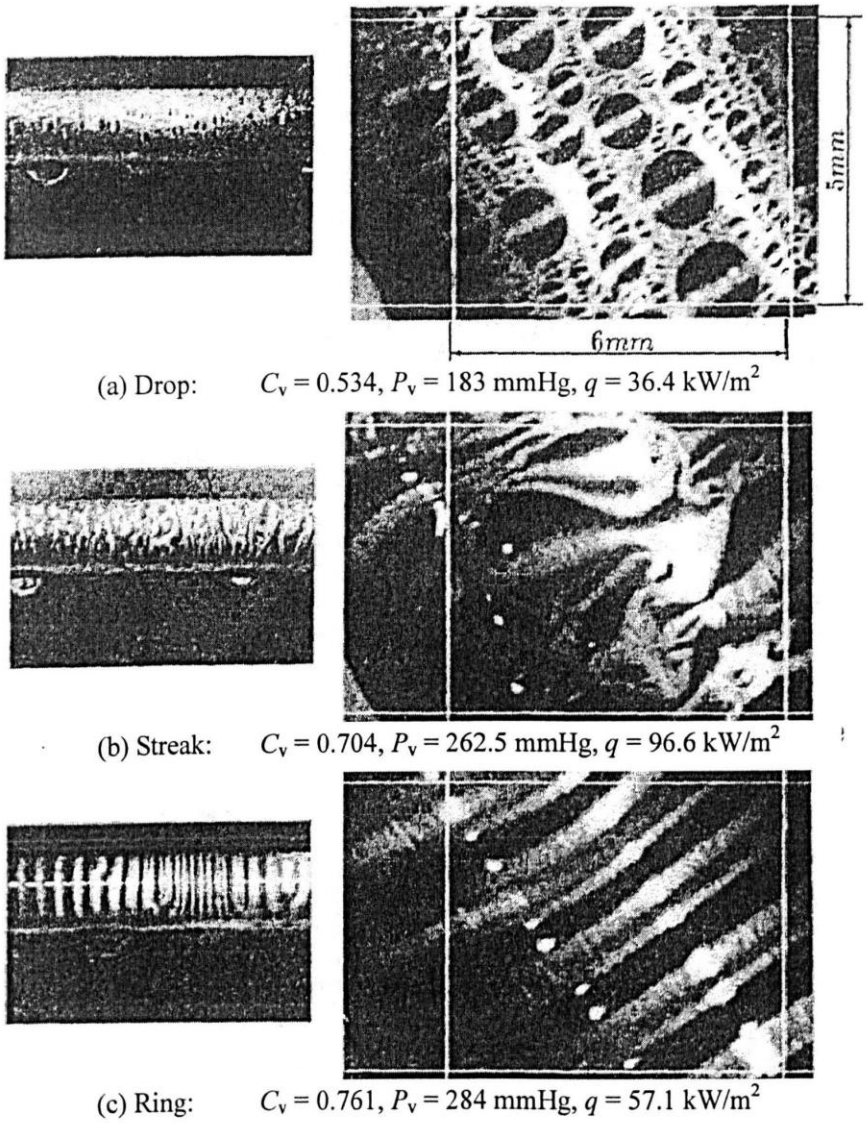

Figure 3-6: condensate appearance during condensation of steam-ethanol mixtures on the horizontal tube (Fujii et al. (1993))

Hashimoto et al. (1994) conducted the similar experiments for steam-ethanol mixtures under atmospheric conditions as Fujii et al. (1989, 1993), using a vertical copper tube of diameter 30 mm and active heat-transfer length of 90 mm. similar condensate appearances were observed as Fujii (1993). Heat-transfer coefficients on the vertical tube were also found to be 3 times higher than Nusselt (1916) when the condensate appearance was dropwise.

Utaka and Terachi (1995) experimentally investigated the condensation of steam-ethanol mixtures on a vertical plane surface of length 71mm and width 30mm. Vapour mass concentration of 0.17% to 0.71% was used. They determined the dependence of heat transfer characteristics along the length of the plane. Condensate appearance varied

along the vertical position of the plane. Heat transfer coefficient and heat flux were found to decrease from top to bottom. Heat flux and heat transfer coefficients were maximum at the top position due to a large amount of condensate generated. Lastly, they found that ethanol mass concentration increases at the higher position as a less volatile component would condensate first. They also divided the heat transfer curves into three main domains against vapour-to-surface temperature difference. The steep increase of heat flux and heat transfer coefficient, heat flux and heat-transfer coefficient reaching a maximum value and the decrease of heat flux and heat transfer coefficient. Finally, the curves follow the film-wise trend with a further increase in vapour-to-surface temperature difference. The curves obtained from Utaka and Terachi is shown in Figure 3.7.

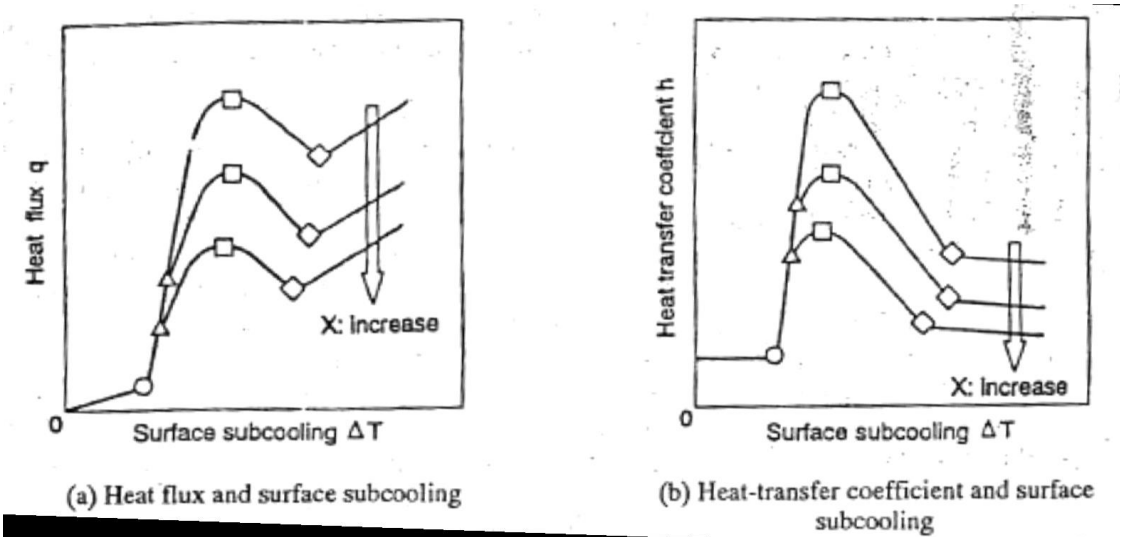

Figure 3-7: Heat flux and heat-transfer characteristic curves for steam ethanol mixtures (Utaka and Terachi (1995)).

Hijikata et al. (1996) used the horizontal copper tube of diameter 30 mm as a condensate surface to investigate the condensate appearance under an absolute pressure of 135mmHg. The condensate of the steam-ethanol mixture was periodically wiped to remove droplets from the tube surface. They note four important observations: firstly, thin condensate film always existed and drops float on it. Secondly, movement of drops is more frequent on the surface in pseudo-dropwise compared to pure steam dropwise condensation. Thirdly, droplets are always formed from the same place where small scratches existed; and lastly, drop diameter was 20 times smaller than pure steam dropwise condensation and was around 0.5 mm.

Morrison and Deans (1997) also experimentally investigated the condensation binary mixture but this time using different fluid; steam-ammonia. They used horizontal stainless-steel tube of diameter 25 mm and length of 145 mm. At the lowest concentration (0.1%) contrary to steam-ethanol heat transfer was found to be less than Nusselt (1916). However, for the mass concentration of 0.22 to 0.88% found enhancements of up to 1.13. Table 3.3 shows the experimental conditions and results.

Table 3-3: Steam-ammonia condensation results from Morrison and Deans (1997).

Exp No	X_v (wt%)	ΔT (K)	Film Type	q (kW/m^2)	α (kW/m^2 K)	ε
1	0.1	14.5	S	132.2	9.1	0.86
2	0.23	15.2	SR	171.3	11.3	1.04
3	0.39	14.6	RB	173.3	11.8	1.09
4	0.52	15	RB	175.2	11.7	1.07
5	0.71	14.9	R	184.2	12.4	1.13
6	0.88	14.8	R	178.6	12.1	1.10
7	2.05	18.3	R	168.7	9.2	0.89
8	2.20	15	B	127.6	8.5	0.75

*S = Smooth, B = Banded, R = Rippled

Morrison et al. (1998) then extended his experimental work by using steam-methylamine as a binary mixture. Visual observation shows the pseudo-dropwise mode of condensation and condensate film behaved vigorously and turbulently. Maximum enhancements were similar to steam-ammonia case 1.3 but at the vapour concentration of 0.2%. Table 3.4 summarises the experimental conditions and results.

Table 3-4: Steam-methylamine condensation results from Morrison and Deans (1998).

Exp No	X_v (wt%)	ΔT (K)	Film Type*	q (kW/m^2)	α (kW/m^2 K)	ε
1	0.00	16.1	S	172.6	10.7	1.0
2	0.03	7.9	SR	126.6	16	1.2
3	0.03	10.1	RB	192.2	19	1.6
4	0.2	6.4	PD	198.7	31.2	2.3
5	0.22	5.6	BR/PD	136.2	24.4	1.7
6	0.22	7.8	PD/BR	203.1	26.2	2.0
7	1.04	6.2	PD	133.8	21.6	1.6
8	1.04	9.2	PD	202.0	22.0	1.8
9	2.31	11	PD	190.0	17.2	1.5
10	4.29	15.7	PD	173.8	11	1.0

*S = Smooth, B = Banded, R = Rippled, PD = Pseudo-dropwise

Utaka and Kobayashi (2001) studied the effect of vapour velocity on Marangoni condensation of steam ethanol on the short vertical flat plate. They found that the heat transfer coefficient increases with the increase in vapour velocity regardless of ethanol vapour concentration over the entire range of vapour-to-surface temperature difference. Increasing velocity decreases the diffusion resistance as the concentration of the more volatile component decreases in the vapour phase of the liquid-vapour interface.

Later, Utaka and Nishikawa (2003) used the laser extinction method to measure the film thickness for various condensate appearances. The minimum film thickness of 1 μm was always found after drops rolling off from the condensing surface.

Philpott and Deans (2004) extended the work of Morrison and Deans (1997) and explored the heat transfer characteristics of condensation of steam-ammonia inside the horizontal tube. Dimensions of the tube were 20 mm × 150 mm and vapour concentrations of 0-10% were used at the inlet. Maximum increased in vapour concentration along the length of the tube was 26%. At lower vapour concentration of ammonia, 0.9%, maximum enhancement of 1.3 times compared to pure water was obtained. As ammonia concentration increases heat transfer rate decreases. At bulk ammonia concentration of 18%, only 20 % of predicted pure steam heat-transfer coefficient was achieved.

Utaka and Wang (2004) further explored the steam-ethanol condensation under atmospheric pressure on a vertical surface of 20 mm × 10 mm. Vapour concentrations were varied from 0 to 32% and vapour velocities from 0.4 to 1.5 m/s. Figure 3.8 and 3.9 shows the heat flux and heat-transfer coefficient against vapour-to-surface temperature difference. Enhancements of around 8 times were reported compared to the pure steam case. At the point of maximum heat transfer coefficient, condensate film thermal resistance was minimum.

They also investigated the ternary mixture of water, nitrogen and ethanol. Ethanol vapour concentration of 0.01%, 0.017%, 0.25% and 0.45% were used with maximum nitrogen mass fraction of 498×10^{-6} %. Vapour velocity was 0.5 m/s. Effect of non-condensable gas was found to be relatively small compared to the vapour diffusion effect of ethanol. However, it was maximum in dropwise region and minimum at diffusion region. The maximum heat flux shifts towards the right as non-condensable gas concentration increases. They also proposed a correlation developed from the least square method.

$$q_{max} = a_1 + a_2 \ln(C_g) \times 10^6 \quad (3.8)$$

where,

$$a_1 = 1872.2 + 6452\, C_e + 58634.9\, {C_e}^2 - 120699.1\, {C_e}^3 - 78304.1\, {C_e}^4 \quad (3.9)$$

$$a_2 = -168.4 + 445.5\, C_e + 3960.3\, {C_e}^2 - 5175.5\, {C_e}^3 \quad (3.10)$$

$$\alpha_{max} = b_1 + b_2 \ln(C_g) \times 10^6 \quad (3.11)$$

$$b_1 = 172.2 + 1107.5\, C_e + 4023.8\, {C_e}^2 - 7262.3\, {C_e}^3 - 4961.7\, {C_e}^4 \quad (3.12)$$

$$b_2 = -13.4 + 44{,}8 - 41\, {C_e}^2 \quad (3.13)$$

where,

q_{max} is the maximum heat flux

α_{max} is the maximum heat-transfer coefficient

C_g is nitrogen gas concentration

C_e is ethanol concentration

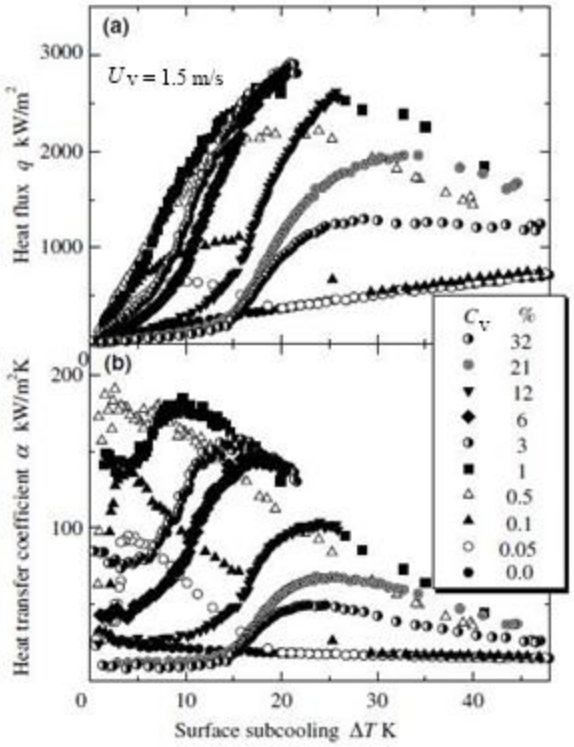

Figure 3-8: Utaka and Wang (2004) results of heat flux and heat transfer coefficient against vapour-to-surface temperature difference.

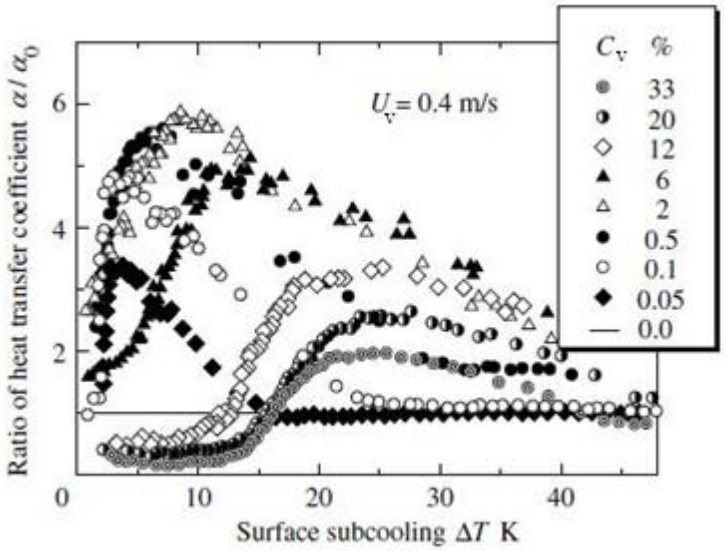

Figure 3-9: Utaka and Wang (2008) results of heat flux against vapour-to-surface temperature difference for different ethanol concentrations

Effect of macroscopic temperature gradient was experimentally investigated by Hu et al. (2007) on a horizontal copper block. The dimensions of the copper block were 25 mm × 40mm. vapour velocities of 2, 4 and 6 m/s at a pressure of 31.2, 47.4 and 84.5 kPa were investigated. Ethanol vapour concentrations of 0.5%, 1%, 2%, 5%, 10%, 20% and 50%

were used. Heat transfer coefficient increases with vapour velocity and pressure and the maximum Heat transfer coefficient was found at 1% ethanol concentration. The credit of enhancement was given to surface temperature gradient causing convection resulting in higher heat and mass transfer.

Wang (2007) performed the similar experiment as Hu et al. (2007) but on a vertical flat plate and the results of both the experiments were in good agreement with each other.

Yan et al. (2007) and Yang et al. (2008) also studied the condensation heat transfer on a vertical plane with a dimension of 12mm × 42 mm. they demonstrated the effect of concentration, velocity and pressure. It was concluded that with an increase in pressure and velocity enhancements increases and maximum enhancement of up to 7.5 times was found compared to the pure steam case. Figure 3.10 shows the condensate appearances observed by Yan et al. (2007).

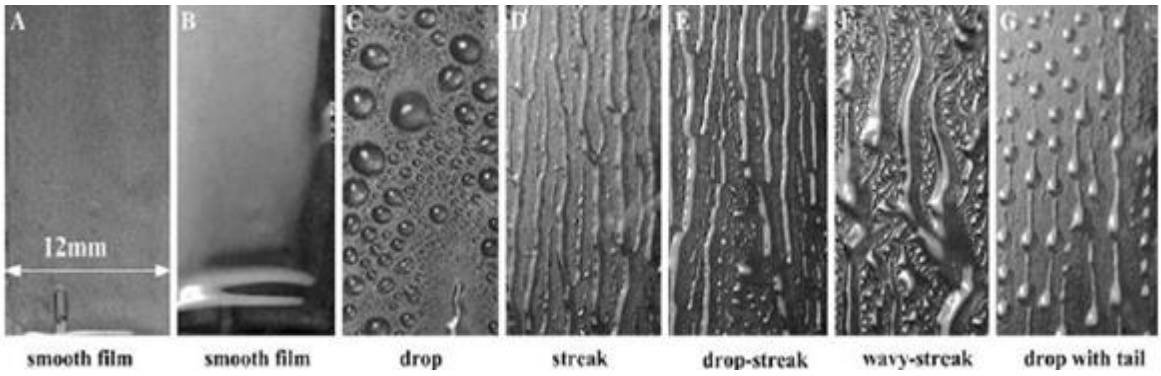

Figure 3-10: condensation modes ranging from smooth film to dropwise (Yan et al (2007)).

Lie et al. (2008) and Wang et al. (2009) experimented with the Marangoni condensation of steam ethanol mixtures on the vertical copper tube with a diameter of 20mm and lengths of 40mm and 50mm. vapour concentration were 0%, 0.5%, 1%, 2%, 5%, 10%, and 50%. Figure 3.11 shows the comparison of the condensation heat-transfer coefficient of steam-ethanol mixtures and different pressure and ethanol concentrations. The visual observation showed the transition of condensation modes from film to rivulets, rivulets to drops and from drops back to rivulets + drop. The maximum enhancement of 9 times was obtained at 1% mass concentration.

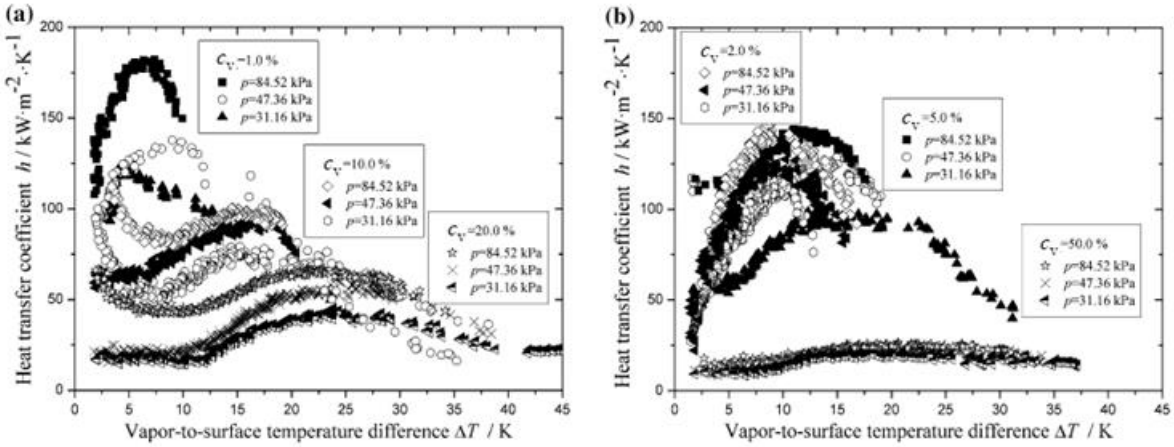

Figure 3-11: Heat-transfer results of Wang et al (2009).

In 2007 Murase et al. investigated heat transfer characteristics of Marangoni condensation using steam-ethanol mixtures on a horizontal smooth tube at atmospheric conditions. The tube diameter was 12.2 mm and length of 90 mm. vapour concentrations of 1.1%, 2%, 5.4% and 10% were used and vapour velocities were 0.15, 0.24, 0.35, 0.56 and 0.75 m/s. enhancements of around 4 times compared to pure steam were reported at vapour concentrations of 1.1 and 2%. The results were also compared with Utaka and Wang (2004) and were in good agreement. Graph of heat flux against vapour-to-surface temperature difference is shown in figure 3.12.

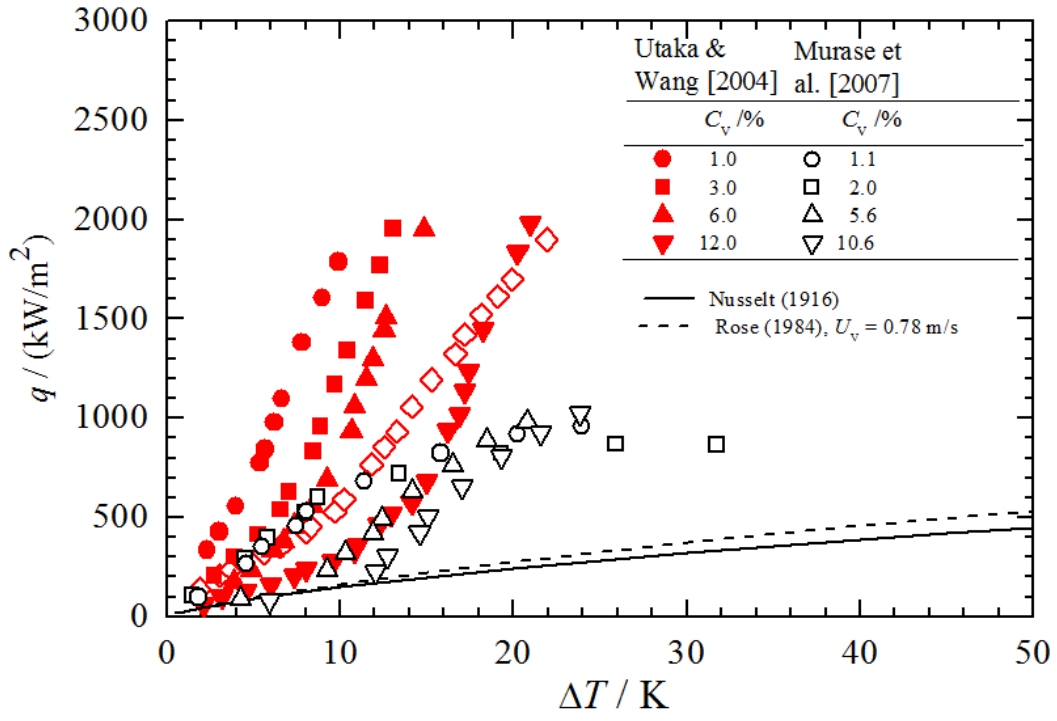

Figure 3-12: Comparison of heat flux against vapour-to-surface temperature difference for varying ethanol mass concentration (Murase et al. (2007)).

Ali (2012) extended the work of Murase et al. (2007) by experimenting on steam-ethanol mixtures at atmospheric and sub-atmospheric conditions of 14 kPa, 55 kPa and 101 kPa. Three types of condensation surfaces were used: horizontal smooth tube, horizontal bank of smooth tubes and low-finned tubes. Tests were conducted at higher vapour velocities of 0.78, 1.6, 2.4, 3.2, 4.9 and 7.5 m/s and ethanol mass concentrations of 0.05%, 0.1%, 0.5% and 1%. At atmospheric condition he also used lower concentration of 0.001%, 0.005%, 0.01%, 0.017% and 0.025%. Enhancements of up to 4 were found in case of steam-ethanol mixtures at the mass composition of 0.017 % to 0.1%. In case of low finned tubes enhancements of up to 3 was obtained at an ethanol concentration of 0.025%, for Bank of tubes enhancements of around 2 were reported when sufficient vapour was available on the last rows.

3.2.6 Theoretical investigations

Owing to the complex phenomenon of Marangoni condensation a complete theory is still not developed. However, Yan et al (2009) investigated the drop size distribution of Marangoni condensation. They analyse the dependence of drop diameter and drop cycle time on the vapour-to-surface temperature difference, vapour velocities and test section pressure. Similar condensate appearances as earlier investigations were found with drops and rivulets. Drop diameter was found to be less than 1mm for 70% of drops and cycle time was 0.2 to 2 sec. Drop diameter increases with vapour-to-surface temperature difference and vapour velocity but was not affected by vapour pressure. Maximum drop diameter was about 1.5 to 5 mm. For maximum diameter, a formula was devised and is given as:

$$D_{maz} = 1.95\,(100 \times C_v)^{0.25}$$

where,

C_v is the equilibrium ethanol vapour concentration.

In 2011 Li et al. proposed a semi-empirical model to predict the heat flux for Marangoni condensation of steam-ethanol mixtures on vertical tube. The model was based on Sparrow and Marchall (1969), the theory of diffusion of binary mixtures, and LeFevre and Rose (1966), the theory of dropwise condensation of pure steam. The contact angle of the condensate drop was assumed to be 90 degrees and the thin film that exist between

the drops was neglected. ethanol concentration along the condensate was also assumed to be uniform. The average heat flux was calculated using integration of drop radii.

$$q = \int_{rmin}^{rmax} q_{b.\pi r^2.N(r)dr} \tag{3.14}$$

where,

$N(r)$ is the drop size distribution function (same as Lefevre and rose (1966) proposed for pure steam dropwise condensation).

q_b is heat flux through the base of the hemispherical drop

r_{max} is maximum drop radius

r_{min} is minimum drop radius

Ma et al. (2012) used a surface free energy difference to explain theoretically the transition mode of condensate from film-wise to dropwise. The surface free energy was defined as:

$$\Delta\sigma = \sigma_c - \sigma_f \tag{3.15}$$

where,

$\Delta\sigma$ is the difference in surface free energy

σ_c is the surface free energy of condensate

σ_f is the surface free energy of thin film

σ_c and σ_f were calculated at condensate and thin film temperatures using these assumptions.

$$T_c = T_v \tag{3.16}$$

$$T_f = T_v - \frac{\Delta T}{2} \tag{3.17}$$

Results were promising when compared to experimental results of Utaka and Terachi (2004). It shows that condensate appearance changes from film-wise to drop-wise with an increase of surface free energy. Heat transfer coefficient was compared against change in surface free energy and similar results were obtained.

3.3 Self-rewetting fluids

The term self-rewetting fluids are associated with the dilute aqueous solutions of alcohols having carbon atoms greater than or equal to four (such as butanol, Pentanol, Hexanol, Heptanol or Octanol). Theses fluid due to their properties associated with the non-linear dependency of surface tension with temperature tends to enhance the heat transfer coefficients. As discussed in the previous section, non-azeotropic mixtures in contrast to single component fluid, due to the concentration gradient (Marangoni effect) at the liquid-vapour interface leads to instability of liquid film. This film deformation would expect to give higher interface temperature where the film is thicker (crest) and lower interface temperature at the valley (where the film is thinner). The surface tension gradient due to concentration causes the liquid in the film to be drawn towards the crest. Hence, marking the start of pseudo dropwise mode of condensation. For ordinary liquids (such as Ethanol), Figure 3.13, the derivative of surface tension with respect to temperature is less than zero i.e. the surface tension is a decreasing function of temperature. In such a case, where the less volatile component has the higher surface tension is known as the positive mixture and surface tension effect favours the heat transfer. However, the thermocapillary effect as shown in Figure 3.14 deteriorates the heat transfer. If both the thermocapillary effect and the surface tension effect move in the same positive direction than appreciable heat transfer can be expected in the process of phase change of the binary mixture. For this to be realized, the fluid must have a favourable relation between surface tension and temperature i.e. derivative of the surface tension with respect to temperature should be greater than zero or in other words, the surface tension is an increasing function of temperature.

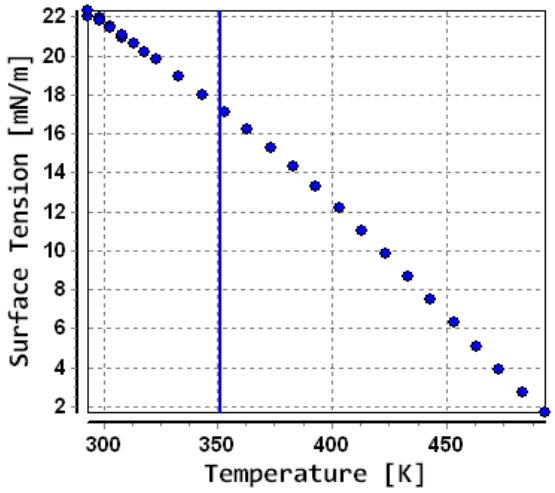

Figure 3-13: variation of the surface tension of ethanol with temperature.

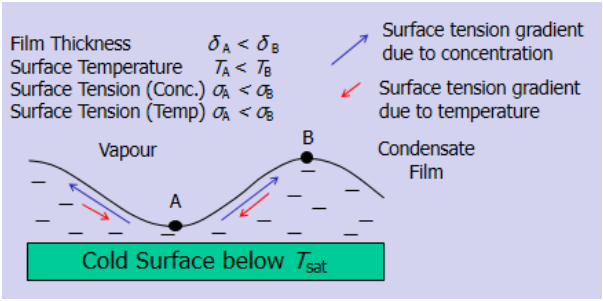

Figure 3-14: Surface tension effect and thermocapillary effect in Marangoni condensation of binary mixtures of steam-ethanol

For self-rewetting fluids, Vochten and Petre (1973) depicted that surface tension as a function of temperature has a nonlinear decreasing trend for some range of temperature until it reaches a minimum at a certain temperature and then increases for the higher range of temperatures as shown in Figure 3.15. These types of aqueous alcohol (such as Steam-Butanol) are known as negative mixtures since alcohol is a less volatile component in contrast to steam ethanol mixture. However, in a small concentration of less than 1%, they behave like positive mixtures. Therefore, the Marangoni effect (surface tension effect) and the thermocapillary effect should cooperate to further enhance the heat transfer coefficients as shown in Figure 3.16.

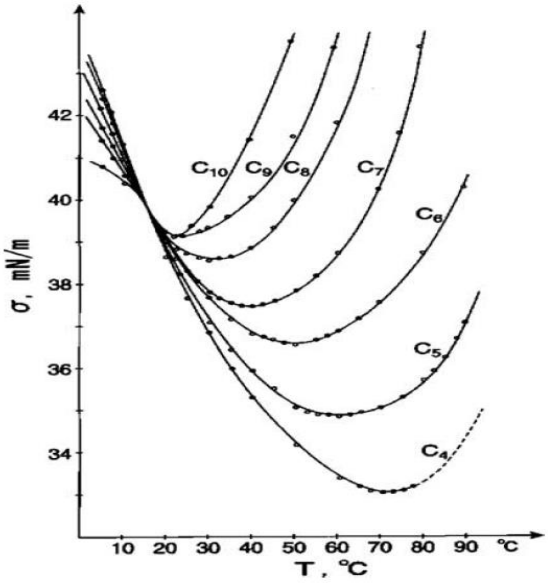

Figure 3-15: variation of surface tension with temperature for self-rewetting fluids.

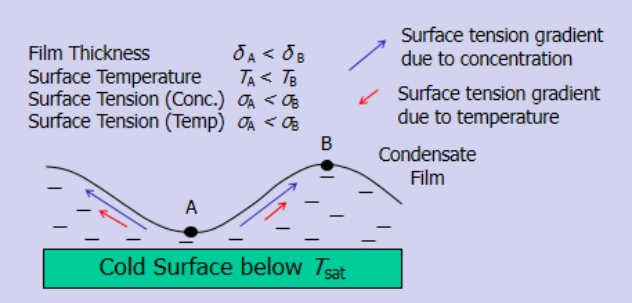

Figure 3-16: Surface tension effect and thermocapillary effect in Marangoni condensation of binary mixtures of steam-butanol.

3.3.1 Boiling heat transfer enhancements in heat pipes under microgravity conditions

This phenomenon was first experimentally demonstrated by Kuramae and Suzuki (1993) in a microgravity boiling using ethanol aqueous solution. It showed that for zeotropic compositions ethanol rich areas of liquid evaporates in the evaporation region and condenses in the condensation region. Resulting in the condensate to flow towards the hot surface due to the concentration gradient between condensing and evaporating regions.

Later the phenomenon was repeated in boiling of ethanol aqueous solution under microgravity conditions by Abe et al. (1994). They compared the boiling heat transfer coefficients (HTC) in microgravity with that of the terrestrial condition of 1G. The

transparent heater was employed to observe the behaviour of the bubble-heater contact area. It was observed that HTC for microgravity was 20 to 60 % higher than the 1G conditions but the critical heat fluxes (CHFs) in microgravity were lower than that in 1G and were nearly the same for CHFs of single component fluids. The comparison can be seen in Figure 3.17. However, the behaviour observed at the bubble-heater contact area for aqueous solutions was different than that of the single component fluid. Observation depicted that bubble was first developed on heater surface and then grew with a liquid layer of certain thickness at the bubble-heater contact area. The inflow of liquid due to surface tension gradient, push away the bubble grown on the heater-surface contact area. The existence of the liquid layer was later confirmed using the interferometer by Abe & Iwasaki (2000).

In 2002 abe & Iwasaki, measured the flow velocity, using tracer particle method, of the liquid developed along the interface (vapour-liquid) due to thermocapillary effect from the bubble base to the top. Results confirmed the theory that thermocapillary flow suppresses the bubble from being detached from the heater surface. For the subcooled temperature difference of 3K velocity of 50mm/s was observed. The schematic of the confirmed phenomenon from abe & Iwasaki is in Figure 3.18.

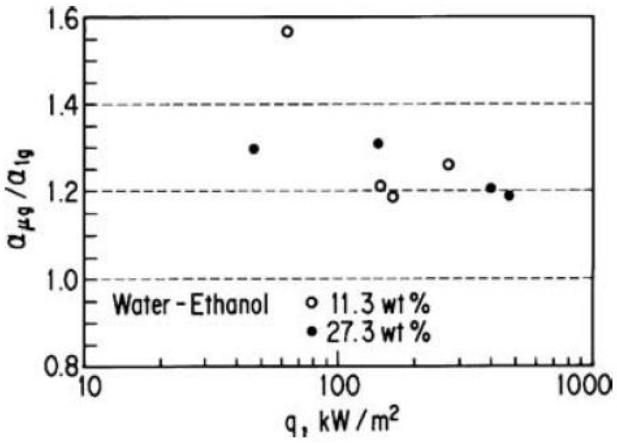

Figure 3-17: Results of Abe & Iwasaki (2000)

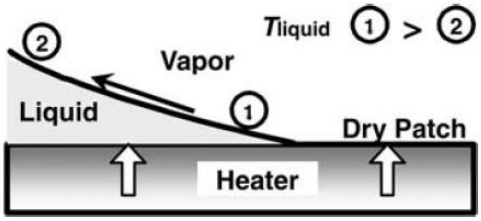

Figure 3-18: The schematic of the phenomenon of thermocapillary effect. Abe & Iwasaki (2002)

Abe et al. (2004) extended the phenomenon to self-rewetting fluids i.e. 1-butanol aqueous solution and observed flow pattern and velocity using the transparent heater and tracer particle method. 1.5 wt% of 1-butanol and 20wt% of ethanol aqueous solutions were used in the wickless heat pipe. To measure temperature distribution and velocity of the returning liquid experiments were conducted in a glass tube with thermocouples and tracer particles as shown in Figure 3.19. The flow direction due to thermocapillary effect was observed to be inwards from top to bottom in contrast to the flow direction observed with a single fluid. Overall velocity (thermocapillary and surface tension) of the liquid inflow to the nucleation site for 1-butanol (1.5 wt%) was up to 15 mm/s and for ethanol (20 wt%) was 0.7 mm/s. Thus, confirming that the higher velocity for 1 butanol is the result of the combined positive effect of surface tension gradient and temperature gradient.

Abe et al. (2005) performed detailed experiments on the heat transfer performance of the wickless heat pipes. Using three heat pipes and two aqueous solutions to compare the heat transfer enhancements; 1-butanol aqueous solution in the wickless heat pipe, the 1-butanol aqueous solution in wicked heat pipe and ethanol aqueous solution in the wickless heat pipe. Among the three heat pipes, the 1-butanol aqueous solution in wickless heat pipe showed highest heat transfer rates, heat flux and dry out limits with lowest thermal resistance. Ethanol aqueous solution in wicked heat pipe performed most poorly among the three. The results are summarised in the Figure 3.20.

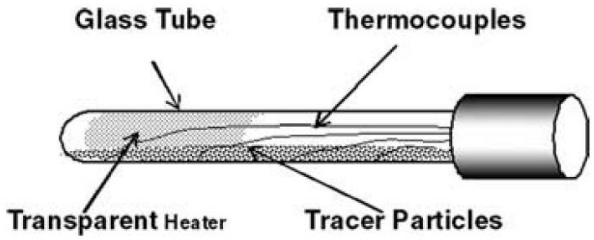

Figure 3-19 Glass tube apparatus with tracer particles used by Abe et al. (2004)

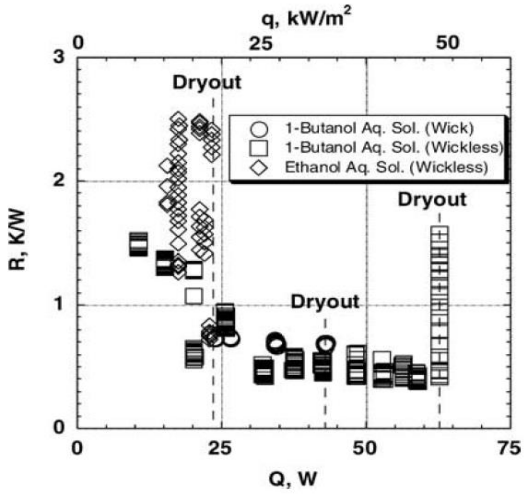

Figure 3-20: Thermal performance of heat pipe (Abe et al. (2004))

3.3.2 Boiling heat transfer enhancements under terrestrial (1G) conditions

Application of self-rewetting fluids is not only applicable to microgravity but also in devices under terrestrial conditions. In nucleate boiling, significant heat transfer enhancements have been found with self-rewetting aqueous solutions compared to water. Van et al. (1956) and Suzuki et al (2005) have shown two to three times higher critical heat fluxes (CHFs). Carry and co-workers (1996 & 1999) demonstrated the same phenomenon using an aqueous solution of 2-propanol (1.5 mol%) under pressure conditions of 7 kPa. The CHF was double compared to water and significant higher Heat Transfer Coefficient (HTC) than water was reported. Results concluded that strong Marangoni effect was due to the concentration gradient of the mixture in the liquid.

Abe (2006) conducted pool boiling experiments for four different fluids; water, 4.8wt% of the 2-propanol aqueous solution, 2wt% of the 1-pentanol aqueous solution and 6wt% of the 1-butanol aqueous solution under atmospheric conditions. The author compared the results in Figure 3.21 with heat transfer correlation of natural convection boiling of water by Stephen & abdelsalam (1980). The main findings were the significant enhancement of the heat transfer coefficient of up to 20% with 1-butanol and 1- pentanol aqueous solutions as compared to the Stephen-abdelsalam's correlation for water. However, no significant advantage in the CHFs was found. 2-propanol aqueous solution performed

poorly that pure water and HTC and CHF were both appreciably low. Moreover, he also showed the photographic evidence in Figure 3.22 for the reduction in bubble size of the pool boiling behaviour of the 1-butanol aqueous solution compared to water and associated this attribute to end the drawback of microscale boiling heat transfer devices with water.

Abe et al. (2006) also extended the experimental work to ordinary heat pipes i.e. wicked heat pipes to further understand the effect of self-rewetting fluids in terrestrial applications. Two different diameters of heat pipes were used, 4mm and 8mm, and tested in vacuum chambers. Former diameter pipes with 1- butanol aqueous solution showed 40% better results than water and 15% less thermal resistance. Whereas later size pipe showed a 40% reduction in thermal resistance. The results are shown in Figure 3.23.

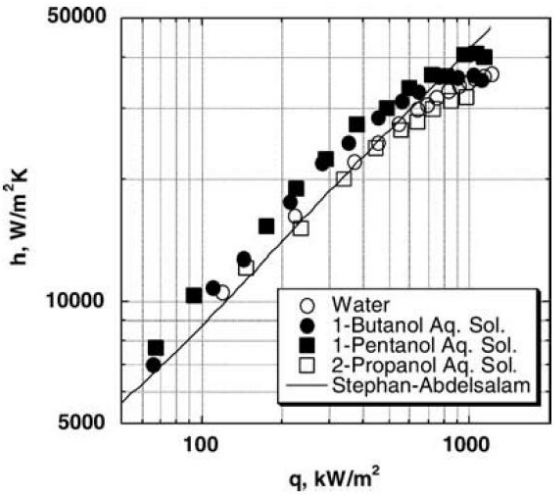

Figure 3-21: Comparison of results of Abe (2006) and Stephen-Abdelsalam (1980) Correlation.

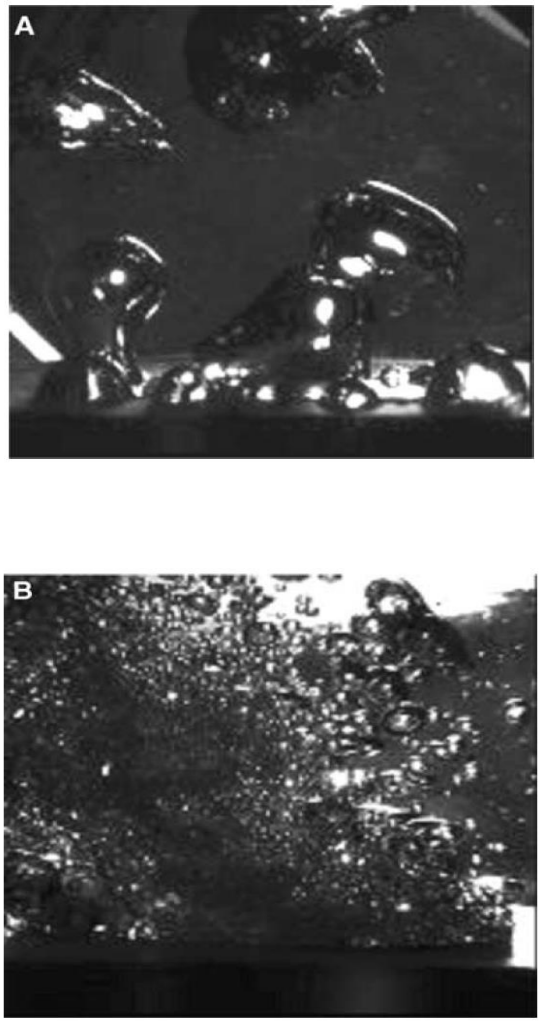

Figure 3-22: Photographic evidence showing a reduction in bubble size for (A) 1-butanol aqueous solution compared to (B) water (Abe, 2006).

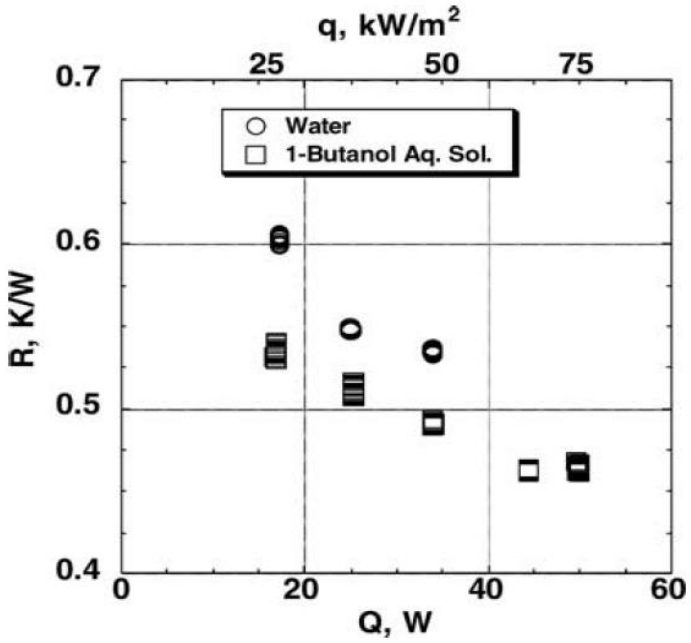

Figure 3-23: Results of Abe (2006).

In 2014 Hu et al performed a series of experiments to clarify the heat transfer mechanism and characteristic of pool boiling with self-rewetting liquid. They used dilute aqueous heptanol solution as a fluid and a horizontal heated wire as a boiling source. Video of nucleation boiling process was also recorded with the aid of the high-speed video cameras. The main findings of their results were the comparison of the critical heat flux (CHF) of heptanol aqueous solution with CHF of pure water. They concluded the following:

1. Surface tension gradient induces the Marangoni effect in the heptanol aqueous solution which enhanced the heat transfer process and reduces the dry out phenomenon. The CHF of heptanol aqueous solution was 2.52 times higher than that of water (Figure 3.24).
2. The bubbles of Heptanol aqueous solutions are smaller than that of water (Figure 3.25).
3. Due to Marangoni convection, a thick film is maintained between the bubbles which makes coalescence difficult.
4. This thickening of the liquid film between bubbles is beneficial as it promotes bubbles on the heated surface to detach easily (Figure 3.26).
5. At certain critical heat flux, microbubble emission boiling was observed. Under which the bubble would collapse on the heated surface and many microbubbles

were released from the surface. These emissions of microbubbles create turbulence and enhanced the heat transfer process (Figure 3.27).

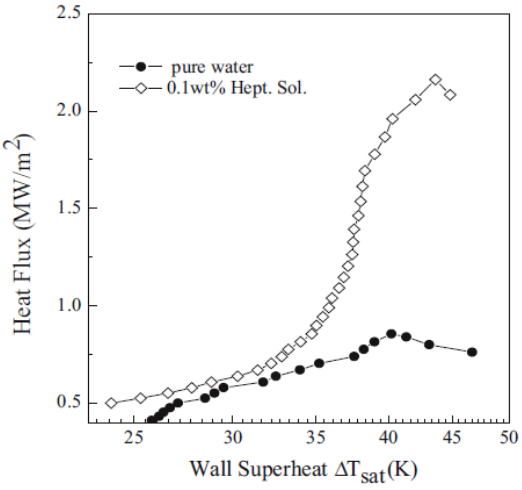

Figure 3-24: Heat flux against wall superheat temperature difference (Hu, et al., 2014).

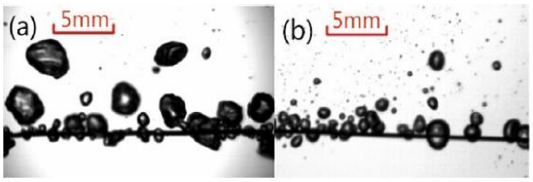

Figure 3-25: Comparison of the bubble diameter of water and heptanol; (a) water (b) Heptanol (Hu, et al., 2014).

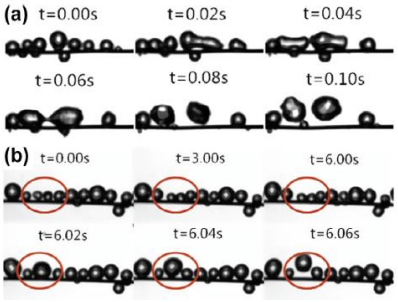

Figure 3-26: observation with time lapse (a) water (b) Heptanol *(Hu, et al., 2014)*.

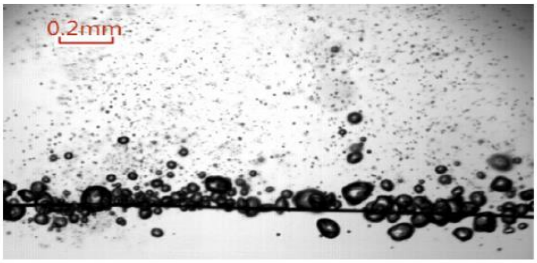

Figure 3-27: emission of microbubbles creating turbulence *(Hu, et al., 2014)*.

Hu et al (2015) further extended the research on to subcooled pool boiling (sub-cooling of 1°C, 5°C, 10°C and 15°C) using heptanol aqueous solution with different concentrations of 0, 0.01 wt %, 0.05 wt %, and 0.1 wt %. Results demonstrated higher heat transfer performance and reduced dry out phenomenon with higher subcooled temperature. 0.1 wt % of Heptanol showed the highest critical heat flux. Moreover, they also confirmed the previous finding that Heptanol bubbles were smaller and more compared to water. The findings of the above-mentioned experiment are shown in Figure 3-28.

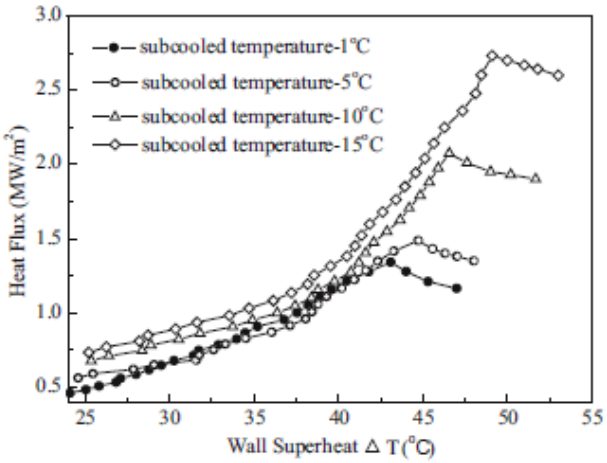

Figure 3-28: The boiling curve of the solution with different subcooled temperature. (Hua, et al., 2015)

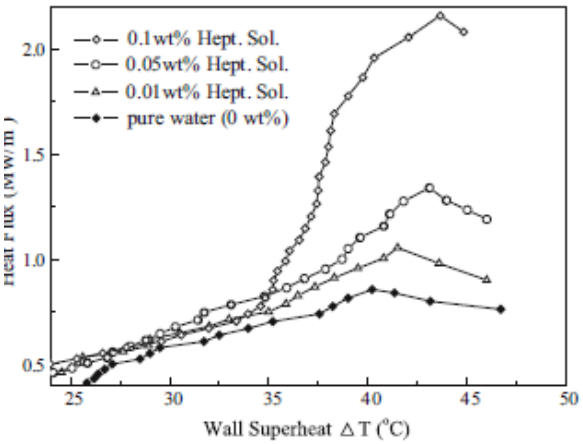

Figure 3-29: The boiling curve of the working fluid with different concentration (Hua, et al., 2015).

Moreover, Sitar & Golobic (2015) conducted the boiling experiments of pure Butanol and n-Butanol aqueous solutions in microchannels of cross section 50×50 µm and 25×25µm.

Illumination sources, microscopes and high-speed cameras were installed for visual observations. For 2% and 6% aqueous butanol solutions, enhanced heat transfer was observed compared to pure water and pure butanol. Maximum temperature also reduced to 10K and 30 K for 2% and 6% Butanol concentration respectively. The results are shown in Figure 3.30. With the help of high-speed visualisation cameras, contact angles and surface roughness was measured. The contact angle of pure water was higher than the aqueous butanol solutions as shown in Figure 3.31. the author concluded that contact angle and surface tension itself are not crucial for enhancement of heat transfer coefficient.

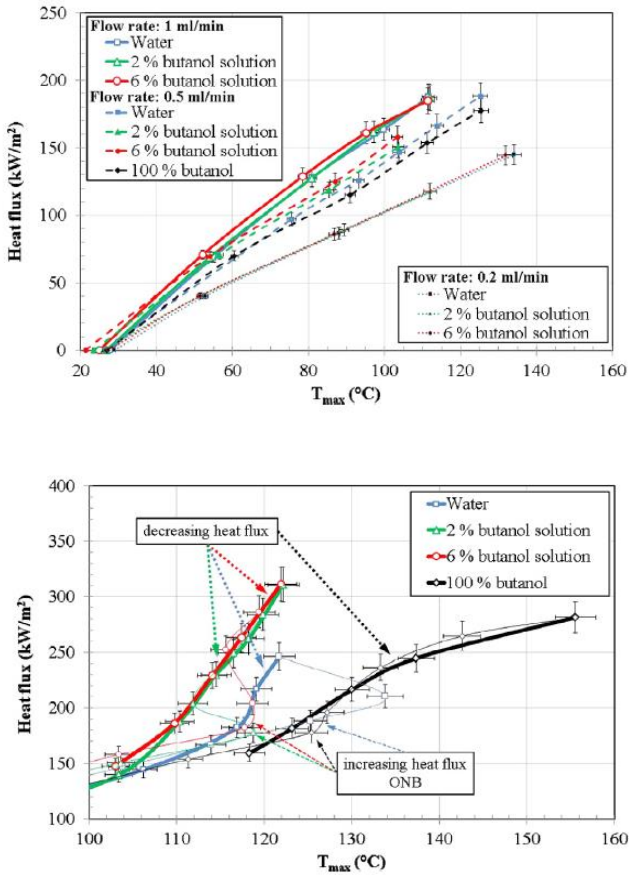

Figure 3-30: Results of Sitar & Golobic (2015)

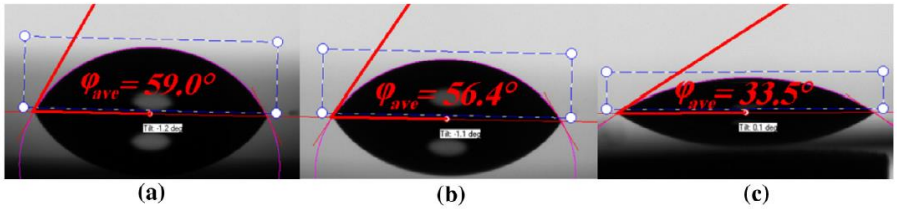

Figure 3-31: Contac tangle of pure water and aqueous butanol (Sitar & Golobic (2015)).

3.4 Summary

List of earlier experimental investigations for Marangoni condensation of mixtures can be seen in Table 3-5. Earlier experiments have demonstrated a significant enhancement in condensation heat transfer adding various additives (ethanol, ammonia and methylamine) in the water on horizontal/vertical planes and horizontal/vertical tubes. The maximum enhancement of around 8 times was reported using ethanol in steam. No experimental evidence is available for steam-butanol or steam-propanol mixtures even though boiling investigations have shown promising results using such fluids. There is also very less research done on a theoretical and empirical aspect of the steam-ethanol mixtures. None of the empirical models covers a wide range of parameters and so far no theory has been developed.

Table 3-5: Summary of previous experimental studies in Marangoni condensation

Authors	Composition (Vapour mass fractions %)	Geometry	Pressure kPa	Vapour velocity m/s	Heat transfer performance/ important points
Missen (1961)	Pentane +methanol, Pentane+methylene dichloride	Vertical tube l = 150 mm, d = 40 mm	101	-	Photographs published, displaying Marangoni condensation
Mirkovich and Missen (1963)	Pentane +methanol, Pentane+methylene dichloride	Vertical tube l = 150 mm, *d = 40 mm*	101	-	Reduction in overall heat transfer due to diffusion resistance
Ford and Missen (1968)	-	-	-	-	Devised necessary but not the sufficient condition for film stability
Ford and McAleer (1971)	-	Circular plane t = 0.63 mm, d_o = 2.54 mm	101	-	Measurement of drop sizes for Marangoni condensation
Fujii et al. (1989)	Steam + methanol 0.08 - 0.85 Steam + ethanol 0.28 - 0.92	Horizontal tube l = 385 mm, d = 18 mm	113-14	-	No significant enhancement due to lower vapour-to-surface temperature difference
Utaka and Terachi (1995)	Steam + ethanol 0.17 - 0.74	Vertical plane (31 mm × 71 mm)	101	-	Significant enhancement α_{max} = 33 kW/m2 K (Cv = 0.34 %)
Morrison and Deans (1996)	Steam + ammonia 0.23 - 0.88	Horizontal tube l = 145 mm, *d = 25 mm*	101	-	*ε = 1.13 times* (C_v = 0.71 %)

Morrison et al. (1998)	Steam + methyleamine 0.03 - 4.3	Horizontal tube l = 145 mm, d = 25 mm	101	-	*ε = 2.3 times* (C_v = 0.2 %)
Philpot and deans (2004)	Steam + ammonia 0 - 26%	Horizontal shell and tube condenser l = 150 mm, *d = 20 mm*	101	-	*ε = 1.34 times* (C_v = 0.9 %)
Utaka and Wang (2004)	Steam + ethanol 0 - 32	Vertical plane (10 mm × 20 mm)	101	0.4, 1.5	*ε = 8 times* α_{max} = 180 kW/m2 K (C_v = 1.0 % Uv = 1.5 m/s)
Wang and Utaka (2004)	Steam + ethanol-nitrogen. C_e = 0.01-0.45 C_g = 9×10-6 - 498 × 10-6	Vertical plane (10 mm × 20 mm)	101	0.5	α_{max} = 180 kW/m2 K (C_e = 0.01 %, C_g = 9×10-6 %)
Peng et al. (2004)	Steam + ethanol 0.5, 1, 3, 22, 37	Vertical flat plane with temperature gradients (40 mm × 120mm)	101	0.3	*ε = 2.8 times* (C_v = 22%)
Hu et al. (2007)	Steam + ethanol 0.5, 1, 2, 20, 50	Vertical flat plane with temperature gradients (25 mm × 40 mm)	84.53, 47.36, 31.16	2, 4, 6	α_{max} = 210 kW/m2 K (C_v = 1.0 %, U_v = 2 m/s P_v = 84.53 kPa)
Yan et al. (2007)	Steam + ethanol 0.5, 1.0, 5.1, 9.8, 22, 50	Vertical flat plane (12 mm × 42 mm) *	84.53, 47.36, 31.16	1 - 5	ε = 1.8 times α_{max} = 42 kW/m2 K (C_e = 1 %)
Murase et al. (2007)	Steam + ethanol 1.1, 2.0, 5.4, 10.0	Horizontal tube l = 90 mm, *d = 12.2 mm*	101	0.15 - 0.75	*ε = 4 times* (C_v = 2 % Uv = 0.75 m/s)
Yang et al. (2008)	Steam + ethanol 0.5,1, 5, 10, 22, 51	Vertical flat plane (12 mm × 42 mm)	84.53, 47.36, 31.16	2	ε = 7.5 times α_{max} = 150 kW/m2 K (C_v = 1.0 %, U_v = 2 m/s Pv = 84.53 kPa)
Li et al. (2008)	Steam + ethanol 0, 0.5, 1, 2, 5, 10, 20, 50	Vertical half tube l = 40 mm d = 20 mm	84.53, 47.36, 31.16	2, 4, 6	ε = 9 times α_{max} = 175 kW/m2 K (C_v = 1.0 %, U_v = 4 m/s Pv = 84.53 kPa)
et al. (2009)	Steam + ethanol 0, 0.5, 1,2, 5, 10, 20, 50	Vertical flat plane with temperature gradient (25 mm × 40 mm)	84.53, 47.36, 31.16	3, 4, 6	α_{max} = 235 kW/m2 K (C_v = 1.0%, U_v = 4 m/s, P_v = 84.5 kPa)
Wang et al. (2009)	Steam + ethanol 0, 0.5, 1, 2, 5, 10, 20, 50	Vertical half tube l = 55 mm d = 10, 12.2, 20 mm	84.53, 47.36, 31.16	2, 4, 6	ε = 7.5 times α_{max} = 175 kW/m2 K (C_v = 1.0 %, Pv = 84.53 kPa)
Yan et al. (2009)	Steam + ethanol 0.5, 1, 2, 5, 10, 20, 50,100	Vertical flat plane (12 mm × 42 mm)	84.53, 47.36	1	α_{max} = 210 kW/m2 K (C_v = 1.0%, *Pv = 84.5 kPa)*

Chapter 4

4 The methodology of the experimental study

The experimental apparatus used has a long history in condensation heat transfer and had provided very reliable data up to present investigation. The apparatus was first designed in 1980's to investigate the condensation heat transfer on a single horizontal tube at low vapour velocity and atmospheric pressure. In 1985 Masuda used the apparatus to study the condensation heat transfer on integral-fin tubes using ethylene glycol and R-113 as condensing fluid. The work on integral-fin tubes was extended by Wen (1990) when he used the same apparatus to investigate the condensation heat transfer of steam and ethylene glycol on instrumented integral-fin tubes. Huang (1995) then further used it to investigate the effect of condensation of steam and R-113 on integral-fin tubes made of different materials. Later, the apparatus was adapted by Briggs (2003) and Baiser & Briggs (2009) to examine the condensation of steam and R-113 on Pin fin tubes. In 2007, Murase made use of the same apparatus and studied the Marangoni Condensation of the steam-ethanol mixture on smooth tubes. Finally, the apparatus was used by Ali (2011) to extend the work of condensation on Pin fin tubes, after which the apparatus was dismantled. The apparatus is now reassembled in the sustainable energy laboratory under the supervision of Dr HS Wang to extend the work on Marangoni condensation using the steam-butanol and steam-propanol mixtures as a condensing fluid.

4.1 General layout

Figure 4.1 shows the general layout of the experimental equipment used. It consists of a stainless-steel boiler where the vapour is generated using four electrically controlled immersion heaters. The heaters can be operated individually with total electric power ranging from 0 to 12 kW. One heater was connected to a variable resistor enabling varying heating powers to obtain different vapour velocities. The boiler is fitted with a sight glass to indicate the liquid level inside the boiler. Sight glass was marked to ensure minimum liquid level that would completely immerse heaters in liquid. Vapour generated in the boiler condenses on a test tube after journeying through 180° calming section and passes vertically down into the test section. Excess vapour is condensed in the auxiliary condenser and finally, the condensate returns to the boiler under gravity. Coolant for

condensing tube and auxiliary condenser is supplied through a centrifugal pump and the coolant flow rate is measured using a float type flow meter.

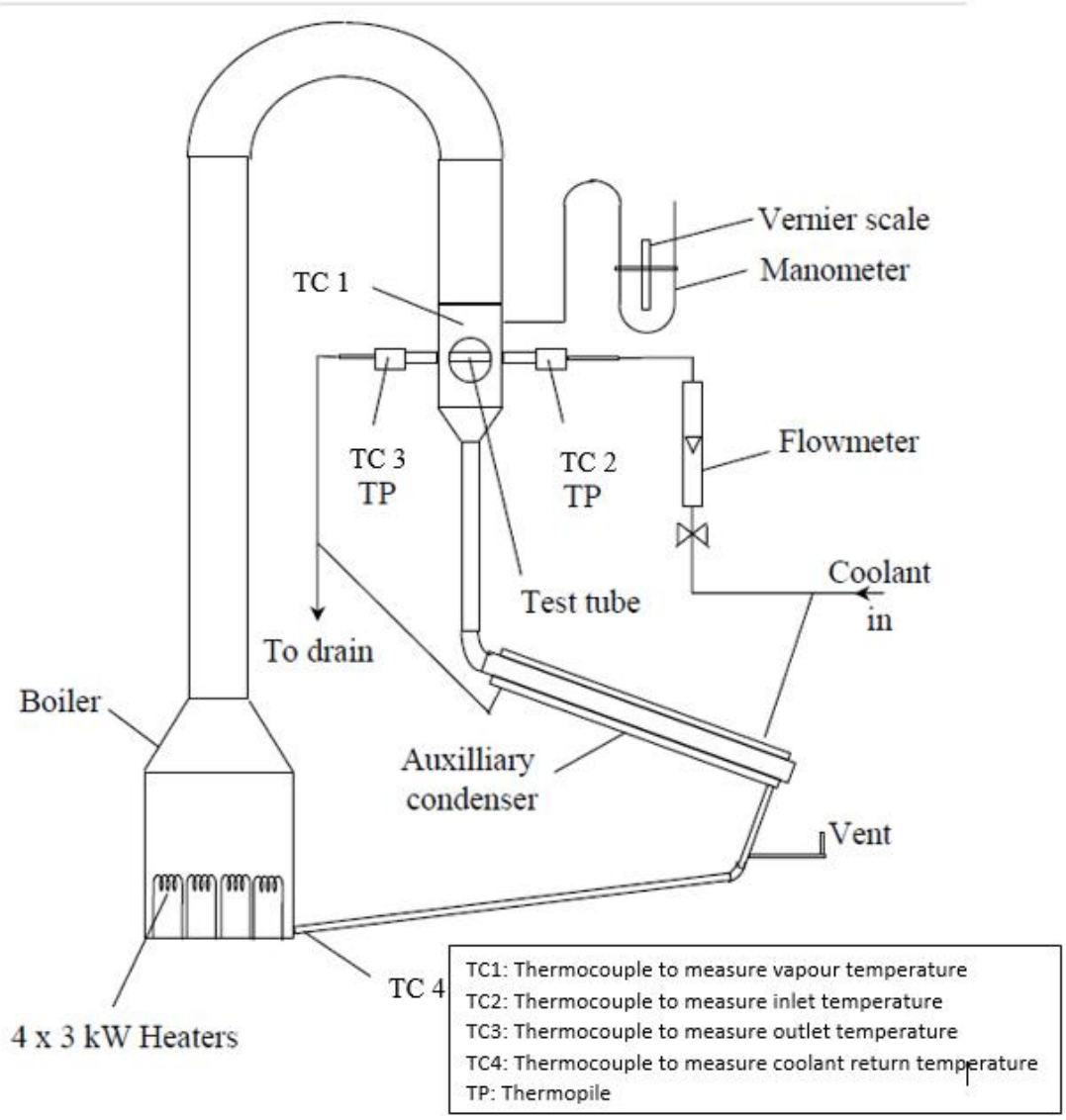

Figure 4-1: Schematic of experimental apparatus used for condensation investigations (the image was originally taken from Ali (2011)) and modified).

4.2 Test section

Figure 4.2 shows the schematic of the test section with an inside diameter and active condensing length of 100mm. For visual observation, a circular Pyrex glass window is located at the front of the test section. Horizontally mounted test tubes were fitted with PTFE (Poly-tetra-fluoro-ethylene) bushes to thermally insulate test tubes from the test section. The inside of the test tube was also thermally insulated using PTFE inserts in order to circumvent axial conduction from the tube and to ensure equal inside and outside surface available for the heat transfer. Mixing chambers made of PTFE at the inlet

and outlet of the test tubes were fitted to obtain mean coolant inlet and outlet temperatures. The coolant temperature rise was measured using ten-junction thermopile with an accuracy of 0.0005 K. Vapour temperature was measured using a K-type (Nickel-Chromium / Nickel-Aluminium) thermocouple inserted in a close thermocouple pocket protruded just above the test tube in the upstream area of the test section. Fortin barometer and U-tube mercury manometer were used to measure the atmospheric pressure and test section pressure respectively. One end of manometer was connected to test section just above the test tube and the other end was open to atmosphere.

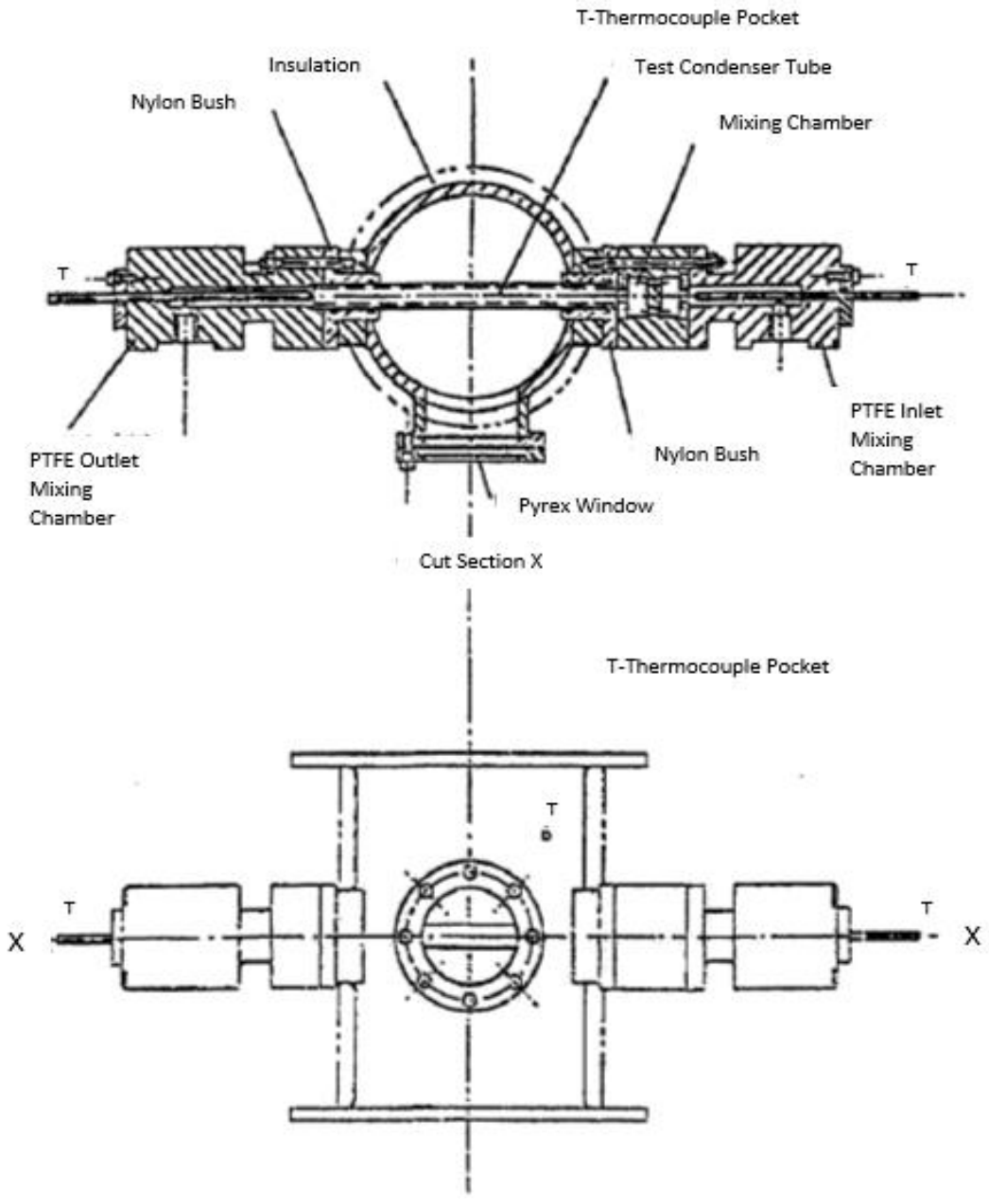

Figure 4-2: Schematic drawing of Test section reproduced from Murase et al (2007).

4.3 Test tube

Single smooth instrumented copper tube with an outer diameter of 12.7mm and inner diameter if 8.35mm was used in all the experiments. The total length of the tube was 300 mm of which 100 mm was exposed to the condensing vapour. To measure the surface temperature directly during condensation four thermocouples were embedded in the wall of the copper tube located at an interval of 90^{o} with an offset of 22.5^{o} from the vertical plane. The measuring junction of the thermocouple was placed at exactly half the length of the tube exposed to the vapours. Figure 4.3 shows the schematic of the cross-section of the copper tube with embedded thermocouples.

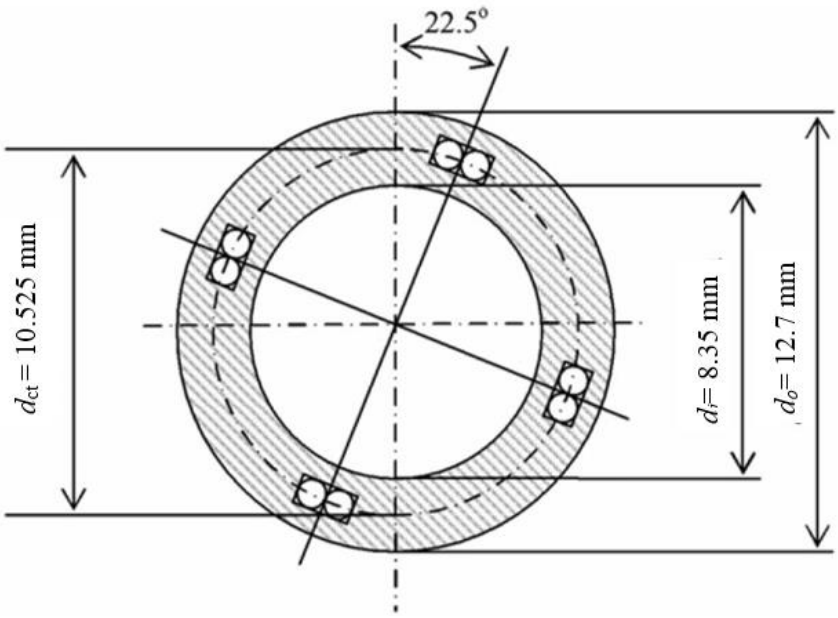

Figure 4-3: Schematic drawing of thermocouples embedded in the smooth copper test tube.

.

Instrumented tubes were manufactured in-house by the technicians. The procedure of manufacturing the instrumented tube is shown in figure 4.4. Four rectangular channels in the longitudinal direction were cut in the outer surface of the copper tube. Each channel was 2.6mm deep and 1mm wide and was equally spaced around the tube. A thermocouple was then placed in the channel ensuring the measuring junction is at the centre of the tube length. After placing the thermocouples in channel rectangular copper strips were soldered in placed and later machined on the lathe for a smooth finish. Finally, the smooth tubes were thinly copper plated by electroforming.

(a)

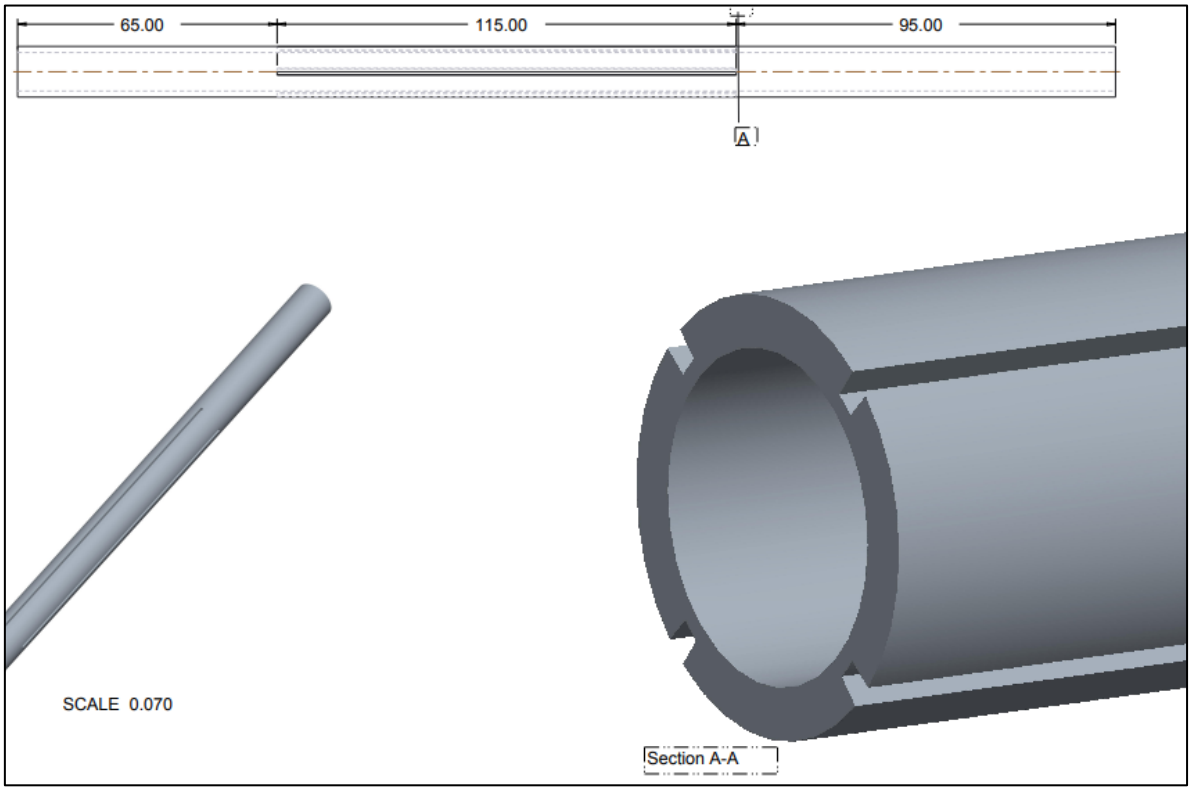

(b)

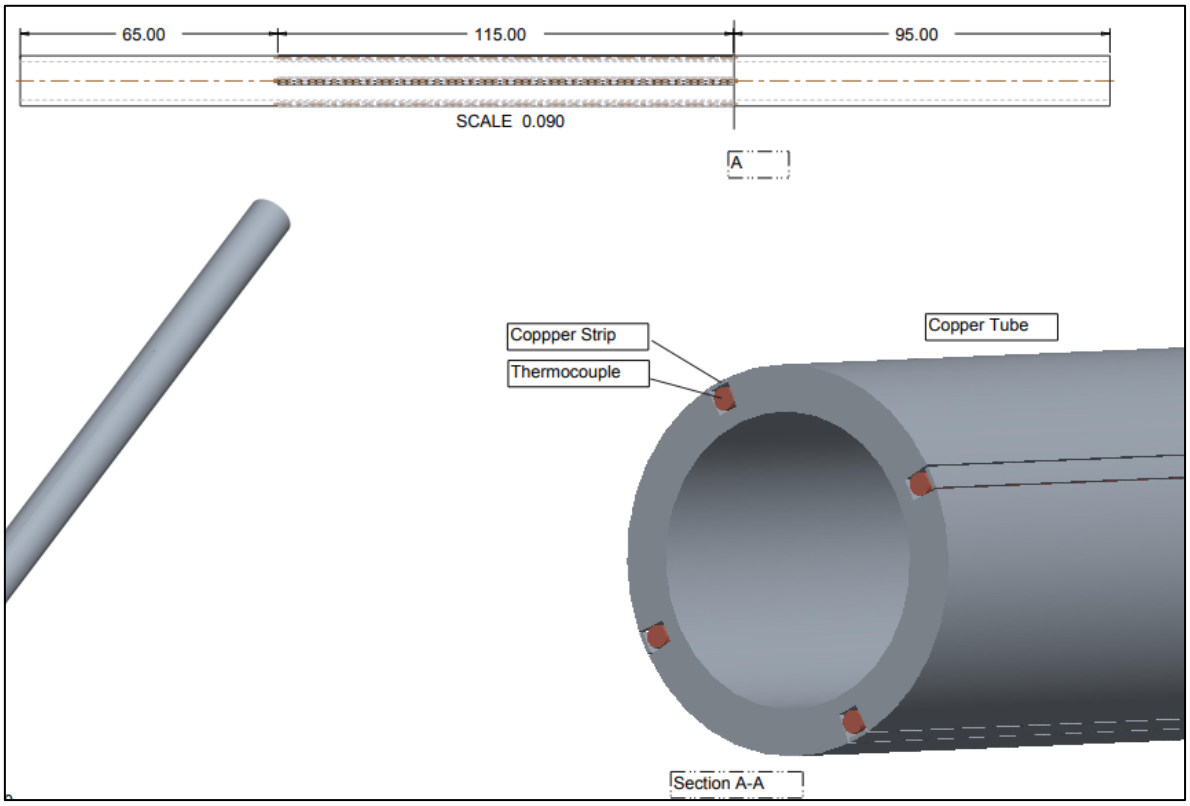

Figure 4-4 Instrumented tubes, (a) four thermocouple groves cut into longitudinal direction. (b) thermocouples embedded in the groves and covered with the copper strip.

4.4 Auxiliary condenser

Centrifugal pump was used to supply cooling water to the auxiliary condenser. All the uncondensed vapour from the test section was condensed in the auxiliary condenser and returned to the boiler. Between the auxiliary condenser and boiler, a closed thermocouple pocket was protruded to measure the temperature of returning liquid to the boiler. This pocket is marked as TC 4 in figure 4.1.

4.5 Boiler power

To calculate the input power to the boiler, the electrical resistance of each heater and the voltage drop across it was measured using a digital multi-meter. Table 4.1 shows the electric resistance of each heater.

Table 4-1: Resistances of each electric power heater used in the boiler.

Heater Number	1	2	3	4
Resistance / Ω	19	17.6	16.8	18.4

4.6 Coolant flow rate

Flow rate to the auxiliary condenser was not necessary to measure and therefore was supplied directly from the centrifugal pump installed in the building basement. The flow rate of cooling water to the test tube was measured using variable aperture, float type flow meter. It had a range of 3-30 l/min.

4.7 Temperatures

Temperature measurements were taken using K-type thermocouple for the vapour temperature in the test section, coolant inlet temperature in the mixture chamber, temperature rise across test tube and the temperature of the returning condensed liquid to the boiler.

Figure 4.5 shows the schematic of the thermocouple. One end of the thermocouple and the copper wire was soldered and placed into the cold junction of crushed and melting distilled ice mixture. While the other ends of the thermocouple wires were fused

together. A digital DC voltmeter was used to measure the thermo-emf from the thermocouples. The voltmeter has a resolution of 1μV equivalent to 0.025 K.

To accurately measure the coolant water temperature, rise a ten-junction thermopile was used. Figure 4.6 shows the arrangement of 10 inlet and 10 outlet junctions of the thermopile in a stainless-steel pipe. The stainless-steel pipe was inserted in the coolant water mixing chamber shown in figure 4.1.

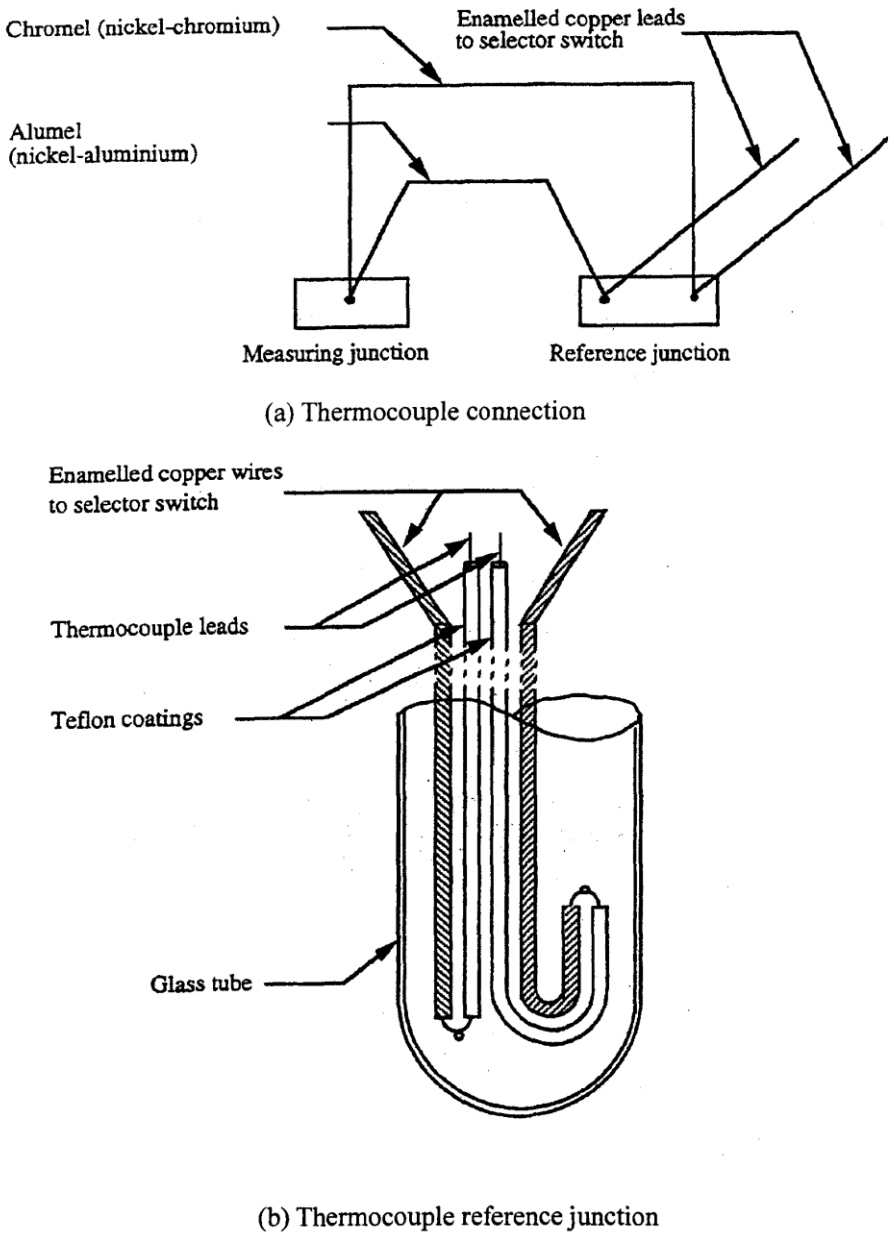

Figure 4-5: Single Junction Thermocouple, reproduced from Murase (2007). Glass tube inside diameter is 10mm and length immersed in ice is 250mm.

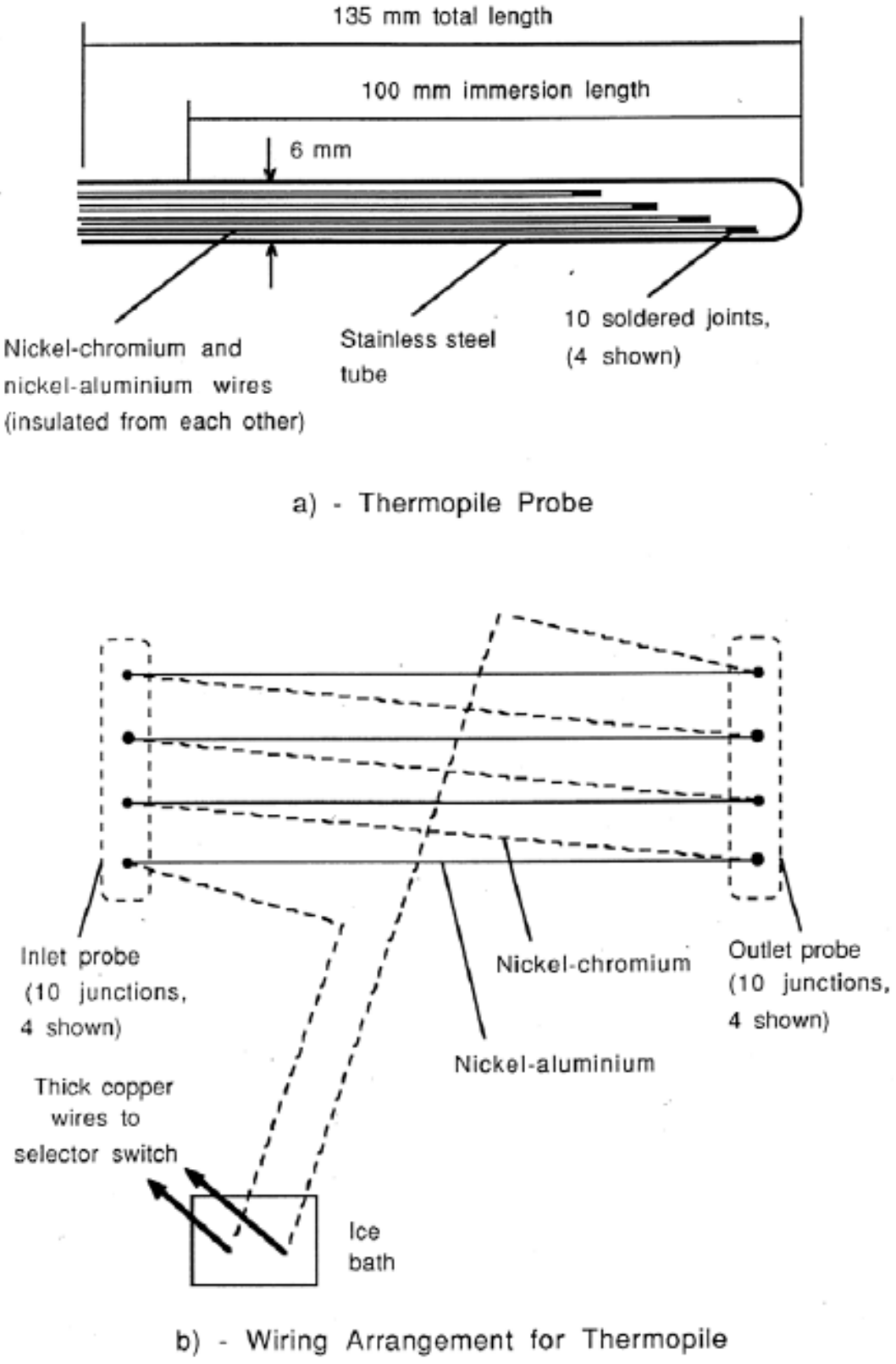

Figure 4-6: Ten-junction thermopile, reproduced from Ali. et al (2011).

4.8 Test section vapour pressure

U tube mercury and test fluid manometer were used to measure the pressure inside the test section. One end of the manometer was connected to test section while other was open to atmosphere. The manometer was fitted with a Vernier scale and precision rule to measure the fluid level in the manometer. Fortin barometer located in the laboratory was used to measure the atmospheric pressure.

4.9 Safety switches

Two safety switches are also fitted with the equipment to ensure cut down of the equipment in case of limited cooling water or excess pressure. Table 4.2 gives the details of the operating conditions of the safety switches. The warning buzzer is sounded in case of an emergency and the safety switches are triggered to disconnect the power supply to the boiler.

4.10 Experimental procedures

Before the experiments, it was ensured that inside of the rig and test tube are thoroughly clean and there are no traces of alcohol contamination due to prior use. Distilled water was filled in the boiler, condensed and then drained out several times (7 to 8 times) to remove impurities. Every run data was collected to match with Rose 1984 pure steam theory. A good agreement with the theory would indicate that the rig is pure from any contaminations. The data was repeated twice to ensure the good repeatability.

4.11 Safety procedure

Before the apparatus could run, few safety measures were taken which are as follows:

1. Always check the level of liquid in the boiler to ensure heaters are well immersed
2. Vent valve should be opened.
3. Coolant water supply should be turned on.
4. Once the coolant flow has reached steady conditions, heaters can be switched on.
5. Keep monitoring the internal pressure of the test section at regular intervals during the experiment.

4.12 Prevention of dropwise condensation in case of pure steam

Before the experiment test tubes were cleaned by immersing in coca cola for at least 5 hours. The tube was then rinsed with distilled water. The tube was then installed in the test section. This ensures film-wise condensation in case of pure steam.

4.13 Procedure for experimental test runs

After following the safety procedure apparatus was left to run for at least one hour to reach steady state conditions. This also ensures removal of air through the vent. The following set of readings were taken at several different flow rates:

1. Manometer readings for pressure calculation.
2. Thermo-emf readings for the coolant thermocouples at inlet and outlet mixing chambers.
3. Thermo-emf reading of the vapour temperature above the test section.
4. Thermo-emf reading of the condensate returning to the boiler.
5. Thermo-emf reading of the thermopile.
6. Coolant flow rate readings of the test tube.
7. Ambient temperature and pressure readings from the barometer placed in the laboratory.

The test tubes were monitored visually through the observation window in the test section. The above-mentioned steps were taken for varying flow rates in ascending order. 15 minutes were given after every change of coolant flow rate to ensure steady state conditions.

On completion of the experimental run, heaters were first turned off while cooling water was kept running for several hours to ensure proper cooldown of the system and complete cease of condensation. After the all the experiments using one fluid is completed the rig was thoroughly cleaned again by draining the mixture and filling distilled water. Pure steam results were repeated, and the rig was made ready for another fluid.

4.14 Data processing and data reduction

The chapter below describes the procedure used in data reduction for various quantities. The fluid properties were obtained using the equations listed in Appendix A.

4.14.1 Atmospheric pressure

Fortin barometer was used to measure the Atmospheric Pressure Atmospheric pressure, P_{atm} in mm Hg. The equation below is tabulated by the manufacturer for temperature correction.

$$P_{atm} = \left\{ P_B - \left[0.015 + \left(1.6229 T_B - 0.1188 \right) \times 10^{-4} \right] \right\} \tag{4.1}$$

Where T_B is the temperature reading of thermometer in °C and P_B is the pressure reading on the barometer in mm Hg.

4.14.2 Test section vapour pressure

In the test section, Vapor pressure, P_v, was calculated by means of mercury manometer, using Eq (5.2).

$$P_v = P_{atm} - g\left[\rho_{Hg}\left(H_2 - H_1 \right) + \rho_{TF}\left(H_3 - H_2 \right) \right] \tag{4.2}$$

Where ρ_{TF} and ρ_{Hg} are the densities of the test fluid and mercury and respectively. H_1, H_2 and H_3 are liquid levels in the manometer.

4.14.3 Temperature measurements

The temperature measurements were obtained using Calibrated K-type thermocouples. Details of the calibration are given in Appendix C. The calibration data were fitted by the Eq (5.3)

$$T = 273.15 + 0.025091E - 7.56632 \times 10^{-8} E^2 - 1.73740 \times 10^{-10} E^3 + 3.66 \times 10^{-14} E^4 - 2.1105 \times 10^{-18} E^5 \tag{4.3}$$

where T is the absolute temperature in K and E is the thermo-e.m.f in μV.

4.14.4 Coolant temperature rise

The ten-junction thermopile was used to measure the coolant temperature rise. A minor prearranged alteration was made because of dissipative temperature rise of coolant in the mixing chamber and tube. The equation below represents the rise in coolant temperature due to condensation of steam on the tube using thermopile.

$$\Delta T_{\mathrm{c}} = \left(\frac{\Delta E - \Delta E_{\mathrm{friction}}}{10} \right) \times \left(\frac{dT}{dE} \right)_{\mathrm{E=Em}} \tag{4.4}$$

Where ΔE is the e.m.f reading using ten-junction thermopile. $\Delta E_{\mathrm{friction}}$ is the predetermined correction for dissipative temperature rise in the absence of condensation (details are given in Appendix C) and $\left(\frac{dT}{dE}\right)_{E=E_{\mathrm{m}}}$ was obtained by differentiating Eq. (5.3) as follows.

$$\left(\frac{dT}{dE} \right)_{\mathrm{E=Em}} = 0.02563 - 4.066 \times 10^{-7} \times 2E_{\mathrm{m}} - 6.973 \times 10^{-12} \times 3E_{\mathrm{m}}{}^{2} + 1.325 \times 10^{-14} \times 4E_{\mathrm{m}}{}^{3} - 9.704 \times 10^{-19} \times 5E_{\mathrm{m}}{}^{4} \tag{4.5}$$

Mean thermo-e.m.f, E_{m}, could be calculated as follows

$$E_{\mathrm{m}} = E_{\mathrm{in}} + \frac{1}{2} \times \frac{\left(\Delta E - \Delta E_{\mathrm{friction}} \right)}{10} \tag{4.6}$$

Where, E_{in} is the thermo e.m.f reading using the thermocouple at the inlet.

4.14.5 Heat transfer rate

The heat transfer rate through the tube, Q, was calculated based on Eq. (5.7), as follows

$$Q = \rho_c V_c C_{pc} \Delta T_C \tag{4.7}$$

Where V_{c} is the volume flow rate of a flowing coolant through the tube, ρ_{c} is the density, ΔT_{c} is the coolant temperature rise and C_{pc} is the specific isobaric heat capacity of the

coolant. Reference temperature, T_{ref}, defined below was used for all thermo-physical properties.

$$T_{\mathrm{ref}} = T_{\mathrm{c,in}} + \frac{1}{2}\Delta T_{\mathrm{c}} \tag{4.8}$$

where $T_{\mathrm{c,\,in}}$ is the coolant temperature at the inlet. The heat flux, q, based on the outside diameter of the smooth tube, d, was calculated from the following equation

$$q = \frac{Q}{\pi d l} \tag{4.9}$$

where l is the active length of the tube, exposed to the vapour.

4.14.6 Vapour-to-surface temperature difference

Four thermocouples were embedded along the circumference of the tube used to measure the wall temperature of the plain tube. Throughout the tube, predetermined correction for depth of thermocouples below the condensing surface was considered with the assumption of uniform radial heat conduction. The outside surface temperature, $T_{\mathrm{wo,k}}$, was estimated by Eq. (5.11)

$$T_{\mathrm{wo,k}} = T_{\mathrm{w,k}} + \frac{Q}{2\pi k_{\mathrm{w}} l}\ln\left(\frac{d}{d_{\mathrm{t}}}\right) \tag{4.10}$$

Where d_{t} is the diameter of thermocouple location within the tube. $T_{\mathrm{w,k}}$ is a measured temperature within the tube by thermocouple respectively at the k^{th} thermocouple position. The average outer wall temperature, T_{wo}, was taken as the arithmetic average of the four local exterior wall temperatures.

$$T_{\mathrm{wo}} = \frac{T_{\mathrm{wo,i}} + T_{\mathrm{wo,\,j}} + T_{\mathrm{wo,k}} + T_{\mathrm{wo,l}}}{4} \tag{4.11}$$

The vapour-to-surface temperature difference, ΔT, is given by

$$\Delta T = T_{\mathrm{v}} - T_{\mathrm{wo}} \tag{4.12}$$

where T_{v} is the vapour temperature measured by the thermocouple located at the vapour upstream of the test section.

4.14.7 Vapour mass flow rate and velocity

Steady flow energy balance between boiler and outlet of the auxiliary condenser under the assumption of negligible potential and kinetic energy changes was used to calculate the vapour mass flow rate of a vapour approaching a smooth tube.

$$m_{\mathrm{v}} = \frac{Q_{\mathrm{B}} - Q_{\mathrm{L}}}{h_{\mathrm{fg}} + C_{\mathrm{p}}\left(T_{\mathrm{sat}} - T_{\mathrm{cr}}\right)} \tag{4.13}$$

where Q_{L} is the thermal heat loss from the well-insulated test loop (see Appendix B), Q_{B} is the electric power of the heaters to the boilers, T_{sat} is the saturation temperature, T_{cr} is the condensate temperature returning to the boiler, h_{fg} is the specific enthalpy of the vapour at a saturated temperature T_{sat} and C_{p} is the specific heat capacity of the condensate. A vapour velocity in the test-section, U_{v} at the approach to the condensing tube would be:

$$U_{\mathrm{v}} = \frac{m_{\mathrm{v}}}{\rho_{\mathrm{v}} A_{\mathrm{ts}}} \tag{4.14}$$

Where A_{ts} is the cross-sectional area of the test section and ρ_{v} is the density of an upstream vapour.

4.14.8 Ethanol vapour concentration

Equations 4.15 and 4.16 can be used to obtain an equilibrium ethanol mass fraction of liquid, C_{L}, and an equilibrium ethanol mass fraction of vapour, C_{v}.

$$C_{\mathrm{v}} = \frac{M_{\mathrm{e}} y_{\mathrm{e}}}{(M_{\mathrm{e}} - M_{\mathrm{w}}) y_{\mathrm{e}} + M_{\mathrm{w}}} \tag{4.15}$$

$$C_{\mathrm{L}} = \frac{M_{\mathrm{e}} x_{\mathrm{e}}}{(M_{\mathrm{e}} - M_{\mathrm{w}}) x_{\mathrm{e}} + M_{\mathrm{w}}} \tag{4.16}$$

Where M_{w} and M_{e} are the molar masses of water and ethanol respectively. Equilibrium mole fraction of liquid, x_{e} and vapour, y_{e} can be determined using Raoult's law, as given in equations 4.15 to 4.21.

$$y_{\mathrm{e}} = \frac{x_{\mathrm{e}} \gamma_{\mathrm{e}} P_{\mathrm{e}}}{P_{\mathrm{V}}} \tag{4.17}$$

$$P_v = x_e \gamma_e P_e + x_w \gamma_w P_w \tag{4.18}$$

Equation (4.18) can be re-written as follows

$$x_e = \frac{P_V}{P_e \gamma_e + \left(\frac{P_w \gamma_w}{\alpha} \right)} \tag{4.19}$$

where

$$x_e = 1 - x_w \tag{4.20}$$

$$\alpha = \frac{x_e}{x_w} \tag{4.21}$$

Activity coefficients (γ_e and γ_w) are dependent on the type of liquid and composition. These can be calculated from equations proposed by Fujii et al. (1983), originally proposed by Kogan et al. (1974). Starting values of x_w and x_e were given in Eq. (4.17) and Eq. (4.18), which are assumed as initial liquid water and ethanol concentration at room temperature.

$$RT_v \ln\gamma_e = 2187.6x_w^2 - 2407.2x_w^3 + 5398.7x_w^4 \tag{4.22}$$

$$RT_v \ln\gamma_w = 9374.3x_e^2 - 11989.4x_e^3 + 5398.7x_e^4 \tag{4.23}$$

R is molar ideal gas constant and T_v is the measured vapour temperature of the mixture. Resulting values of γ_e and γ_w are substituted back into Eq. (4.19) and iteration continued until successive values of x_e and x_w agreed to within 0.001%. Equation 4.24 can be used to calculate the saturation pressure for each of the ethanol and water-ethanol can be using the measured vapour temperature of the mixture. (Pooling et al. (2001)) as follow:

$$\ln P = A - \frac{B}{T_v - C} \tag{4.24}$$

For ethanol: A = 16.8958, B = 3795.17, C = 42.23

For water: A = 16.3872, B = 3885.70, C = 42.98

Range of ethanol liquid and vapour concentration at equilibrium are listed in Tables 4.2 at pressures of 101 by taking into account the uncertainty in measurements of temperature ($\pm$ 0.1 K) and pressure ($\pm$ 100 Pa).

Table 4-2 Ethanol initial liquid, equilibrium vapour concentrations at P_v = 101 kPa

C_{iL} / %	C_v / %
0.025	1.1 ± 1.0
0.05	1.4 ± 1.0
0.1	1.6 ± 1.2
0.5	6.4 ± 1.2
1.0	10.7 ± 1.1

4.15 Uncertainty analysis

It was not possible to reproduce the exact same conditions of vapour velocity, coolant flow rate and pressure for the present experiments. Method of Kline and McClintock (1953) suggested that statistical methods of calculating variance cannot be applied to a single set of experiments. Hence, they recommended the following method of estimating uncertainties for a single set of experiments.

The uncertainty, δ_x, in a variable is expressed in terms of the best estimate of the variable x and measured experimental value x_{meas}.

$$x = x_{meas} \pm \delta_x \tag{4.25}$$

The final result of the experiment, x_R, will depend on several measured quantities each having a different uncertainty level as shown in Eq. (4.26)

$$x_R = F(x_1, x_2 \ldots\ldots\ldots x_n) \tag{4.26}$$

The following equation was proposed by Kline and McClintock (1953) for calculating the resulting uncertainty level, δx_R, in the dependent variable

$$\delta x_R = \left[\left(\frac{\partial F}{\partial x_1} \delta x_1 \right)^2 + \left(\frac{\partial F}{\partial x_2} \delta x_2 \right)^2 + \ldots\ldots\ldots + \left(\frac{\partial F}{\partial x_n} \delta x_n \right)^2 \right]^{1/2} \tag{4.27}$$

Equation (5.27) can be dimensionless to give

$$\frac{\delta x_{\mathrm{R}}}{x_{\mathrm{R}}} = \left[(X_1 \delta x_1)^2 + (X_2 \delta x_2)^2 + ... + (X_{\mathrm{n}} \delta x_{\mathrm{n}})^2 \right] \tag{4.28}$$

$$X_{\mathrm{n}} = \frac{\left(\frac{\partial F}{\partial x_{\mathrm{n}}} \right)}{x_{\mathrm{R}}} \tag{4.29}$$

Where the fractional uncertainty level x_{R} is known as $\frac{\delta x_{\mathrm{R}}}{x_{\mathrm{R}}}$.

In the current study, the uncertainty analysis was performed for significant factors such as test section vapour velocity, U_{V}, test section vapour pressure, P_{∞}, vapour-to-surface temperature difference, ΔT and heat flux, q, outside of the test tube.

4.15.1 Test section vapour pressure

The pressure in test section was calculated as

$$P_{\mathrm{V}} = P_{\mathrm{atm}} + g(H1 - H2)\rho_{\mathrm{Hg}} + g(H3 - H2)\rho_{\mathrm{TF}} \tag{4.30}$$

Where Fortin barometer was used for measuring P_{atm} due to temperature correction is given by Eq. (4.1). Memory (1989) proposed that uncertainties in temperature correction and measurement of ambient temperature, T_{A} is insignificant, hence uncertainty in test section pressure is dependent on manometer levels (H_1, H_2, H_3) and barometric pressure, P_{B}, reading.

$$\frac{\delta P_{\mathrm{v}}}{P_{\mathrm{v}}} = \left[\left(X_{\mathrm{P_B}} \delta x_{\mathrm{P_B}} \right)^2 + \left(X_{\mathrm{H_1}} \delta x_{\mathrm{H_1}} \right)^2 + \left(X_{\mathrm{H_2}} \delta x_{\mathrm{H_2}} \right)^2 + \left(X_{\mathrm{H_3}} \delta x_{\mathrm{H_3}} \right)^2 \right] \tag{4.31}$$

Differentiating Eq. (4.31) with respect to the barometric pressure reading, gives the following expression

$$X_{\mathrm{P_B}} = \frac{\left(\frac{\partial P_{\mathrm{v}}}{\partial P_{\mathrm{B}}} \right)}{P_{\mathrm{v}}} \tag{4.32}$$

$$X_{\mathrm{P_B}} = \frac{1}{P_{\mathrm{v}}} \tag{4.33}$$

Differentiating Eq. (4.31) with respect to the manometer levels (H_1, H_2, H_3), giving the following expressions

$$X_{\mathrm{H}_1} = \frac{g\rho_{\mathrm{Hg}}}{P_{\mathrm{v}}} \tag{4.34}$$

$$X_{\mathrm{H}_2} = \frac{g\left(\rho_{\mathrm{TF}} - \rho_{\mathrm{Hg}}\right)\rho_{\mathrm{Hg}}}{P_{\mathrm{v}}} \tag{4.35}$$

$$X_{\mathrm{H}_3} = -\frac{g\rho_{\mathrm{TF}}}{P_{\mathrm{v}}} \tag{4.36}$$

The uncertainty level in barometric pressure reading, δx_{PB}, is estimated to be $\pm$0.2 mmHg and the uncertainty in the values of manometer level readings, $\delta x_{\mathrm{H}_1}, \delta x_{\mathrm{H}_2}, \delta x_{\mathrm{H}_3}$, are estimated to be $\pm$0.0005 m.

4.15.2 Test section vapour velocity

Test section vapour velocity was calculated from Eq. (4.14) and can be modified as follows

$$U_{\mathrm{V}} = \frac{RT_{\mathrm{sat}}(P_{\mathrm{V}})m_{\mathrm{V}}}{\left(\frac{\pi d_{\mathrm{ts}}}{4}\right)P_{\mathrm{V}}} \tag{4.37}$$

Therefore, within the test section vapour velocity, overall fractional uncertainty level due to the fractional uncertainty levels within each of the test-section, vapour pressure, vapour mass flow-rate and diameter (shown in the above Eq. (4.37)) can be expressed as follows

$$\frac{\delta U_{\mathrm{v}}}{U_{\mathrm{v}}} = \left[(X_{P\mathrm{v}}\delta x_{\mathrm{P\,v}})^2 + (X_{\mathrm{dts}}\delta x_{\mathrm{dts}})^2 + (X_{\mathrm{m_v}}\delta x_{\mathrm{m_v}})^2\right] \tag{4.38}$$

Differentiating Eq. (4.38) with respect to the vapour pressure would give as follow

$$X_{P\mathrm{v}} = \frac{1}{T_{\mathrm{sat}}(P_{\mathrm{v}})}\frac{\partial T_{\mathrm{sat}}}{\partial P_{\mathrm{v}}} - \frac{1}{P_{\mathrm{v}}} \tag{4.39}$$

where $\frac{\partial T_{sat}}{\partial P_{\infty}}$ can approximated from equations in Appendix A. Differentiating Eq (4.38) with respect to test-section diameter, as well as vapour mass flow-rate to give the following equations

$$X_{\mathrm{dts}} = -\frac{2}{d_{\mathrm{ts}}} \tag{4.40}$$

$$X_{\mathrm{mv}} = \frac{1}{m_{\mathrm{v}}} \tag{4.41}$$

The uncertainty in d_{ts} was estimated from manufacturing tolerances i.e $\pm$0.0005 m and the uncertainty level in P_v can be calculated from Eq. (4.31). Vapour mass flow rate m_v was calculated from the Eq. (4.14). Lee (1982) suggested 1.5% uncertainty in the mass flow rate of vapour. The vapour mass flow rate was calculated from Eq. (4.13) and was compared at the exit of the auxiliary condenser with actual mass of condensate.

4.15.3 Heat flux

Equation 4.10 was used to calculate heat flux to the condensing tube and can be written as follow

$$q = \frac{m_c C_{\mathrm{pc}} \Delta T_{\mathrm{c}}}{\pi d l} \tag{4.42}$$

According to Memory (1989), uncertainty in C_{pc} due to uncertainty in measuring coolant temperature was negligible therefore causing the fractional error within heat flux in Eq. (4.42). This is represented below as

$$\frac{\delta q}{q} = \left[(X_{\mathrm{mc}} \delta x_{\mathrm{mc}})^2 + (X_{\Delta \mathrm{Tc}} \delta x_{\Delta \mathrm{Tc}})^2 + (X_{\mathrm{d}} \delta x_{\mathrm{d}})^2 + (X_{\mathrm{l}} \delta x_{\mathrm{l}})^2 \right] \tag{4.43}$$

where

$$X_{\mathrm{mc}} = \frac{1}{m_{\mathrm{c}}} \tag{4.44}$$

$$X_{\Delta \mathrm{T_c}} = \frac{1}{\Delta T_{\mathrm{c}}} \tag{4.45}$$

$$X_{\mathrm{d}} = -\frac{1}{d} \tag{4.46}$$

$$X_{\mathrm{l}} = -\frac{1}{l} \tag{4.47}$$

The uncertainty level in the coolant mass flow rate was $\pm$0.5 l/min. To ensure high accuracy, A 10-junction thermopile was used to measure coolant temperature with the uncertainty of $\pm$0.005K. The uncertainty in the tube dimensions (estimated from manufacturing tolerances) were, X_{l}= $\pm$0.0005m, X_{d}= $\pm$0.0001m.

4.15.4 Vapour-to-surface temperature difference

From Eq. (4.12), the Vapour-to-surface temperature difference was calculated as follows

$$\Delta T = T_{\mathrm{sat}}\left(P_{\infty}\right) - T_{\mathrm{wo}} \tag{4.48}$$

The fractional uncertainty in vapour-to-surface temperature can be calculated as follows

$$\frac{\delta \Delta T}{\Delta T} = \left[\left(X_{\mathrm{P}\infty}\delta x_{\mathrm{P}\infty}\right)^2 + \sum_{K=1}^{4} \left(X_{\mathrm{Ttc}}\delta x_{\mathrm{Ttc}}\right)^2 \right]^{1/2} \tag{4.49}$$

$$X_{\mathrm{P}\infty} = \frac{\left(\frac{\partial \Delta T}{\partial P_{\infty}}\right)}{\Delta T} = \frac{\left(\frac{\partial T_{\mathrm{sat}}}{\partial P_{\infty}}\right)}{\Delta T} \tag{4.50}$$

$$X_{\mathrm{T\,tc}} = -\frac{1}{4\Delta T} \tag{4.51}$$

where $\frac{\partial T_{\mathrm{sat}}}{\partial P_{\infty}}$ can be calculated from equations in Appendix A. Uncertainty in tube wall thermocouple readings was estimated to be $\pm$0.5 K and the uncertainty level in P_{∞} can be calculated from Eq. (4.31).

Chapter 5

5 Marangoni condensation of steam-ethanol mixtures on a horizontal smooth tube and comparison with earlier experimental data

5.1 Introduction

Experiments were conducted to measure condensation heat transfer of pure-steam and steam-ethanol mixtures over a horizontal smooth tube to validate the apparatus and experimental procedure. Later, the data of lower concentrations at lower velocities which were never conducted before for steam-ethanol mixtures were added. This data is important as it will help in understanding the transition region of Marangoni condensation of steam-ethanol mixtures. Since data collected by Ali et al (2012) at lower concentrations has fewer points in the transition region. It will also help in developing an empirical model of Marangoni condensation for steam-ethanol mixtures.

A smooth copper tube having an outer diameter of 12.75 mm and the inner diameter of 8.65 mm was used for all the experiments. Active heat transfer length was 100 mm with four thermocouples embedded in the outer surface of the tube. Test section pressure was 101 kPa measured using the U-tube manometer. Special care was taken to minimise the errors due to uncondensable gases such as air in the test section. Vapour velocity ranged from 0.2 m/s to 0.75 m/s and was limited by the boiler's maximum electrical power. The coolant flow rate ranged from 3 to 32 l/min and was increased in steps of 1 l/min. At each flow rate four embedded thermocouple temperatures, inlet and outlet coolant temperatures, coolant temperature rise, condensate return temperature and test section gauge pressure were recorded. At several steps, pictures of the condensate film were also recorded for visual observations.

For the comparison purposes, the mass fractions chosen were the same as chosen by Murase et al (2007) and Ali et al (2012) in their experimental work. Mass Fraction of ethanol (initial liquid mass fraction (C_{iL}) of ethanol prepared at room temperature) were 0.001%, 0.005%, 0.01%, 0.025%, 0.05%, 0.1%, 0.5% and 1.0%. For each ethanol mass fraction, the vapour velocity at the approach to condenser tube was varied by adjusting

the boiler power to give 0.2, 0.35, 0.46, and 0.56 m/s. The vapour velocity of 0.75 m/s and 0.78 m/s was also used, former for the first four concentrations and latter for the last four concentrations corresponding to Hassan's and Murase's data. The coolant inlet temperature was always between 24°C to 26 °C. Hassan's data include all the above-mentioned concentrations at velocities above 0.75 m/s. However, Murase's data includes concentration from 0.05% – 1% at velocities lower than 0.75m/s. Therefore, data with lower concentrations of 0.001% to 0.025% at velocities lower than 0.75 m/s is still not known. This chapter aims to collect this missing data and in doing so will also validate the experimental apparatus by reproducing the previous results.

5.2 Pure steam results

Figure 6.1 shows the pure-steam condensation data with heat flux and heat transfer coefficient plotted against vapour-to-surface temperature difference. The data was collected for three different velocities of 0.2, 0.46 and 0.69 m/s. The results are compared with Rose (1984) pure steam theoretical model and seem to be in good agreement. Rose (1984) pure steam theoretical model is represented by equation 5.1.

$$q_{Ro} = 0.728\left[\frac{0.9 + 0.728F^{1/2}}{\left(1 + 3.44F^{1/2} + F\right)^{1/4}}\right]\left(\frac{k\Delta T}{d}\right)Re_{tp}{}^{1/2} \tag{5.1}$$

(Rose (1984))

Figure 5.2 shows a comparison of the dimensionless plot of pure-steam experimental results and Rose (1984) equation 2.7. The results are again in good agreement. Equation 2.7 is written below as equation 5.2.

$$\frac{Nu}{Re_{tp}^{-1/2}} = \frac{0.9 + 0.728F^{1/2}}{\left(1 + 3.44F^{1/2} + F\right)^{1/4}} \tag{5.2}$$

(Rose (1984))

Where Re_{tp} is a two-phase Reynold Number represented by equation (2.4) and F is a dimensionless number represented by equation (2.6).

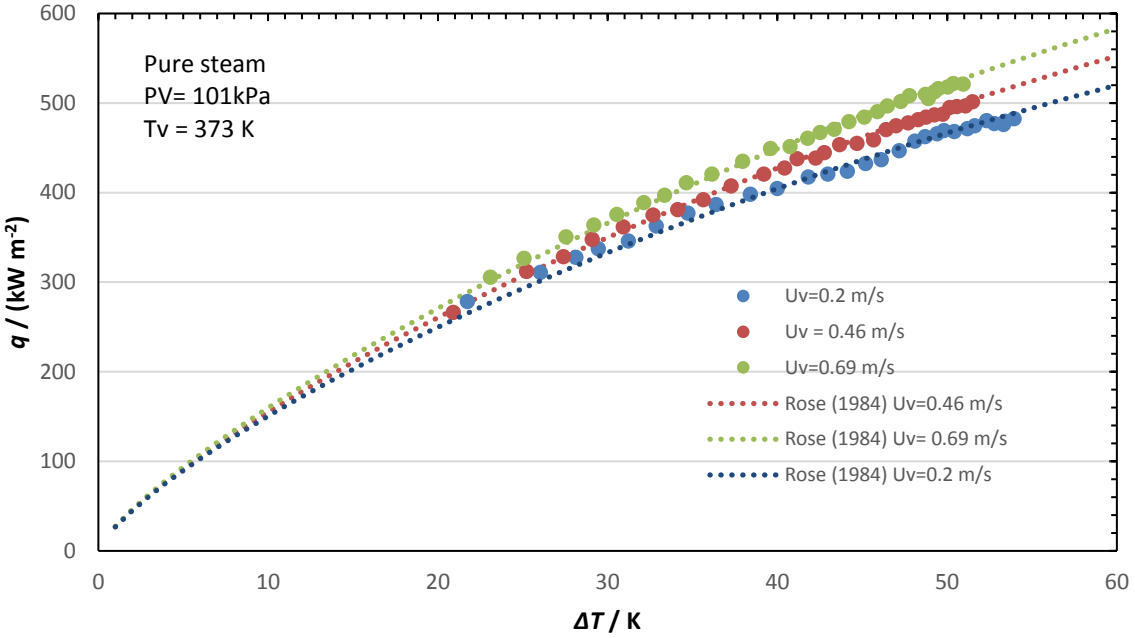

Figure 5-1:Comparison of pure steam data with Rose (1984) equation for three different velocities (U_v = 0.2, 0.46 and 0.69 m/s) at atmospheric pressure of 101 kPa.

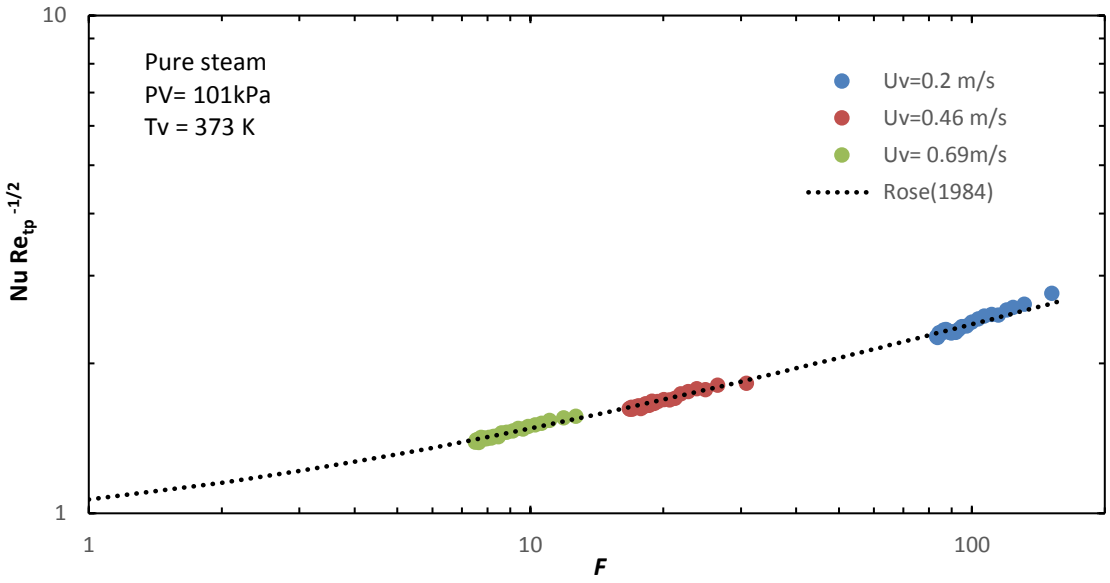

Figure 5-2: Comparison of dimensionless plot with Rose (1984) equation 6.2 for three different velocities (U_v = 0.2, 0.46 and 0.69 m/s) at atmospheric pressure of 101 kPa.

5.3 Steam-ethanol results and discussion

The results of steam-ethanol mixtures are shown in figures 5.3 and 5.4 with heat flux and heat-transfer coefficient plotted against vapour-to-surface temperature difference for different vapour velocities at each ethanol mass fraction (C_{iL}). The solid black line represents the Nusselt (1969) equation for pure steam given by equation (2.1). Whereas, the results predicted by Rose (1984) equation (5.1) is presented in dotted line for the varying vapour velocities respectively. For comparison, previous steam-ethanol experimental data of Hassan et al (2012) and Murase et al (2007) are also plotted. Present data are plotted by closed points and previous data by open points.

The main focus of this chapter was to investigate heat flux and heat-transfer coefficients at the lower concentrations of ethanol. Data at higher concentrations were reproduced for validation purpose. Figures 5.3 (a)-(d) and 5.4 (a)-(d) compares the present data with previous work of Hassan et al. (2012) and figure 5.3 (e)-(h) and 5.4 (e)-(h) compares the present data with the previous work of Murase et al. (2007). All the graphs show good agreement with the previous results and thus provide confidence in the new data collected.

The key finding of this chapter was the identification of the transition phase of condensation mode through visual observations and plotting their corresponding data points on the heat flux against vapour-to-surface temperature difference graph. This transition was clearly observed at lower mass fractions of ethanol except for C_{iL}=0.001%. For the C_{iL}=0.001%, visual observation shows the film-wise mode of condensation dominating the entire tube surface throughout vapour-to-surface temperature difference. Therefore, the heat fluxes and heat-transfer coefficients were almost equal to Rose (1984) equation (see figures 5.3 (a) and 5.4 (a)).

For the concentrations of 0.005%, 0.01% and 0.025% transition from pseudo dropwise to film-wise was clearly visible through visual observations and experimental data. Figures 5.4(b) to (d) showed that the heat transfer coefficient has the maximum value at low vapour-to-surface temperature difference and visual observation showed the pseudo-dropwise appearance of condensate. With the increase in vapour-to-surface temperature difference the heat -transfer coefficient decreases, and the transition from the pseudo-dropwise to film-wise mode was observed. During the transition, the corresponding heat

flux values decrease. These points are marked in orange circles on the heat flux against vapour-to-surface temperature difference graph (see figure 5.3 (b)-(d)). Finally, at higher vapour-to-surface temperature difference complete film-wise mode was observed and the heat transfer coefficient comes close to theoretical Rose (1984) equation (dotted lines). When condensation mode would change from the transition region to filmwise region, a sudden jump in vapour-to-surface temperature difference was observed. These data points assume the start of complete film-wise appearance and are shown in figure 5.3 (b)-(d) in blue circles. The points marked in red circles are assumed to be the start of the transition region. It is necessary to point out here that the transition region may have begun before these points (marked in red circles) and was only visible to the naked eye once the flow rate was sufficiently increased.

However, for the higher concentrations of 0.05%, 0.1%, 0.5% and 1% heat transfer coefficient is relatively low at low vapour-to-surface temperature difference and starts to increase significantly as vapour-to-surface temperature difference increases (figure 5.3 (e) to (h)). Visual observation at this point shows the transition of wavy film-wise to the pseudo-dropwise appearance of condensate. This was only observed for high vapour velocities of 0.35, 0.46, 0.56 and 0.75m/s. Heat-transfer coefficient value reaches a maximum and then starts decreasing as the condensation mode changed to steadier pseudo-dropwise mode. These trends are the results of the combined effect of a change in condensate mode in the liquid phase and the diffusion resistance in the vapour phase and are in agreement with Murase et al (2007) observations.

For the vapour velocity of 0.2 m/s, the decreasing trend of heat transfer coefficient was observed throughout vapour-to-surface temperature difference for all ethanol concentrations (see figure 5.6 (e)). Visual observation confirms that at lower vapour-to-surface temperature difference wavy film condensate was observed and at higher vapour-to-surface temperature difference smooth film condensate was observed. In case of this low vapour velocity, heat-transfer coefficient curves either converges with the Rose (1984) equation with an increase in the vapour to surface temperature difference or dropped below. This may be due to the insufficient amount of vapour supply to the test tube. More than 50% of vapour supplied from the boiler is already condensed on the test tube in the convergence region and vapour velocity just after the test tube was calculated to be less than 0.1 m/s. Due to the very small vapour velocity and the possibility of air

accumulation and higher vapour-phase diffusion layer below the test tube, heat-transfer values are adversely affected. This behaviour is not seen for the higher vapour velocities.

it is evident from the graphs (figures 5.3 (a) to (h) and 5.4 (a) to (h)) that for all the ethanol mass fractions the vapour velocity has a significant influence on the heat transfer. Increase in vapour velocity increases both heat flux and heat transfer coefficient for the given mass concentration and vapour-to-surface temperature difference.

Optimisation of mass concentration was the second important goal of this investigation. For this purpose, figures 5.5 and 5.6 were plotted with heat-transfer coefficient against vapour-to-surface temperature difference for varying mass fractions at each vapour velocity. It is observed from figures 5.6 (a) to (h) that for a given vapour velocity, increase in mass concentration decreases the heat-transfer coefficients at low vapour-to-surface temperature difference. This is attributed to the diffusion resistance in the vapour phase which increases as mass concentration increases. The effect of diffusion resistance is clearly visible at concentrations of 0.5% and 1% in figures 5.5 (a) to (e) and 5.6 (a) to (e). Figure 5.7 explains in detail the effect of diffusion on heat flux and heat-transfer coefficient in the context of phase equilibrium diagram. According to phase equilibrium diagram (figure 5.7 (b)), during condensation of binary vapour mixture, less volatile component (water) condenses more than the volatile component (ethanol). Thus, the concentration of the volatile component increases in the vapour phase at the liquid-vapour interface given that the sum of mass concentration is kept constant in the vapour boundary layer. This phenomenon is accelerated by the constant supply of mass concentration from bulk to vapour-liquid interphase. On the other hand, convective mass transfer takes place to ensure the mass concentration at vapour-liquid interface approaches that in the bulk. These two mechanisms balance out to make the steady distribution of mass concentrations as shown in figure 5.7 (a). Simultaneously, the vapour temperature decreases from bulk to interface and thus the heat transfer rate and condensation rate (Fujii, 1991).

Figure 5.5a and 5.6a shows that at vapour velocity of 0.75 m/s, the optimum concentration (C_{iL}) is 0.01% and 0.025% with the highest heat transfer coefficient values of 112 kW/m^{2}K and 95 kW/m^{2}K at ΔT= 3.43 K and 4.7 K respectively. However, at the same velocity highest heat flux of 102 kW/m^2 was obtained at C_{iL}= 0.5%. The corresponding vapour-to-surface temperature difference (ΔT) was 23.8 K.

(a)

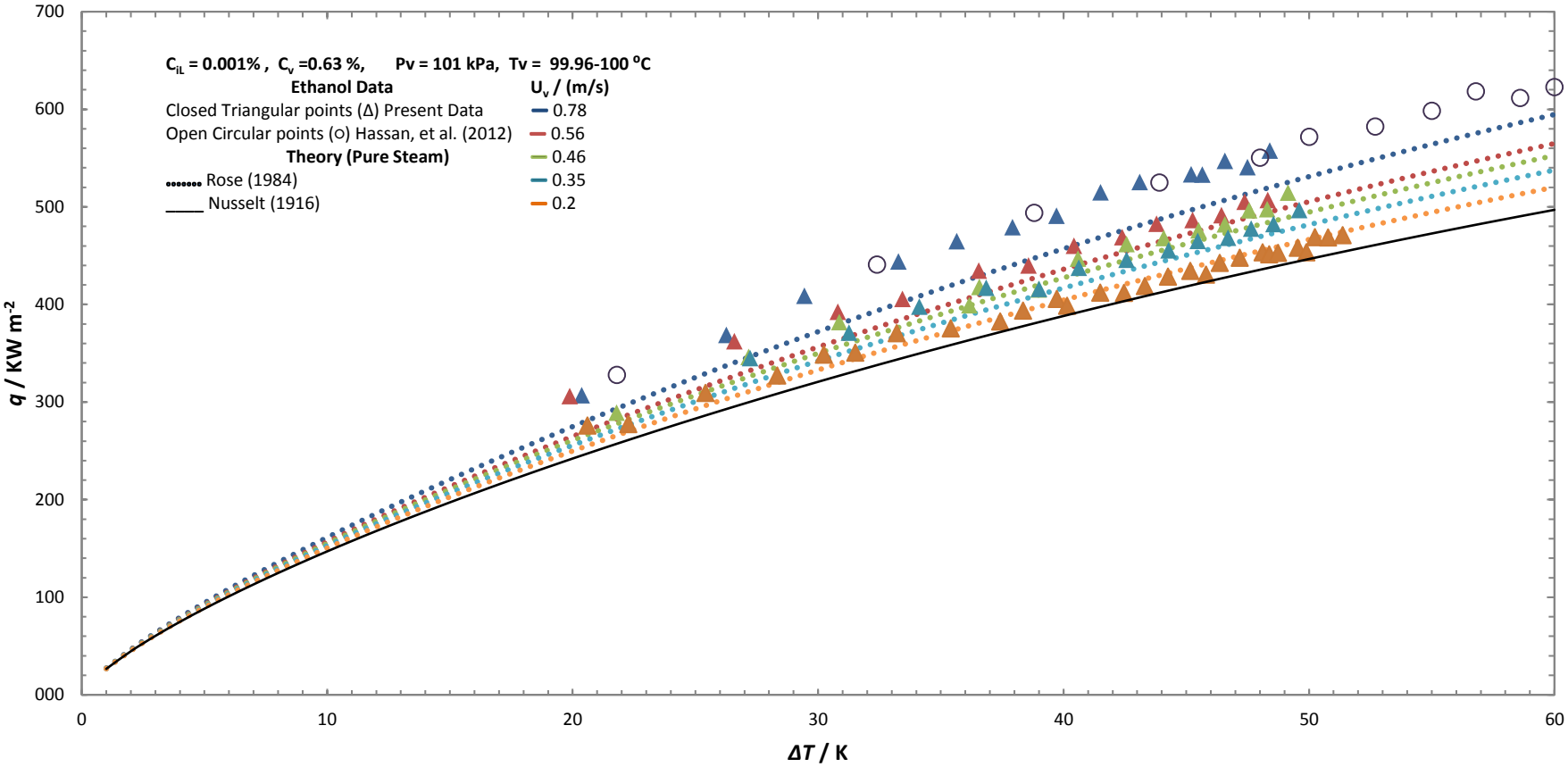

Figure 5-3: (a)-(g) shows variation of heat flux against vapour-to-surface temperature difference for varying vapour velocities at each ethanol mass concentration. (a) C_{iL} = 0.001%, (b) C_{iL} = 0.005%, (c) C_{iL} = 0.01%, (d) C_{iL} = 0.025%, (e) C_{iL} = 0.05%, (f) C_{iL} = 0.1%, (g) C_{iL} = 0.5%, (h) C_{iL} = 1%. Present data is presented with closed points and previous experimental data with open points. Test section vapour pressure is approx. 101 kPa.

(b)

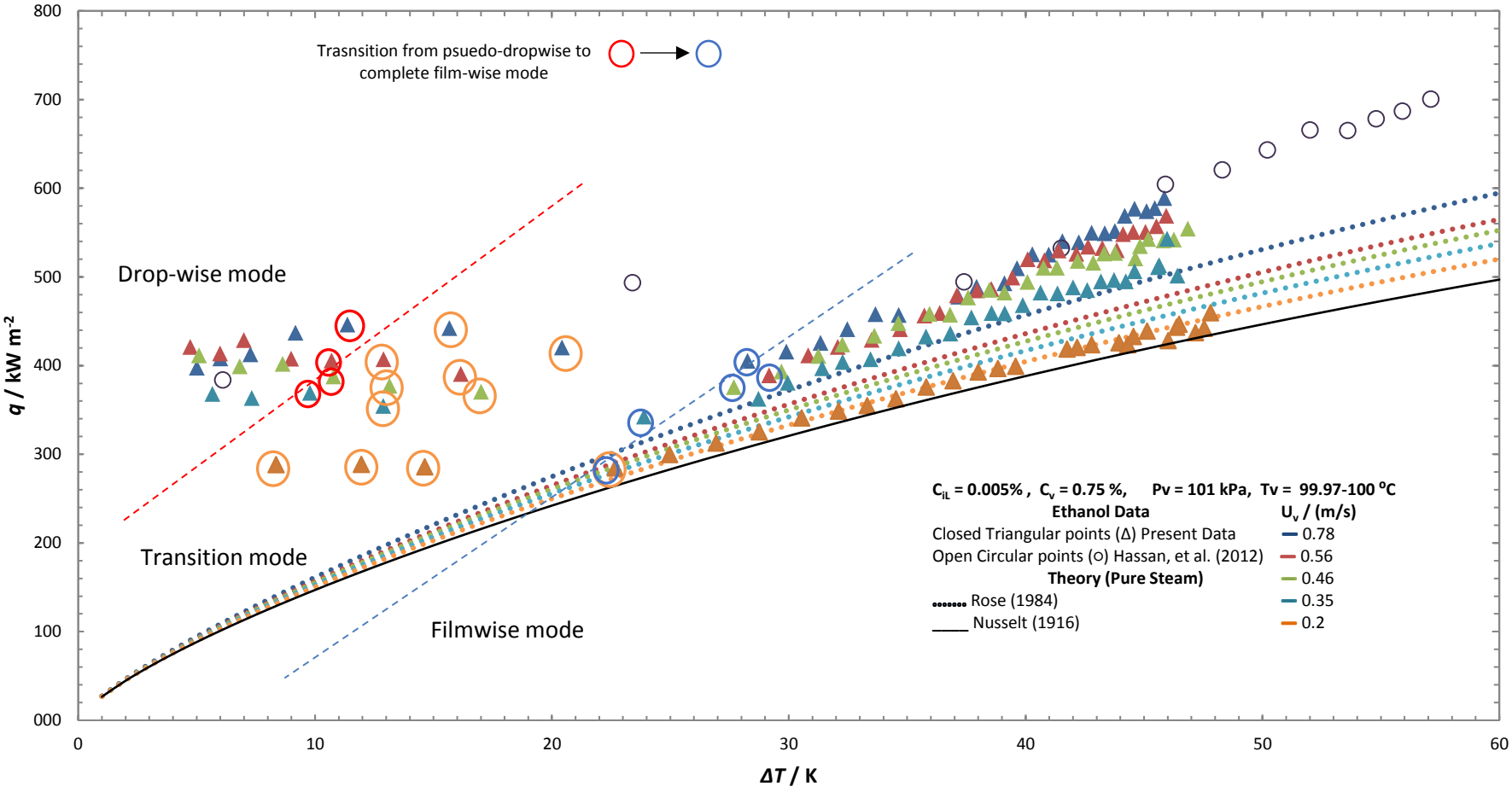

Figure 5.3 (Continued).

(c)

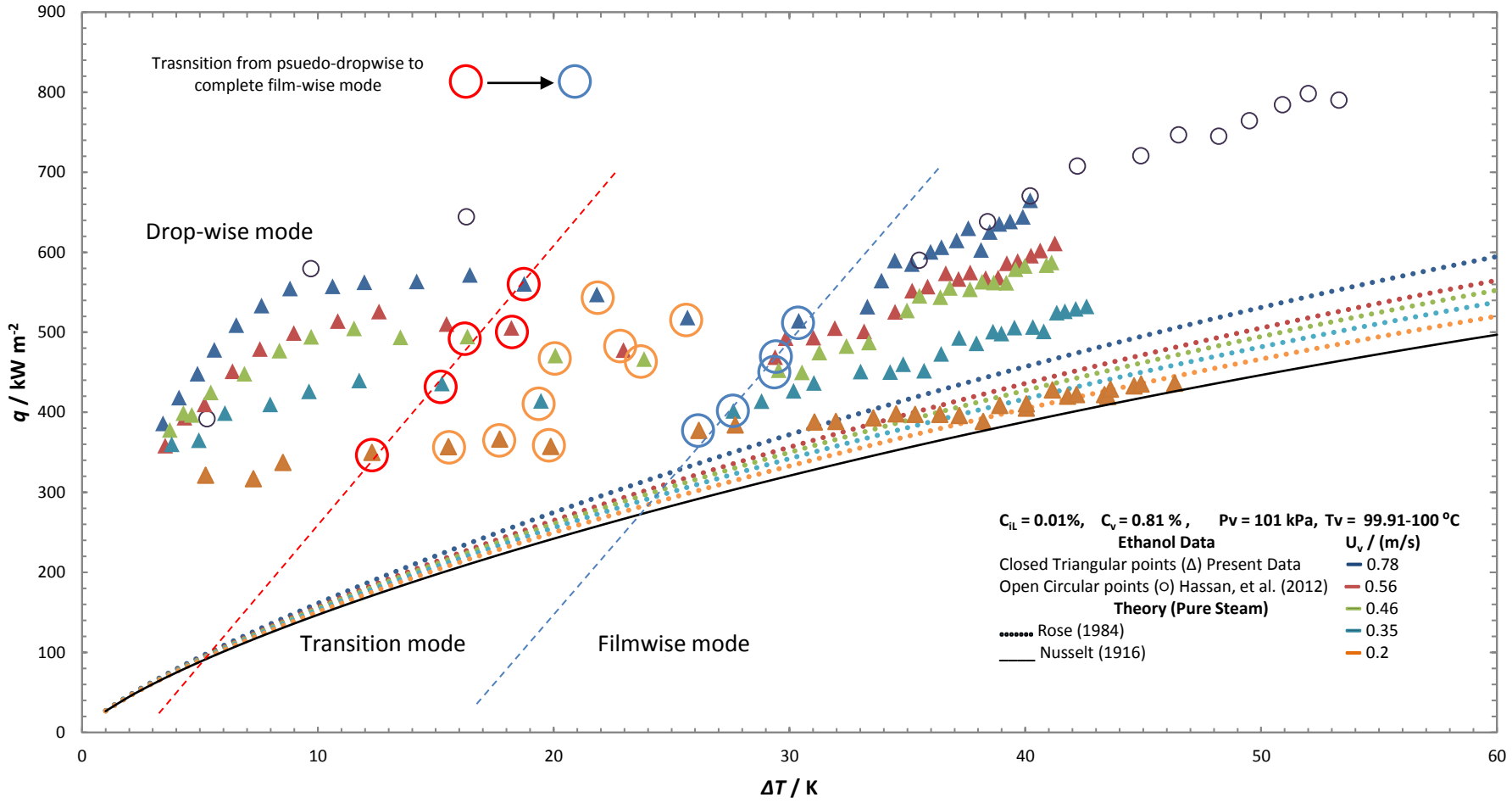

Figure 5.3 (Continued).

(d)

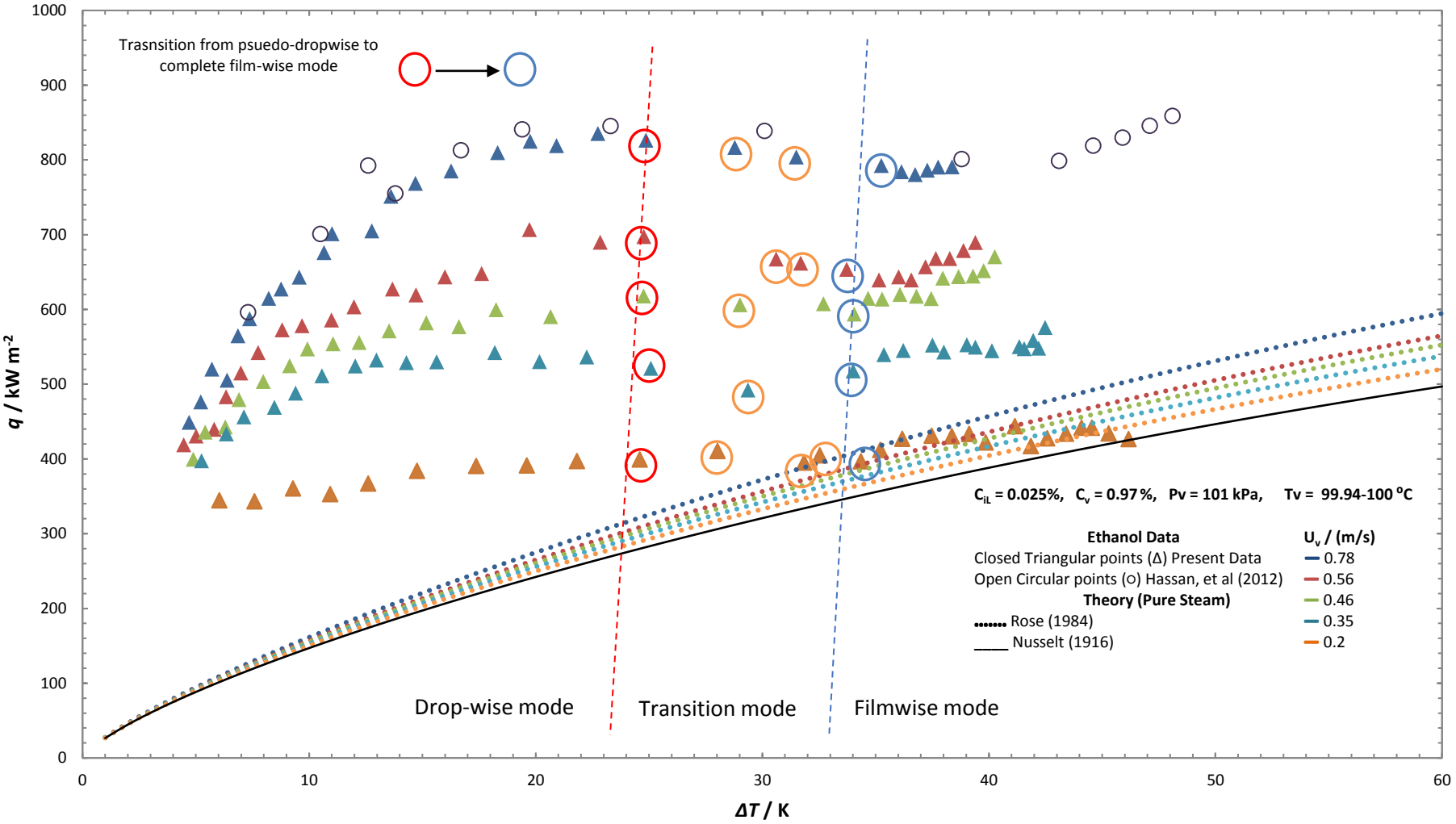

Figure 5.3 (Continued).

(e)

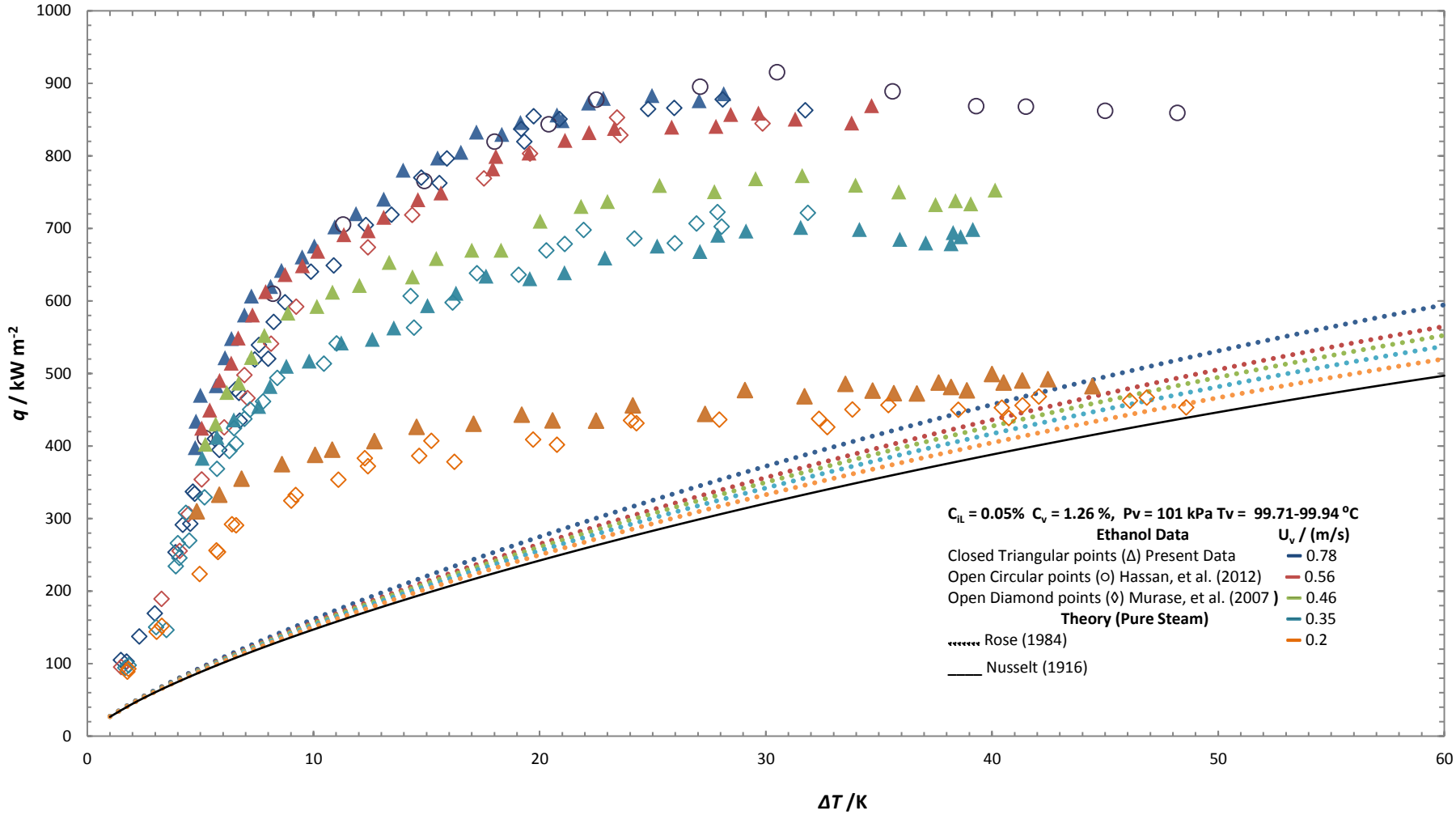

Figure 5.3 (Continued).

(f)

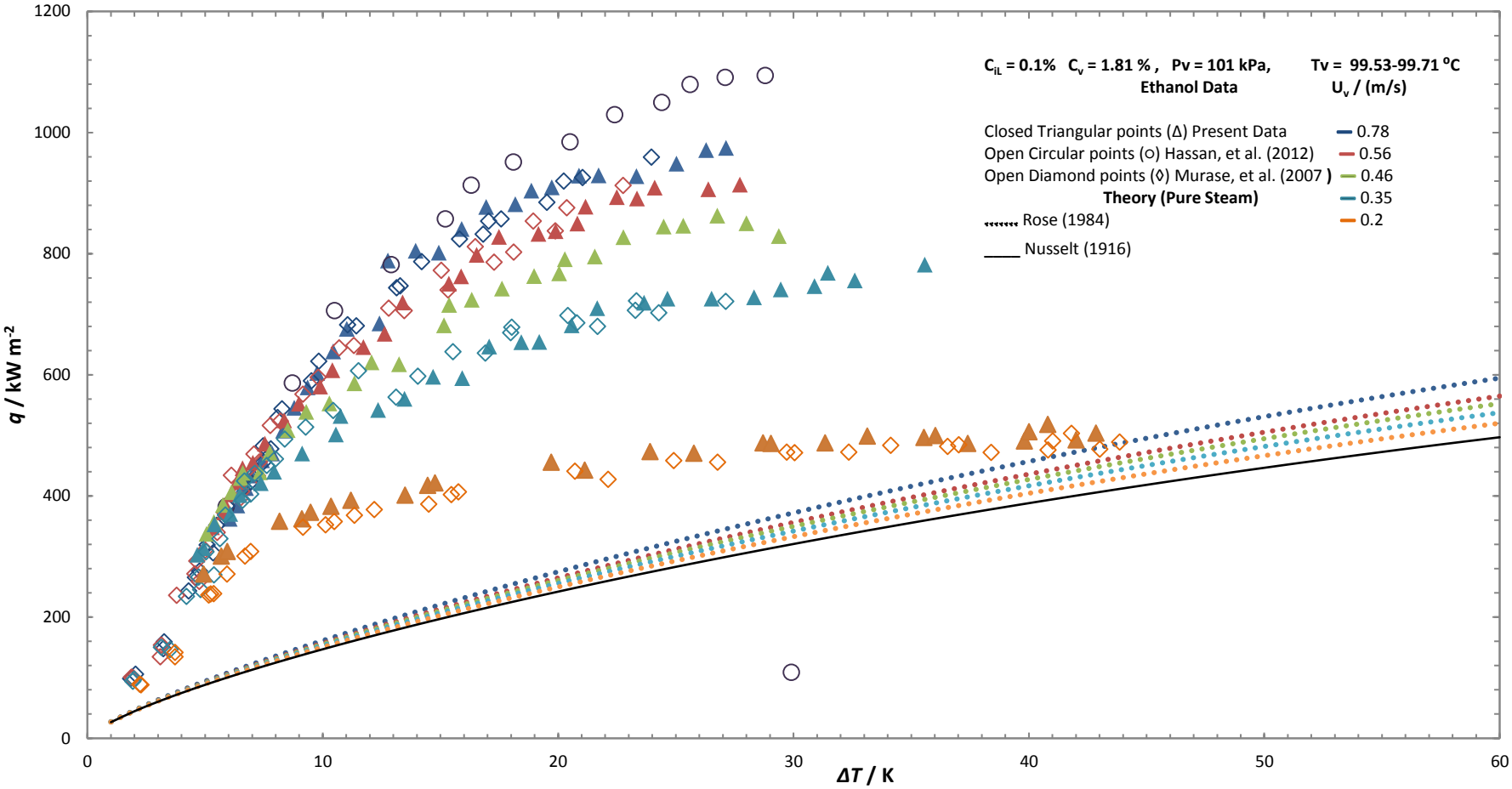

Figure 5.3 (Continued).

(g)

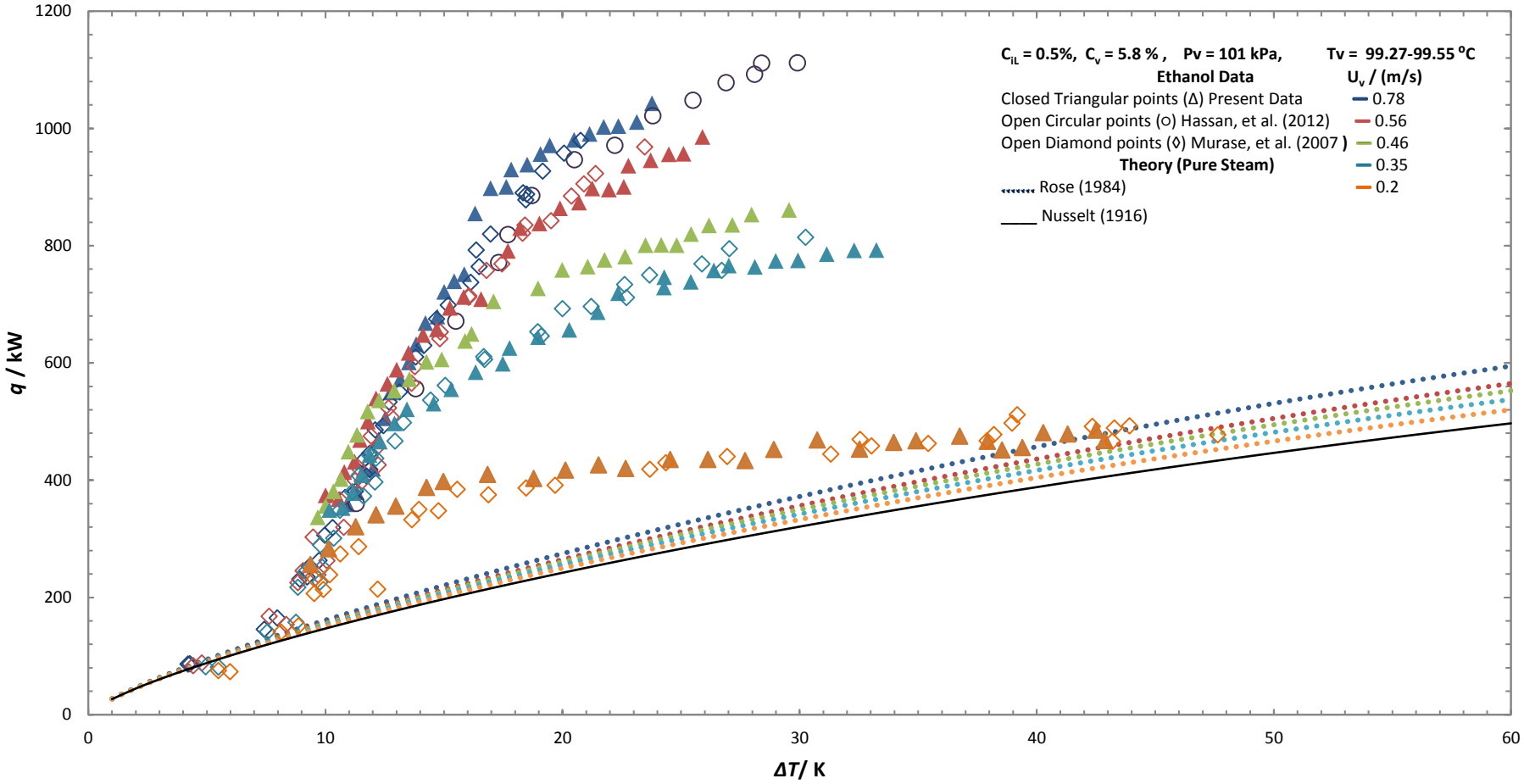

Figure 5.3 (Continued).

(h)

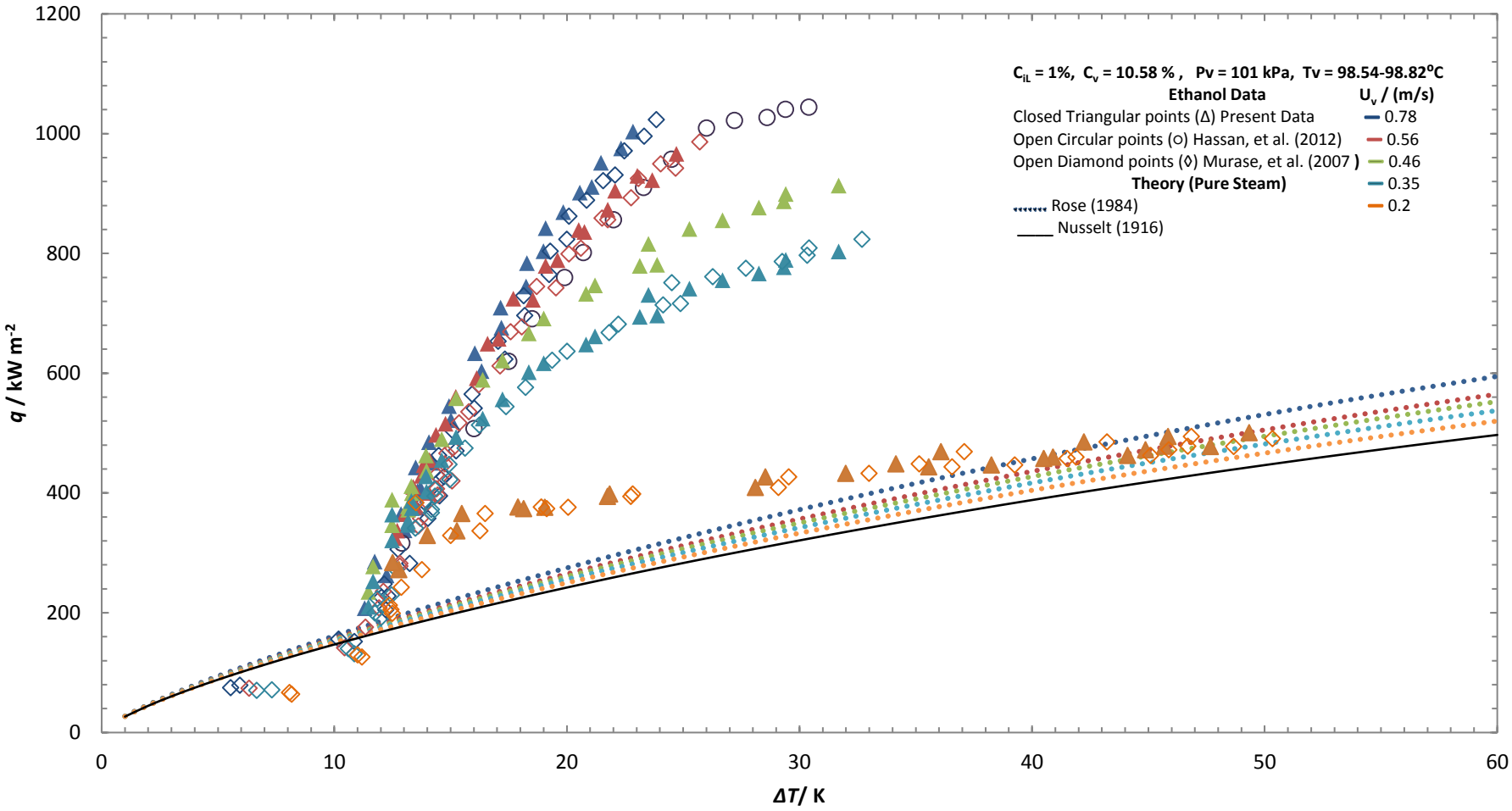

Figure 5.3 (Continued).

(a)

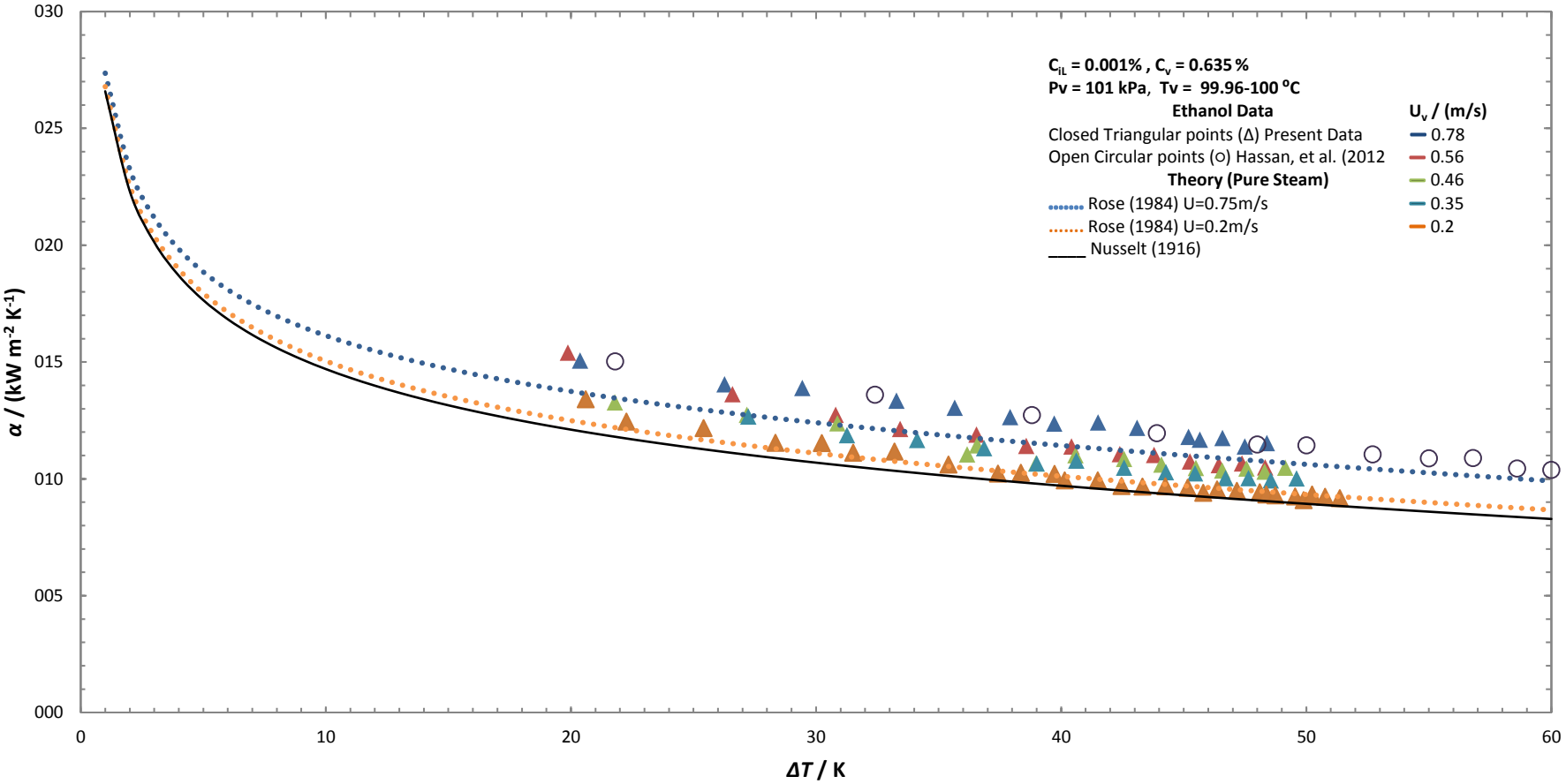

Figure 5-4: (a)-(g) shows variation of heat transfer coefficient against vapour-to-surface temperature difference for varying vapour velocities at each ethanol mass concentration. (a) C_{iL} = 0.001%, (b) C_{iL} = 0.005%, (c) C_{iL} = 0.01%, (d) C_{iL} = 0.025%, (e) C_{iL} = 0.05%, (f) C_{iL} = 0.1%, (g) C_{iL} = 0.5%, (h) C_{iL} = 1%. Present data is presented with closed points and previous experimental data with open points. Test section vapour pressure is approx. 101 kPa.

(b)

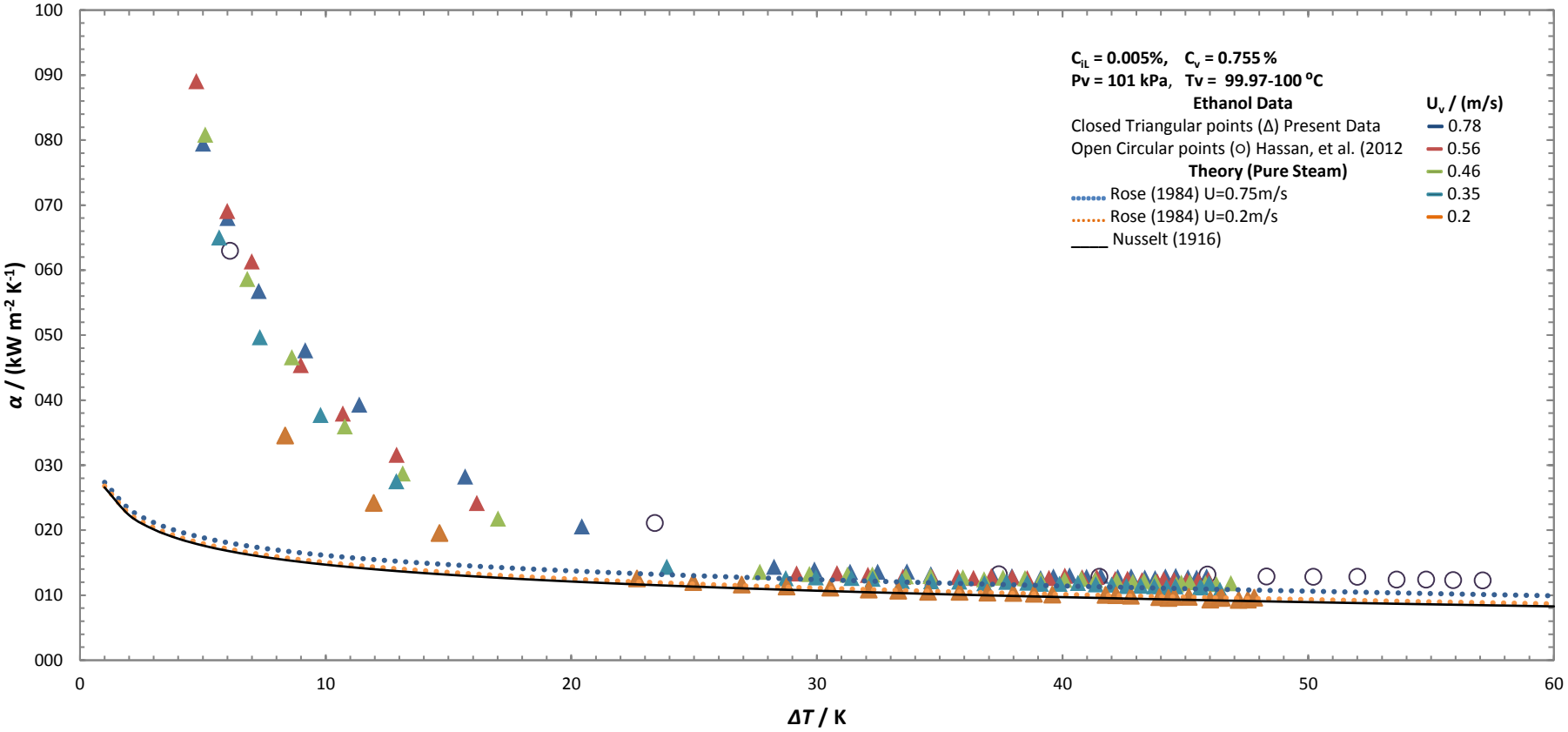

Figure 5.4 (Continued).

(c)

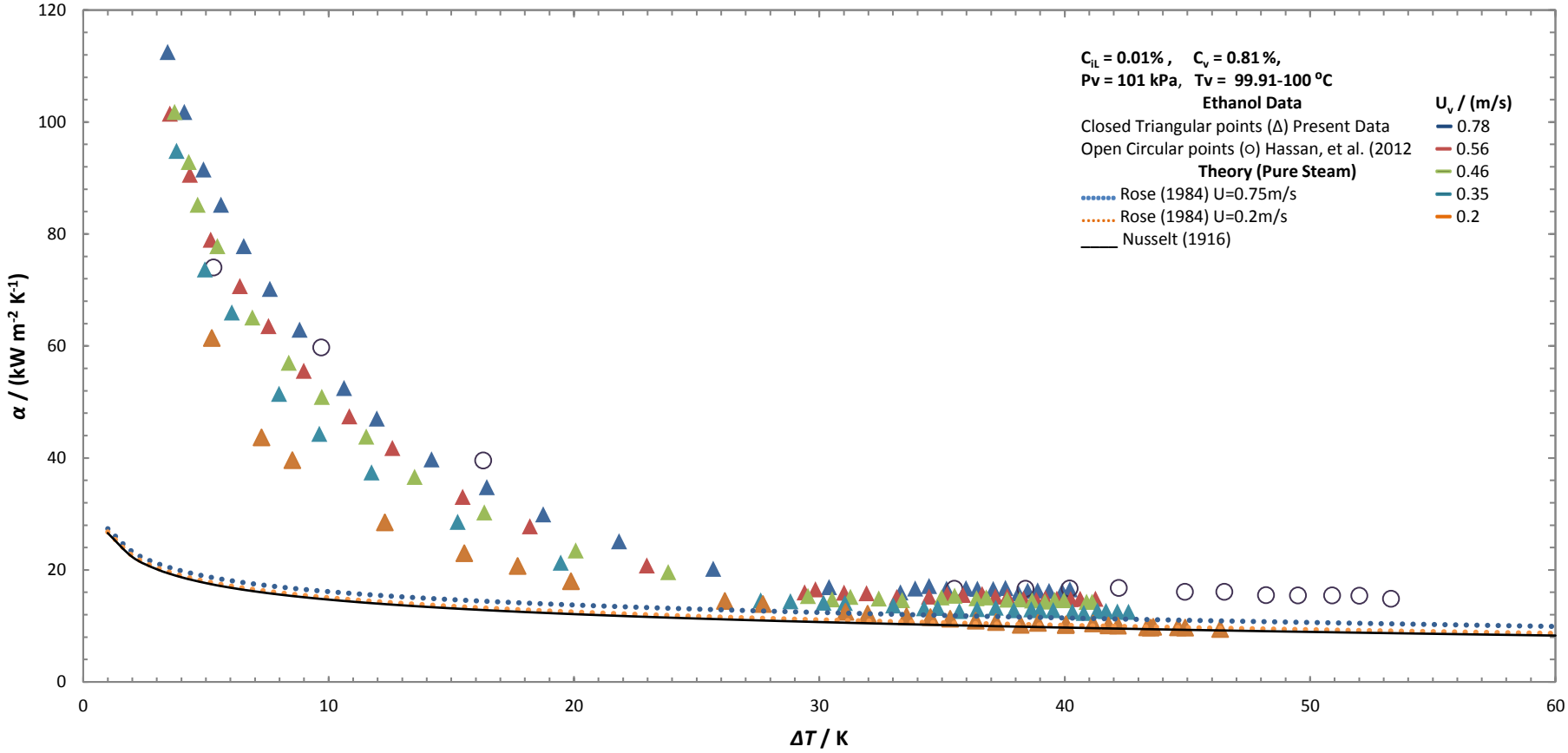

Figure 5.4 (Continued).

(d)

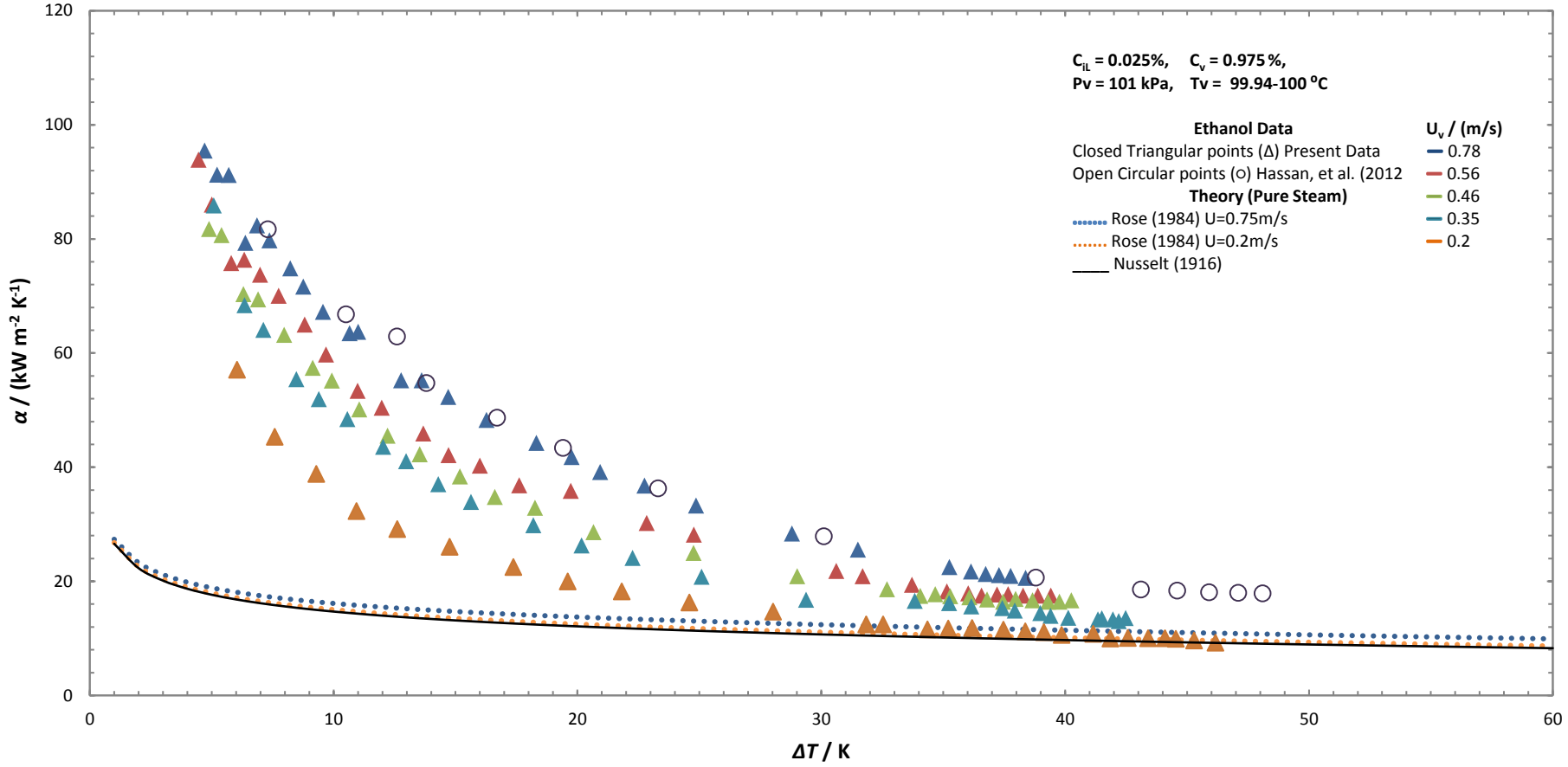

Figure 5.4 (Continued).

(e)

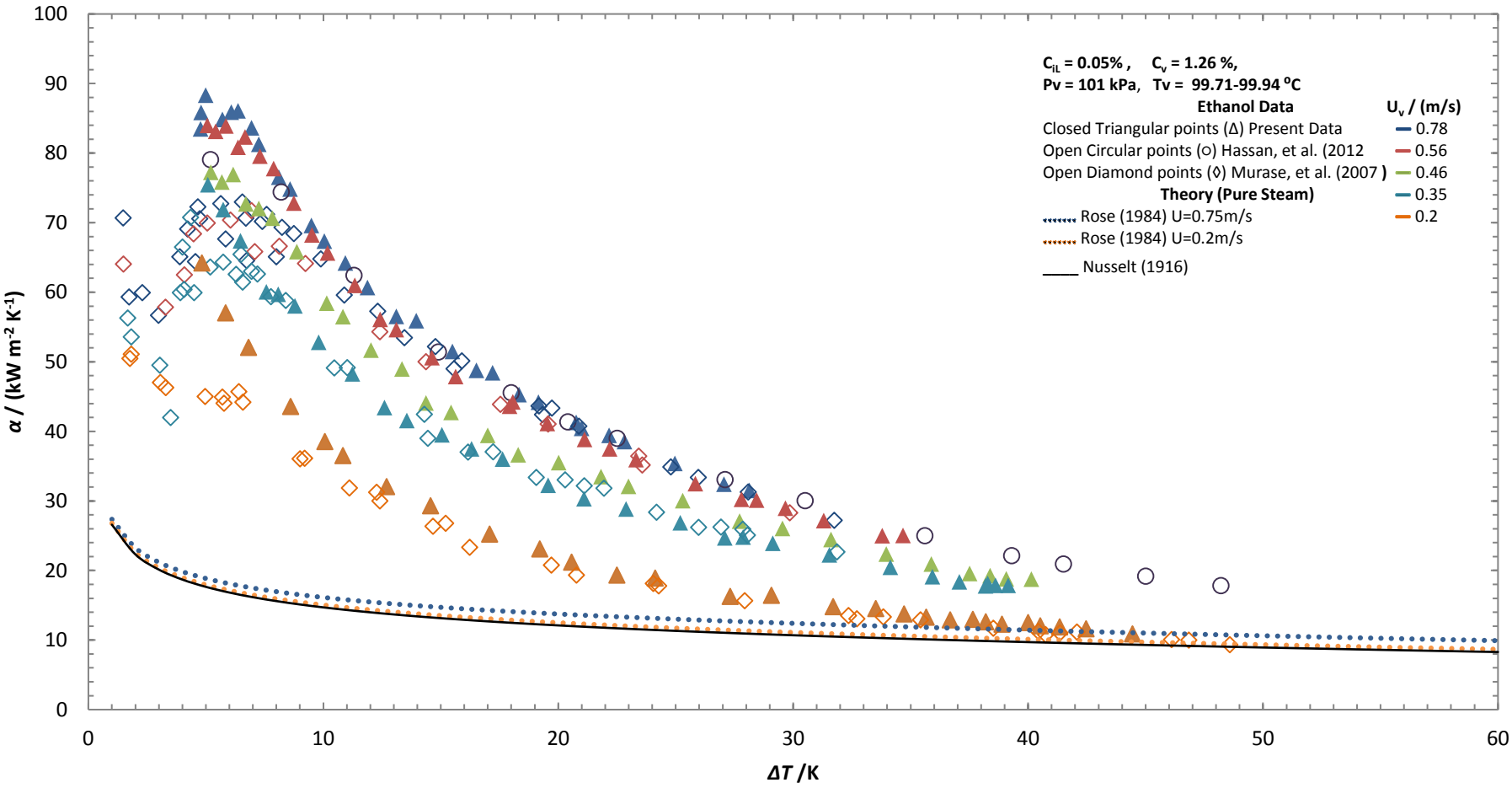

Figure 5.4 (Continued).

(f)

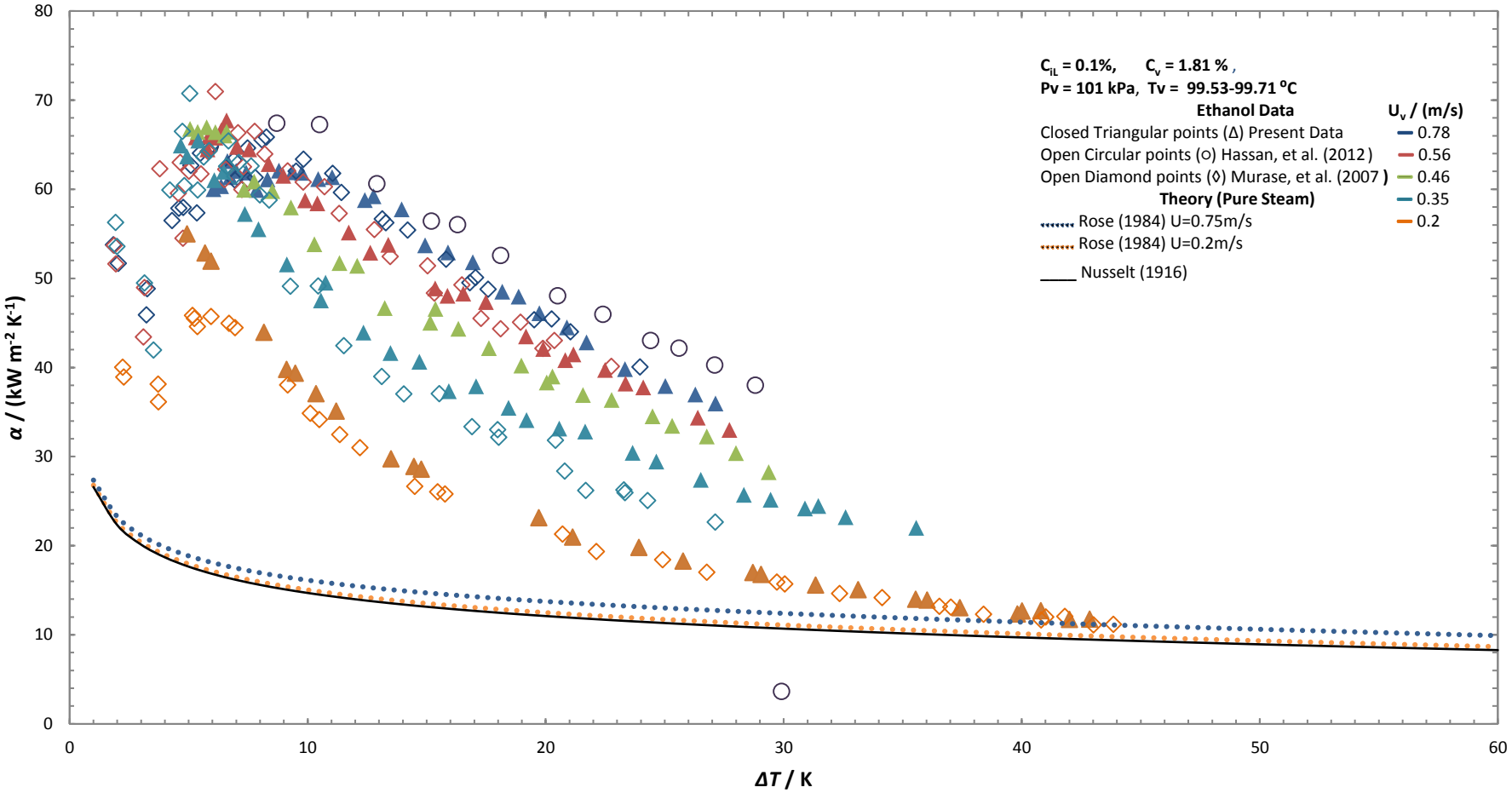

Figure 5.4 (Continued).

(g)

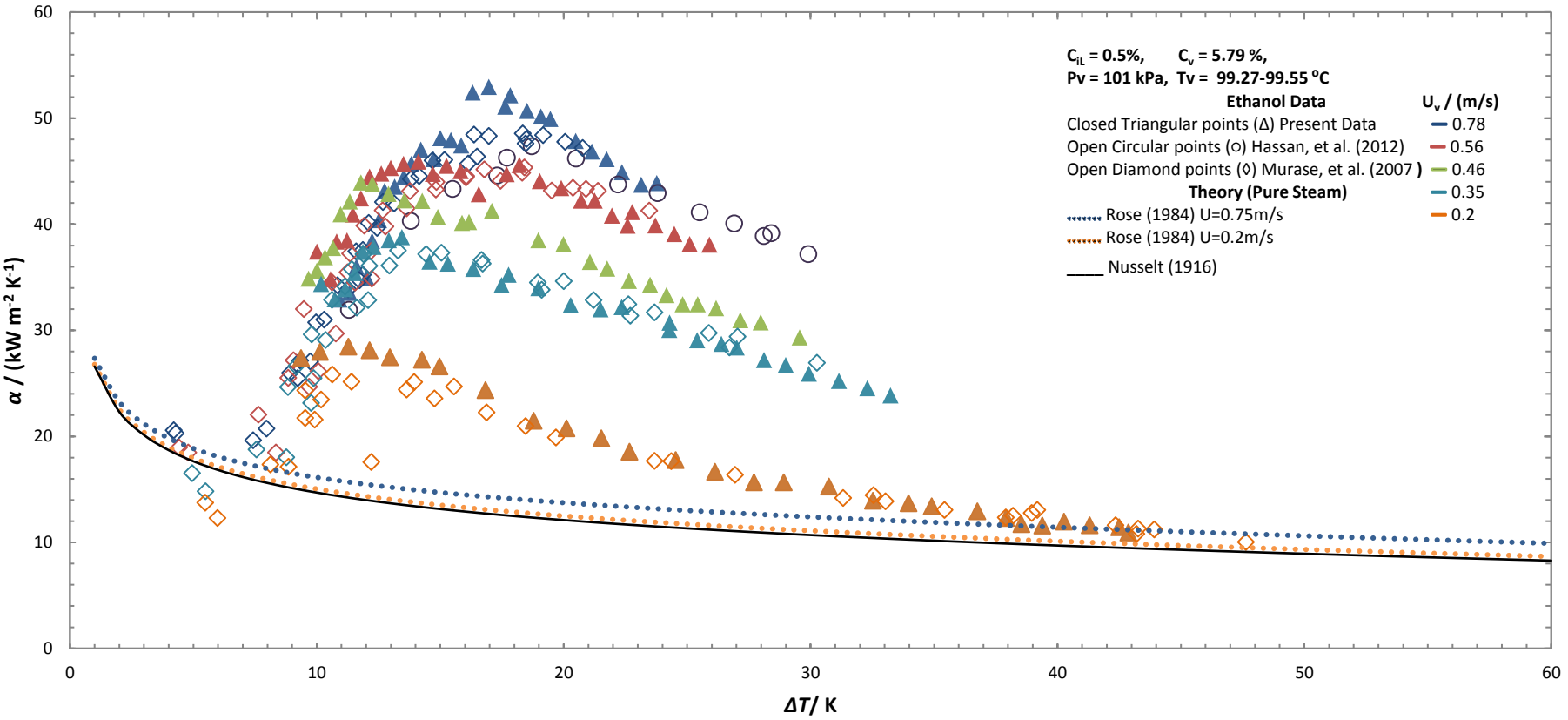

Figure 5.4 (Continued).

(h)

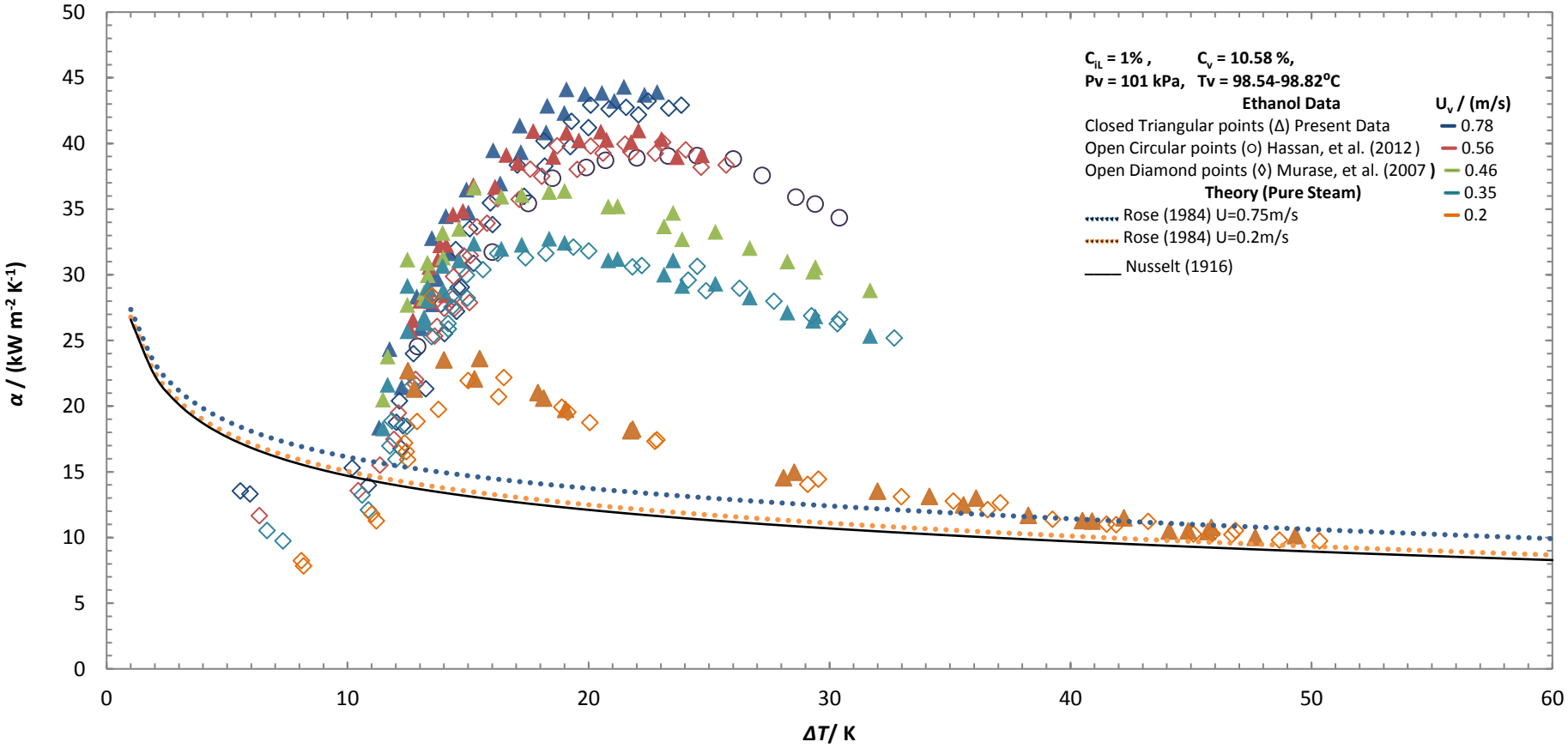

Figure 5.4 (Continued).

(a)

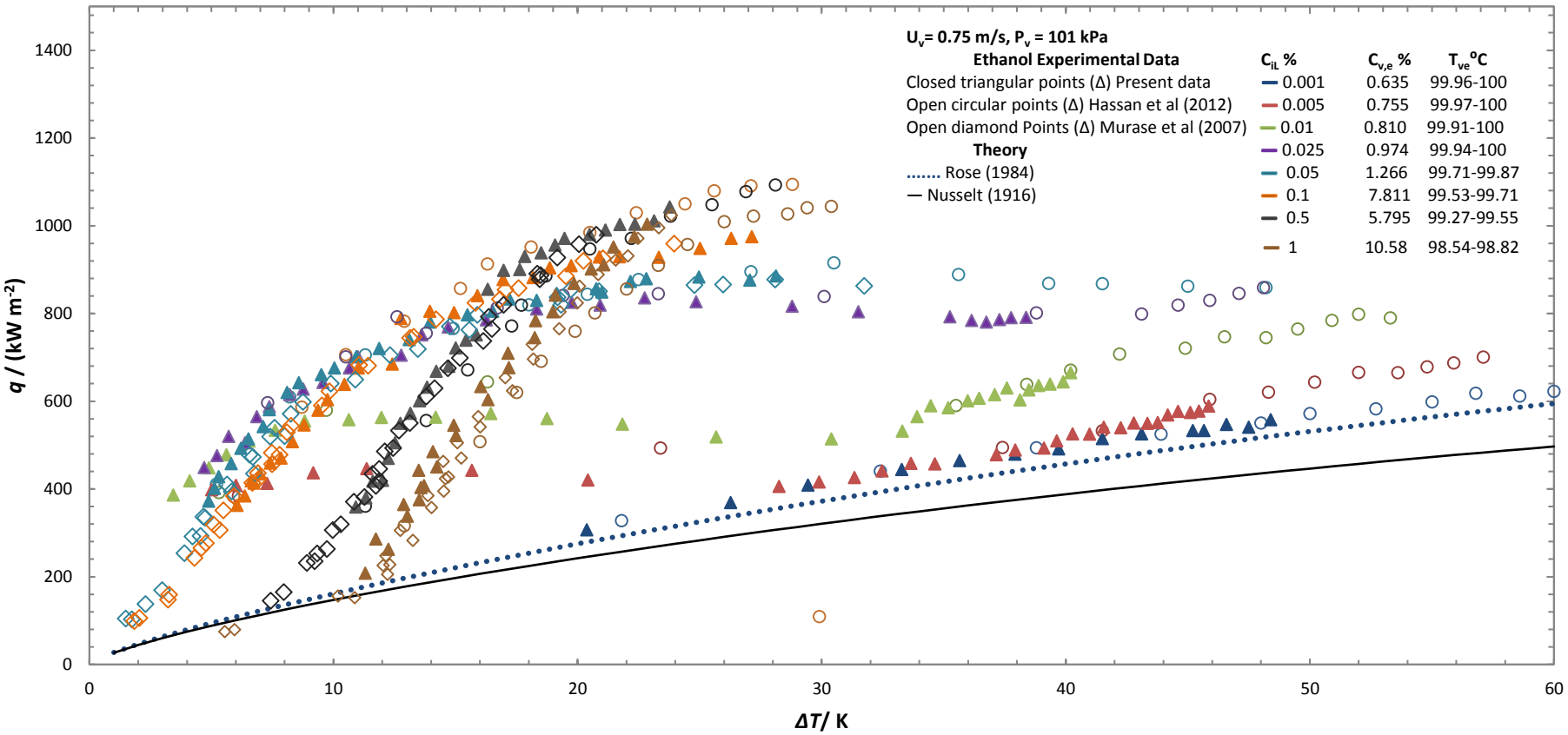

Figure 5-5: (a)-(e) shows variation of heat flux against vapour-to-surface temperature difference for varying ethanol mass concentrations at each vapour velocity. (a) U_v = 0.75 m/s, (b) U_v = 0.56 m/s, (c) U_v = 0.46 m/s, (d) U_v = 0.35 m/s, (e) U_v = 0.20 m/s. Present data is presented with closed points and previous experimental data with open points. Test section vapour pressure is 101 kPa.

(b)

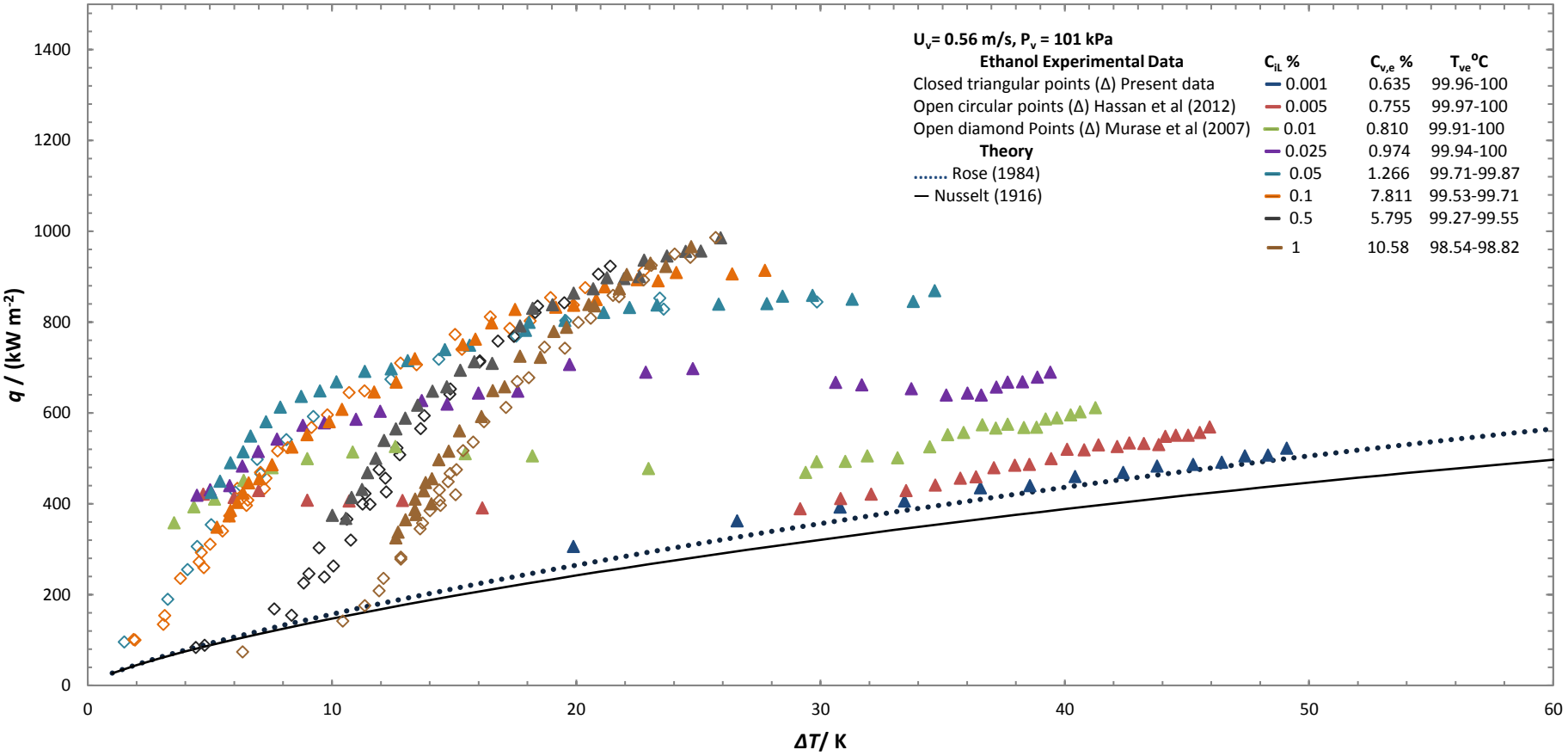

Figure 5.5 (Continued).

(c)

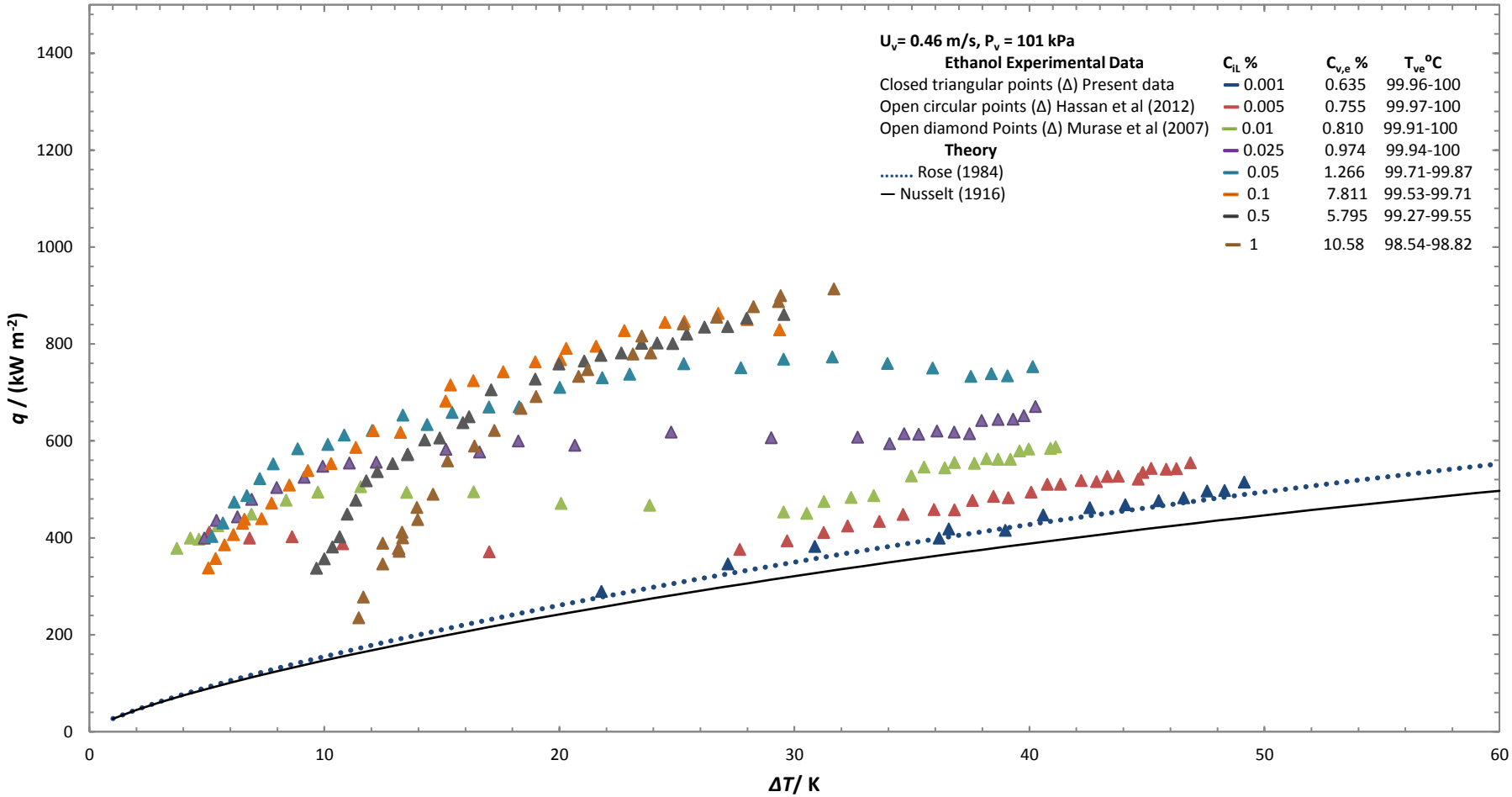

Figure 5.5 (Continued).

(d)

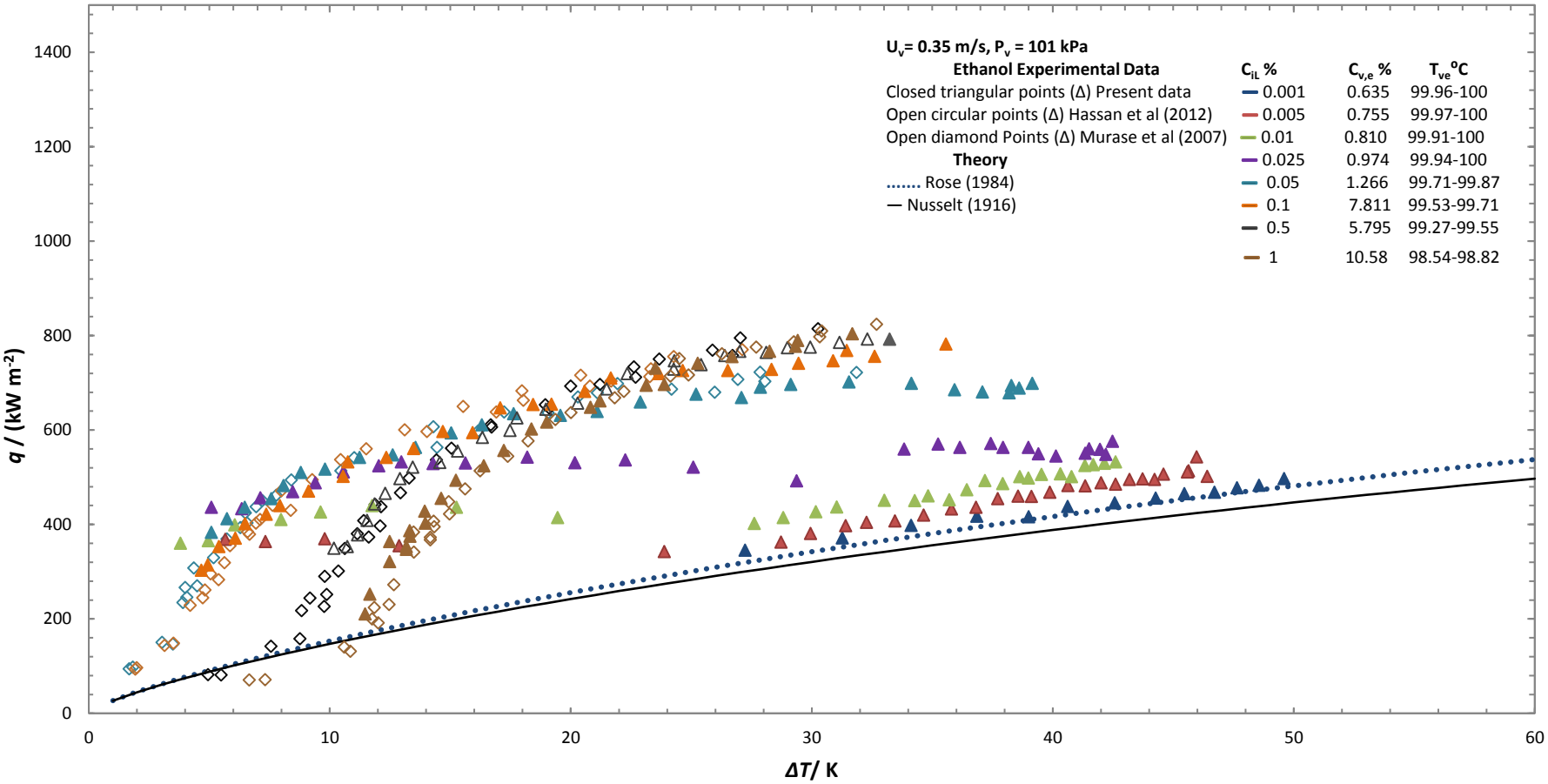

Figure 5.5 (Continued).

(e)

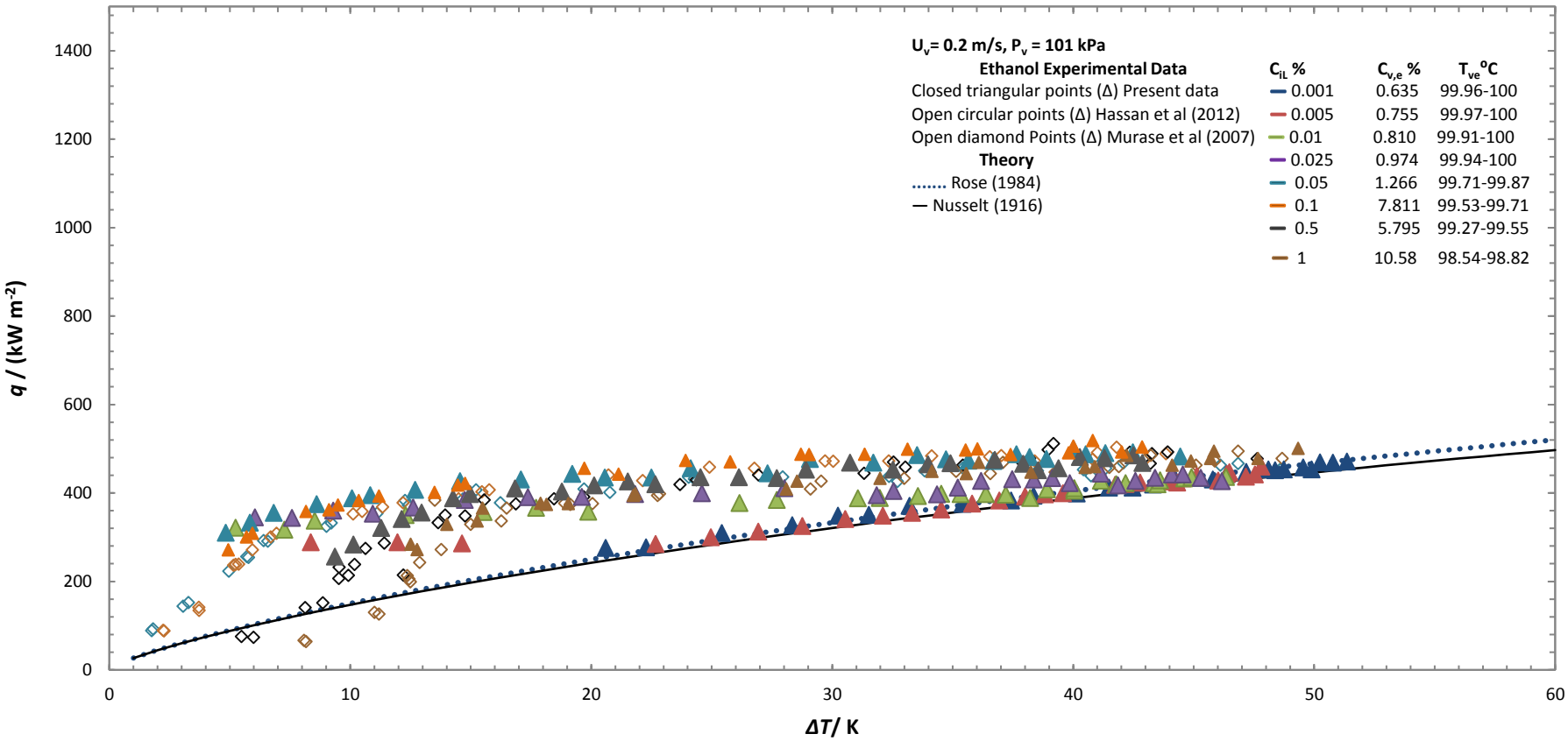

Figure 5.5 (Continued).

(a)

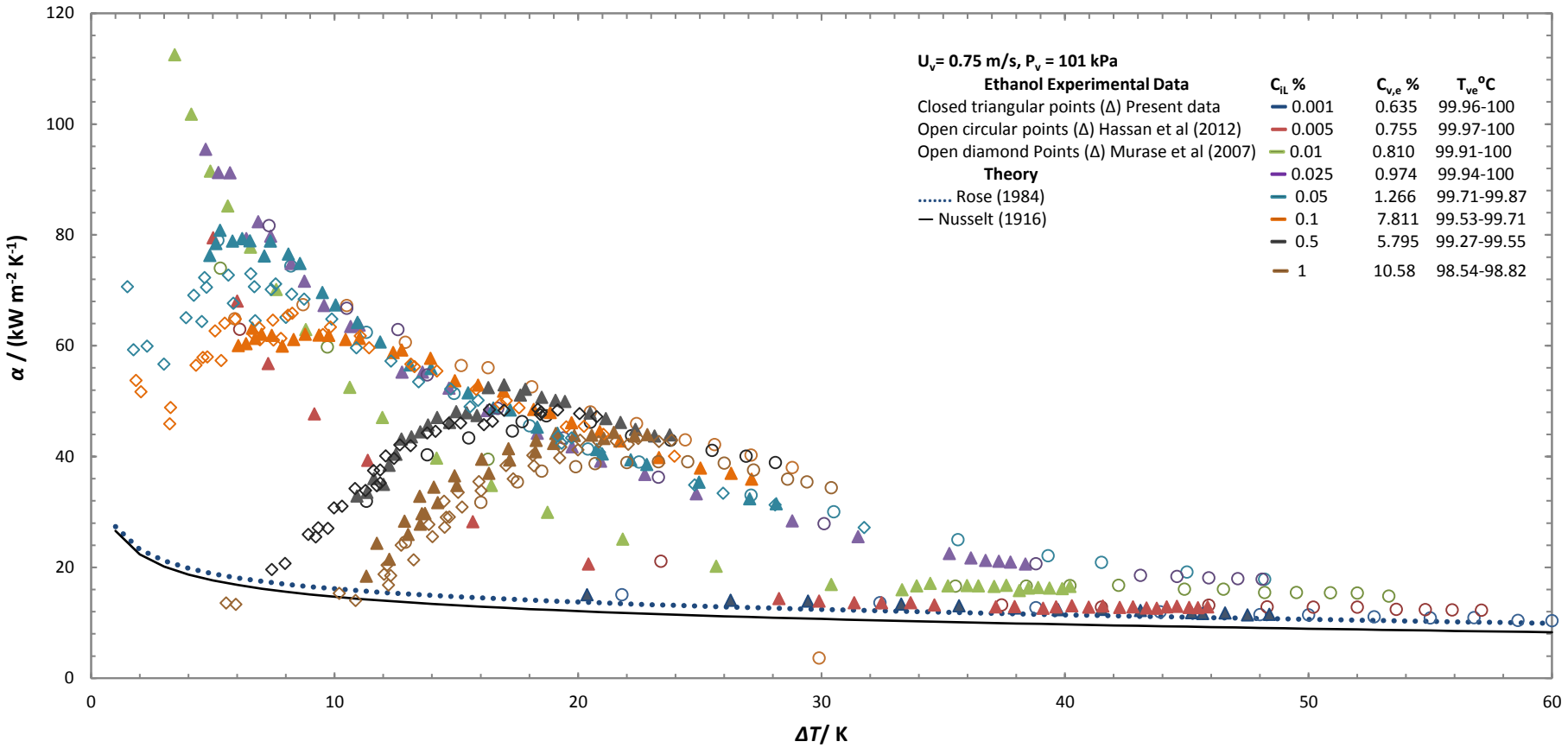

Figure 5-6: (a)-(e) shows variation of heat transfer coefficient against vapour-to-surface temperature difference for varying ethanol mass concentrations at each vapour velocity. (a) U_v = 0.75 m/s, (b) U_v = 0.56 m/s, (c) U_v = 0.46 m/s, (d) U_v = 0.35 m/s, (e) U_v = 0.20 m/s. Present data is presented with closed points and previous experimental data with open points. Test section vapour pressure is 101 kPa.

(b)

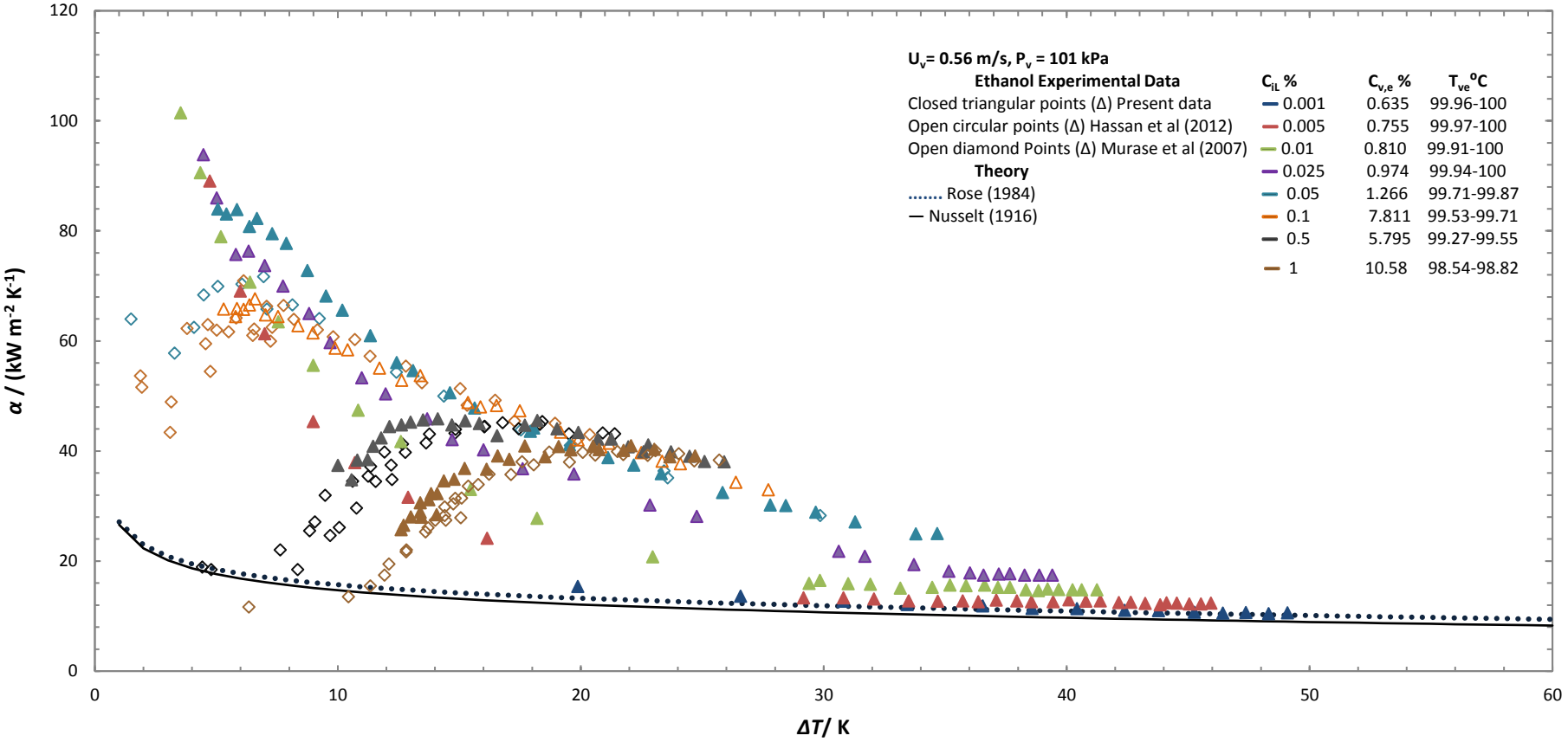

Figure 5.6 (Continued).

(c)

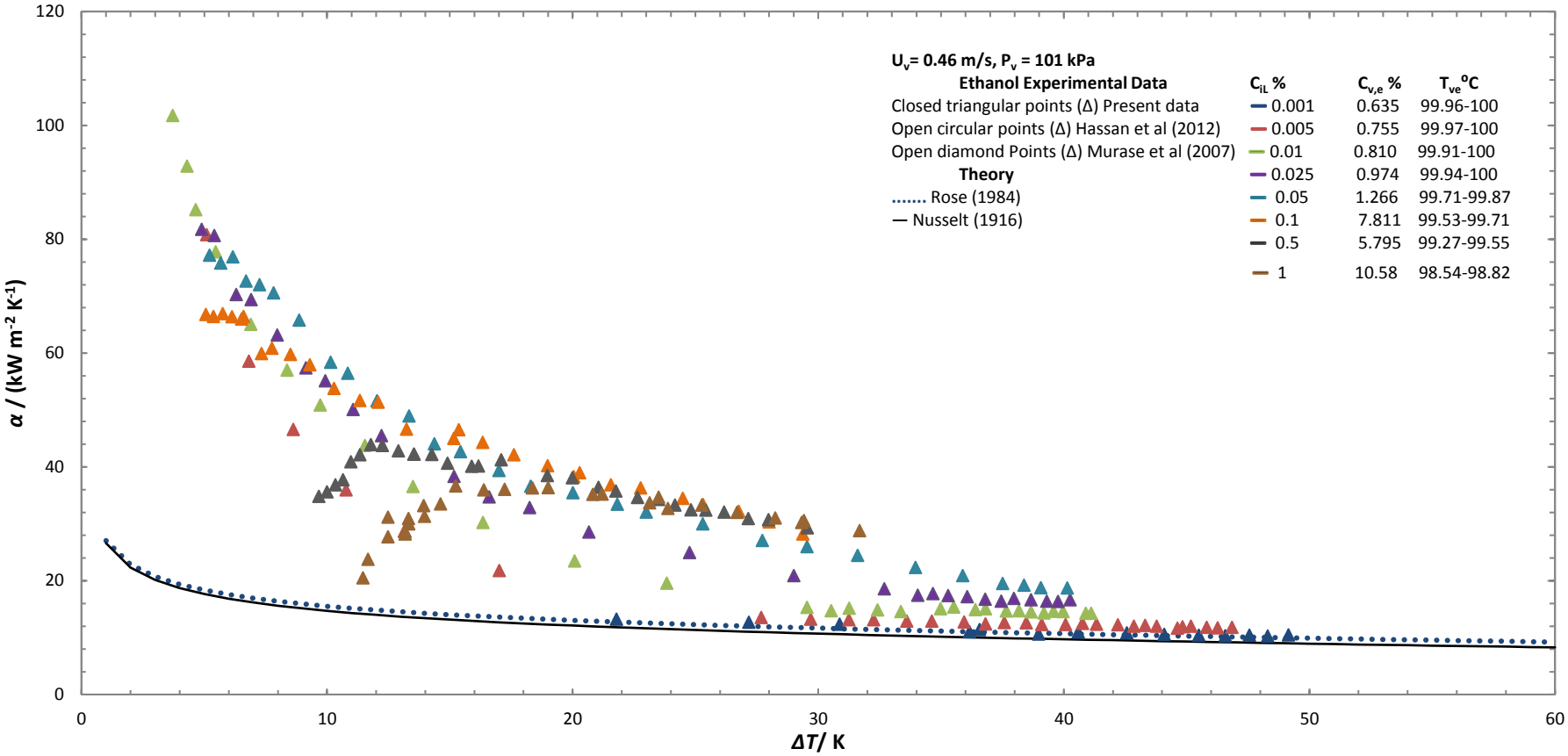

Figure 5.6 (Continued).

(d)

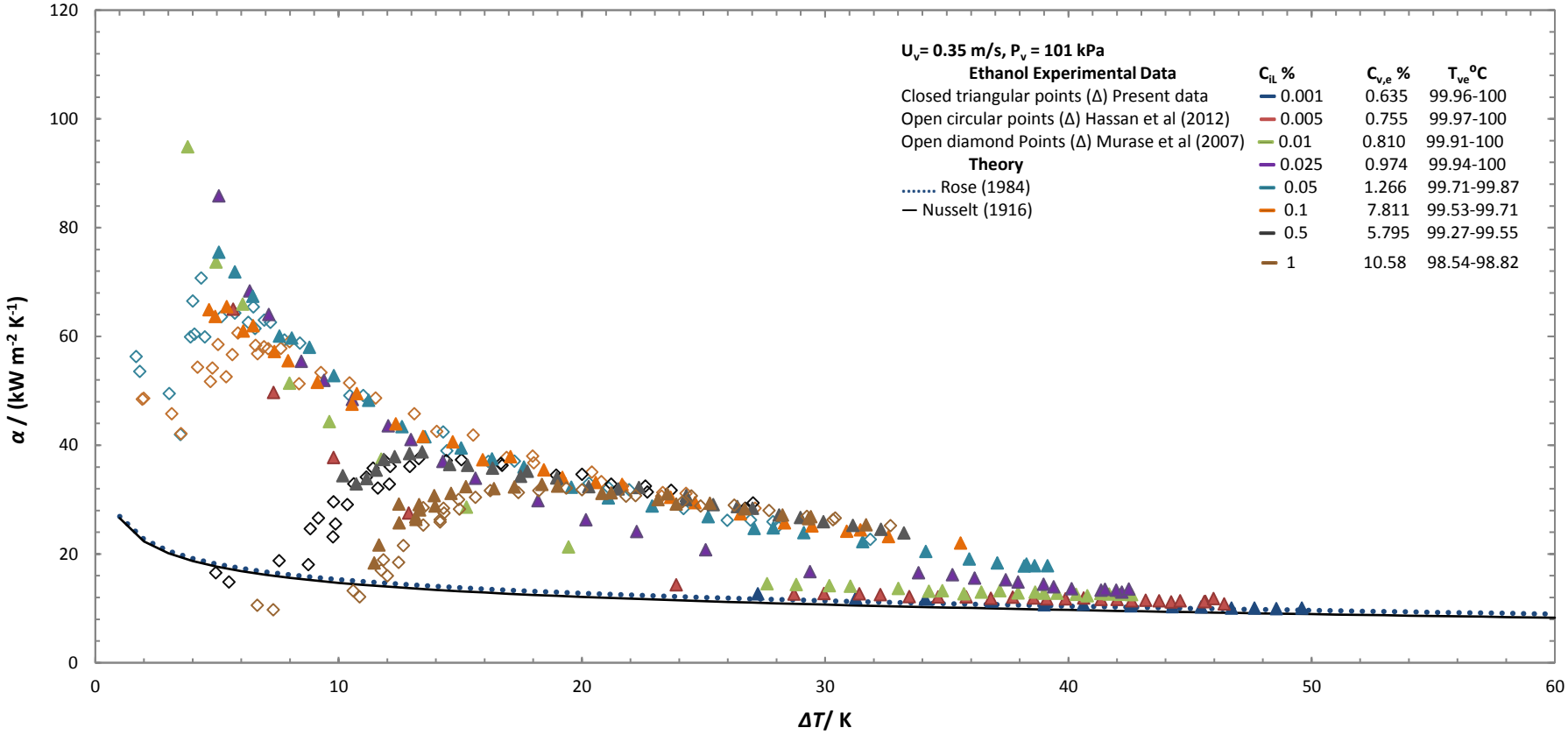

Figure 5.6 (Continued).

(e)

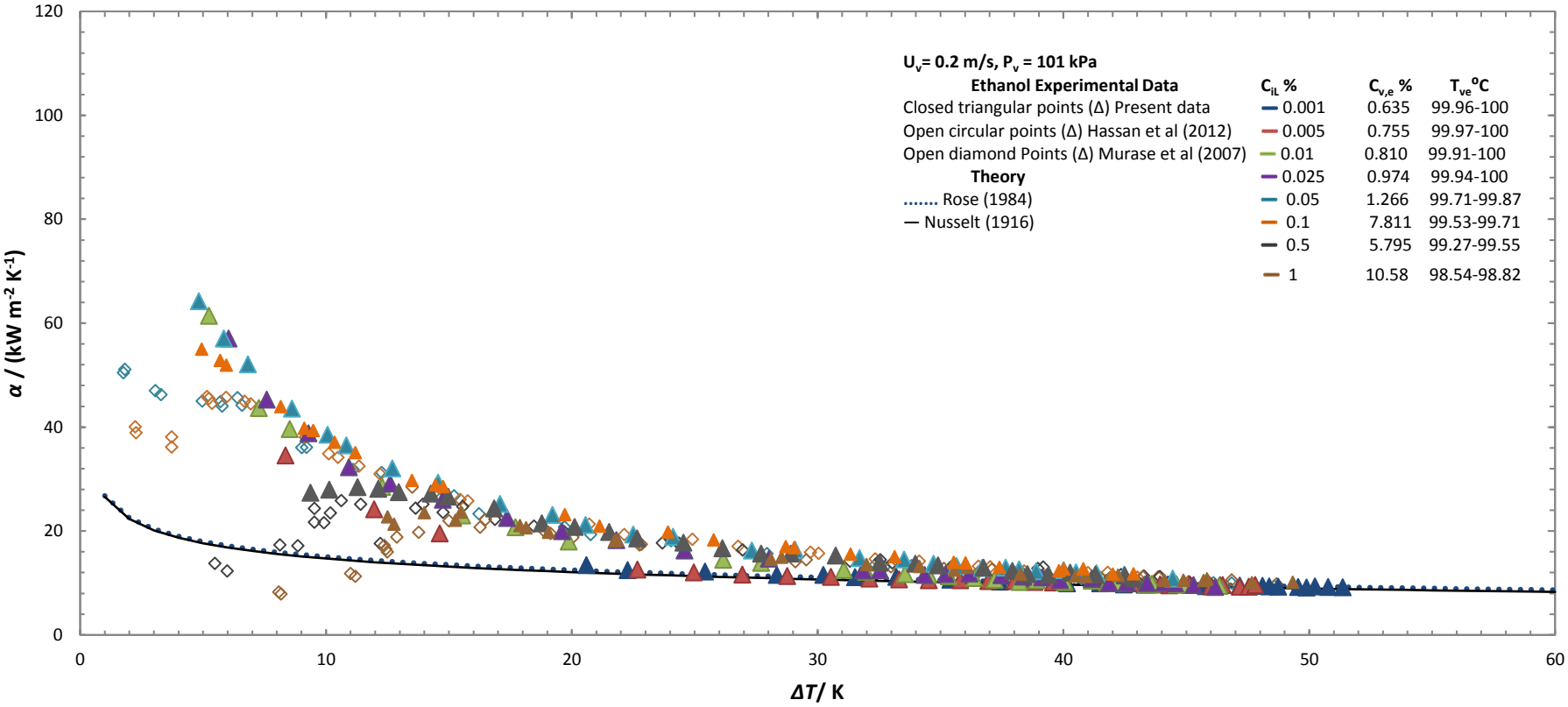

Figure 5.6 (Continued).

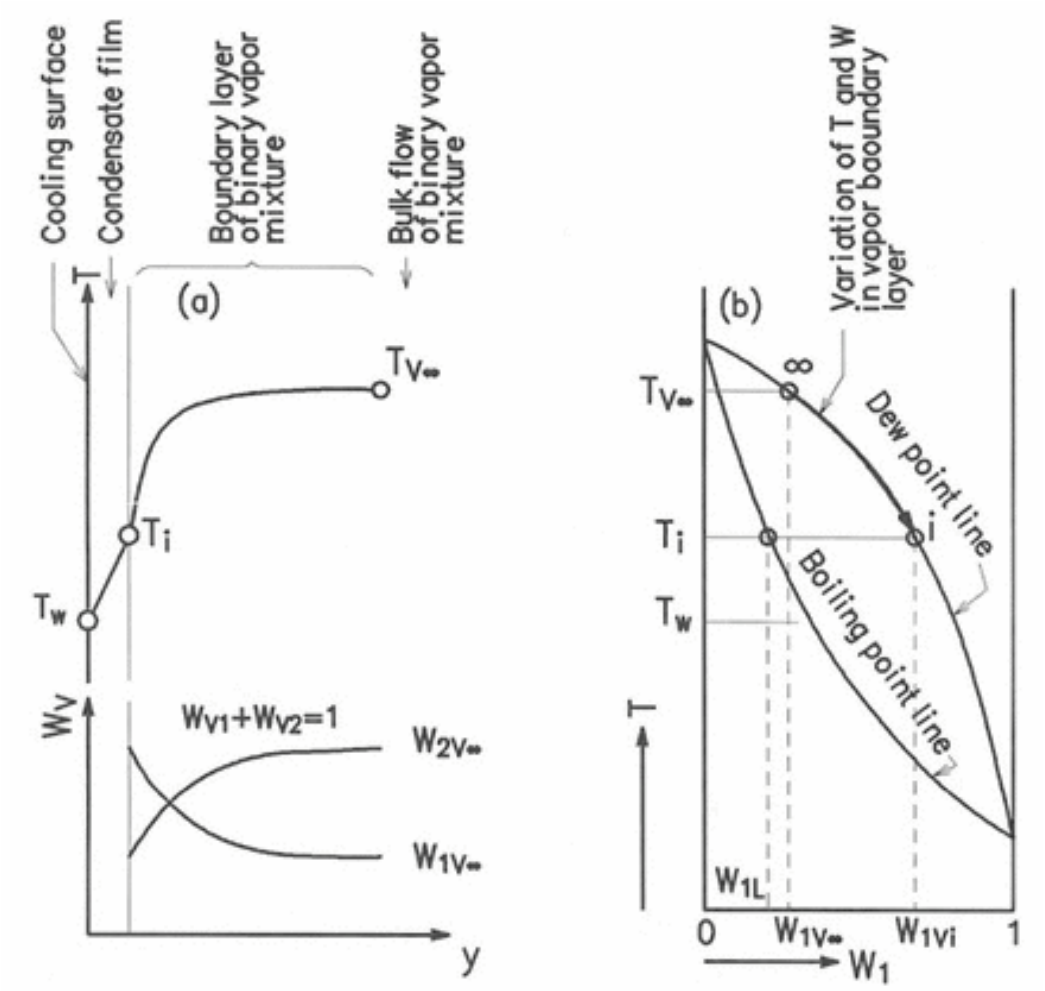

Figure 5-7: (a) distribution of Temperature (*T*) and mass concentration (*W*) in the condensate film and the vapour boundary layer. Y is the normal distance from the surface. (b) Variation of *T* and *W* on a diagram of phase equilibrium. Subscripts: ∞ is bulk, i is vapour liquid interface, w is wall surface, 1 is a volatile component, 2 is a less volatile component, v is vapour and L is liquid.

5.3.1 Enhancement

Enhancement ratio can be defined as:

$$\varepsilon_{se} = \left(\frac{q_{se}}{q_{Ro,ps}} \right)_{\Delta T, U_v} \tag{5.3}$$

where,

ε_{se} is the enhancement ratio of the steam-ethanol mixture at a given vapour velocity and vapour-to-surface temperature difference.

q_{se} is observed heat flux for steam-ethanol mixtures at a given vapour velocity and vapour-to-surface temperature difference.

$q_{Ro,ps}$ is the theoretical heat flux for pure steam obtained by Rose (1984) theory at a given vapour velocity and vapour-to-surface temperature difference.

Figures 5.8 Shows enhancement ratio for steam-ethanol mixtures for various mass compositions and vapour velocities. For all the mass compositions and vapour velocities except U_v= 0.2 m/s, the enhancement ratio exceeds unity over the entire range of vapour-to-surface temperature difference. Enhancement ratio is strongly dependent upon ethanol mass concentration and vapour-to-surface temperature difference. Enhancement ratio increases as ethanol concentration increase from 0.001% to 0.025%. For ethanol concentrations, greater than 0.025% enhancement ratio decreases for a given vapour to surface temperature difference. The trend of enhancement ratio with vapour-to-surface temperature difference is similar to that observed in the heat-transfer coefficient. For lower concentrations (C_{iL} = 0.005%, 0.01% and 0.025%) enhancements are higher at lower vapor-to-surface temperature difference and decreases as vapour-to-surface temperature difference increases. For higher concentrations (C_{iL} = 0.05%, 0.1%, 0.5% and 1%) initially in the beginning enhancement increases with increase in vapour-to-surface temperature difference and reaches a maximum. It then decreases with further increase in vapour-to-surface temperature difference. Enhancements are more significant at higher velocities and lower concentration. However, at higher concentrations velocity seems to have little effect. The highest enhancement ratio of 5.5 was observed at the

lowest vapour-to-surface temperature difference (ΔT= 3.43 K) for the mass composition of 0.01%.

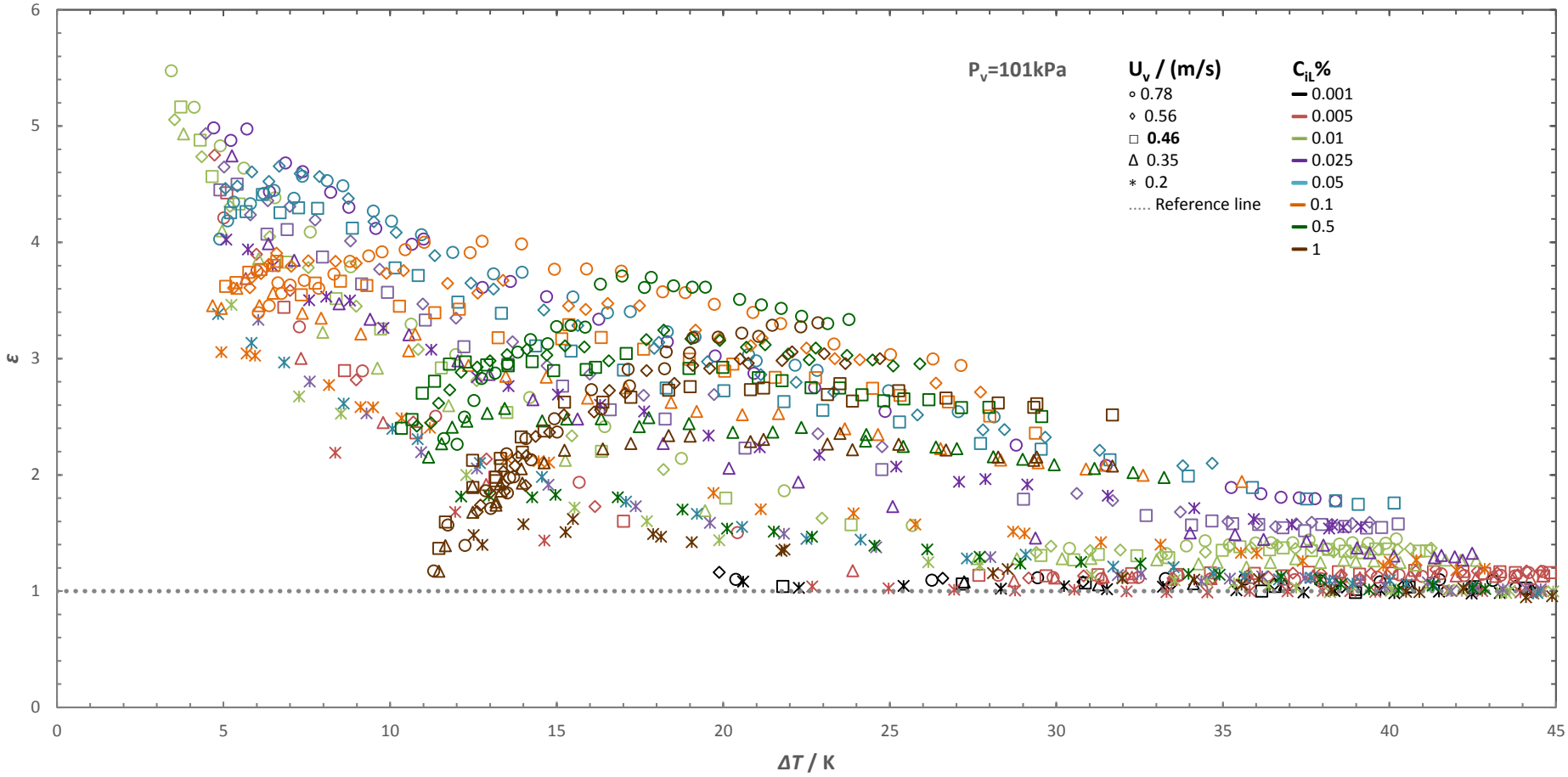

Figure 5-8: Enhancement Ratio of steam-ethanol mixtures of various compositions and vapour velocities. The grey dotted line is the pure steam line used as a reference.

5.3.2 Visual observation

During condensation, videos were taken using 16.1 megapixels Sony Cyber-shot digital camera. Figure 5.9 (a) to (c) shows the change in condensate appearance as the vapour-to-surface temperature increases for mass concentrations of 0.001%, 0.025% and 0.5% at vapour velocity of 0.75 m/s. Visual observation is compared with the heat transfer coefficient graph shown with visual images. The trend of the heat transfer coefficient seems to agree with the mode of condensation. Figure 5.9 (a) shows that for C_{iL} = 0.001% film-wise mode of condensation was observed throughout vapour-to-surface temperature difference and the heat transfer coefficient curve coincides with Rose (1984) theoretical model line. For C_{iL}= 0.025% (figure 5.9 (b)), condensate initially appears to be dropwise with higher heat transfer coefficients and gradually turns into a wavy film as heat transfer coefficient decreases. For C_{iL}= 0.5% (figure 5.9 (c)), heat transfer coefficient initially increases and reaches a maximum value as vapour-to-surface temperature difference increases. Observation shows dropwise mode of condensation with big drops changing into denser smaller drops. Further increase in vapour-to-surface temperature difference changes condensate appearance back to big drops and a hint of the wavy film was observed as heat transfer coefficient decreases. Furthermore, it was also observed that as vapour velocity increases the speed of drops forming and dripping off the test tube increases. This was not possible to see through pictures but was observed through videos.

(a)

C_{iL} **0.001%**

U_v **0.75 m/s**

ΔT = 20.3 K
q = 306 kWm^{-2}
Ɛ=1.1

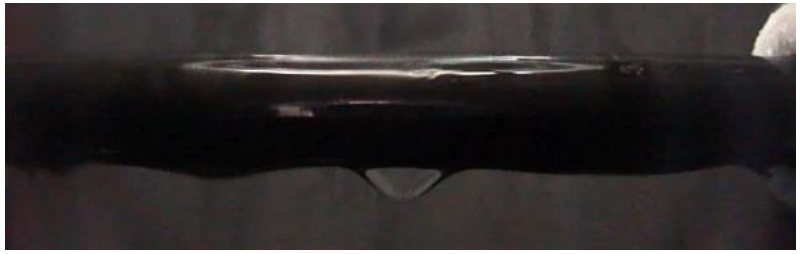

(i) Film-wise

ΔT = 33.27 K
Q = 444 kWm^{-2}
Ɛ=1.10

(ii) Film-wise

ΔT = 39.7 K
Q = 491 kWm^{-2}
Ɛ= 1.08

(ii) Film-wise

ΔT = 43.1K
Q = 525 kWm^{-2}
Ɛ=1.09

(iv) Film-wise

ΔT = 48.4 K
Q = 557 kWm^{-2}
Ɛ=1.07

(v) Film-wise

Heat transfer Coefficient

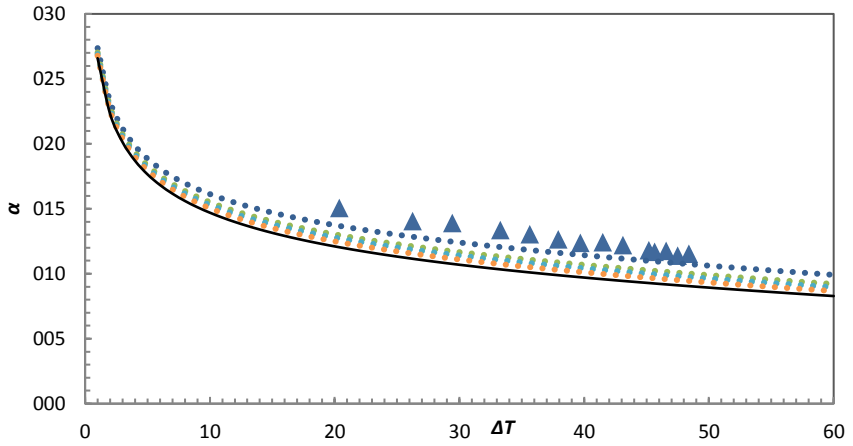

Figure 5-9 Visual observation of steam-ethanol condensation

(b)

C_{iL} **0.025 %**

U_v **0.75 m/s**

ΔT = 4.7 K
q = 448 kWm^{-2}
Ɛ= 4.98

(i) Dropwise: smaller drops

ΔT = 9.5 k
q = 643 kWm^{-2}
Ɛ= 4.11

(ii) Dropwise: bigger drops

ΔT = 14.69k
q = 768 kWm^{-2}
Ɛ= 3.53

(iii) Start of wavy film-wise

ΔT = 22.74 K
q = 835 kWm^{-2}
Ɛ= 2.75

(iv) wavy film wise mode Dominating

ΔT = 38.37 k
q = 790 kWm^{-2}
Ɛ= 1.77

(v) Wavy film-wise dominates

Heat transfer Coefficient

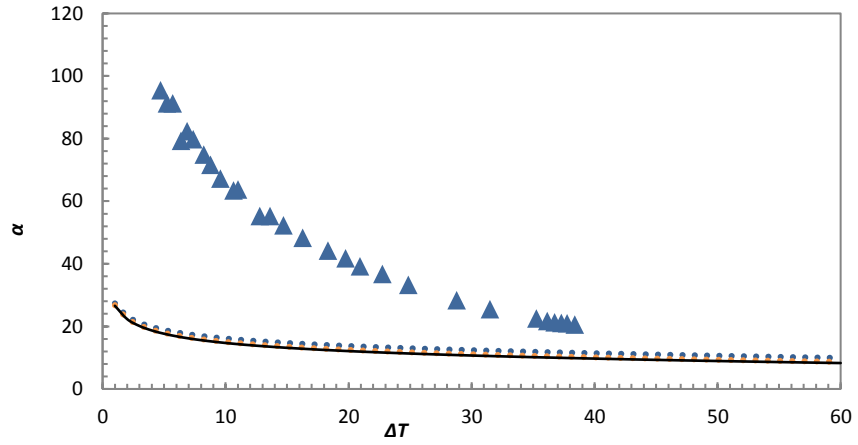

Figure 5-9 Continued.

(c)

C_{iL} **0.5 %**

U_v **0.75 m/s**

ΔT = 10.9 K
q = 358 kWm^{-2}
Ɛ= 2.08

(i) Dropwise: bigger drops

ΔT = 13.8K
q = 632 kWm^{-2}
Ɛ= 3.05

(ii) Dropwise: smaller drops

ΔT = 16.9 K
q = 898 kWm^{-2}
Ɛ= 3.7

(iii) Dropwise: no of smaller drops increases

ΔT = 19.46 K
q = 971 kWm^{-2}
Ɛ= 3.61

(iv) Dropwise: back to big drops

ΔT = 23.7 k
q = 1043 kWm^{-2}
Ɛ= 3.33

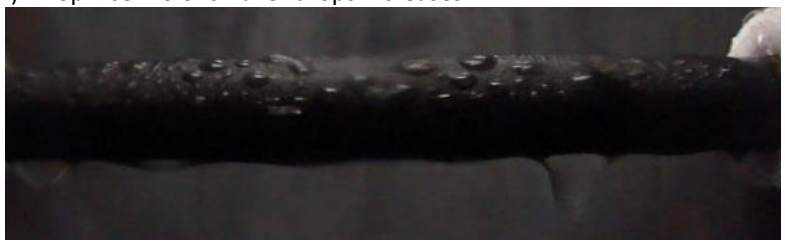

(v) Dropwise: hint of wavy film

Heat transfer Coefficient

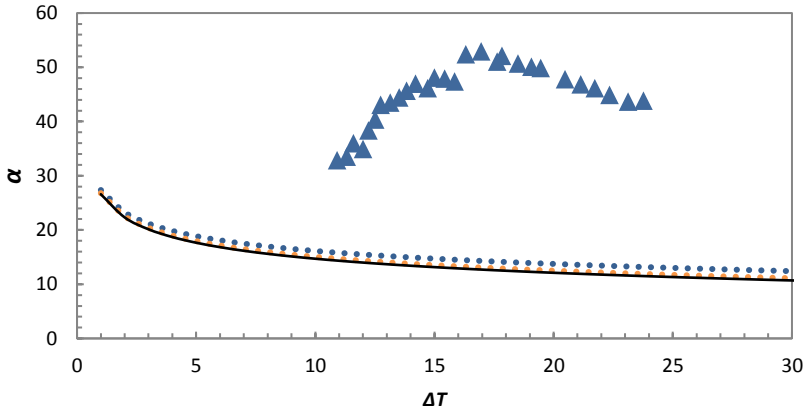

Figure 5.9 continued.

5.4 Summary

The investigations were successful in validating the apparatus and experimental procedure by reproducing the previous data of pure steam and steam-ethanol mixtures. The results were in good agreement for all pure steam experiments and steam ethanol mixtures compared to Rose (1984), Murase (2007) and Hassan (2011) results respectively.

Moreover, the present work has attempted to fill the gap in the data collected by Murase et al. (2007) and Hassan et al. (2012). Data for ethanol mass concentration of 0.001%, 0.005%, 0.01% and 0.025% at velocities of 0.2, 0.35, 0.46 .56 and 0.75 m/s were collected. This data was important in order to understand the transition regions in the Marangoni condensation of steam-ethanol mixtures and would later prove to be beneficial in modelling the semi-empirical model.

Similar to Murase et al (2007) and Hassan et al (2012), results are found to be sensitive to both vapour velocity and surface temperature. Significantly, higher heat fluxes and heat-transfer coefficients were found at low vapour to surface temperature difference for low concentration compared to pure steam condensations. Enhancement plot shows maximum enhancement was achieved at a particular value of vapour-to-surface temperature difference which depends on the ethanol concentration and vapour velocity. The peak value of enhancement ratio occurs at a lower value of vapour-to-surface temperature difference for lower ethanol concentrations and generally has a value around 4.

At this stage, it is still impossible to model this complex phenomenon theoretically. It seems clear that both the temperature drops in the vapour (diffusion resistance in the vapour mixture) and that across the condensate are of comparable magnitude and both are sensitive to composition and vapour velocity. The former (vapour phase diffusion resistance) can be analysed along the lines described by Sparrow and Marshall (1969). The latter (condensate resistance), where the mode of condensation depends on temperature difference as well as composition and vapour velocity, presents a more formidable challenge. However, an attempt is made to create a semi-empirical model based on the dropwise theory of pure steam by Rose (2002). The details of which will follow in chapter 8.

Chapter 6

6 Marangoni condensation of steam-butanol mixtures on a horizontal smooth tube

6.1 Introduction

In this chapter comparative investigation between Marangoni Condensation of steam-butanol and steam-ethanol mixtures has been studied. Experiments for condensation of steam-butanol vapour flowing vertically downward over a water-cooled horizontal tube has been conducted. The Same experimental apparatus and conditions as for the steam-ethanol mixtures were used to measure the heat transfer performance during the condensation of steam-butanol mixtures on a horizontal smooth tube. The same smooth copper tube was used with four thermocouples embedded in the surface. To ensure there were no ethanol footprints left, the tube was thoroughly cleaned using the procedure mentioned in chapter 5 before using it for the steam-butanol case. Test section pressure was 101 kPa measured in the same way as in the steam-ethanol case. Same vapour velocities and coolant flow rates as of steam-ethanol were implied. At each flow rate four embedded thermocouple temperatures, inlet and outlet coolant temperatures, coolant temperature rise, condensate return temperature and test section gauge pressure were recorded. For the purpose of visual observation, videos of condensate film were recorded at several flow rates.

Mass Fraction of butanol (initial liquid mass fraction (C_{iL}) of butanol prepared at room temperature) were 0.001%, 0.005%, 0.01%, 0.025%, 0.05%, 0.1% and 0.5%. For each butanol mass fraction, vapour velocity at approach to condenser tube was varied using the boiler power to give 0.2, 0.35, 0.46, 0.56 m/s and 0.75m/s. Coolant inlet temperature was always around 25 °C with maximum variation of 1 K.

The main purpose of this investigation was to measure the heat transfer properties of steam-butanol mixtures and compare it with the results obtained for steam-ethanol mixtures under the same experimental conditions. It is predicated on the theoretical basis that steam-butanol should perform better than stem-ethanol mixtures.

6.2 Results and discussion

Figures 6.2 and 6.3 shows heat flux and heat transfer coefficient against vapour-to-surface temperature difference for different vapour velocities at each butanol mass fraction (C_{iL}). The solid black line represents the Nusselt (1969) equation for pure steam given by equation 2.1. Whereas, the equation of Rose (1984) including the effect of vapour velocity is presented in blue and orange dotted line for the minimum and maximum vapour velocities respectively. For comparison, steam-ethanol data are also plotted. Steam-butanol data is plotted by closed points and steam-ethanol data using open points.

The key finding of the experiment was the significantly higher heat flux and heat transfer coefficients of steam butanol mixtures, for the given vapour-to-surface temperature difference and mass concentration, compared to the steam-ethanol case. Secondly, the diffusion resistance in steam-butanol mixtures is found to be lower compared to steam-ethanol mixtures for the given mass concentration.

Similar to the steam-ethanol case, for all the butanol mass fractions, the vapour velocity has a significant influence on the heat transfer. Increase in vapour velocity increases both heat flux and heat transfer coefficient for the given vapour-to-surface temperature difference. However, the effect of vapour velocity is much weaker in steam-ethanol mixtures compared to steam-butanol mixtures. This is clearly evident at lower mass concentrations (figure 6.2 (a)-(c)). For example, ethanol mass fractions of 0.01% in figure 6.2 (c), the maximum increase in vapour velocity (0.55m/s) increases the heat flux approximately by 212 kW m^{-2}. For the same butanol mass fractions, the maximum increase in velocity (0.55m/s) increases the heat flux by 635 kW m^{-2}. Giving three times higher heat flux for the given change in velocity.

Figure 6.3 shows that, for the mass fraction of 0.001%, 0.005%, 0.01% and 0.025%, the heat transfer coefficient decreases with the increase in the vapour to surface temperature difference. The heat-transfer coefficient is maximum at low vapour-to-surface temperature difference as a pseudo-dropwise mode of condensation exists. With the increase in vapour-to-surface temperature difference pseudo-dropwise mode transforms into unstable wavy film-wise mode thus decreasing the heat-transfer coefficient. Finally, at higher vapour-to-surface temperature difference complete film-wise mode was observed and the heat-transfer coefficient comes close to theoretical Rose (1984) equation (see figure 6.8 for visual

observations). This trend is similar to what was observed at a lower concentration of steam-ethanol mixtures except for the 0.001%. where the heat flux was almost equal to Rose (1984) equation. However, for the later concentrations of 0.05, 0.1, 0.5 and 1% its heat-transfer coefficient is relatively low at low vapour-to-surface temperature difference and starts to increase significantly as vapour-to-surface temperature difference increases. Visual observation at this point shows the pseudo-dropwise appearance of the condensate. After reaching the maximum value, heat-transfer coefficient decreases when the condensation mode changed to steadier pseudo-dropwise (see Figure 6.10 (k)-(o)).

Figure 6.4 and 6.5 shows heat flux and heat-transfer coefficient plotted against vapour-to-surface temperature difference for varying mass fractions at each vapour velocity. It is observed that mass fraction has a similar effect on the heat flux and heat transfer coefficient of steam-butanol mixtures as steam-ethanol mixtures. For a given vapour velocity higher concentration (0.05, 0.1, 0.5 and 1%) curves of heat transfer coefficient tend to drift away from the origin. However, the drifting is not as strong as in the steam-ethanol case. This drifting is attributed to diffusion resistance in the vapour phase (Murase 2007). Figure 5.7 in chapter 5 explains the effect of diffusion resistance on heat flux and heat transfer coefficients for steam ethanol mixtures, where ethanol was the less volatile component. However, in steam-butanol mixtures, butanol being the less volatile component condenses more. Therefore, the volatile component (in this case water) becomes dense at the vapour liquid interface. According to the phase equilibrium diagram (figure 6.1) decrease in concentration of butanol at vapour-liquid boundary layer in vapour phase minimises the temperature drop from bulk to interface compared to the stem-ethanol case for a given initial mass Concentration (C_{iL}). Thus, lesser diffusion resistance compared to steam-ethanol mixtures.

At the maximum vapour velocity butanol mass fraction of C_{iL} = 0.025% gave the highest heat flux of 1098 kW/m^2 at vapour to surface temperature difference of 9.6 K. For the same velocity butanol mass fraction of C_{iL} =0.01% gave the highest heat transfer coefficient of 282 kW/ m^{2}K at vapour to surface temperature difference of 1.37K

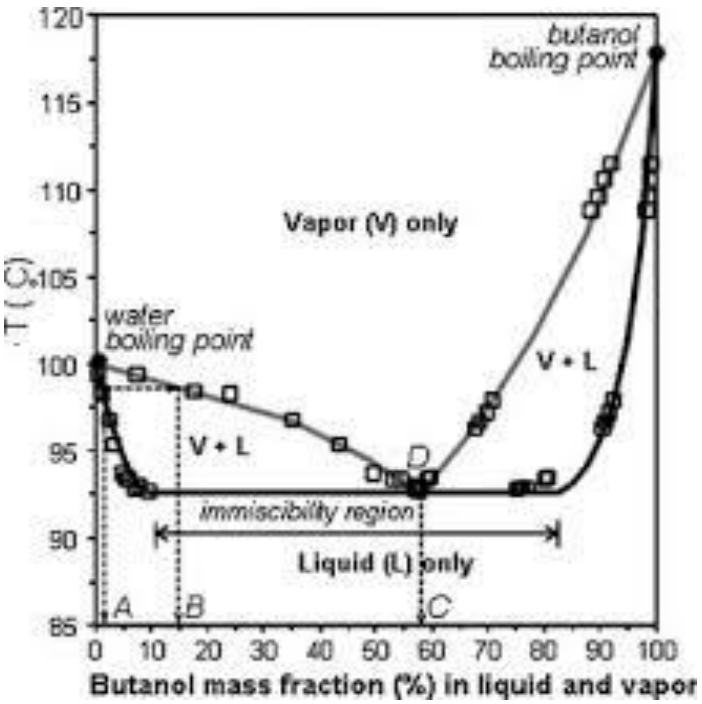

Figure 6-1: Vapour-liquid equilibrium diagram of steam-butanol mixtures at a pressure of 101 kPa.

(a)

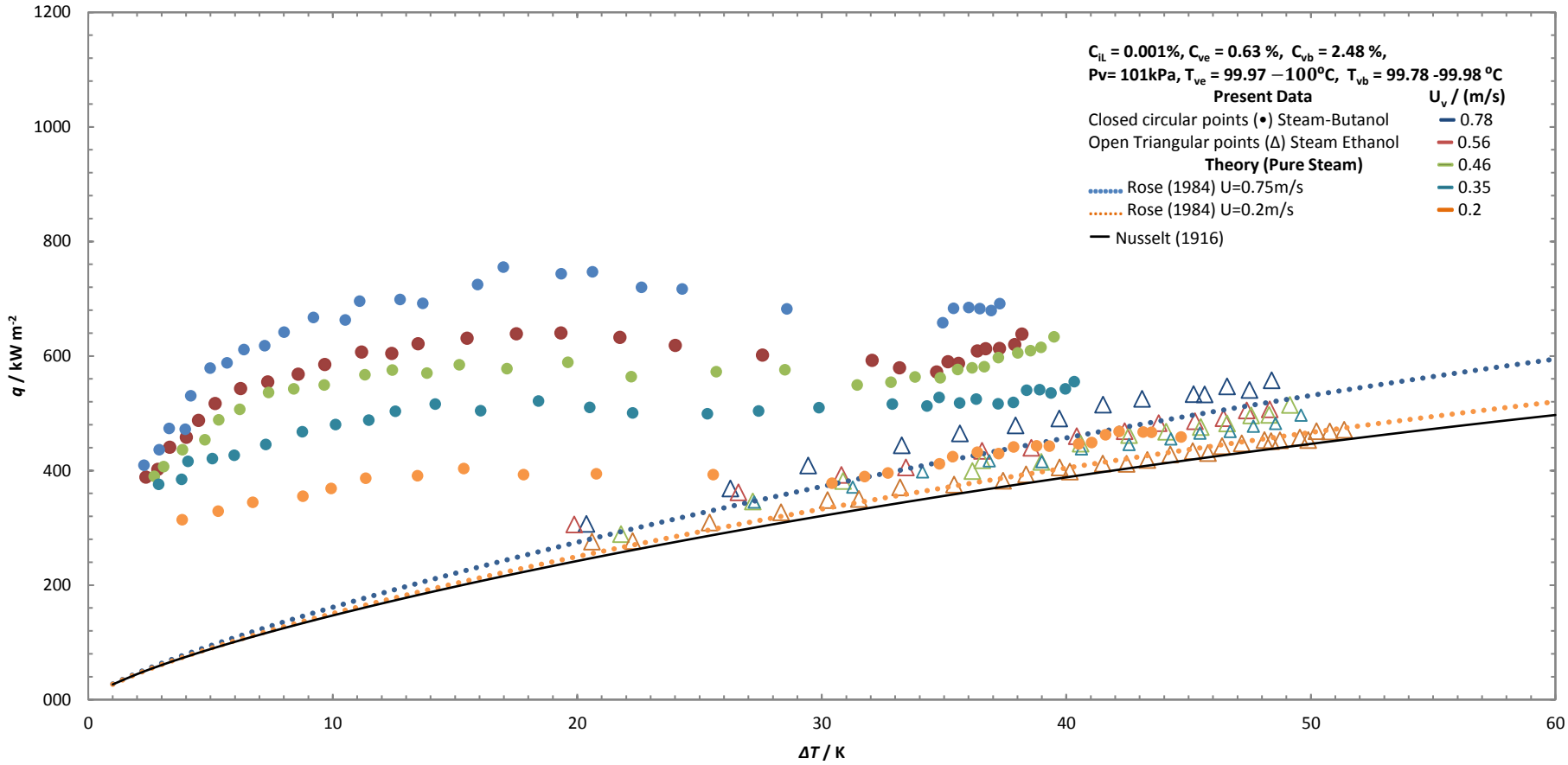

Figure 6-2: (a)-(g) shows variation of heat flux against vapour-to-surface temperature difference for varying vapour velocities at each butanol mass concentration. (a) C_{iL} = 0.001%, (b) C_{iL} = 0.005%, (c) C_{iL} = 0.01%, (d) C_{iL} = 0.025%, (e) C_{iL} = 0.05%, (f) C_{iL} = 0.1%, (g) C_{iL} = 0.5%. Steam-butanol data is presented with closed points and steam-ethanol data with open points. Test section vapour pressure is 101 kPa.

(b)

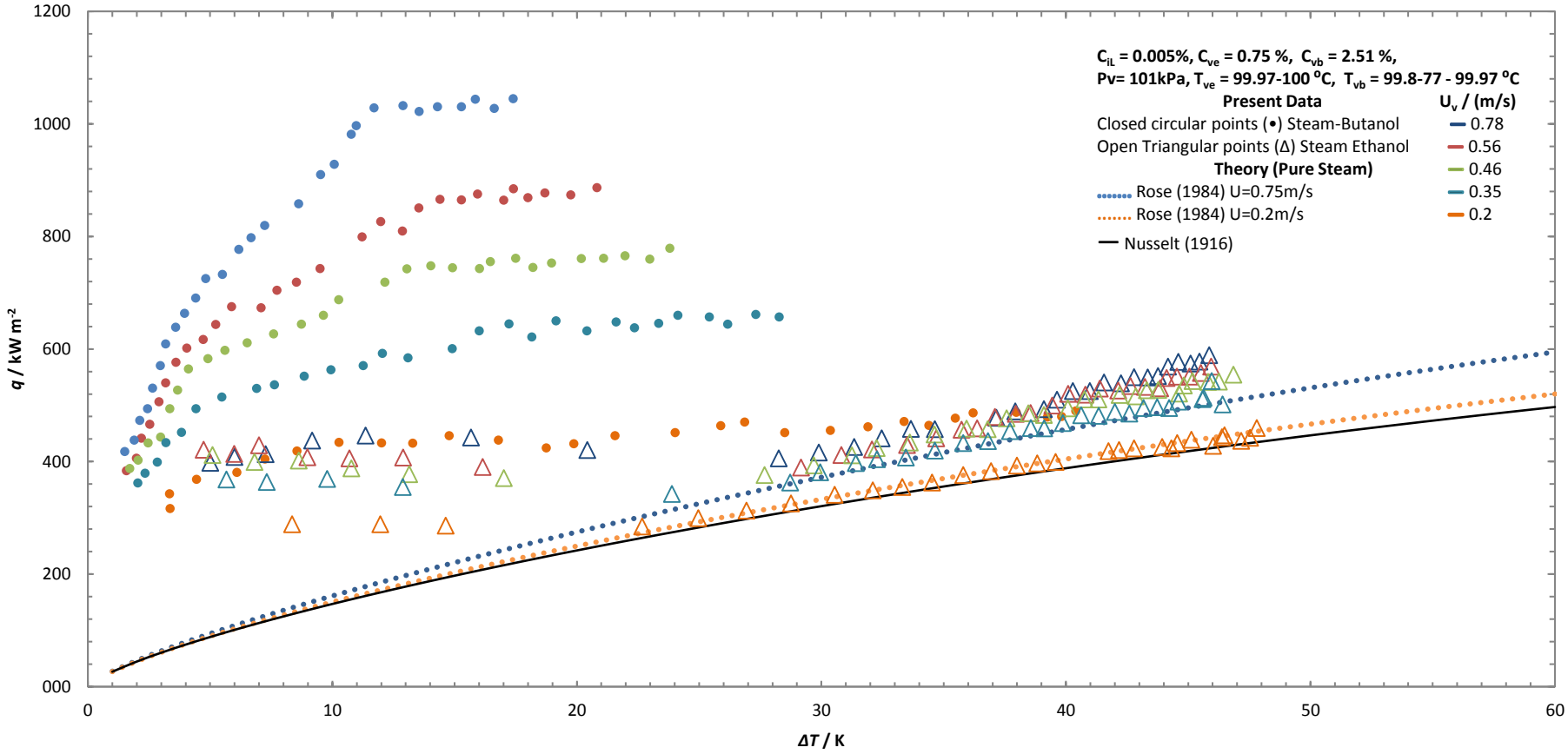

Figure 6.2 (Continued).

(c)

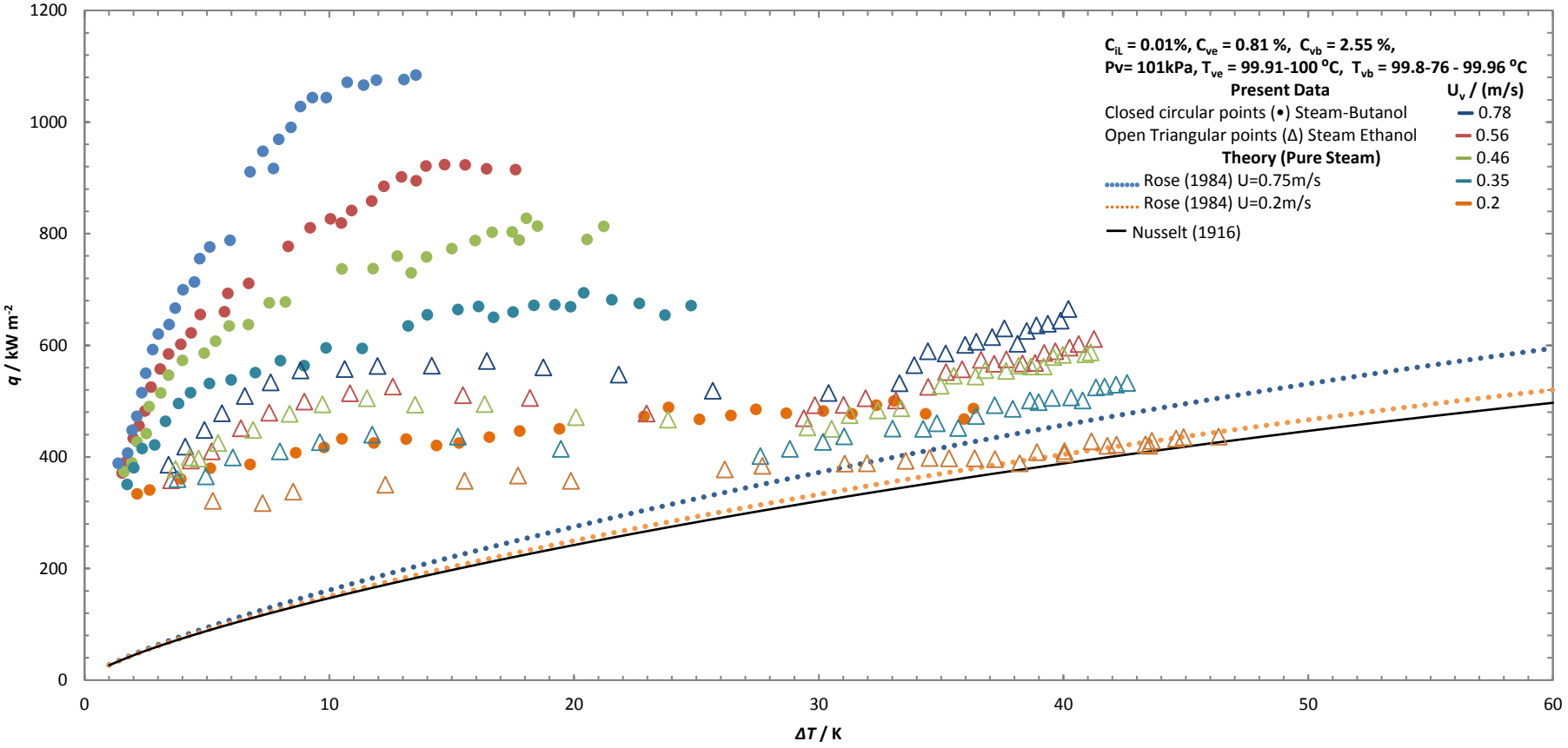

Figure 6.2 (Continued).

(d)

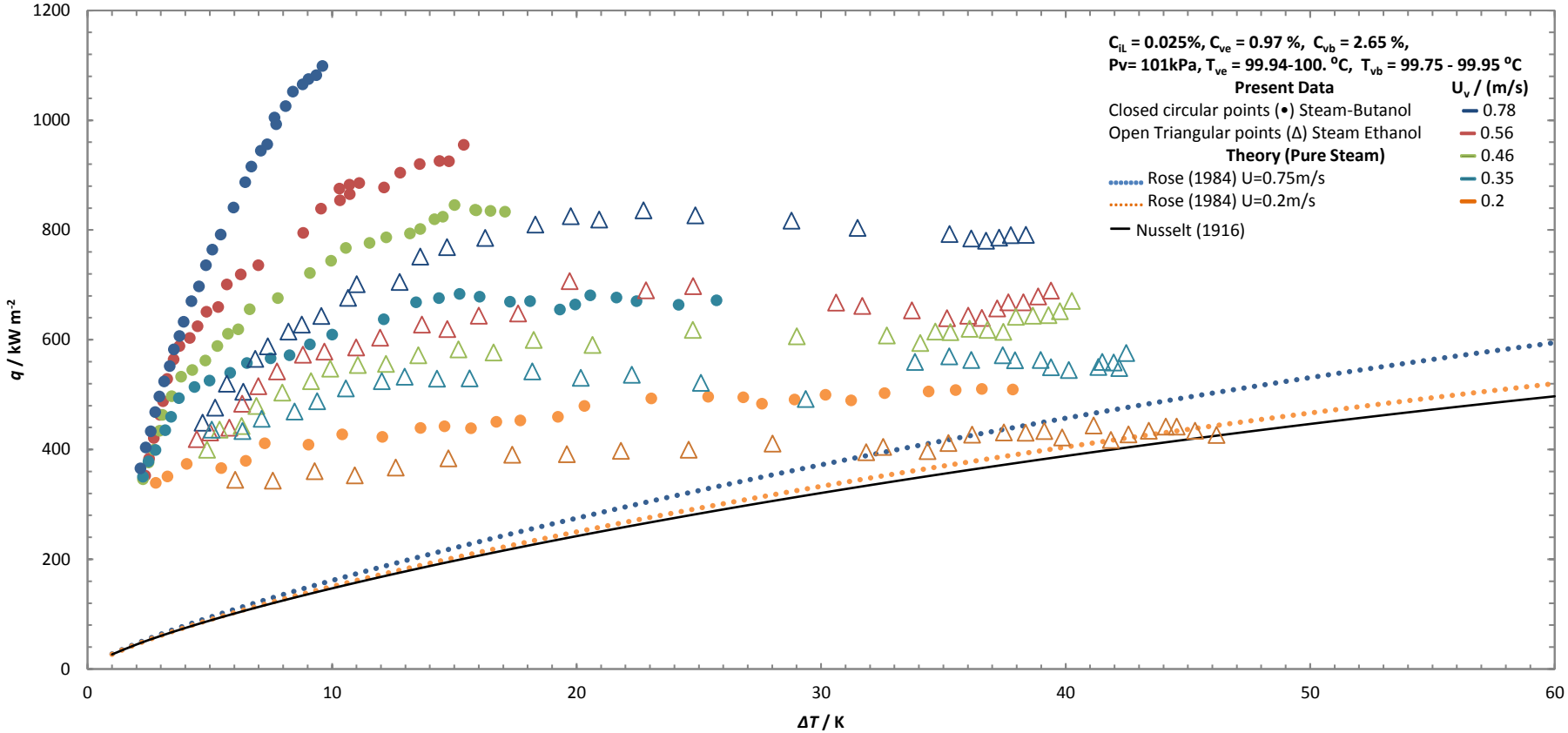

Figure 6.2 (Continued).

(e)

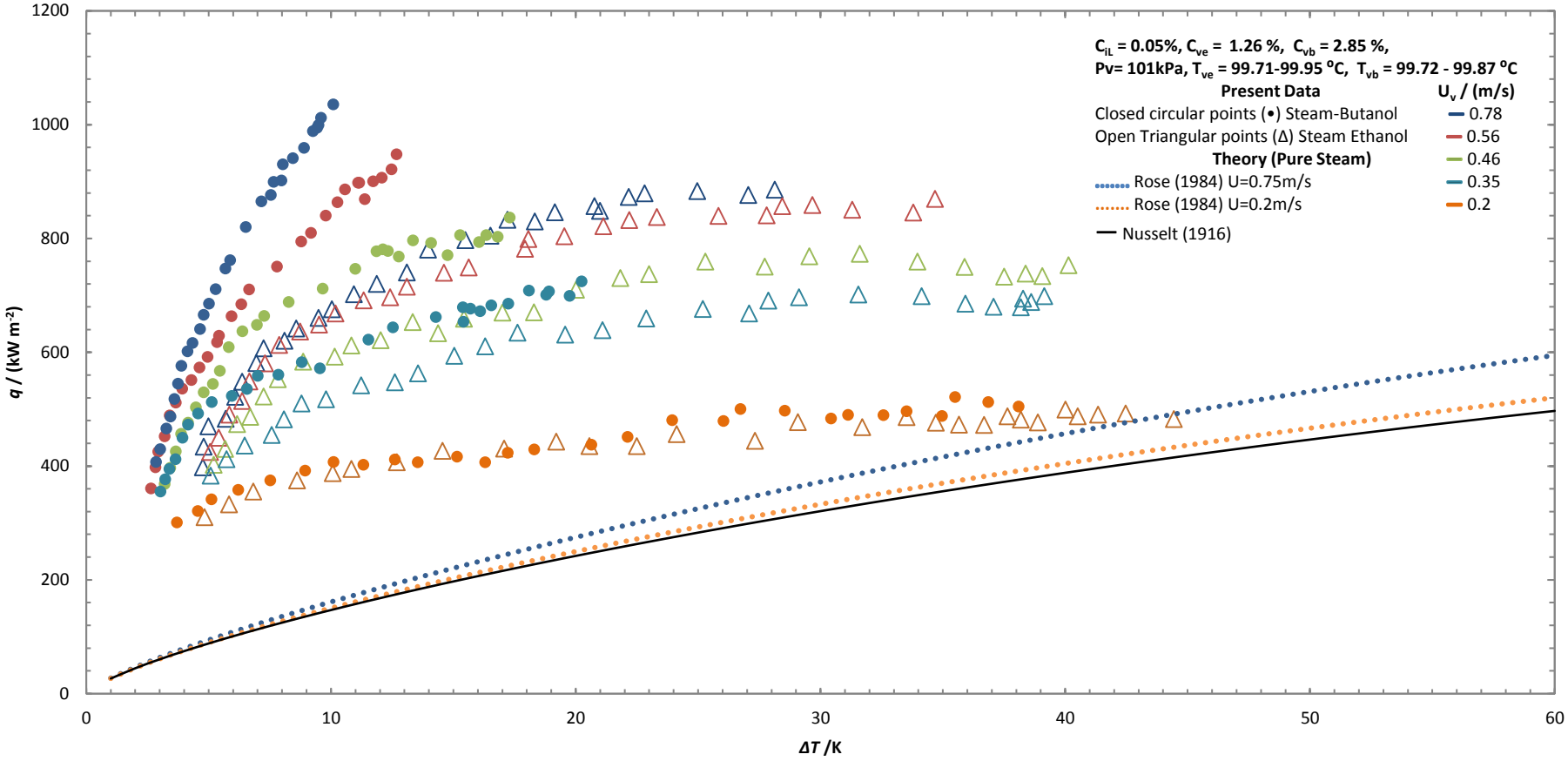

Figure 6.2 (Continued).

(f)

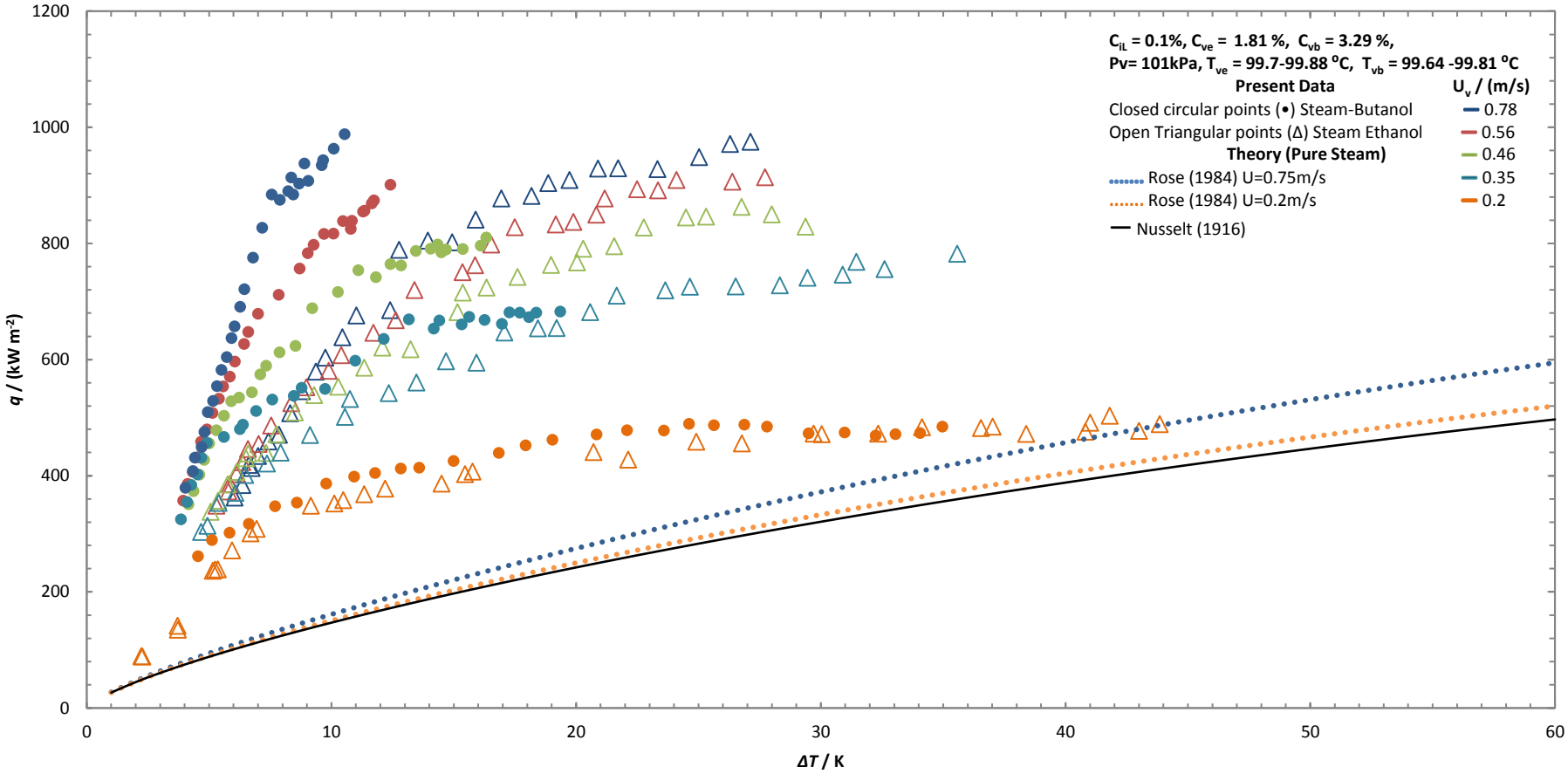

Figure 6.2 (Continued).

(g)

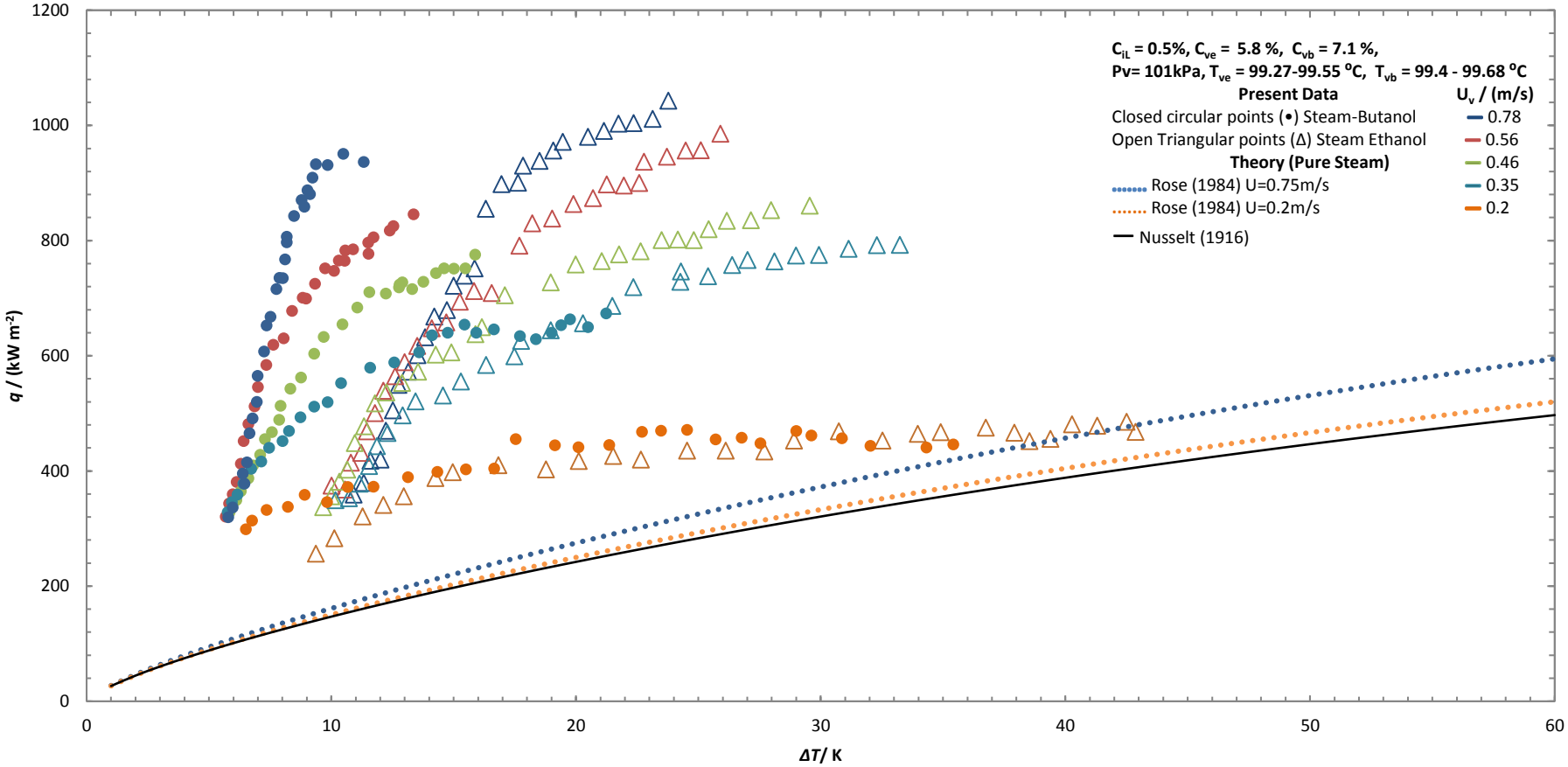

Figure 6.2 (Continued).

(a)

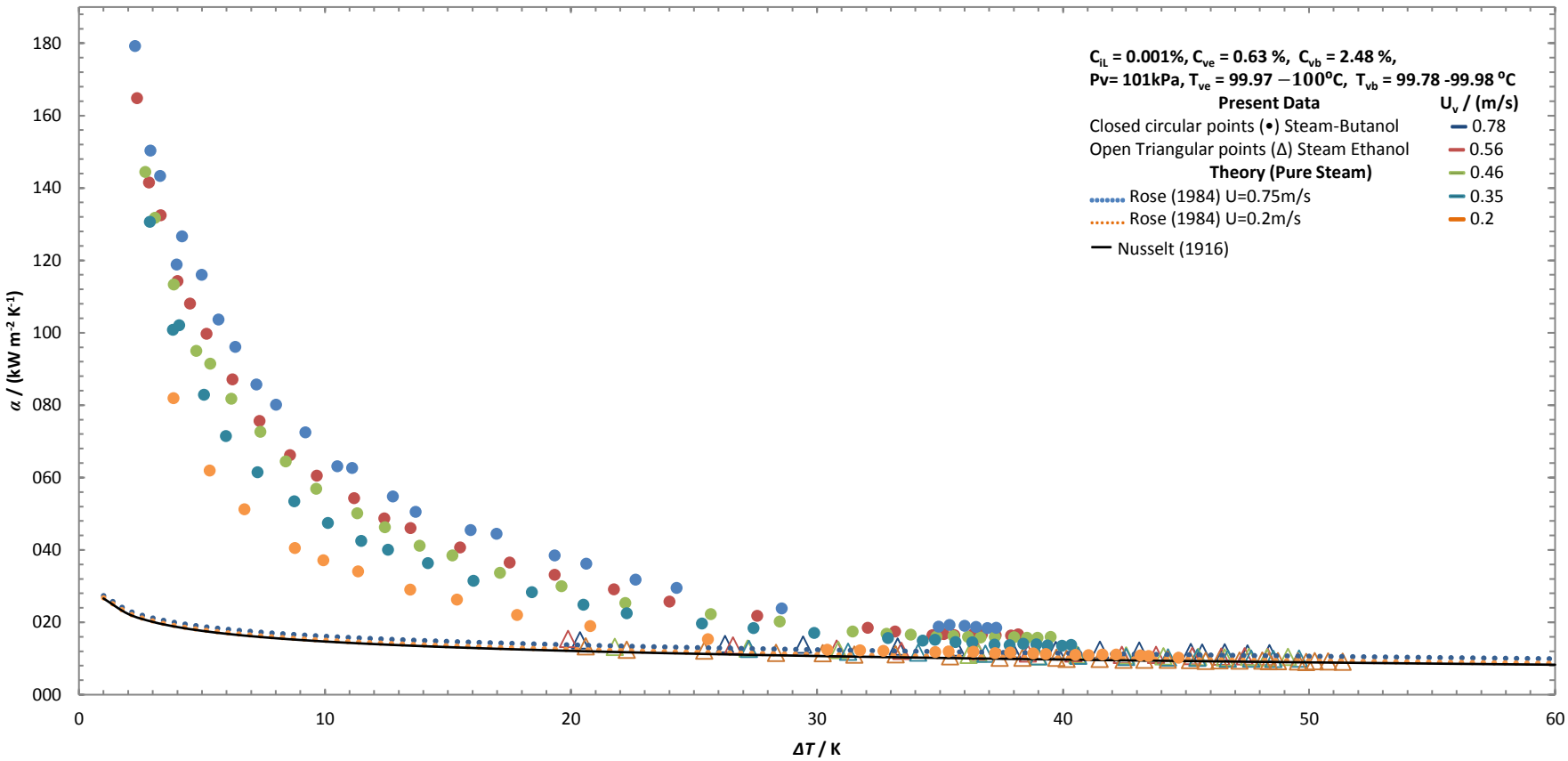

Figure 6-3: (a)-(g) shows variation of heat transfer coefficient against vapour-to-surface temperature difference for varying vapour velocities at each butanol mass concentration. (a) C_{iL} = 0.001%, (b) C_{iL} = 0.005%, (c) C_{iL} = 0.01%, (d) C_{iL} = 0.025%, (e) C_{iL} = 0.05%, (f) C_{iL} = 0.1%, (g) C_{iL} = 0.5%. Steam-butanol data is presented with closed points and steam-ethanol data with open points. Test section vapour pressure is 101 kPa.

(b)

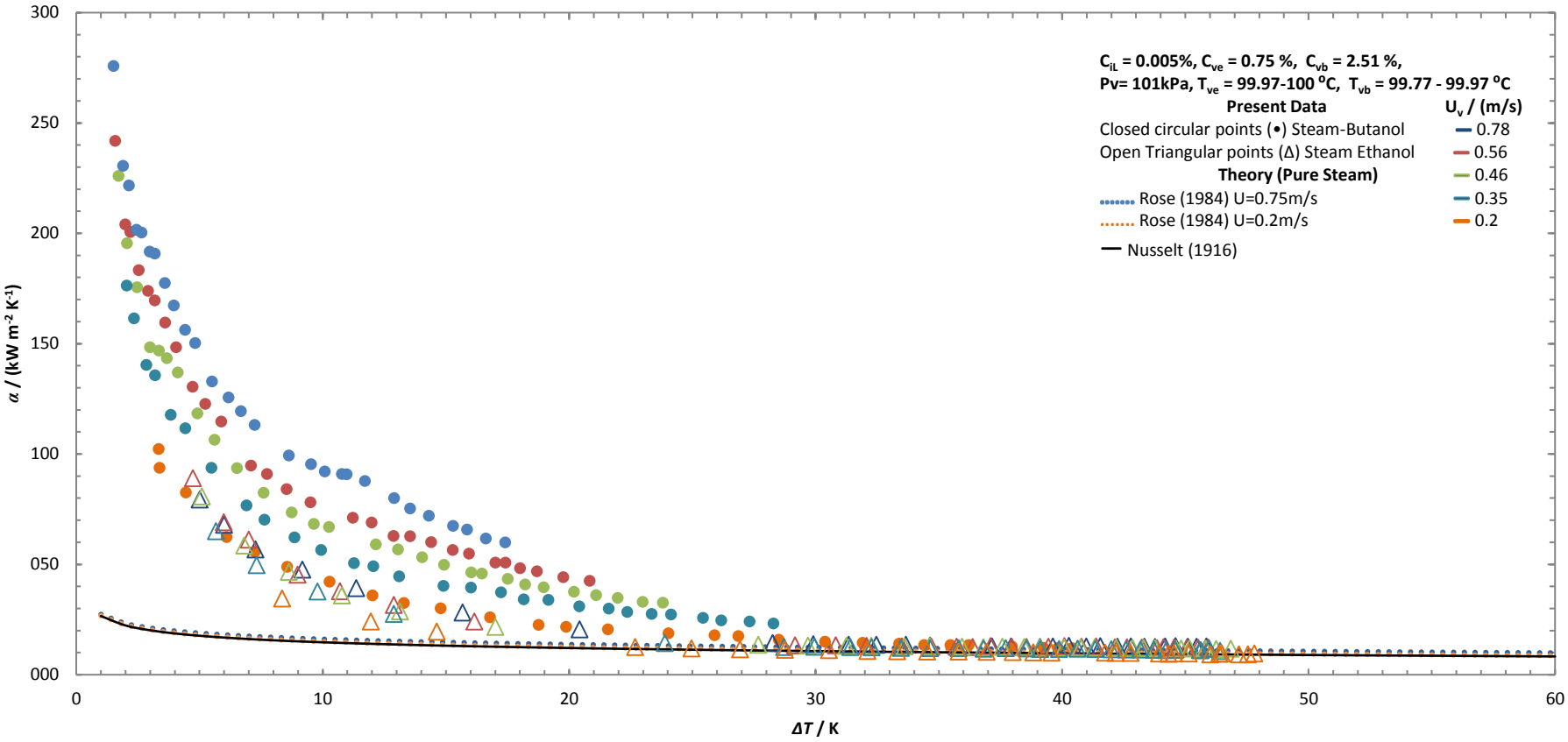

Figure 6.3 (Continued).

(c)

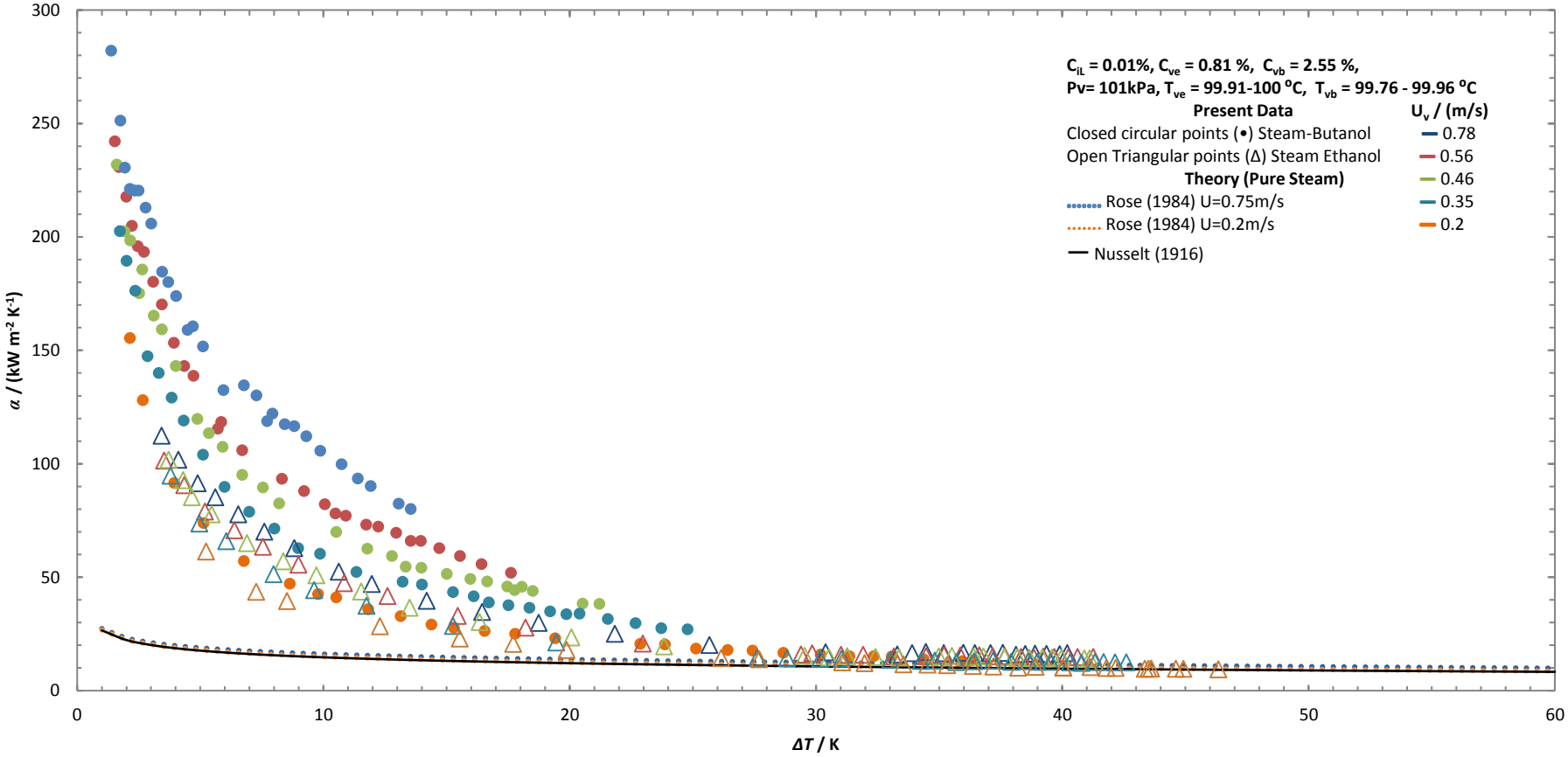

Figure 6.3 (Continued).

(d)

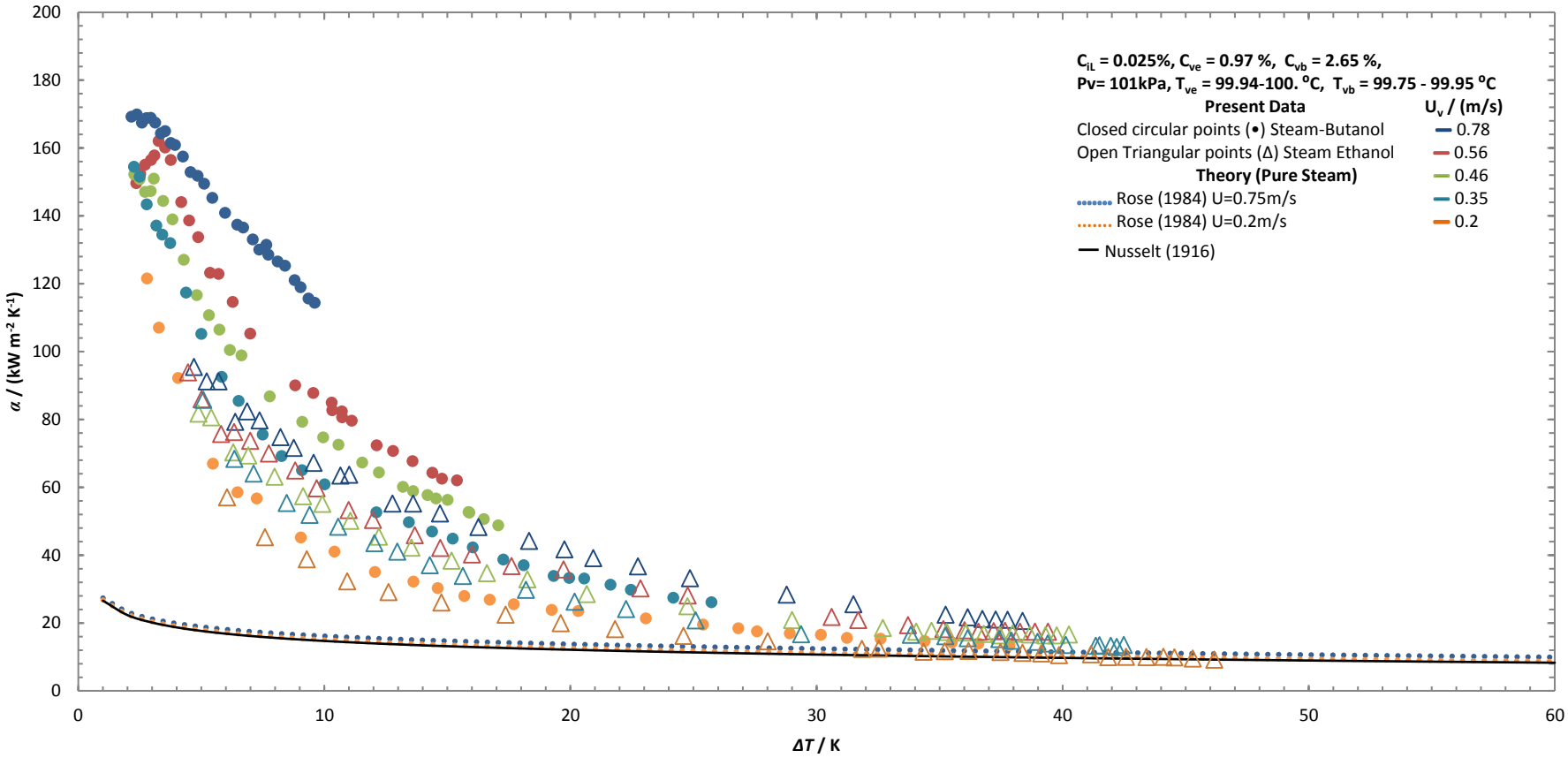

Figure 6.3 (Continued).

(e)

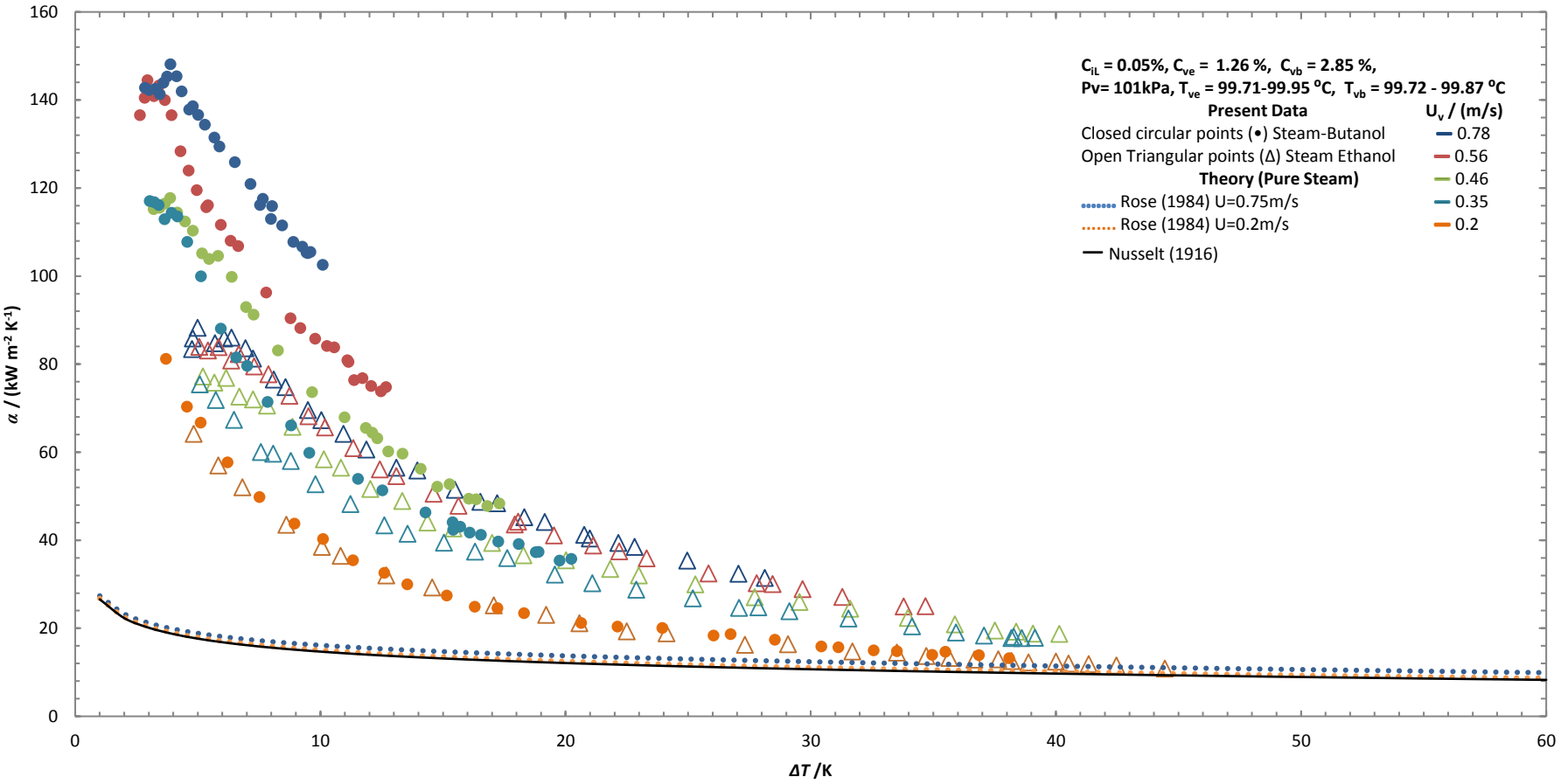

Figure 6.3 (Continued).

(f)

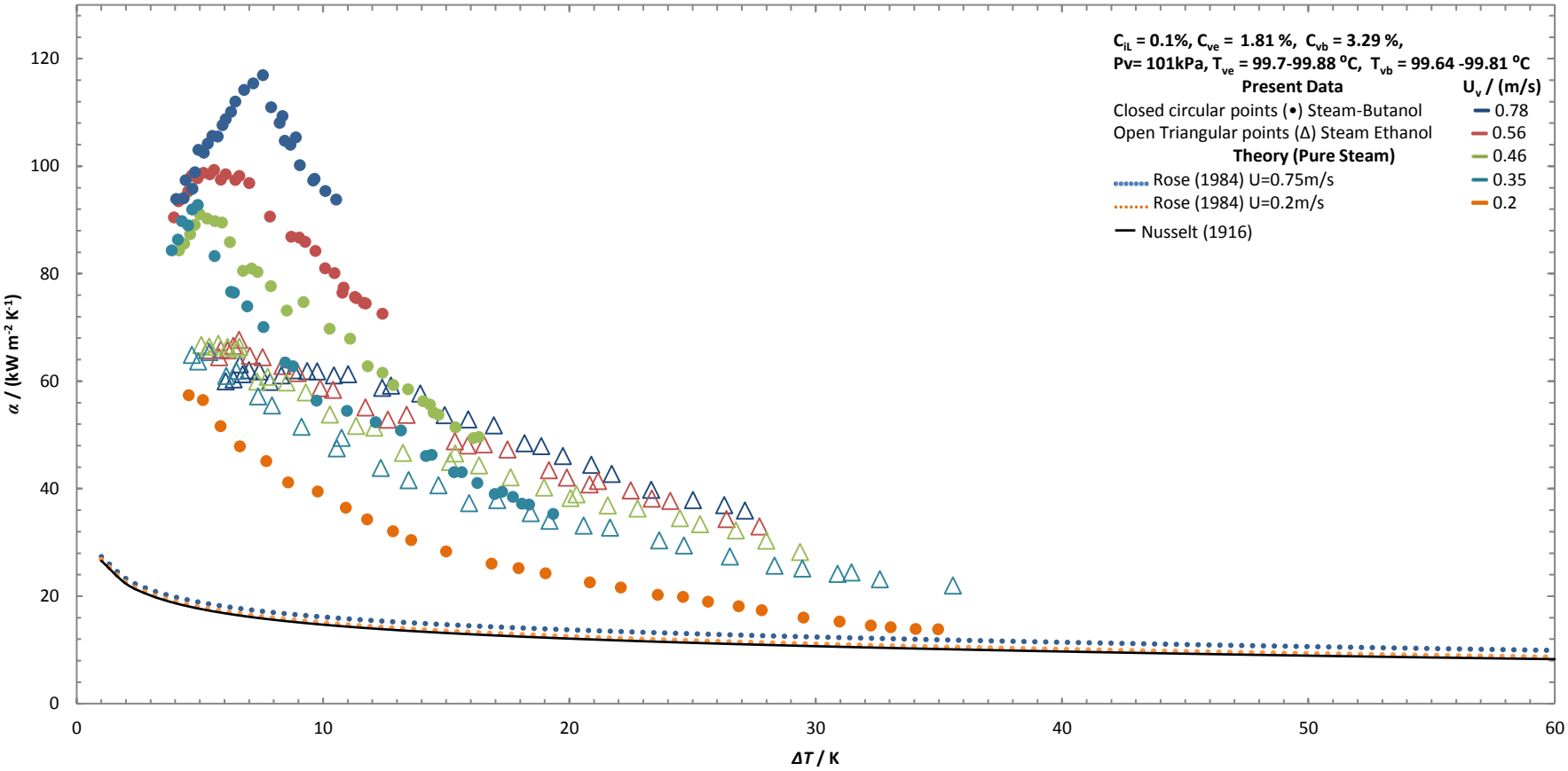

Figure 6.3 (Continued).

(g)

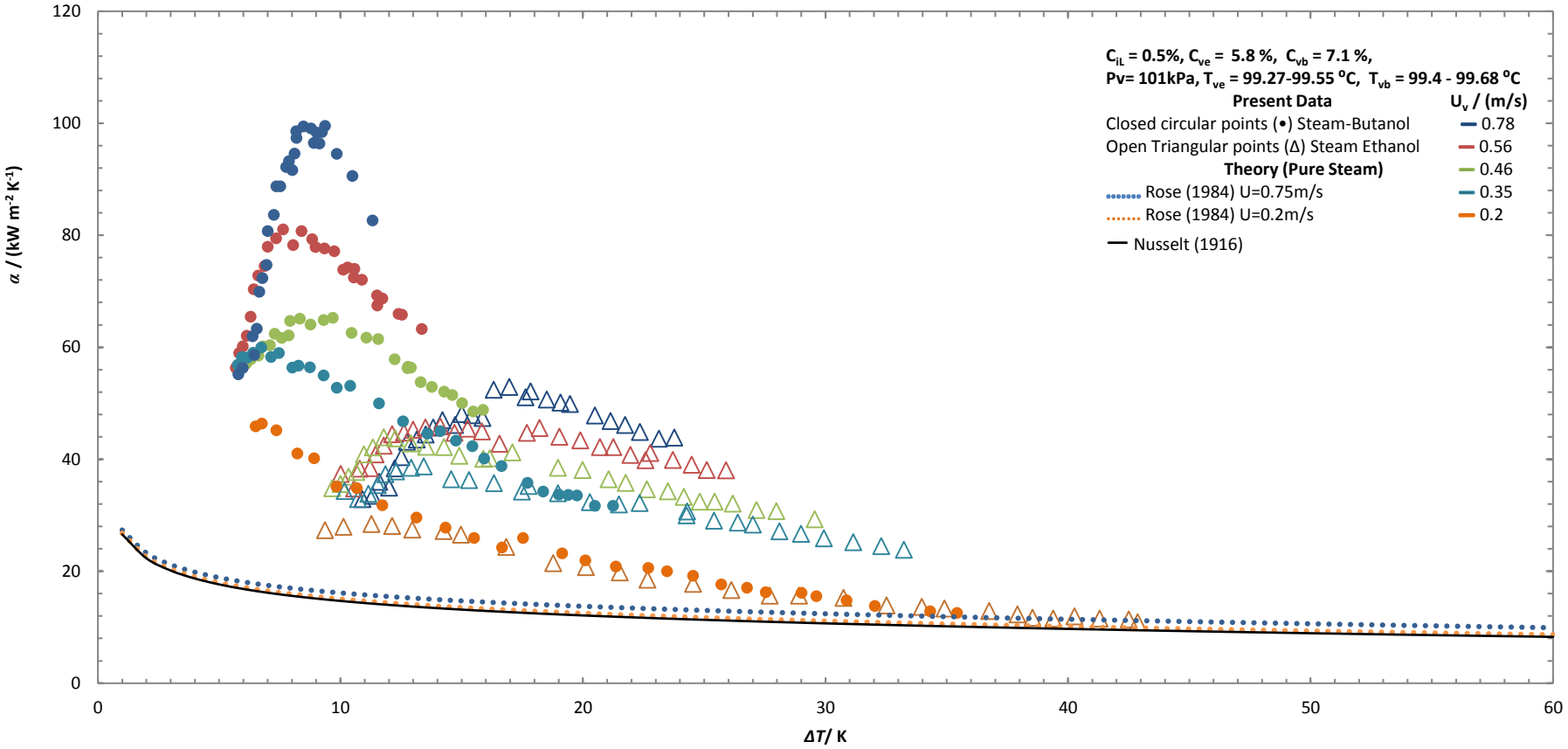

Figure 6.3 (Continued).

(a)

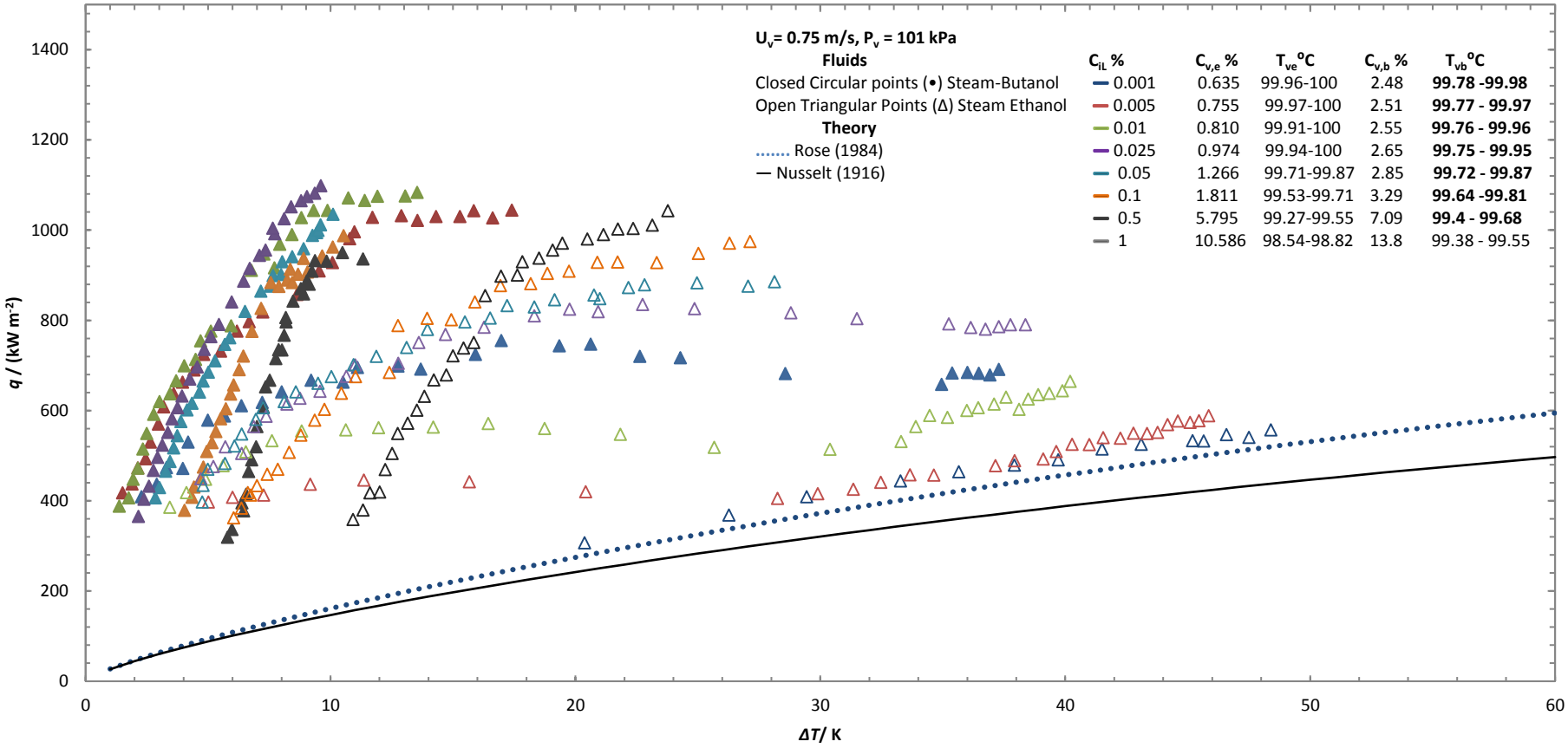

Figure 6-4: (a)-(e) shows variation of heat flux against vapour-to-surface temperature difference for varying mass concentrations at each vapour velocity. (a) Uv = 0.75 m/s, (b) Uv = 0.56 m/s, (c) Uv = 0.46 m/s, (d) Uv = 0.35 m/s, (e) Uv = 0.20 m/s. Steam-butanol data is presented with closed points and steam-ethanol data with open points. Test section vapour pressure is 101 kPa.

(b)

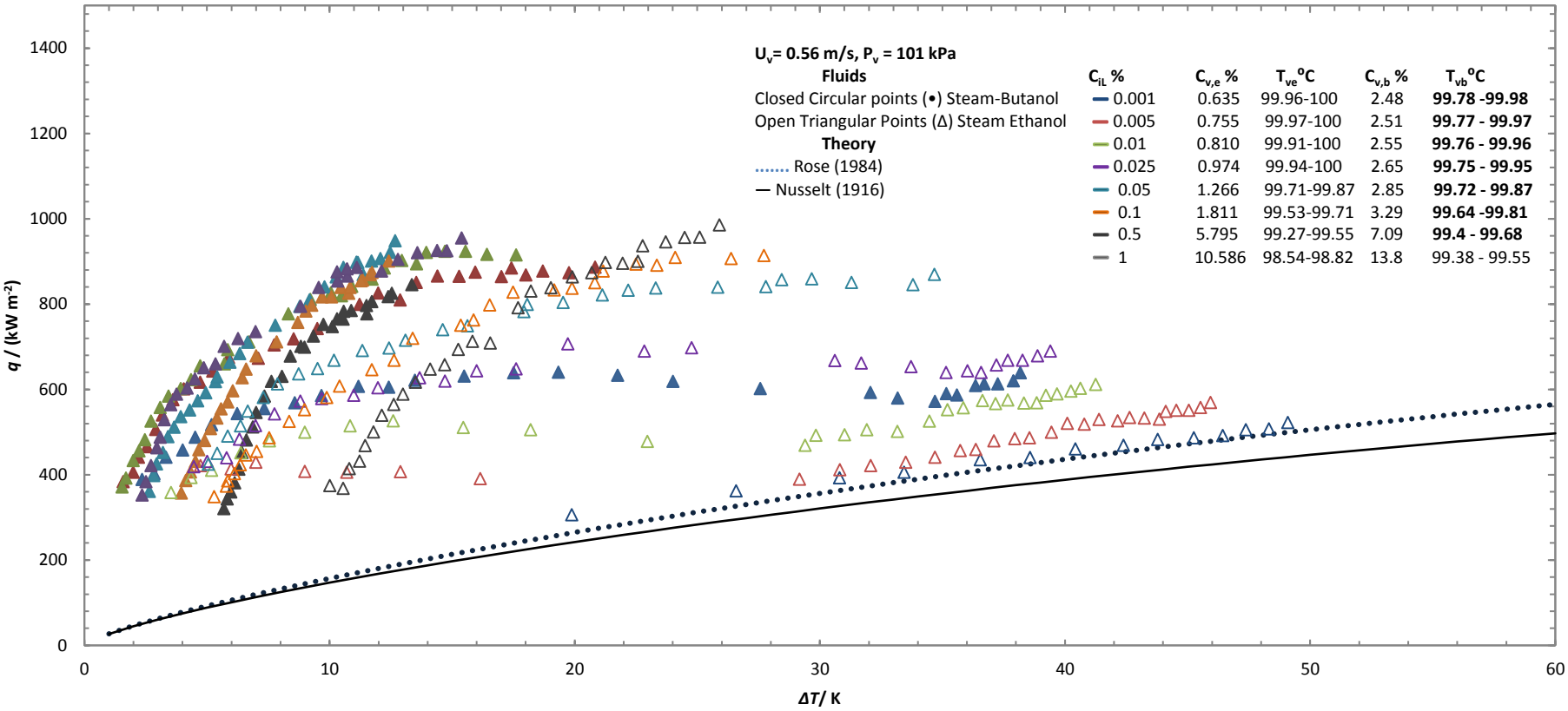

Figure 6.4 (Continued).

(c)

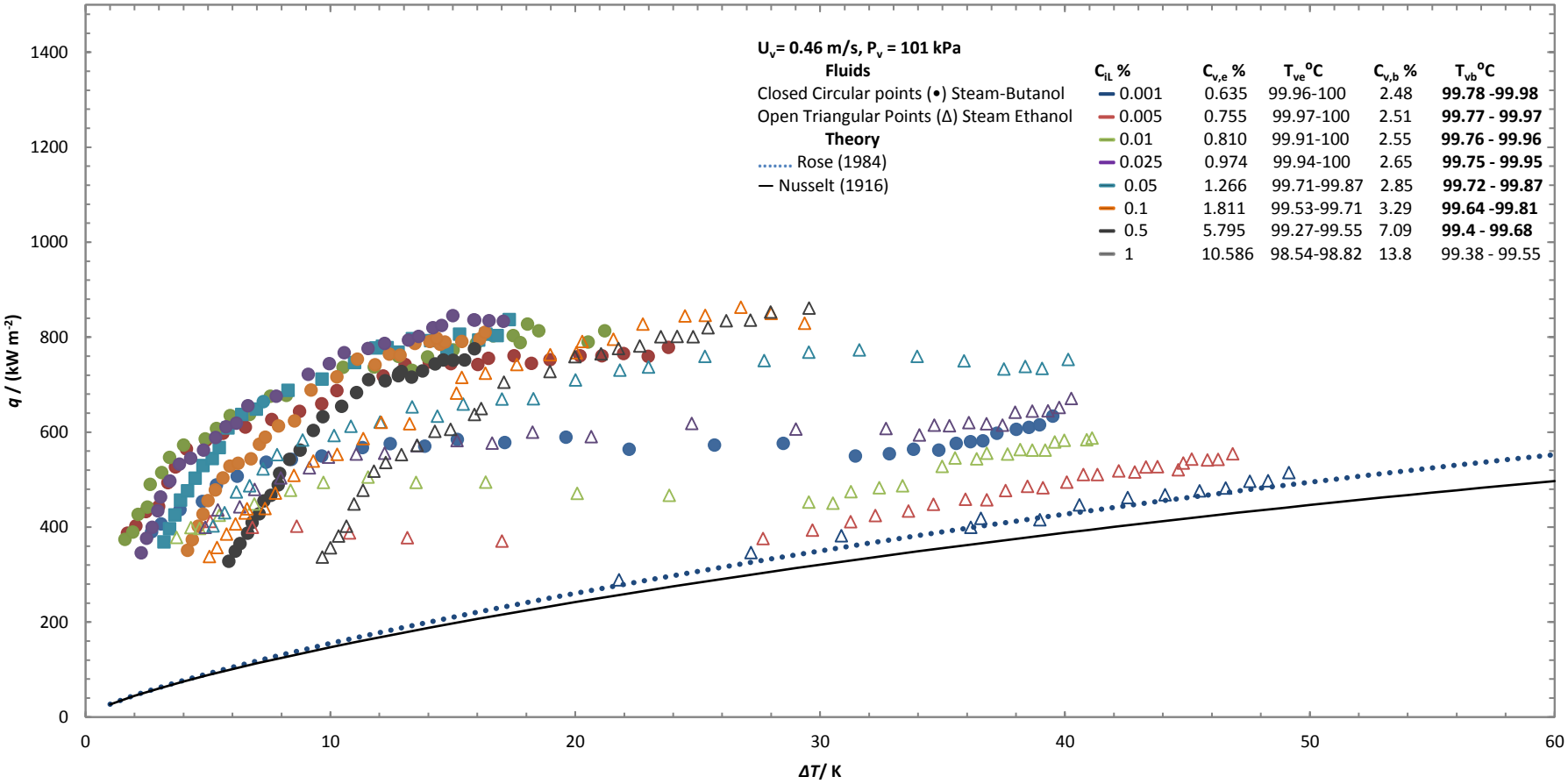

Figure 6.4 (Continued).

(d)

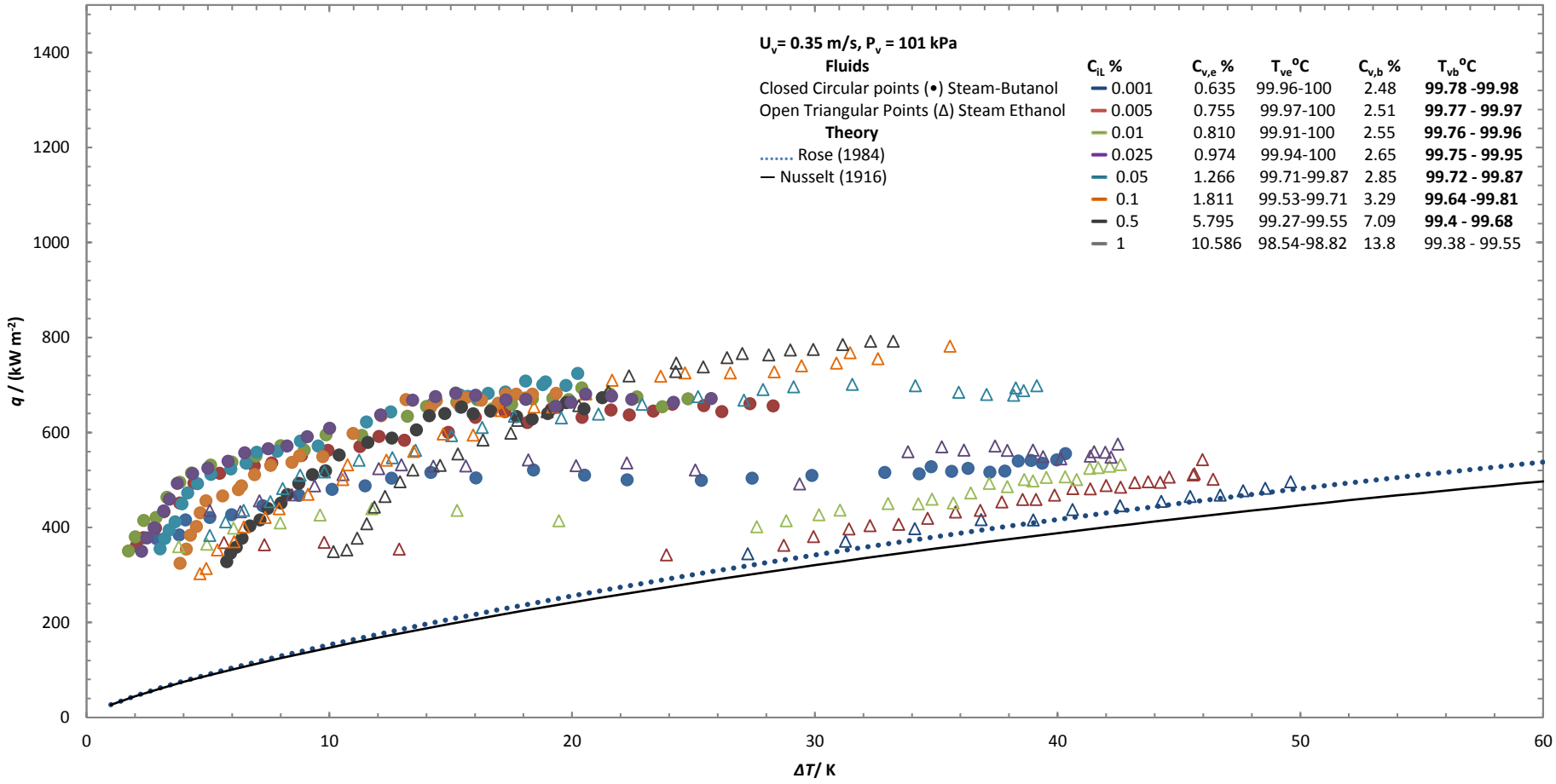

Figure 6.4 (Continued).

(e)

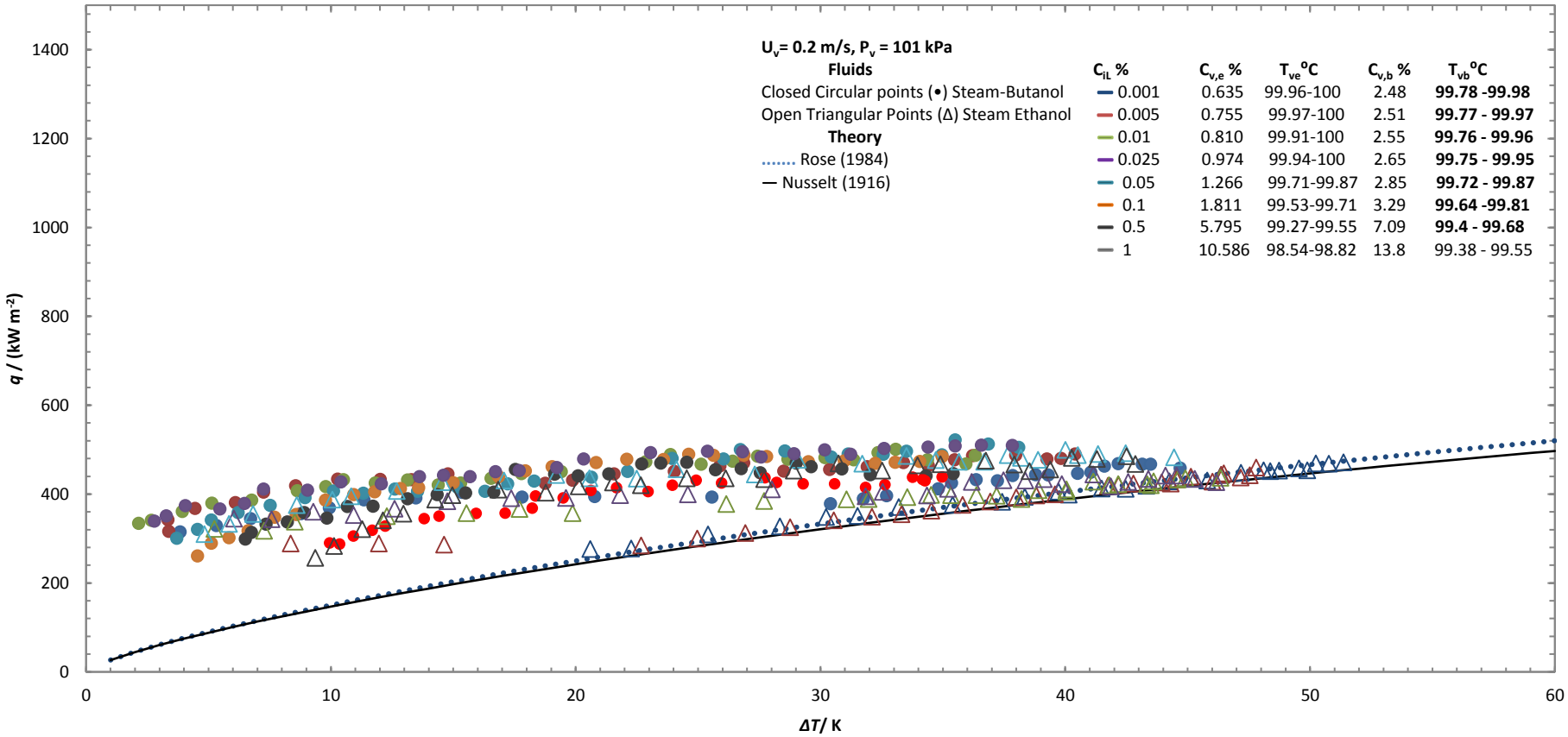

Figure 6.4 (Continued).

(a)

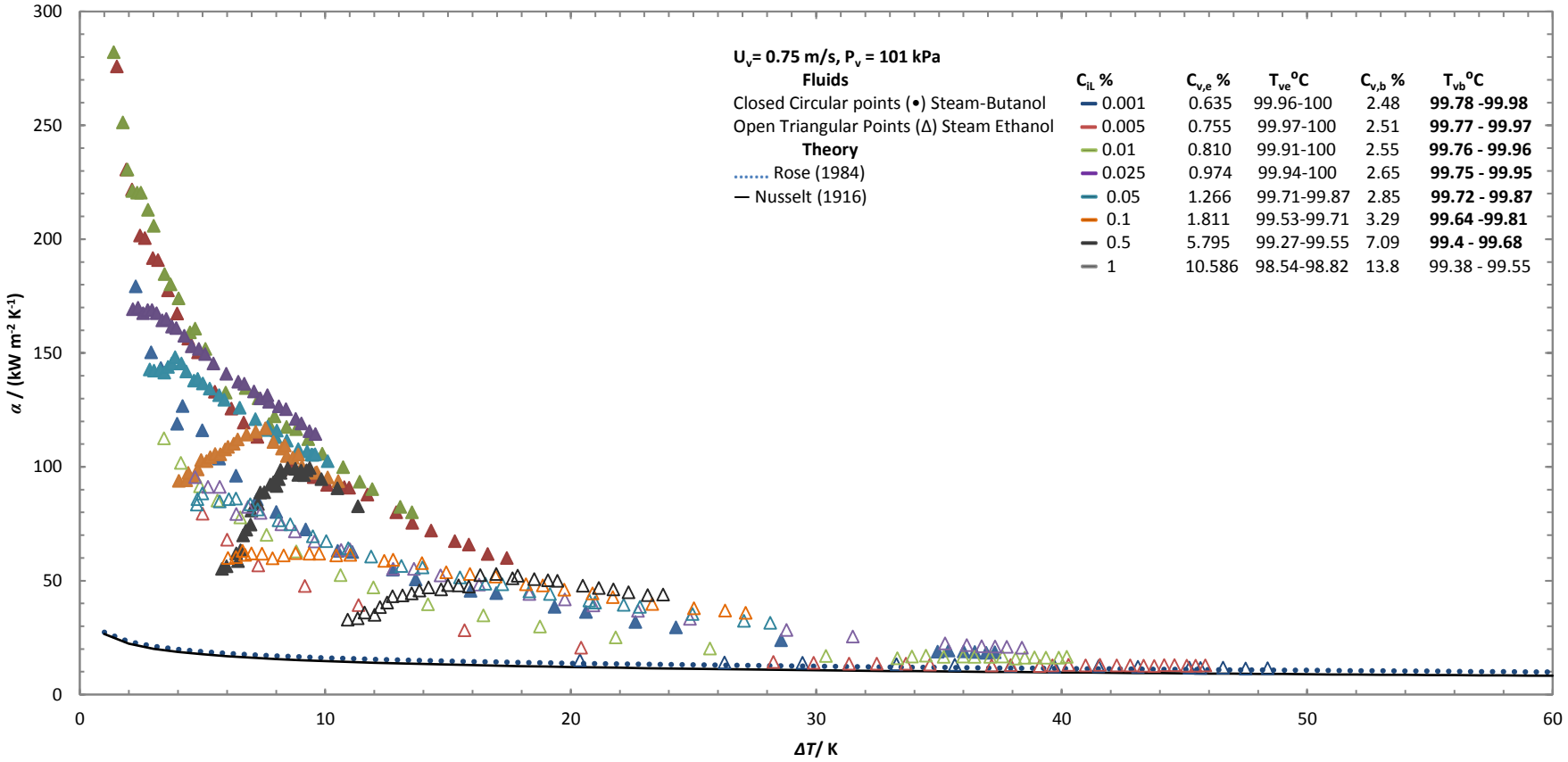

Figure 6-5: (a)-(e) shows variation of heat transfer coefficient against vapour-to-surface temperature difference for varying mass concentrations at each vapour velocity. (a) U_v = 0.75 m/s, (b) U_v = 0.56 m/s, (c) U_v = 0.46 m/s, (d) U_v = 0.35 m/s, (e) U_v = 0.20 m/s. Steam-butanol data is presented with closed points and steam-ethanol data with open points. Test section vapour pressure is 101 kPa.

(b)

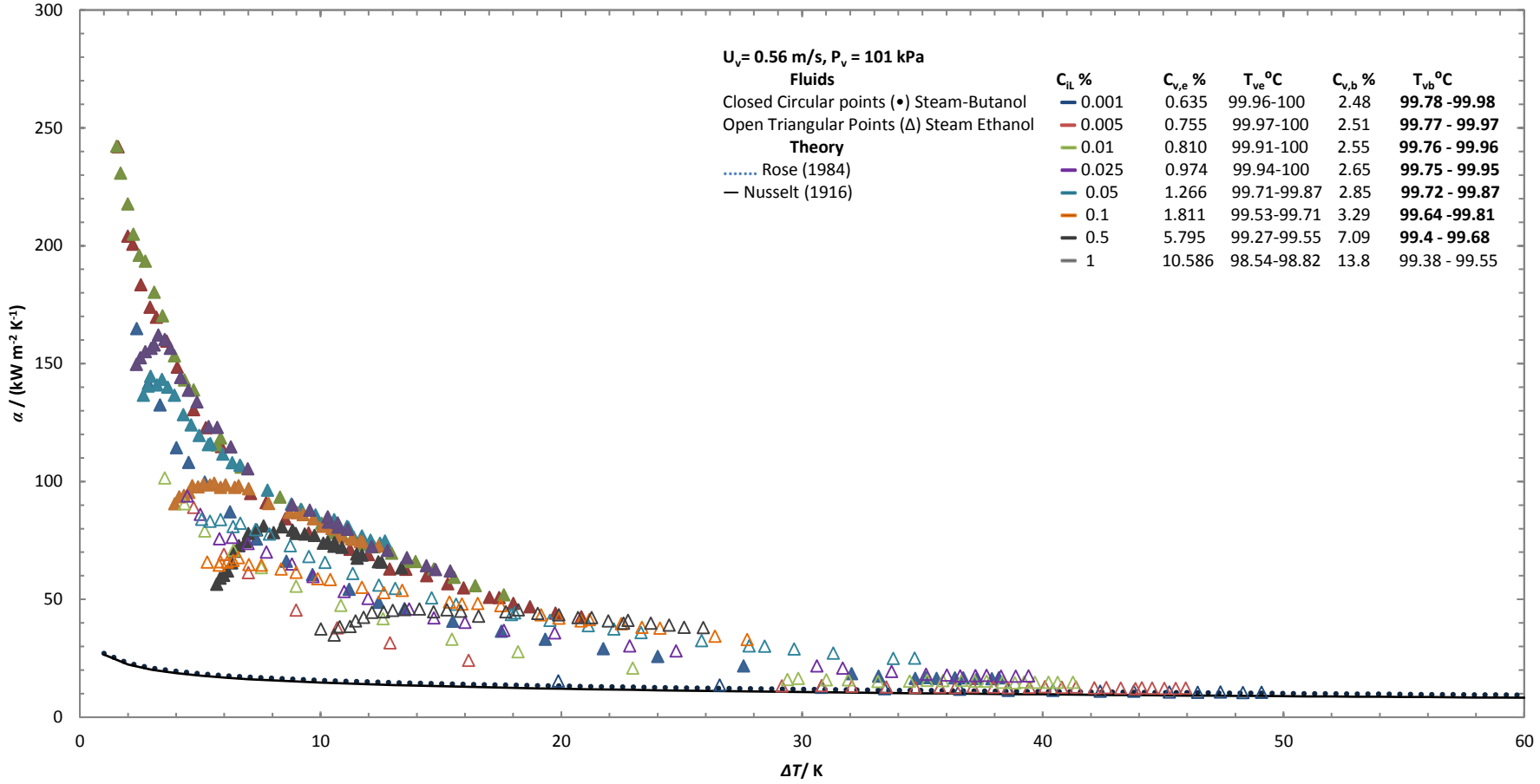

Figure 6.5 (Continued).

(c)

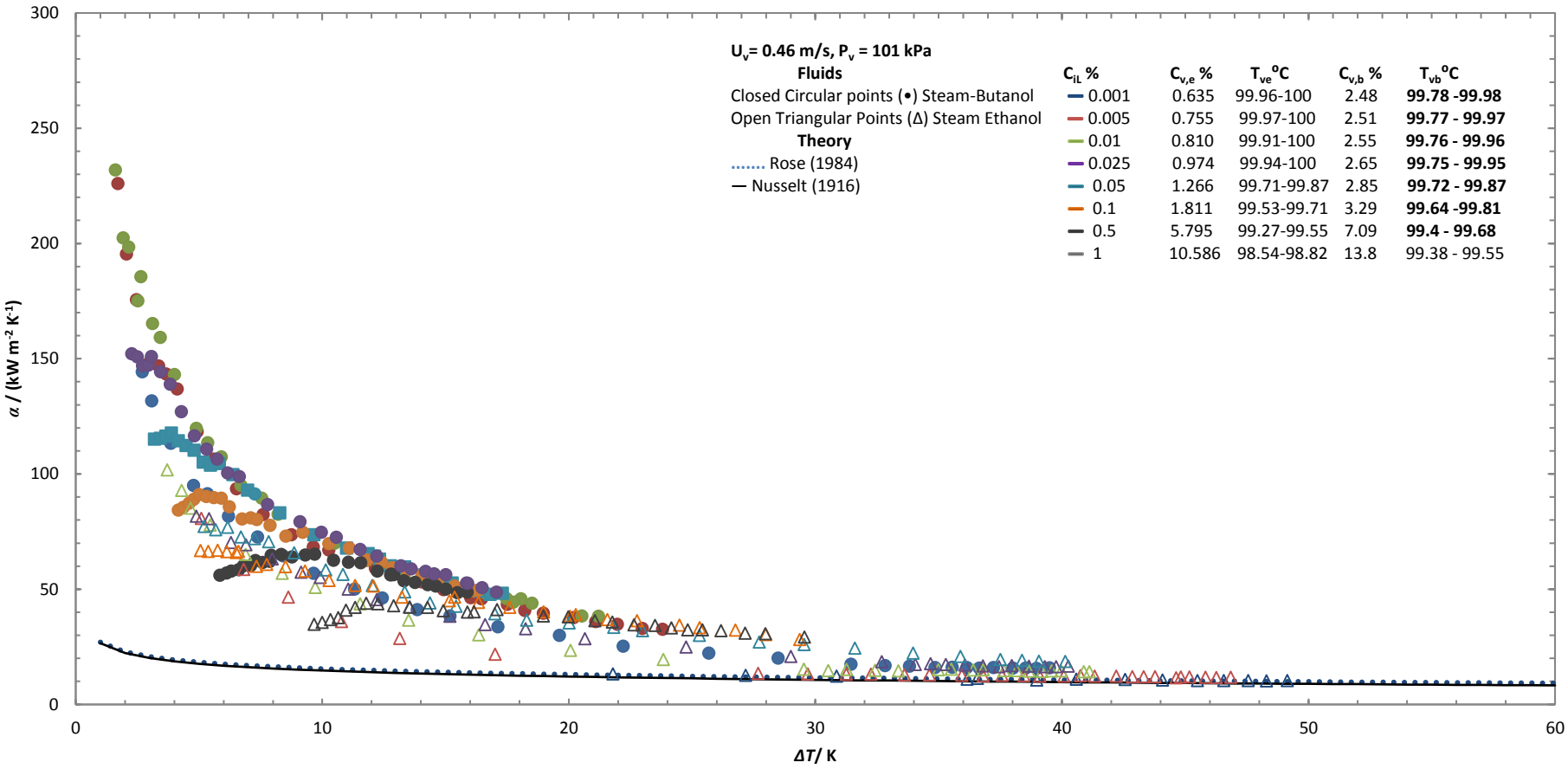

Figure 6.5 (Continued).

(d)

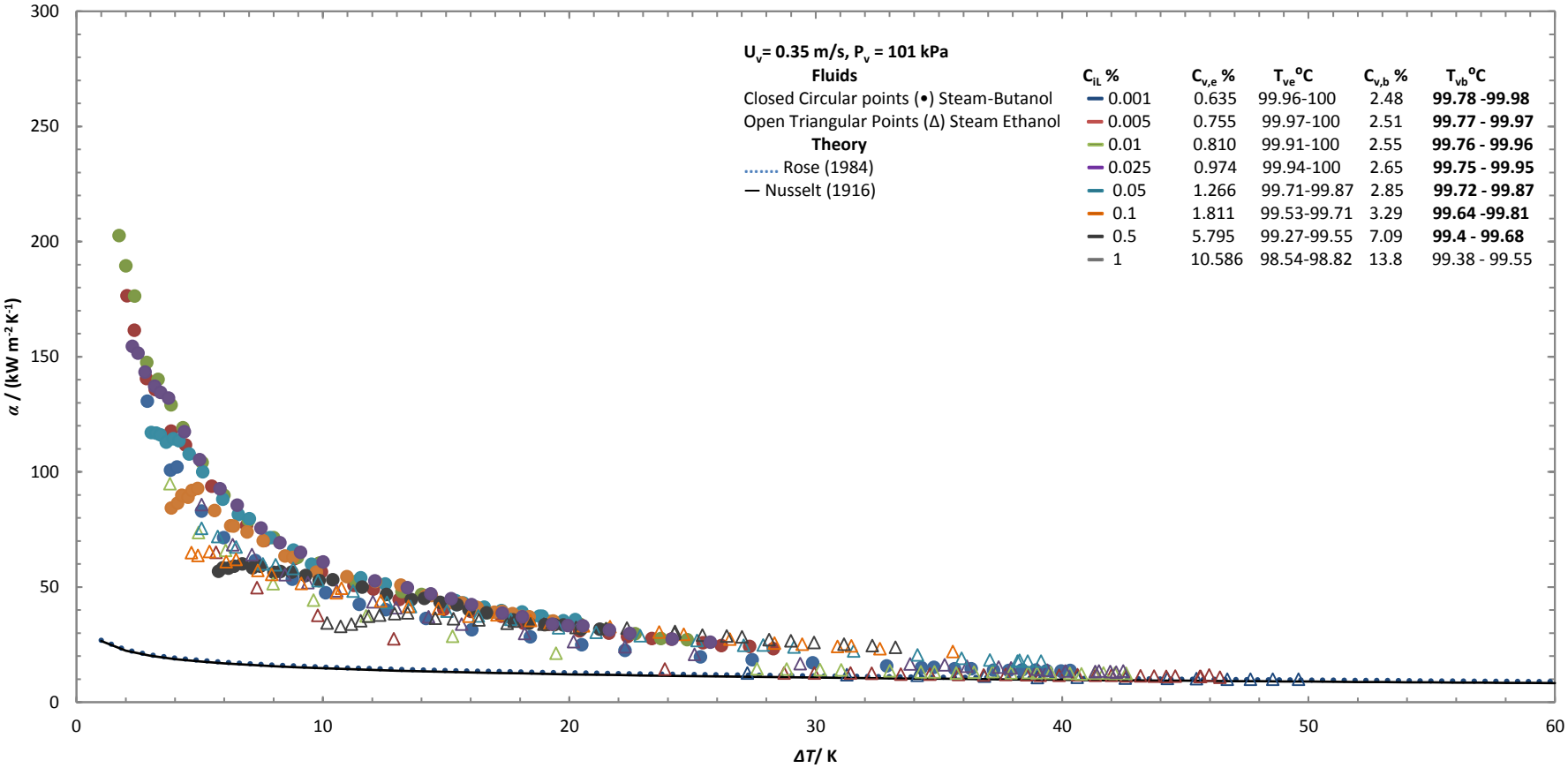

Figure 6.5 (Continued).

(e)

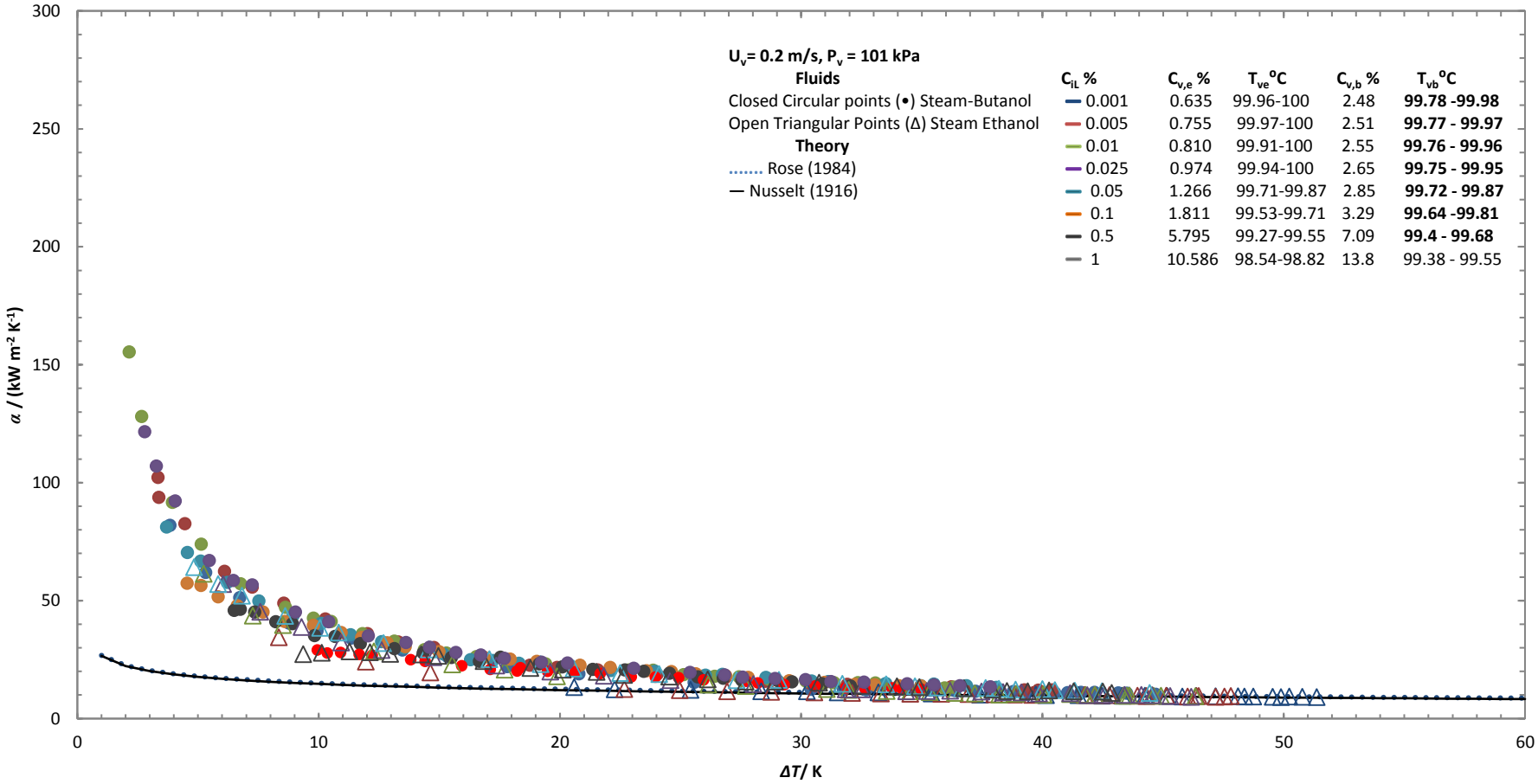

Figure 6.5 (Continued).

6.2.1 Enhancement

Equation 5.3 of enhancement ratio for steam-ethanol mixtures can be modified for steam-butanol mixtures as:

$$\varepsilon_{sb} = \left(\frac{q_{sb}}{q_{Ro,ps}} \right)_{\Delta T, U_v} \tag{6.1}$$

where,

ε_{sb} is the enhancement ratio of the steam-butanol mixture at a given vapour velocity and vapour-to-surface temperature difference.

q_{sb} is observed heat flux for steam-butanol mixtures at a given vapour velocity and vapour-to-surface temperature difference.

$q_{Ro,ps}$ is the theoretical heat flux for pure steam obtained by Rose (1984) theory at a given vapour velocity and vapour-to-surface temperature difference.

For pure steam data, Rose (1984) theory was employed for each vapour velocity as it gives a precise representation of steam experimental data in this investigation (see chapter 5 figures 5.1). Since heat transfer properties are strongly dependent on the vapour-to-surface temperature difference, therefore, the enhancement ratio is also dependent on the vapour-to-surface temperature difference.

Figures 6.6 Shows enhancement ratio for steam-butanol mixtures for various mass compositions and vapour velocities. For all the mass compositions and vapour velocities, the enhancement ratio exceeds unity over the entire range of vapour-to-surface temperature difference. The effect of vapour -to-surface temperature difference is same for steam-butanol mixtures as observed in steam-ethanol case. Butanol concentration has a significant effect on the enhancement ratios at lower vapour to surface temperature difference. At lower mass concentrations, the highest enhancement ratio of 11 was observed at the lowest vapour-to-surface temperature difference (ΔT= 1.37 K) for the mass composition of 0.05% and 0.01%. Vapour velocity also affect enhancement ratio

Figure 6.7 shows the comparison between enhancement ratios of steam-butanol and steam-ethanol mixtures. Enhancements in steam- butanol are almost twice compared to ethanol for the given conditions. Ethanol shows maximum enhancement ratio of 5.47 at vapour

velocity of 0.78m/s for ethanol mass composition of 0.01%. For the same vapour velocity and mass composition, steam-butanol mixture shows an enhancement ratio of 11.

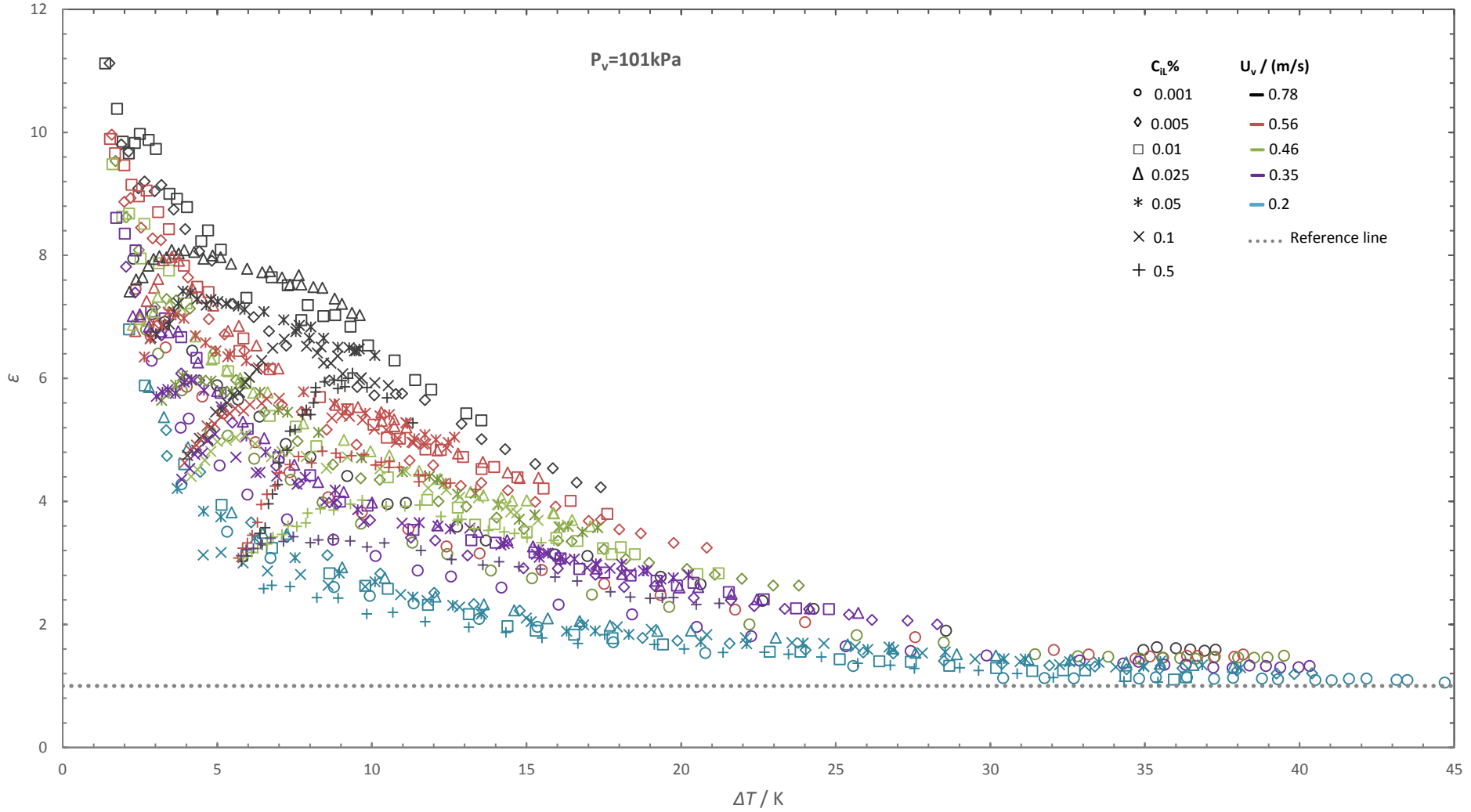

Figure 6-6: Enhancement Ratio of steam-butanol mixtures of various compositions and vapour velocities. The grey dotted line is the pure steam line used as a reference.

(a)

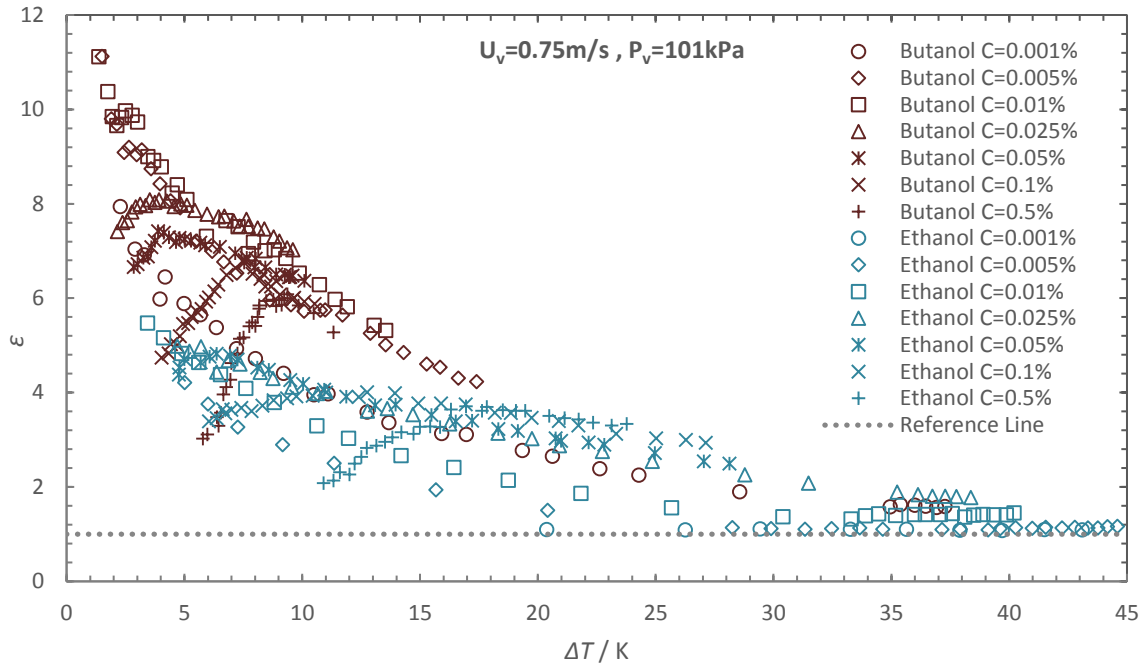

(b)

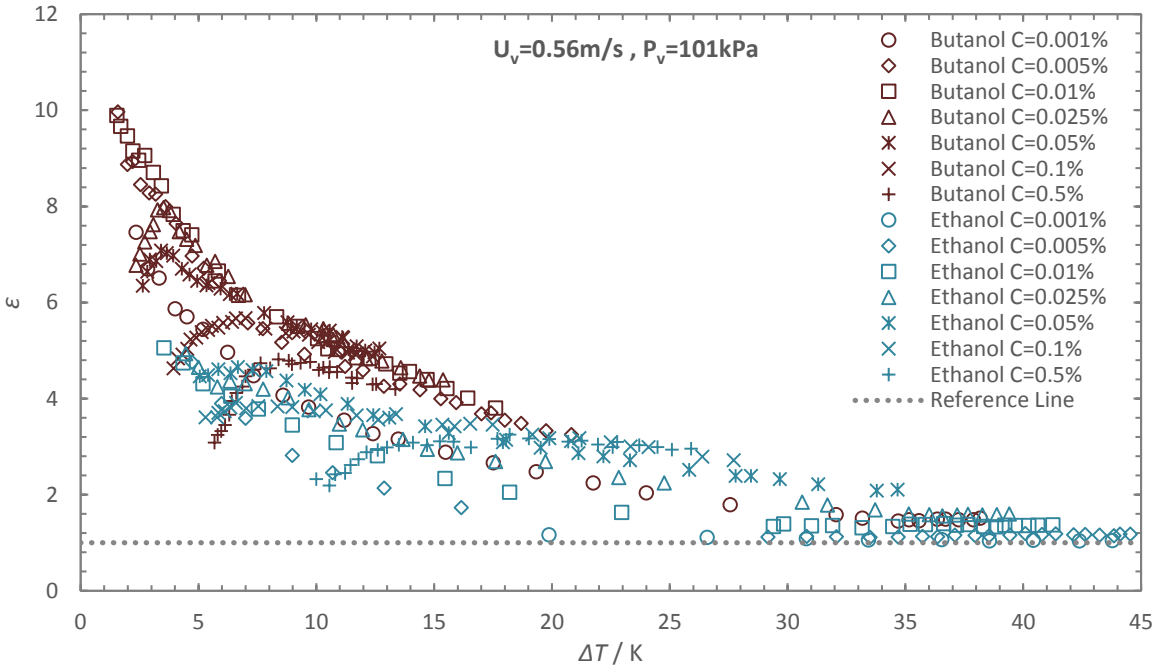

Figure 6-7: Comparison between the enhancement ratio of steam-butanol with steam-ethanol for various mass compositions at each vapour velocity. Steam-butanol results are in dark red colour and steam-ethanol results in cyan colour.

(c)

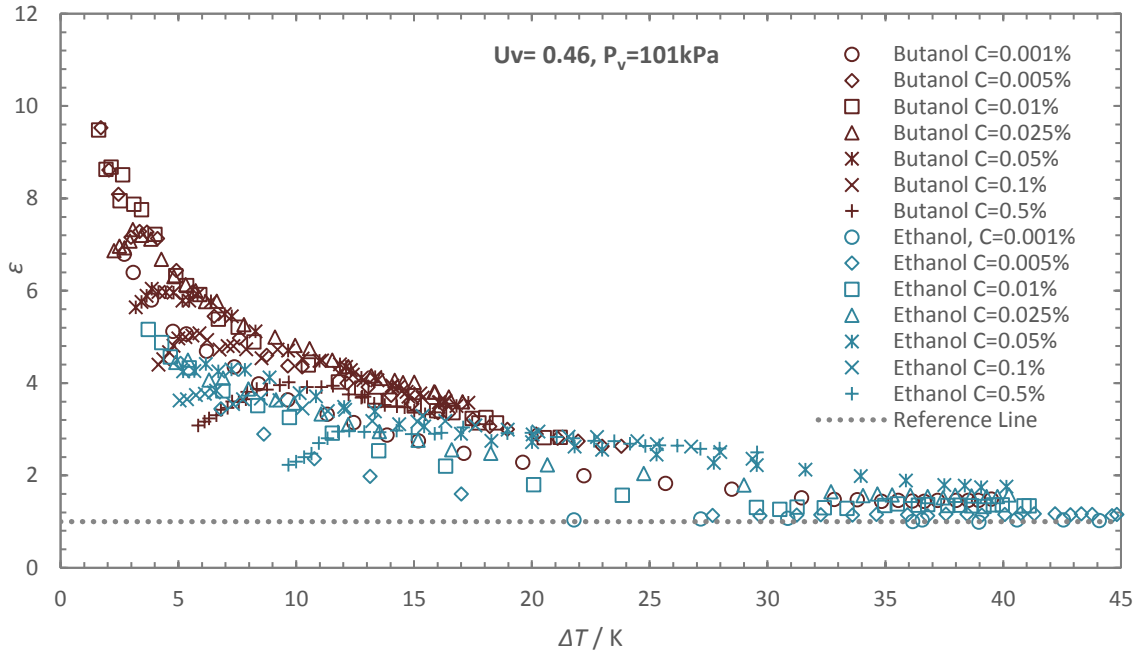

(d)

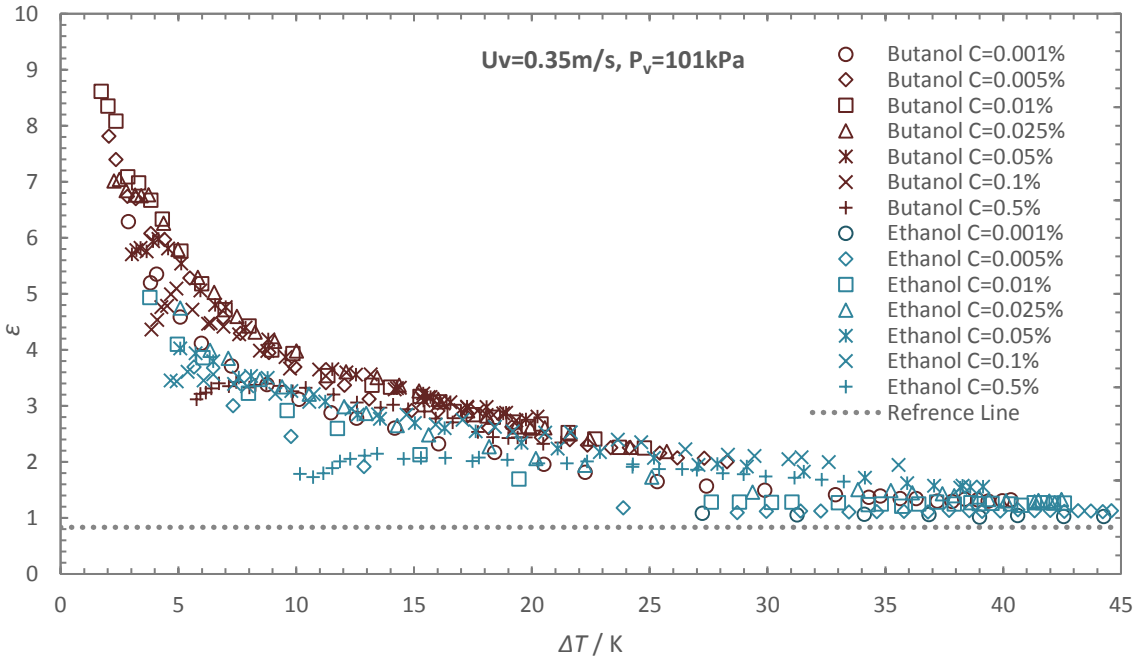

Figure 6.7 (Continued).

(e)

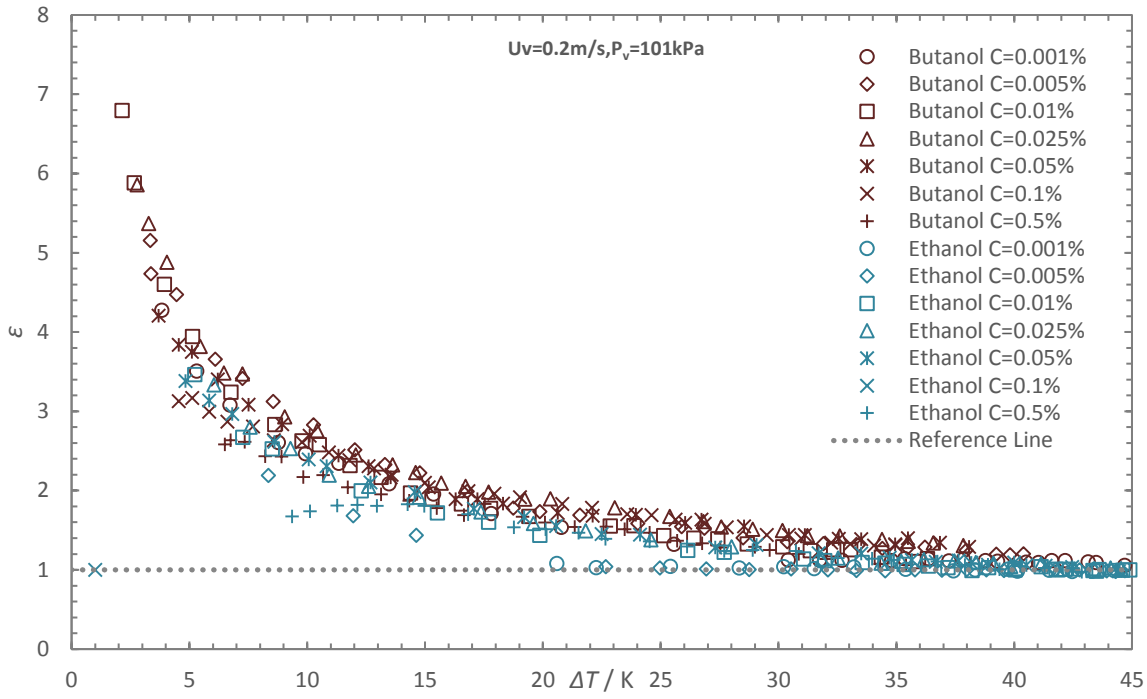

Figure 6.7 (Continued).

6.2.2 Visual observation

Similar to steam-ethanol case videos were made during condensation using 16.1 megapixels Sony Cyber-shot digital camera. Figure 6.8 shows the change in condensate appearance as the vapour-to-surface temperature difference increases for constant mass concentration (0.001%) and three different velocities. It was observed that initially at low vapour velocity condensate appearance is a mixture of drops and rivulets (see table 6.8 (a-c)). With the increase in vapour-to-surface temperature difference, rivulets seem to decrease as more drops are formed and cover the condensing surface (see Figure 7.8 (d-f)). This type of condensation mode can be called pseudo dropwise mode. Further increase in vapour-to-surface temperature difference changes condensate appearance back to rivulets (see Figure 6.8 (g-i)). Finally, the transition from the rivulets mode of condensation to almost complete film-wise mode can be seen in figure 6.8 (j-l). Heat-transfer coefficient and enhancement ratio are seen to decrease during these transitions. Furthermore, it was also observed that as vapour velocity increases the speed of drops forming and dripping off the test tube increases. This was not possible to see through pictures but was observed through videos. Similar sort of pattern was observed for all other mass concentrations at vapour velocity of 2 m/s. However, for U_v > 2 m/s and C_{iL} >0.001% no film-wise mode of condensation was observed this was due to limited availability of coolant flow rate. Condensate appearance was pseudo-dropwise throughout vapour-to-surface temperature difference.

Figure 6.9 is a copy of figure 6.2 (a) with data points in the transition region marked in circles. Data point with red circles marks the start of transition region (pseudo-dropwise mode dominates the condensate surface) and blue circles mark the end of the transition region (film-wise mode dominates the condensate surface). It was also observed that during the transition a jump in vapour-to-surface temperature difference was observed. To minimise this gap extra point was plotted by increasing the flow rate only half a unit. These points are marked with orange circles.

Figure 6.10 shows the condensate appearances at various vapour-to-surface temperature difference for the butanol mass concentration of 0.05%, 0.1% and 0.5%. After observing visual observations, it can be concluded that it is a good idea to compare the condensate appearance with heat-transfer coefficient instead of heat flux. For the C_{iL} =0.05% at U_v= 0.35 m/s and C_{iL} =0.1% at U_v= 0.2 m/s the heat transfer coefficient decreases from maximum

value as vapour to surface temperature difference increases. The visual observation shows the transition of condensate appearance from dropwise to a combination of drops and wavy film. For the C_{iL}= 0.5% at U_v= 0.2m/s. The visual observation shows the dropwise mode of condensation during the steep increase of the heat transfer coefficient. Number of drops increases and become smaller with an increase in the vapour to surface temperature difference. However, after reaching maximum heat transfer coefficient the number of condensate drops decreases (see figure 6.10 (k)-(o)).

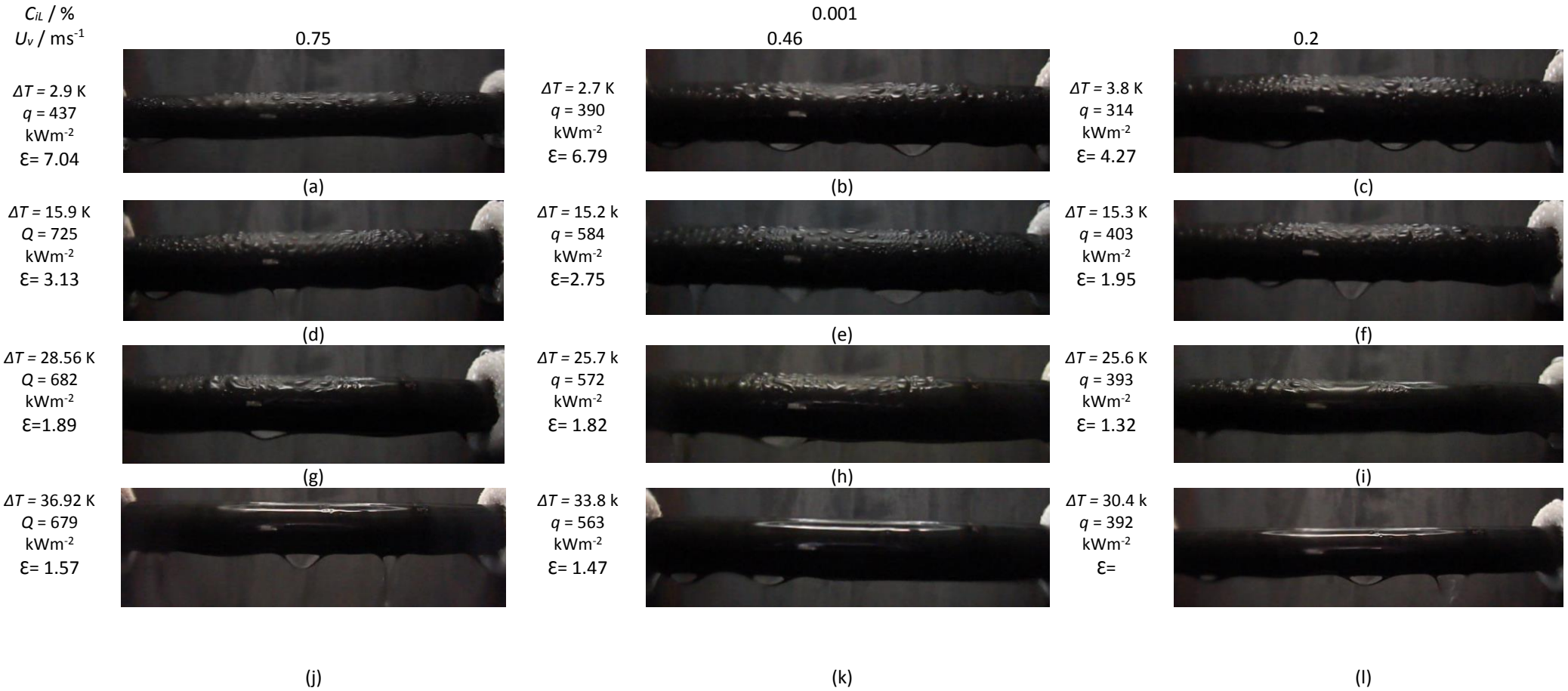

Figure 6-8: Photographs of change of condensation mode with vapour-to-surface temperature difference for U_V= 0.75, 0.46, 0.2 m/s at C_{iL}= 0.001%.

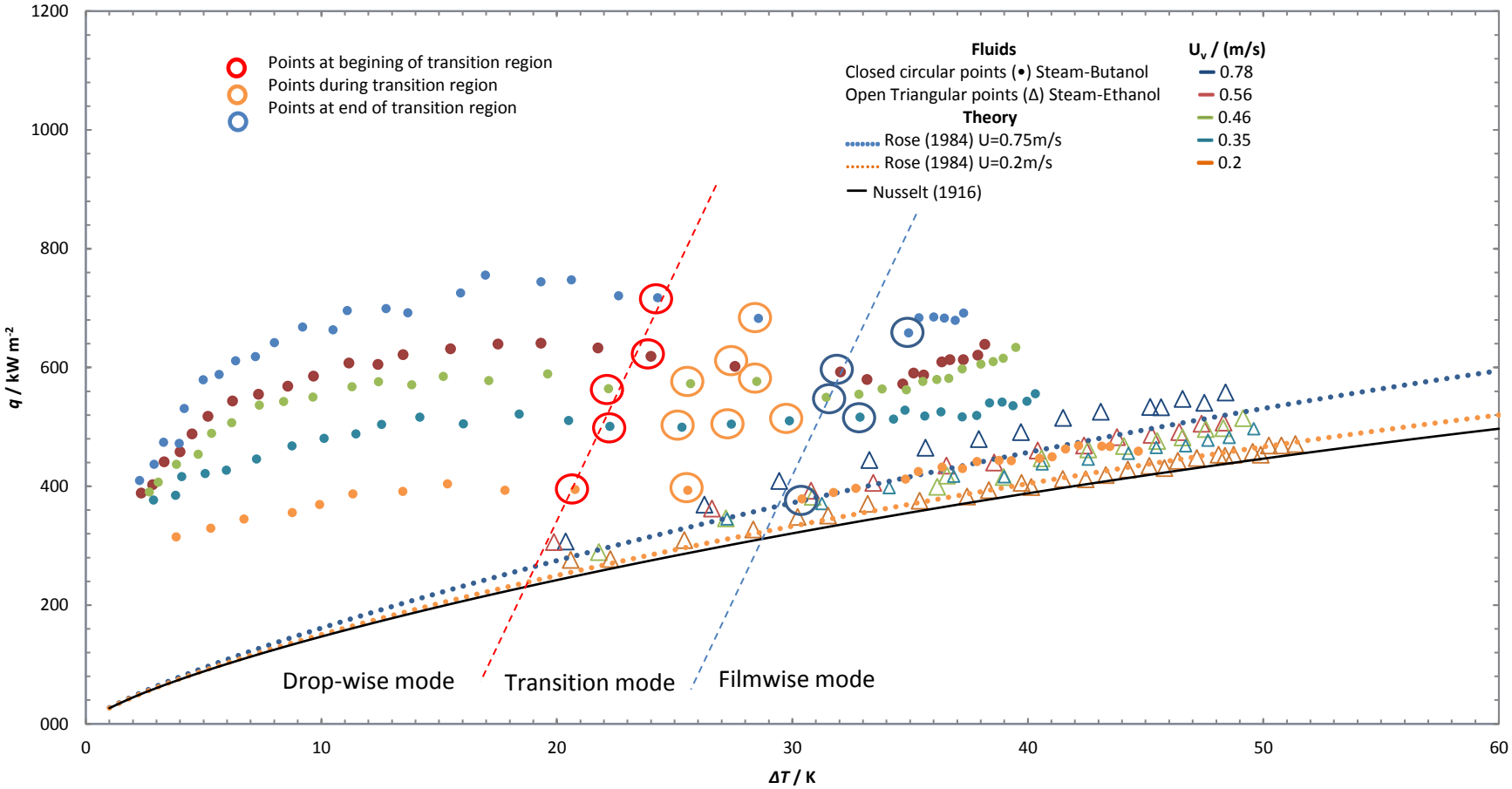

Figure 6-9: Points indicating the start and end of the transition region on the heat flux against vapour-to-surface temperature difference graph for different velocities at C_{iL} =0.001%.

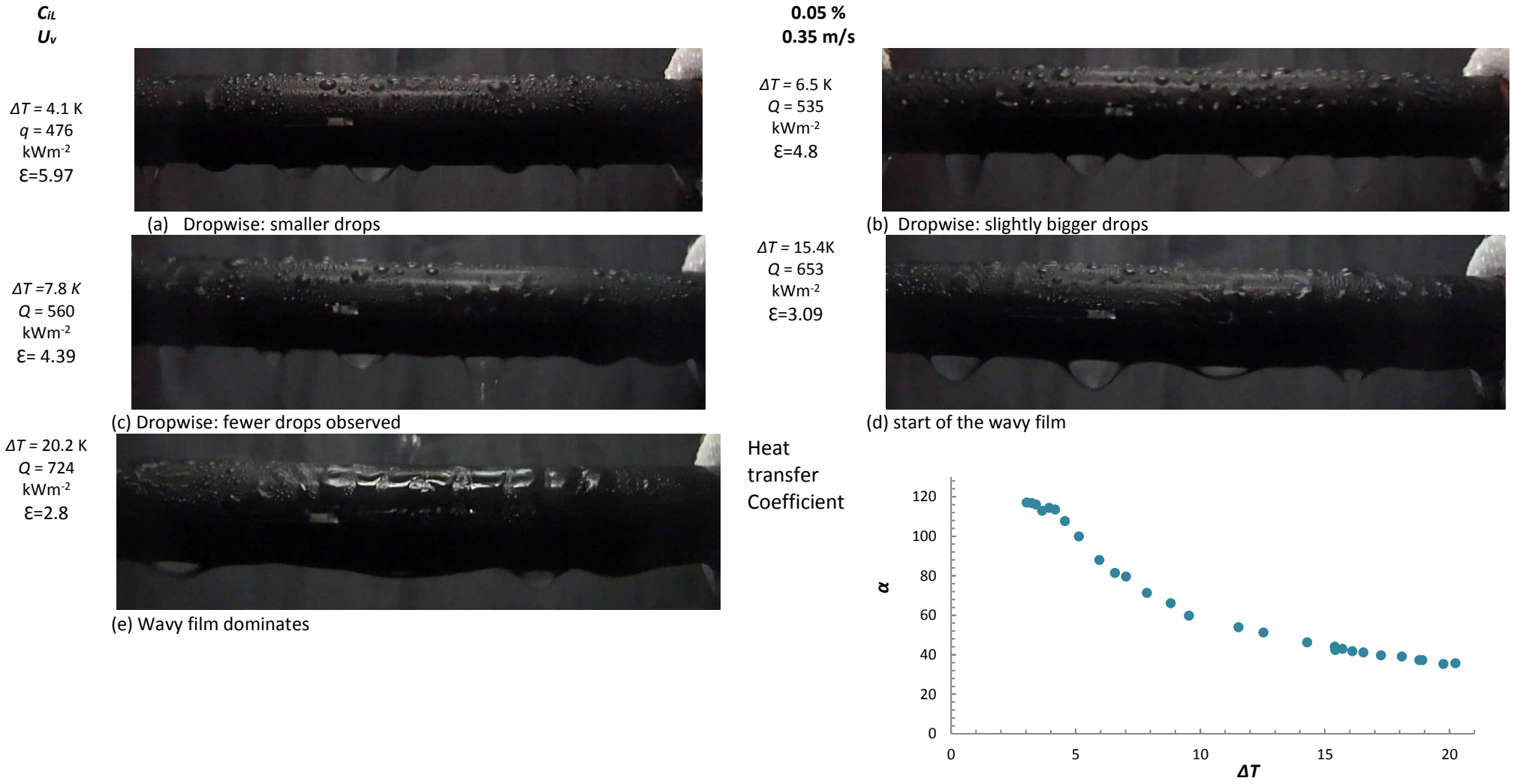

Figure 6-10: Photographic evidences of condensate appearance at CiL = 0.05%, 0.1% 0.5%.

C_{iL} **0.1 %**

U_v **0.2 m/s**

ΔT = 4.54 K
q = 261 kWm^{-2}
Ɛ= 3.12

(f) Dropwise: smaller drops

ΔT = 8.58 k
q = 353 kWm^{-2}
Ɛ= 2.63

(g) Dropwise: bigger drops

ΔT = 9.78 k
q = 386 kWm^{-2}
Ɛ= 2.61

(h) Start of wavy film-wise

ΔT = 16.8
q = 439 kWm^{-2}
Ɛ= 1.99

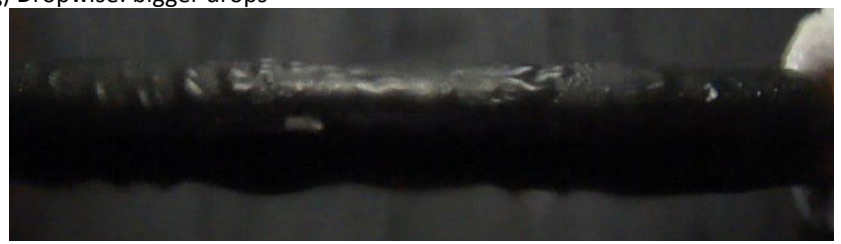

(i) wavy film wise mode Dominating

ΔT = 30.9 k
q = 474 kWm^{-2}
Ɛ= 1.39

(j) Wavy film-wise dominates

Heat transfer Coefficient

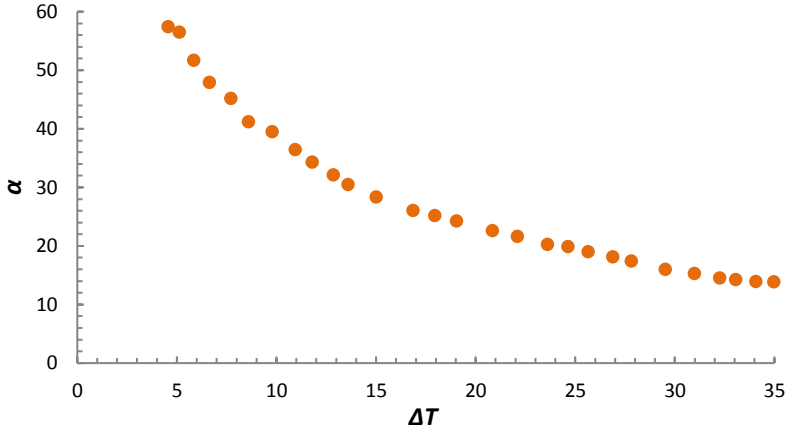

Figure 6-10 continued

C_{iL} **0.1 %**

U_v **0.2 m/s**

ΔT = 5.79 K
q = 319 kWm^{-2}
Ɛ= 3.02

(k) Dropwise: bigger drops

ΔT = 6.78K
q = 491 kWm^{-2}
Ɛ= 4.11

(l) Dropwise: smaller drops

ΔT = 7.88 K
q = 735 kWm^{-2}
Ɛ= 5.4

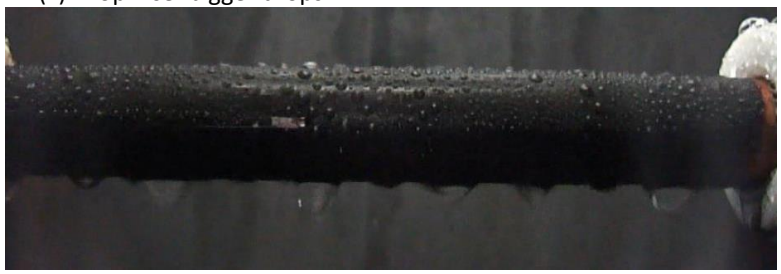

(m) Dropwise: number of drops increases

ΔT = 9.36 K
q = 932 kWm^{-2}
Ɛ= 6.08

(n) Dropwise: more intensity of smaller drops

ΔT = 11.3 k
q = 950 kWm^{-2}
Ɛ= 5.27

(o) Dropwise: smaller drops intensity decreases

Heat transfer Coefficient

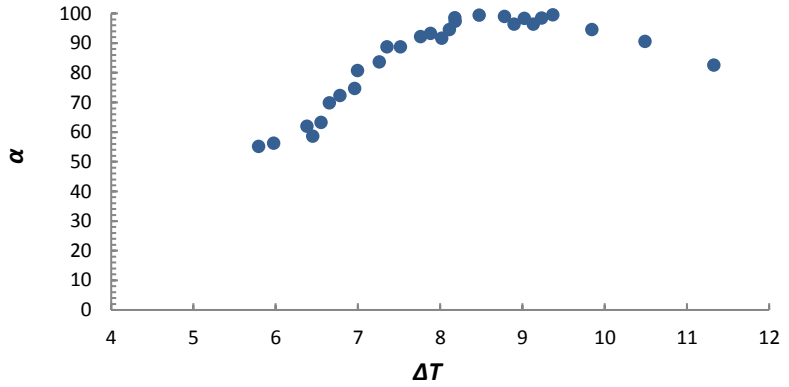

Figure 6-10 continued

6.3 Summary

Measurements of heat transfer during Marangoni condensation of steam-butanol mixtures were conducted successfully and the results were compared with the condensation of steam-ethanol mixtures. Heat flux and heat transfer coefficients for steam butanol mixtures were significantly higher compared to steam-ethanol mixtures, for a given mass concentration and vapour-to-surface temperature difference. Secondly, the effect of diffusion resistance in steam-butanol mixtures is found to be lower compared to steam-ethanol mixtures for the given mass concentrations.

Enhancement ratio was found to be strongly dependant on butanol concentrations at lower vapour to surface temperature difference. Enhancement also depends significantly on the vapour velocity for all mass concentrations. The effect of velocity is more prominent at lower concentrations. Maximum enhancements were achieved at higher velocities and lower mass concentrations at lower vapour-to-surface temperature difference. The peak enhancement value was generally found around 9 at a vapour-to-surface temperature difference of 4K and mass concentrations of 0.005% and 0.01%.

It is noted that in a steam condenser, where the vapour-side resistance might be around one third or more of the total vapour-to-coolant thermal resistance, an enhancement factor of around 9 on the vapour-side could result in significant saving in heat transfer surface and condenser overall size, the latter being especially important in space, marine and offshore applications. Secondly compared to ethanol butanol is less volatile and thus less danger of flammability. Moreover, butanol shows higher performance at much lower concentrations than ethanol further reducing the risk.

Chapter 7

7 Marangoni condensation of steam-propanol mixtures on a horizontal smooth tube

7.1 Introduction

In this chapter comparative investigation between Marangoni Condensation of Steam-propanol, steam-butanol and steam-ethanol mixtures has been studied. The Same experimental apparatus and conditions as for the steam-butanol and steam-ethanol mixtures were used to measure the heat transfer performance during the condensation of steam-propanol mixtures on a smooth horizontal tube. Same test tube with four thermocouples embedded was used. To ensure there were no butanol footprints left, the tube and apparatus were thoroughly cleaned using the procedure mentioned in chapter 5 before using it for the steam-propanol case. Test section pressure was 101 kPa. Same vapour velocities and coolant flow rates as of butanol and ethanol were implied. Mass Fraction of propanol (initial liquid mass fraction (C_{iL}) of propanol prepared at room temperature) were 0.001%, 0.005%, 0.01%, 0.025%, 0.05% and 0.1%. For each propanol mass fraction, vapour velocity at the approach to condenser tube was varied using the boiler power to give 0.2, 0.35, 0.46, 0.56 and 0.75m/s. Coolant inlet temperature was always around 25 °C with a maximum variation of 1 K.

The main purpose of this investigation was to measure the heat transfer properties of steam-propanol mixtures and compare it with the results obtained for steam-butanol and steam-ethanol mixtures under the same experimental conditions. It is predicated on the theoretical basis that steam-propanol should perform better than stem-ethanol mixtures, however, should underperform compared to steam-butanol mixtures.

7.2 Results and discussion

The results of steam-propanol mixtures are shown in figures 7.1 and 7.2 with heat flux and heat transfer coefficient plotted against vapour-to-surface temperature difference for different vapour velocities at each butanol mass fraction (C_{iL}). The solid black line represents the Nusselt (1969) equation for pure steam given by equation (2.1). Whereas, the equation of Rose (1984) including the effect of vapour velocity is presented in blue and orange dotted line for the minimum and maximum vapour velocities respectively. For comparison, steam-ethanol data are also plotted. Steam-butanol data is plotted by closed points and steam-ethanol data using open points.

The key finding of the experiment was that the heat flux and heat transfer coefficients of steam-propanol mixtures lies in between steam-ethanol and steam-butanol mixtures for the given vapour-to-surface temperature difference and mass concentration. Secondly, similar to steam-butanol the diffusion resistance in steam-propanol is found to be lower compared to steam-ethanol mixtures for the given mass concentrations.

Similar to previous cases (steam-ethanol and steam-butanol), for all the mass fractions the vapour velocity has a significant influence on the heat transfer. Increase in vapour velocity increases both heat flux and heat transfer coefficient for the given vapour-to-surface temperature difference. The trend and behaviour of heat-transfer coefficient were also similar to what was observed in steam-ethanol and steam-butanol cases. Figures 7.1, 7.2, 7.3 and 7.4 compares the heat flux and heat transfer coefficient of steam propanol and steam butanol cases. For lower concentration steam-butanol has the higher heat transfer values for a given vapour-to-surface temperature difference. However, as the concentration increases the heat transfer values for steam propanol and steam-butanol seems to come closer to each other.

Figures 7.8 to 7.12 compares the heat flux and heat-transfer coefficient of steam propanol mixtures with steam ethanol mixtures. It was found the steam propanol shows significant enhancements compared to the stem-ethanol case.

Diffusion in the steam-propanol case has a lesser effect compared to the steam-ethanol case. The reason might be the boiling point of propanol (97°C) which is too close to the boiling point of water. Here, propanol is the more volatile component and thus condenses less. The concentration of the propanol in the vapour phase at the vapour liquid interface becomes dense. Thus, temperature drops but since the boiling temperature difference between the two fluid is less the effect is minimised.

At the maximum vapour velocity propanol mass fraction of C_{iL} = 0.025% gave the highest heat flux of 869 kW/m^2 at vapour to surface temperature difference of 9.1 K. For the same velocity butanol mass fraction of C_{iL} =0.01% gave the highest heat transfer coefficient of 180 kW/ m^2K at vapour to surface temperature difference of 1.76 K.

7.2.1 Comparison between steam-butanol and steam-propanol mixtures

(a)

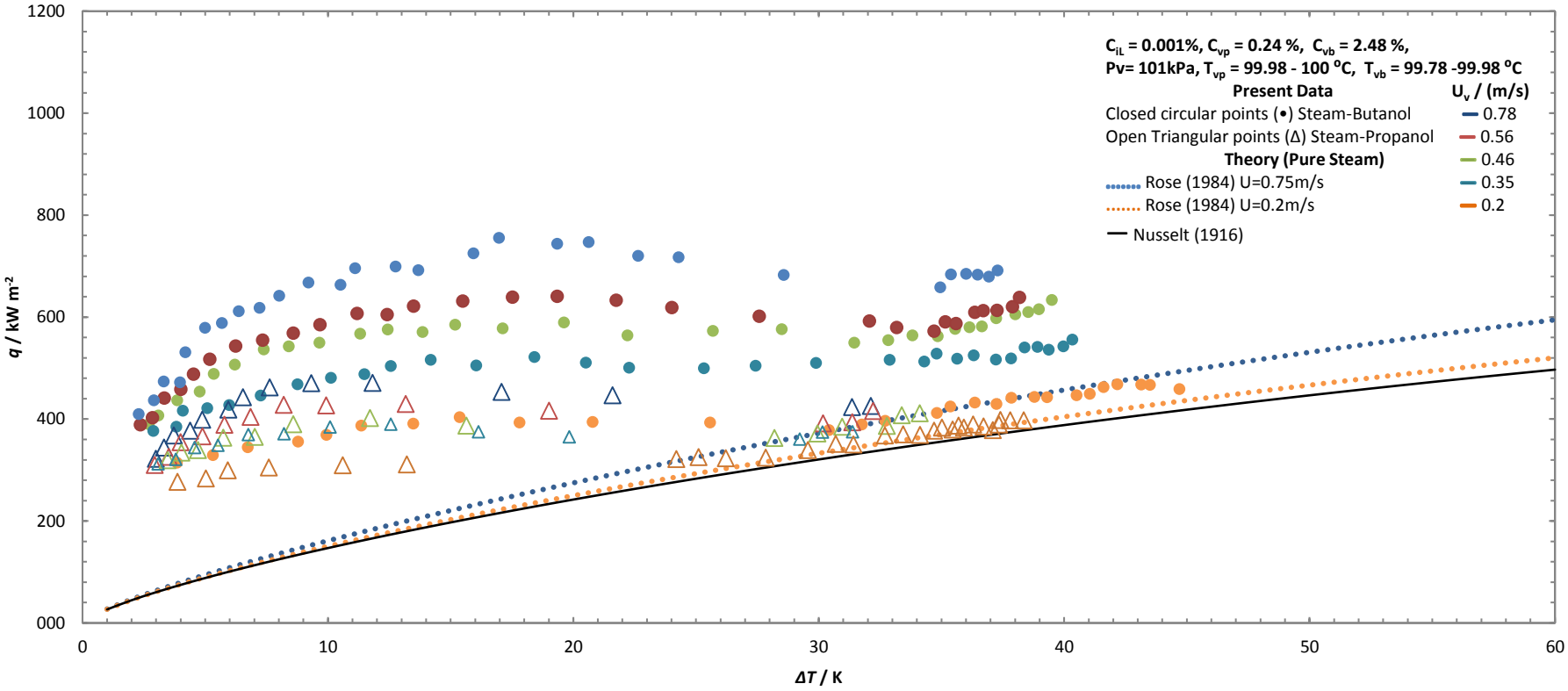

Figure 7-1: (a)-(f) shows variation of heat flux against vapour-to-surface temperature difference for varying vapour velocities at each propanol mass concentration. (a) C_{iL} = 0.001%, (b) C_{iL} = 0.005%, (c) C_{iL} = 0.01%, (d) C_{iL} = 0.025%, (e) C_{iL} = 0.05% and (f) C_{iL} = 0.1%. Steam-butanol data is presented with closed points and steam-propanol data with open points. Test section vapour pressure is 101 kPa.

(b)

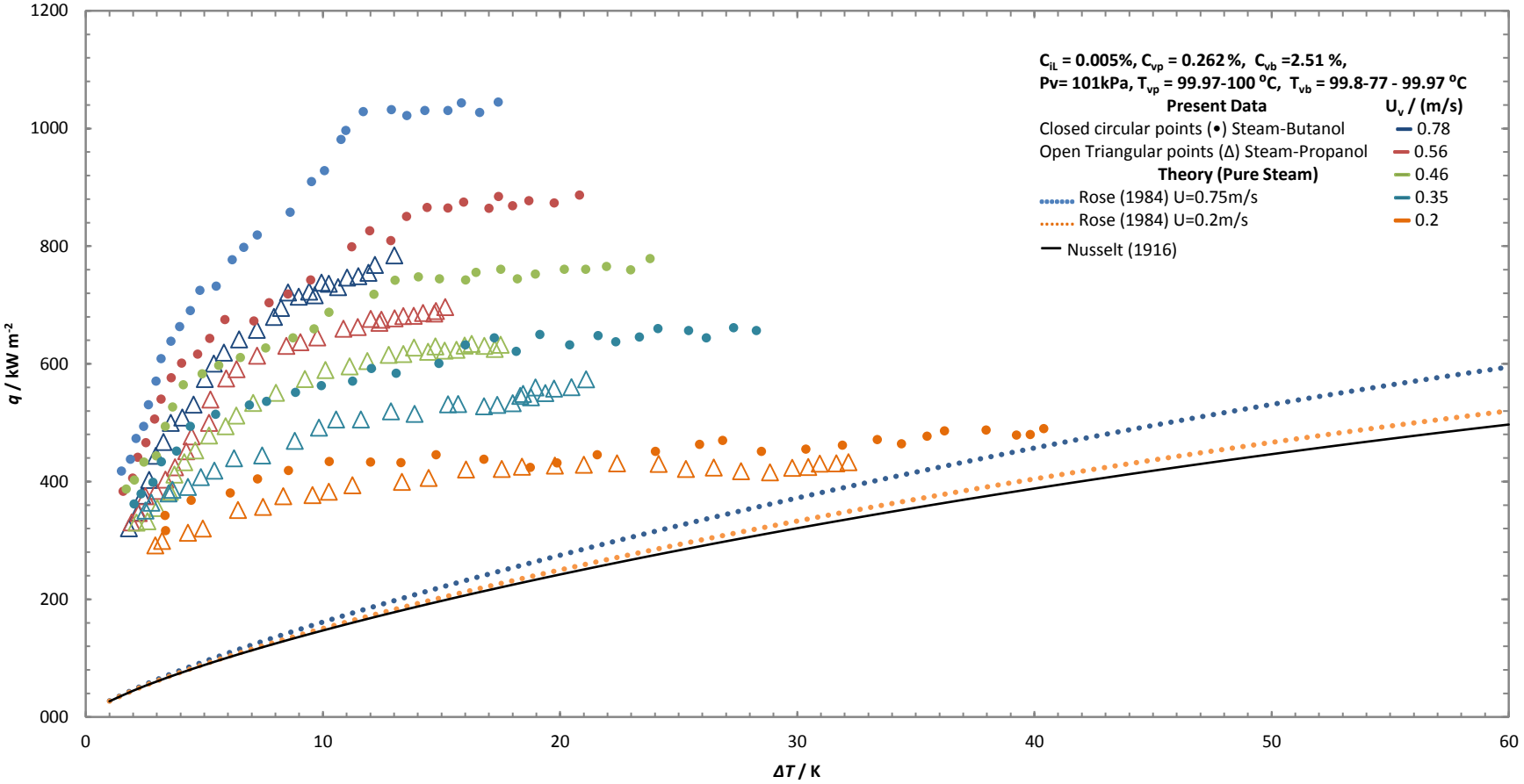

Figure 7.1 (Continued).

(c)

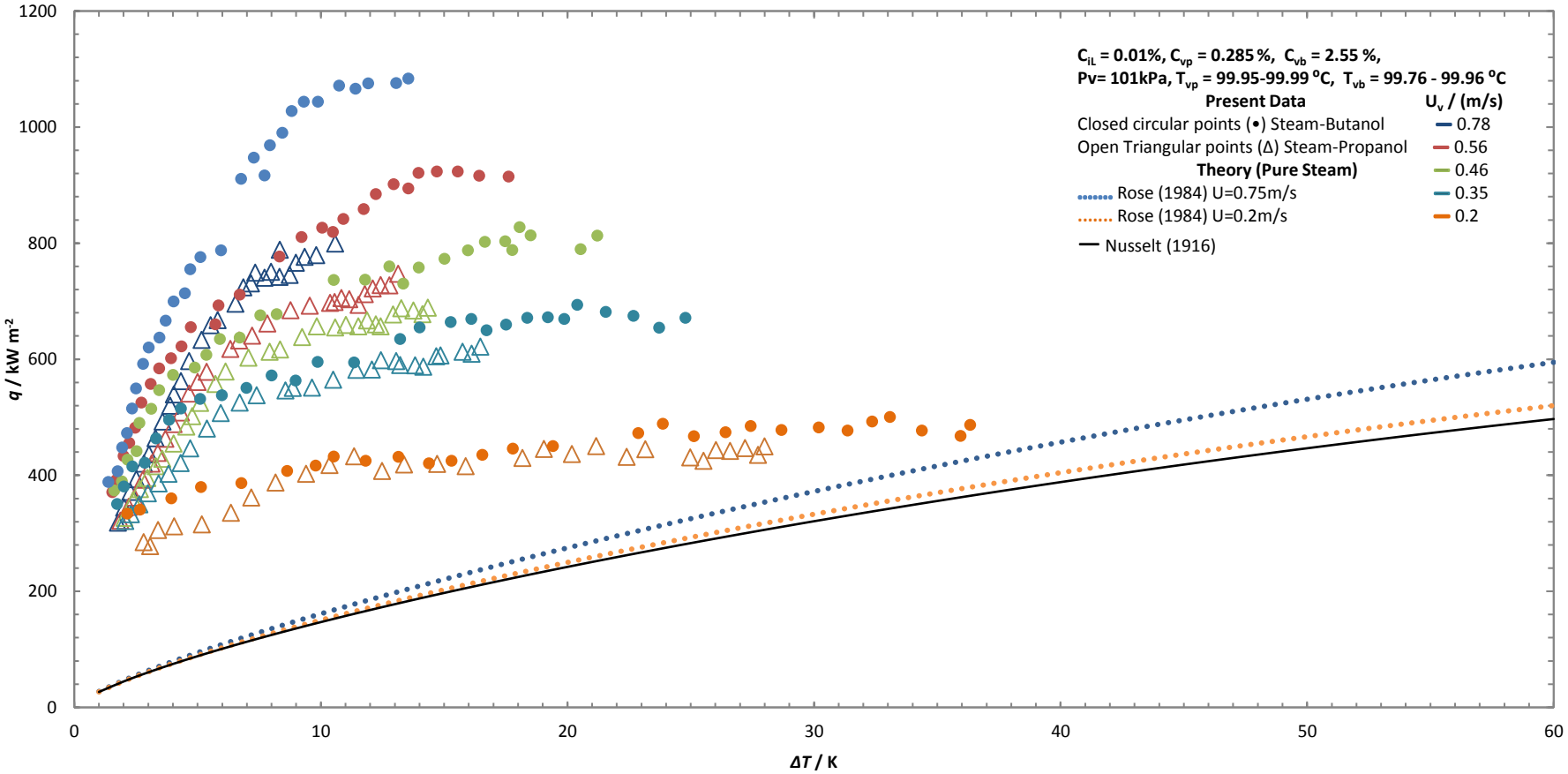

Figure 7.1 (Continued).

(d)

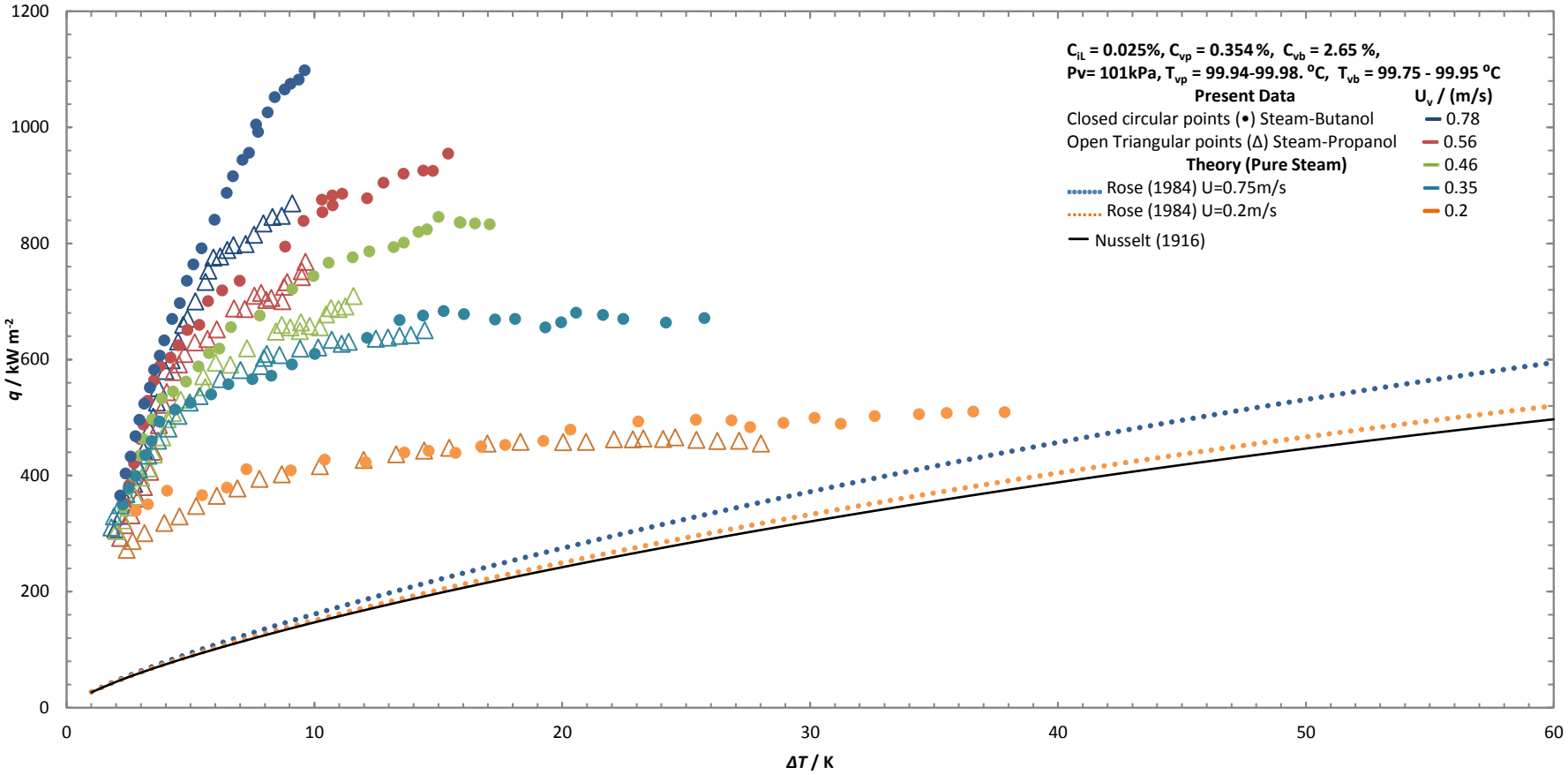

Figure 7.1 (Continued).

(e)

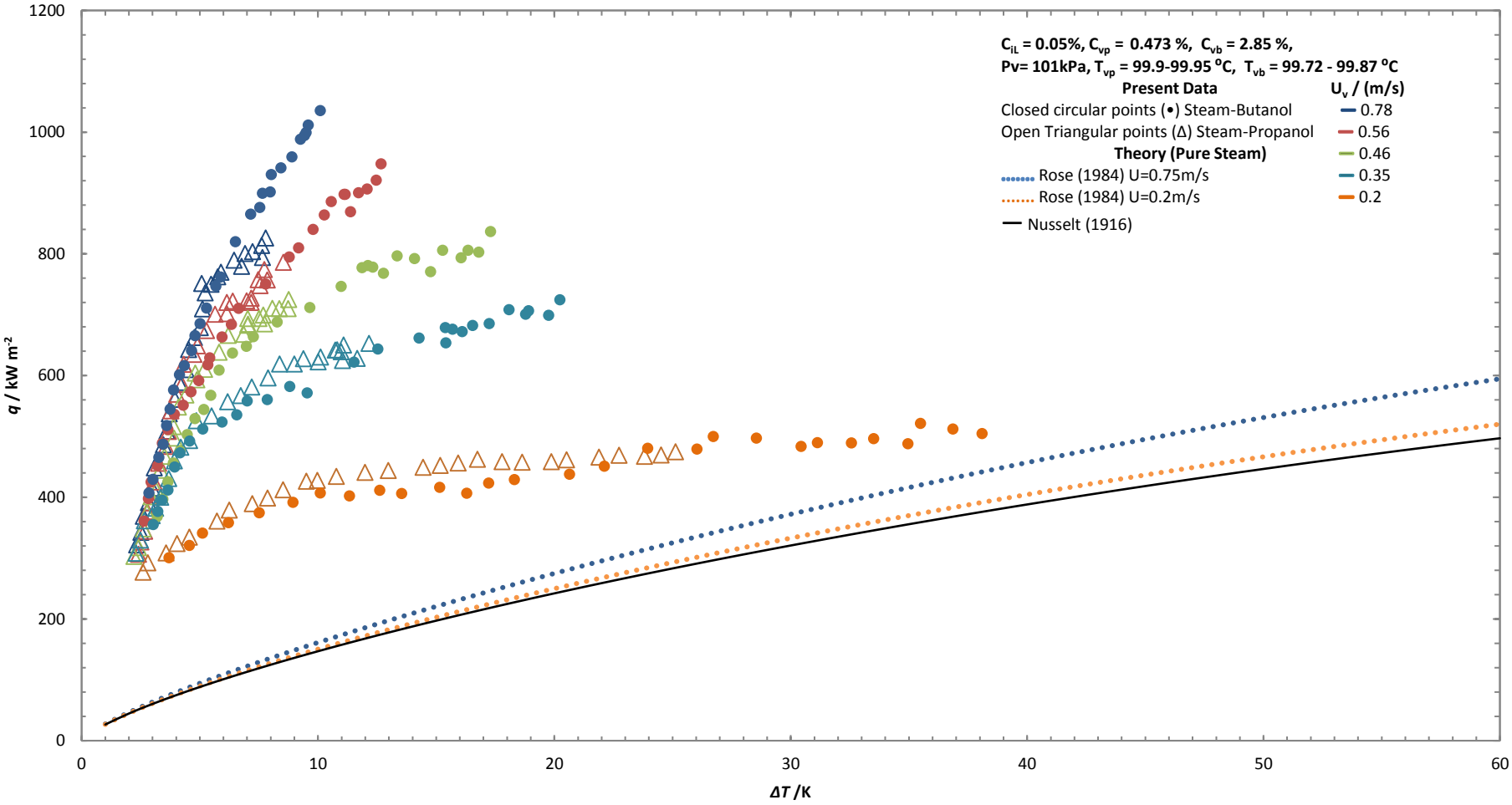

Figure 7.1 (Continued).

(f)

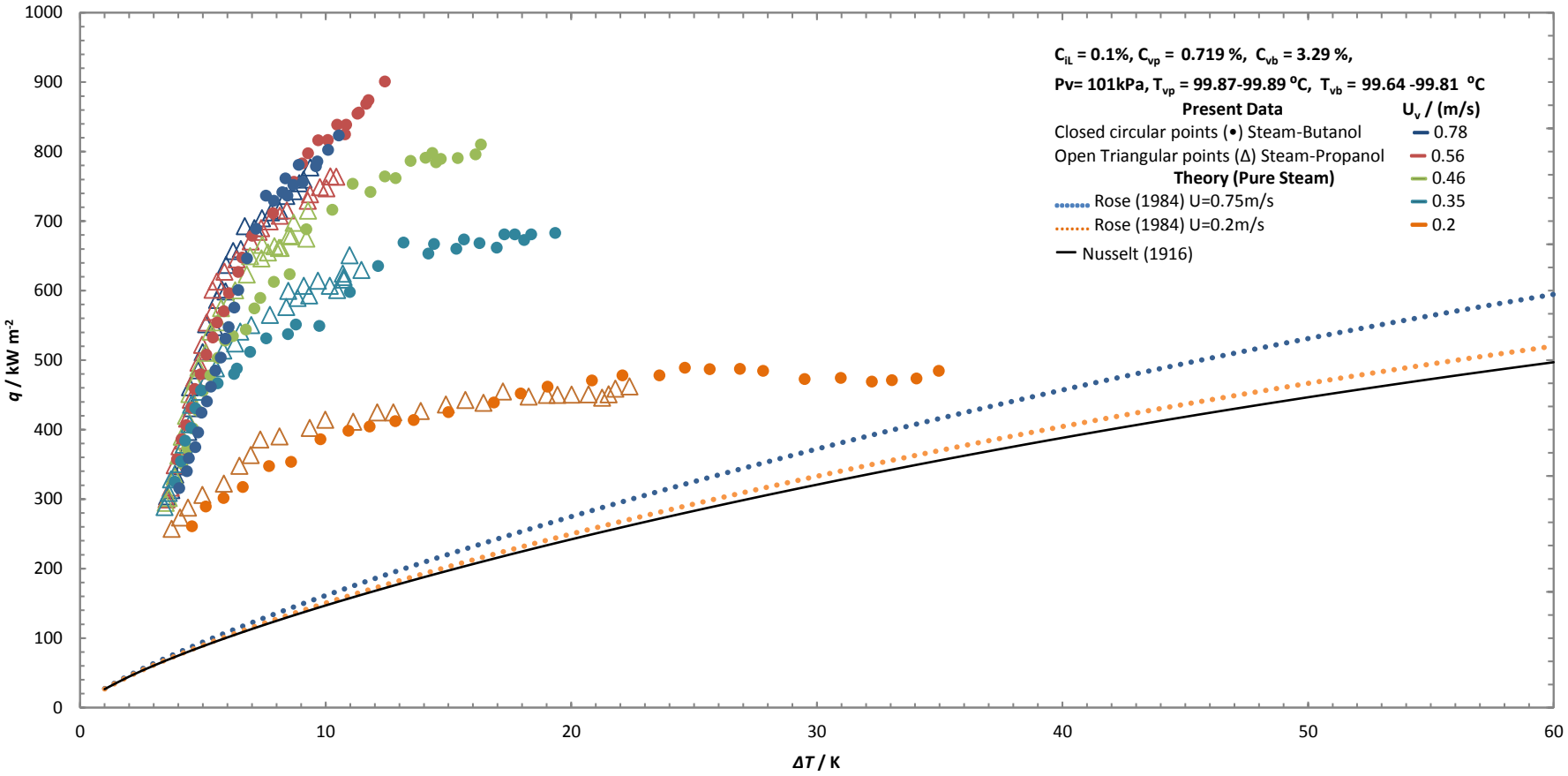

Figure 7.1 (Continued).

(a)

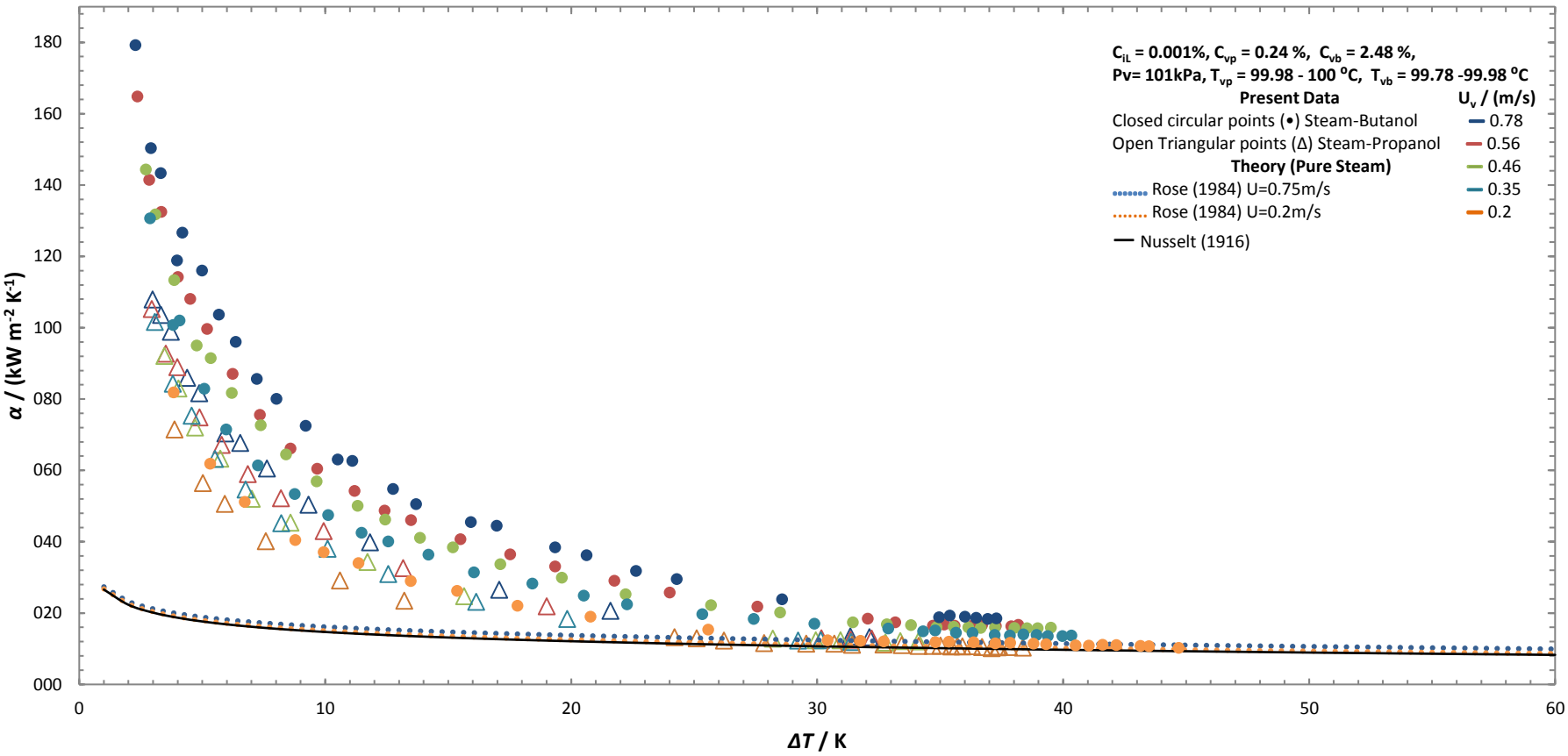

Figure 7-2: (a)-(f) shows variation of heat transfer coefficient against vapour-to-surface temperature difference for varying vapour velocities at each butanol mass concentration. (a) C_{iL} = 0.001%, (b) C_{iL} = 0.005%, (c) C_{iL} = 0.01%, (d) C_{iL} = 0.025%, (e) C_{iL} = 0.05% and (f) C_{iL} = 0.1%. Steam-butanol data is presented with closed points and steam-propanol data with open points. Test section vapour pressure is 101 kPa.

(b)

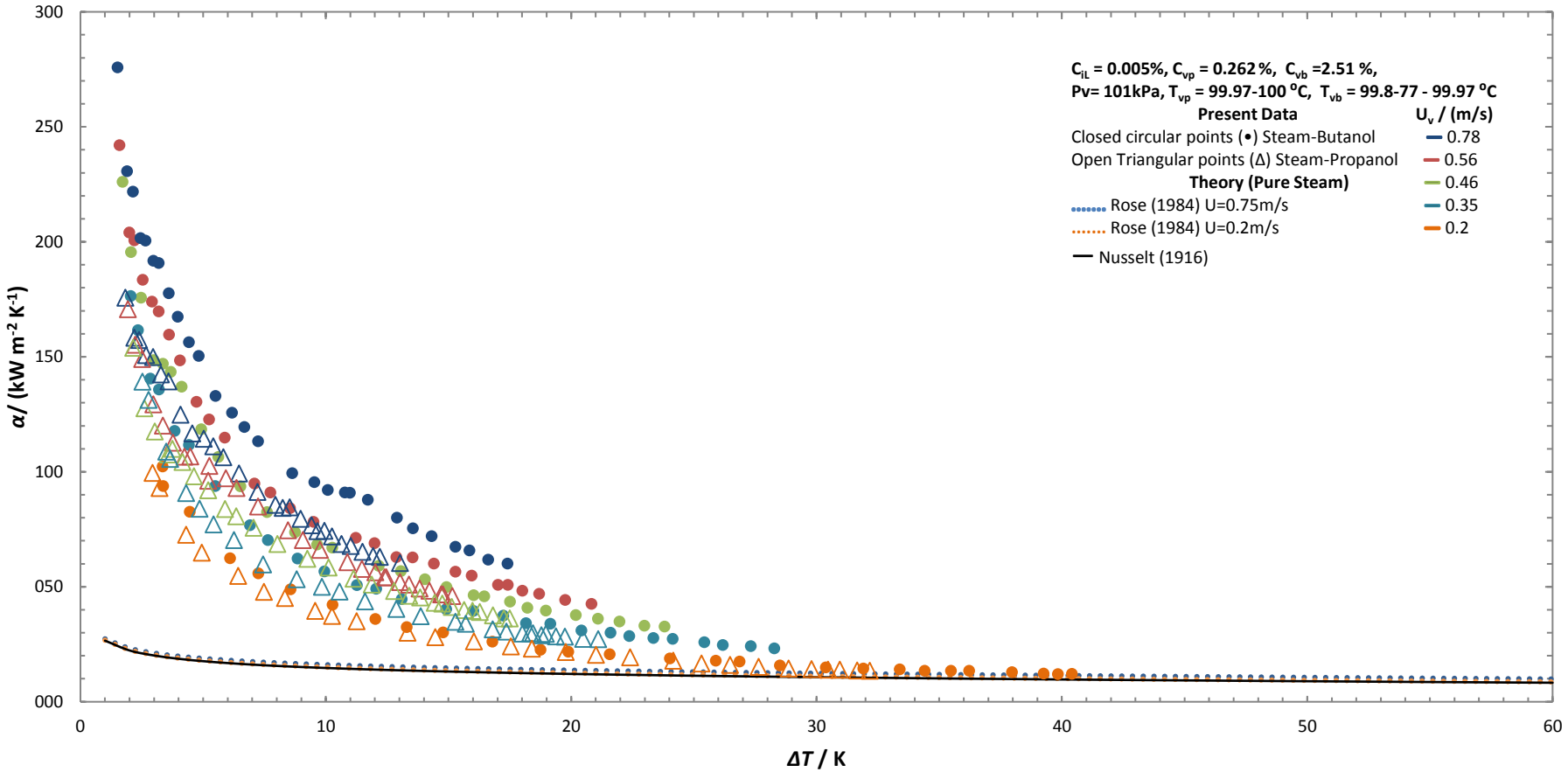

Figure 7.2 (Continued).

(c)

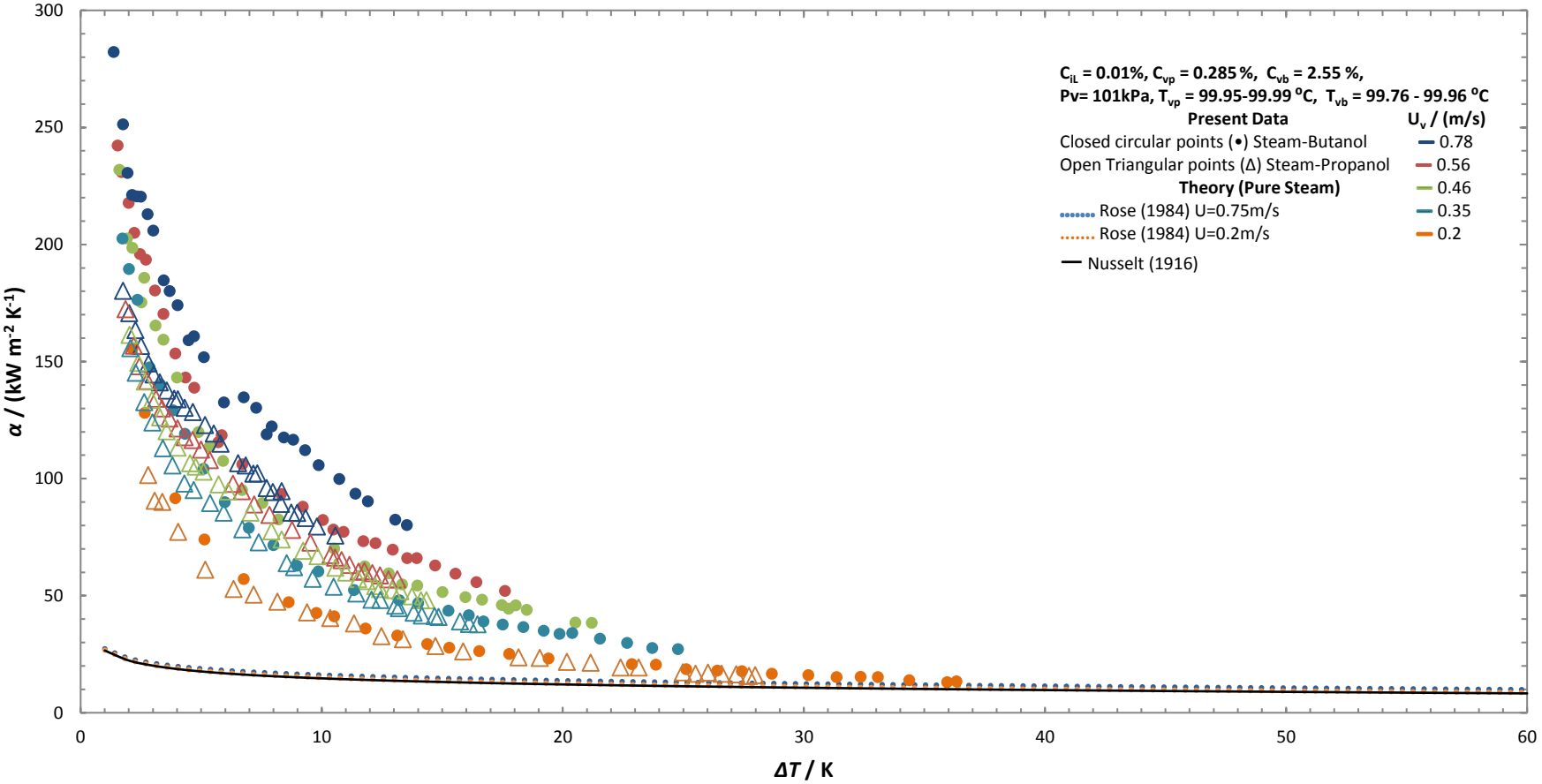

Figure 7.2 (Continued).

(d)

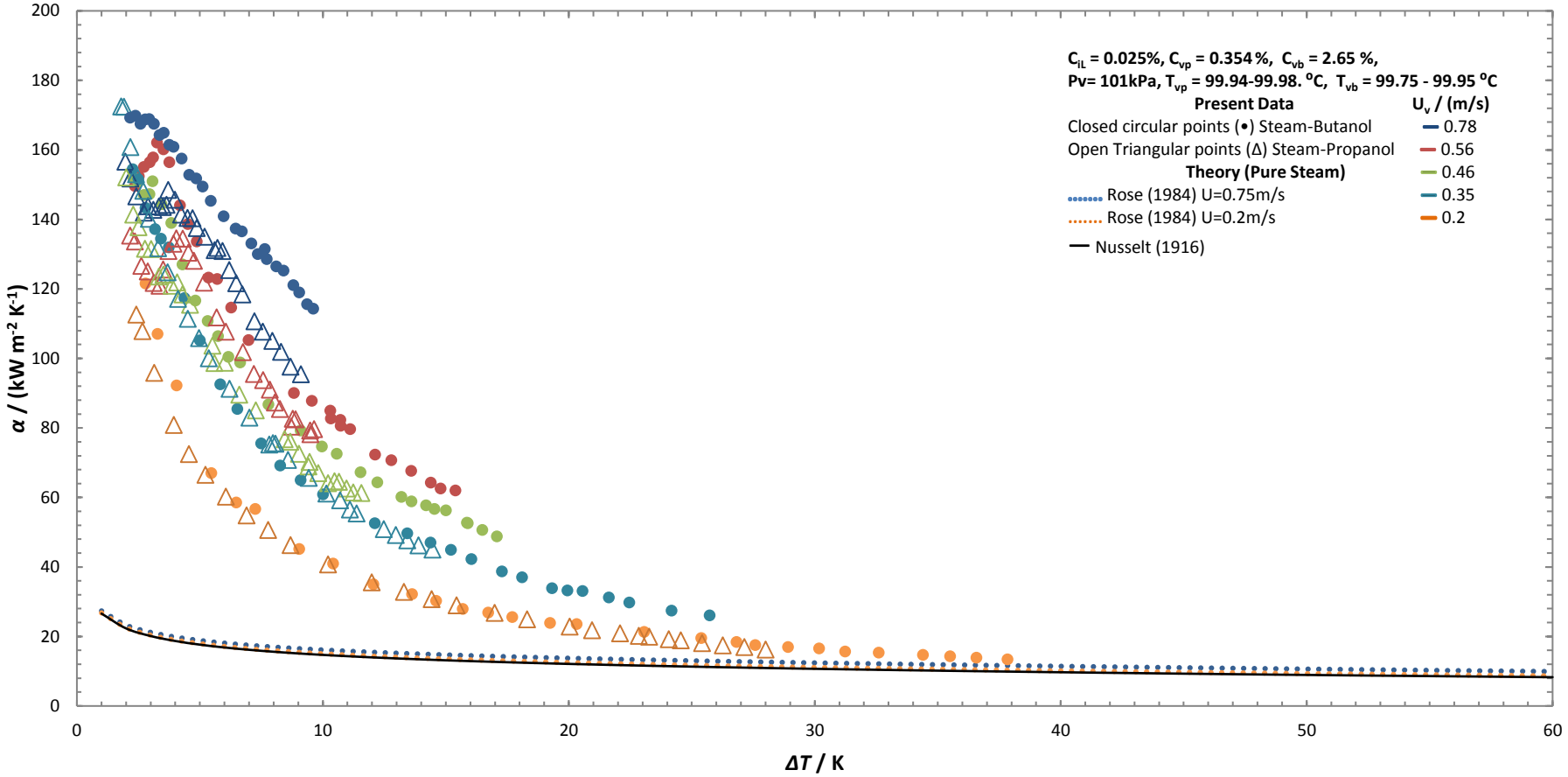

Figure 7.2 (Continued).

(e)

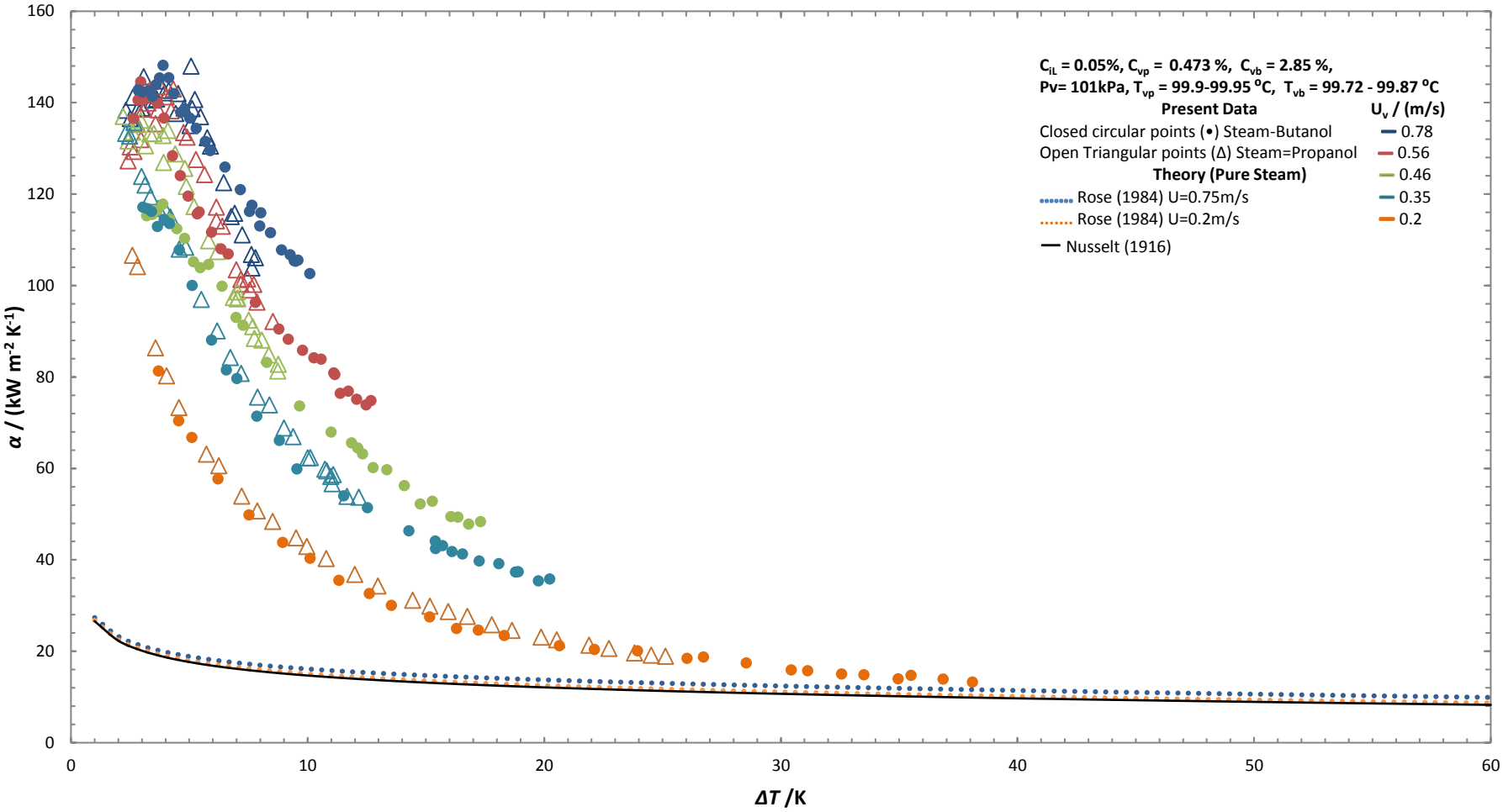

Figure 7.2 (Continued).

(f)

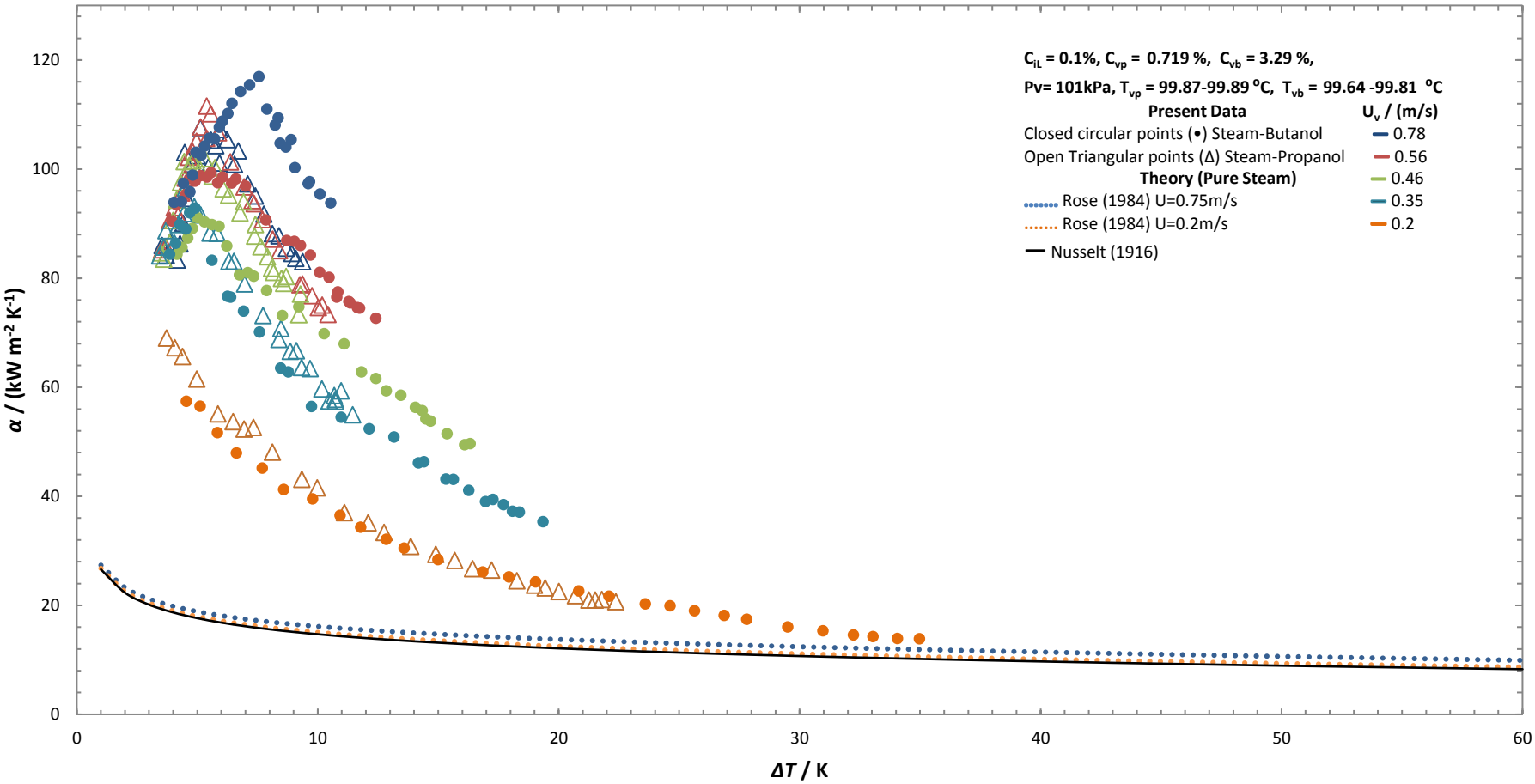

Figure 7.2 (Continued).

(a)

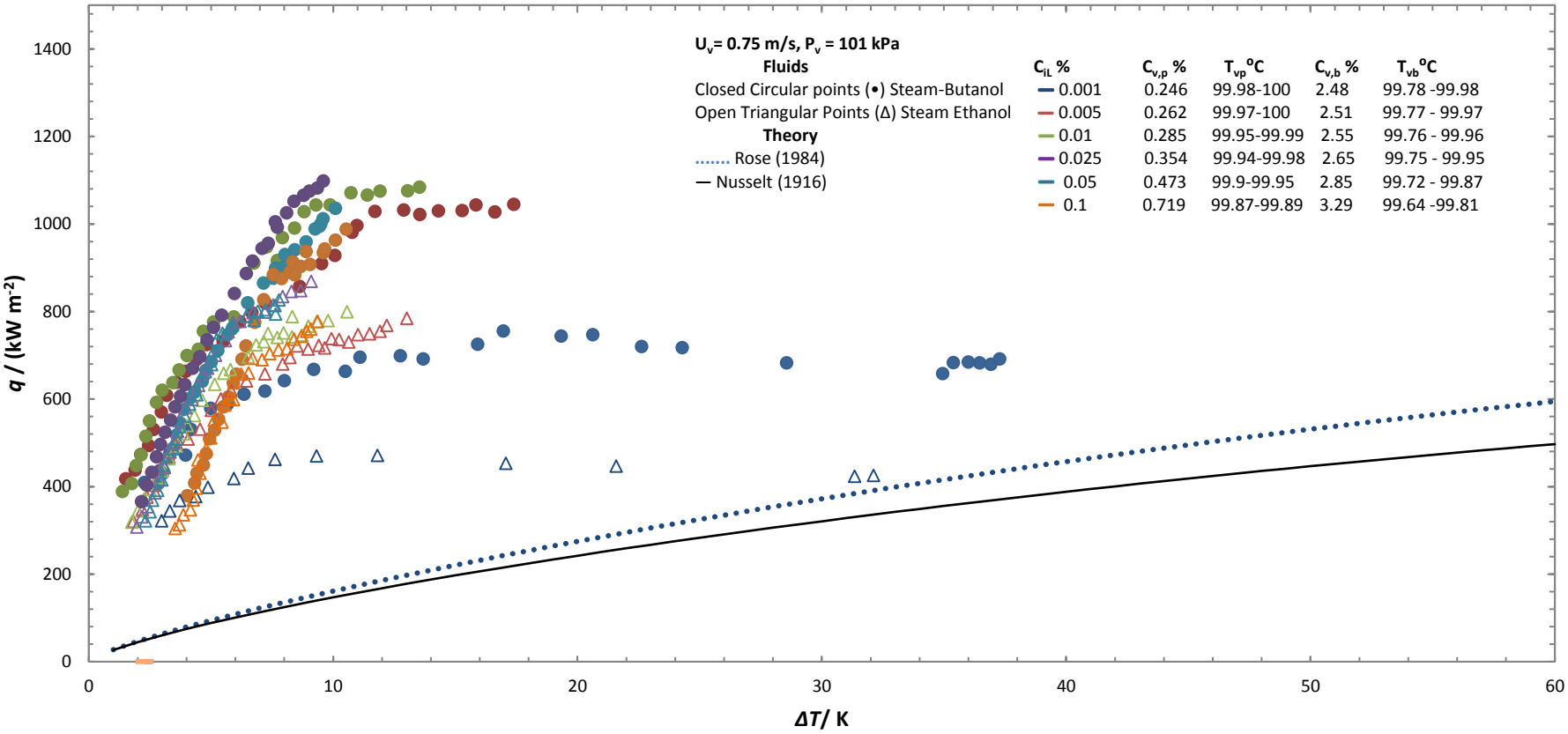

Figure 7-3: (a)-(e) shows variation of heat flux against vapour-to-surface temperature difference for varying mass concentrations at each vapour velocity. (a) Uv = 0.75 m/s, (b) Uv = 0.56 m/s, (c) Uv = 0.46 m/s, (d) Uv = 0.35 m/s, (e) Uv = 0.20 m/s. Steam-butanol data is presented with closed points and steam-propanol data with open points. Test section vapour pressure is 101 kPa.

(b)

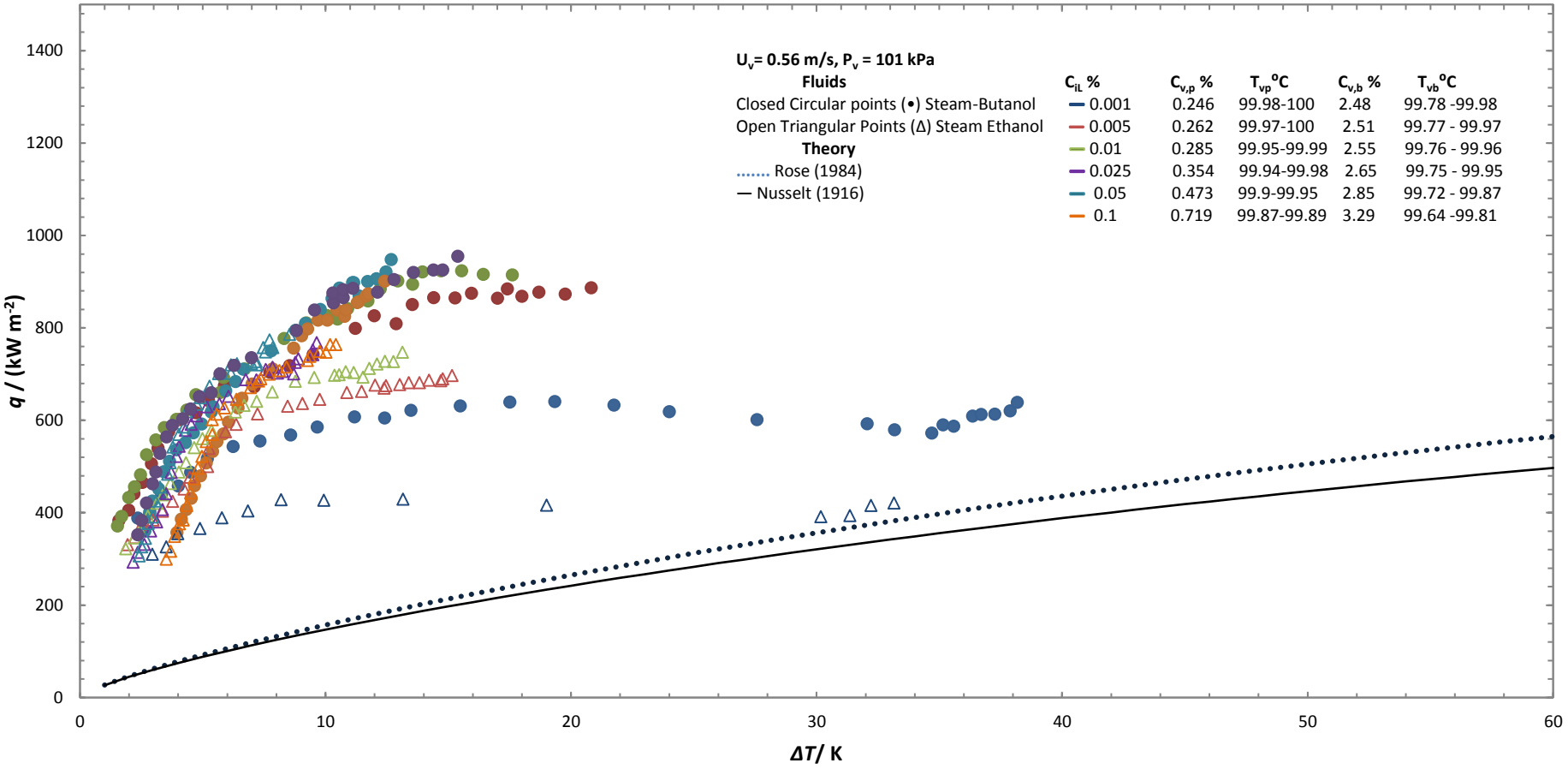

Figure 7.3 (Continued).

(c)

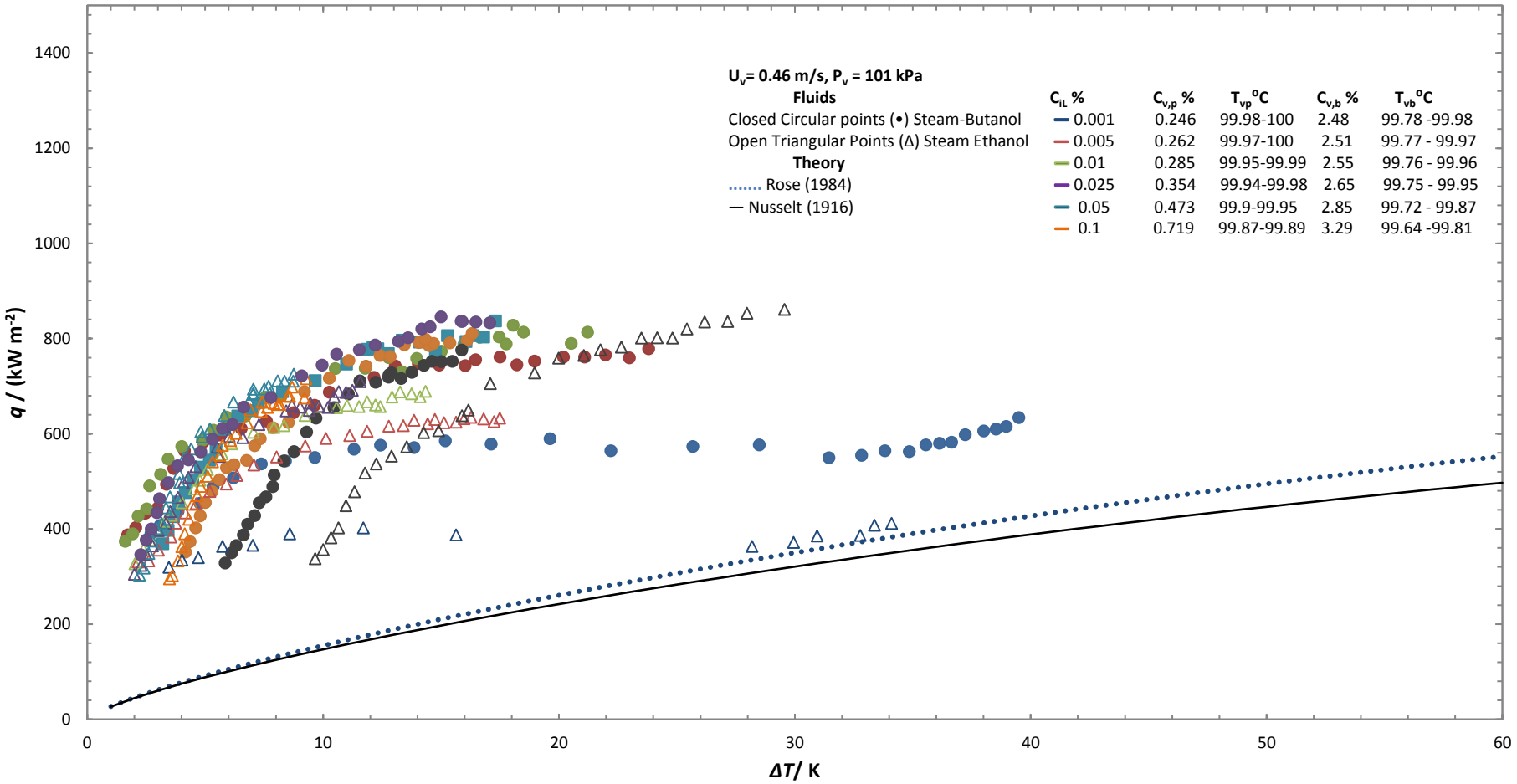

Figure 7.3 (Continued).

(d)

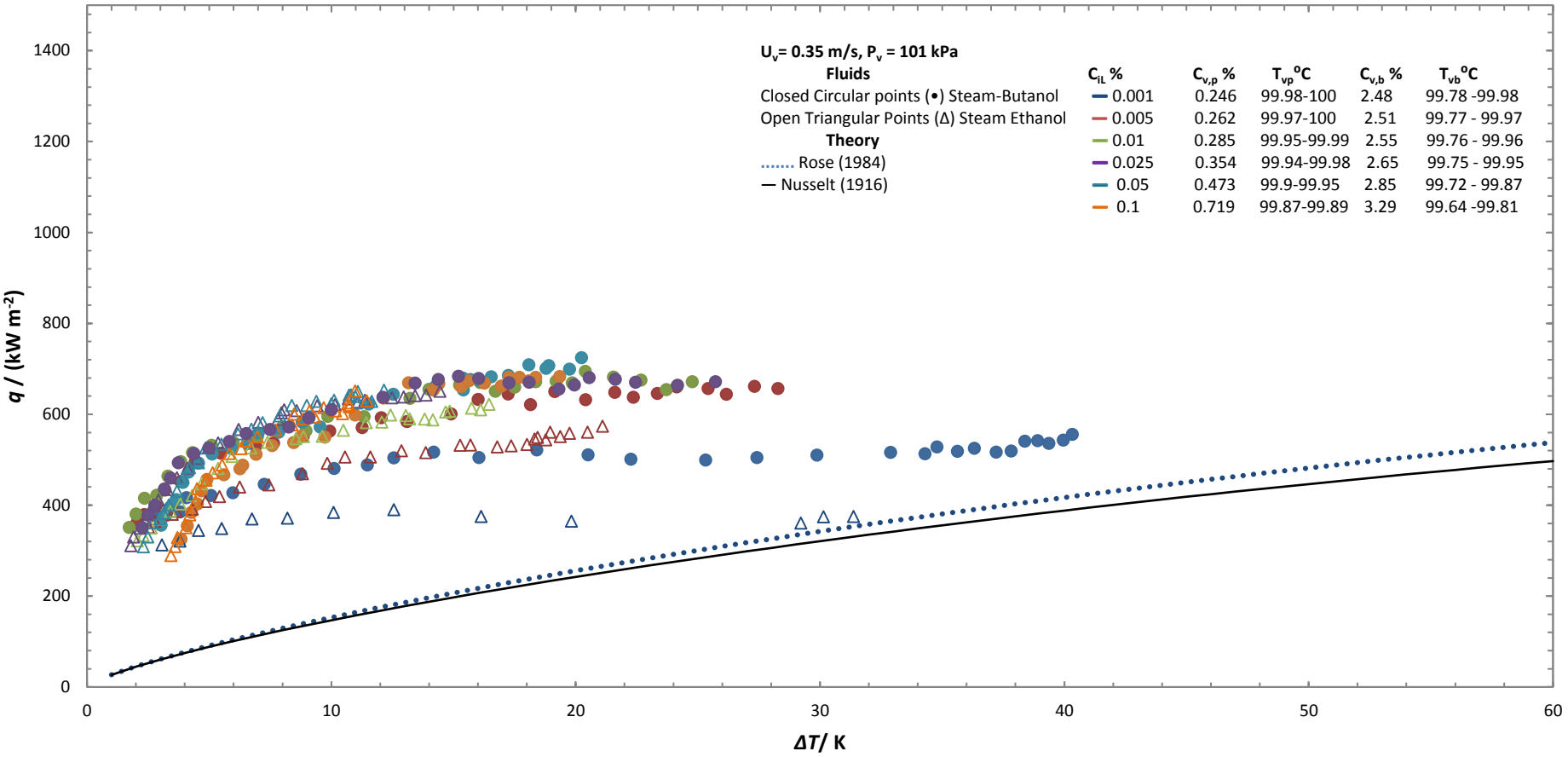

Figure 7.3 (Continued).

(e)

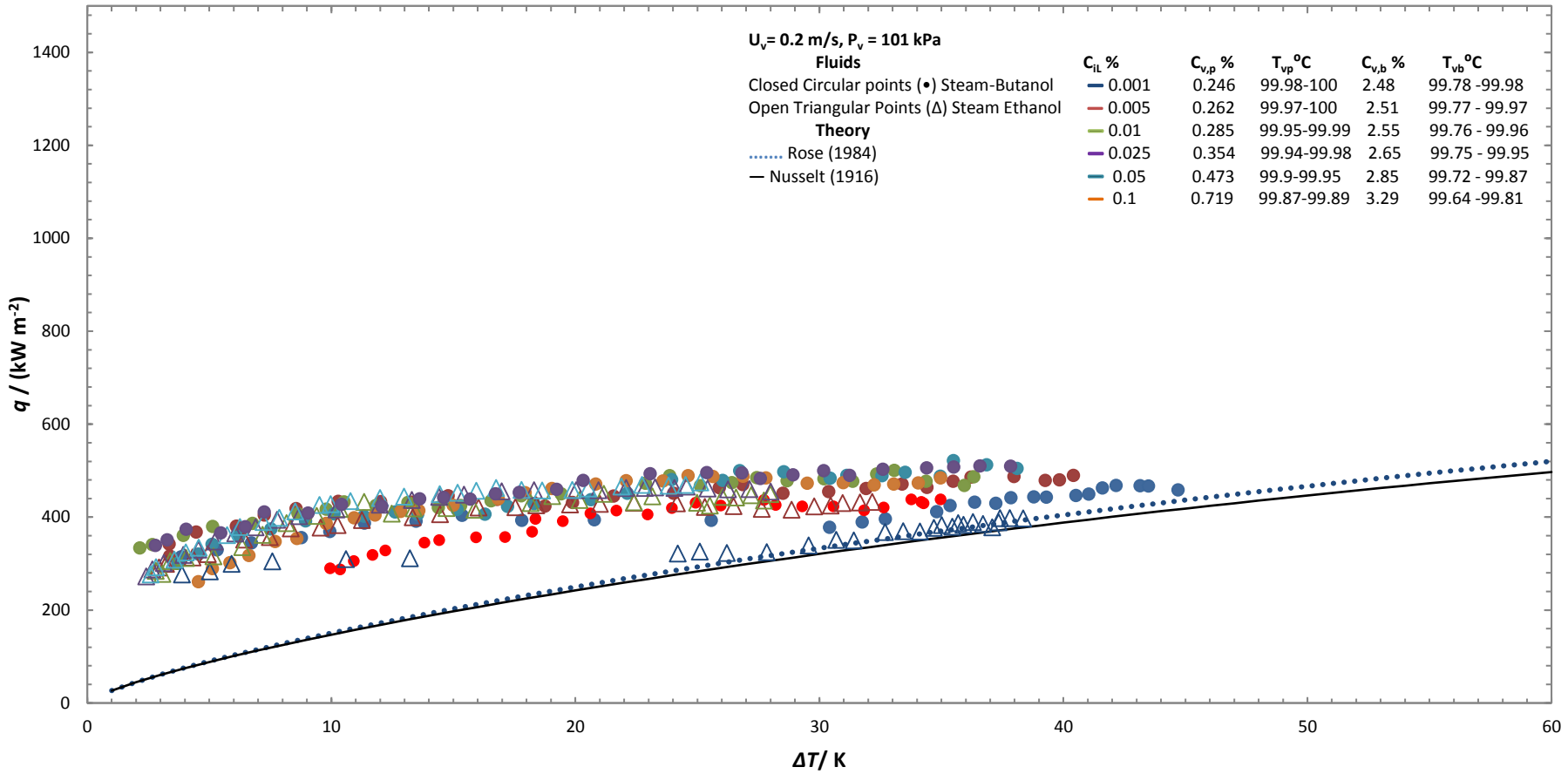

Figure 7.3 (Continued).

(a)

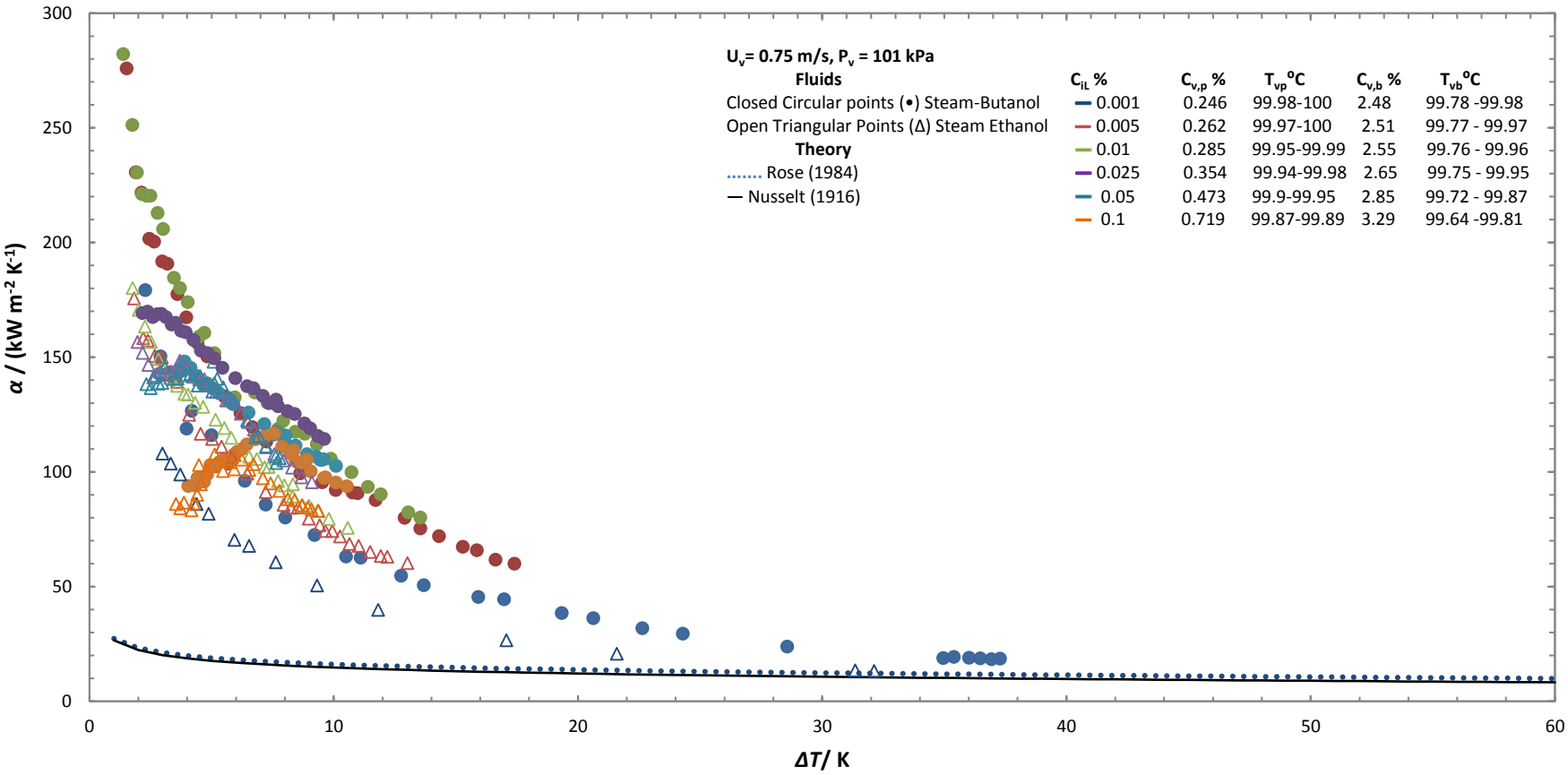

Figure 7-4: (a)-(e) shows variation of heat transfer coefficient against vapour-to-surface temperature difference for varying mass concentrations at each vapour velocity. (a) Uv = 0.75 m/s, (b) Uv = 0.56 m/s, (c) Uv = 0.46 m/s, (d) Uv = 0.35 m/s, (e) Uv = 0.20 m/s. Steam-butanol data is presented with closed points and steam-propanol data with open points. Test section vapour pressure is 101 kPa.

(b)

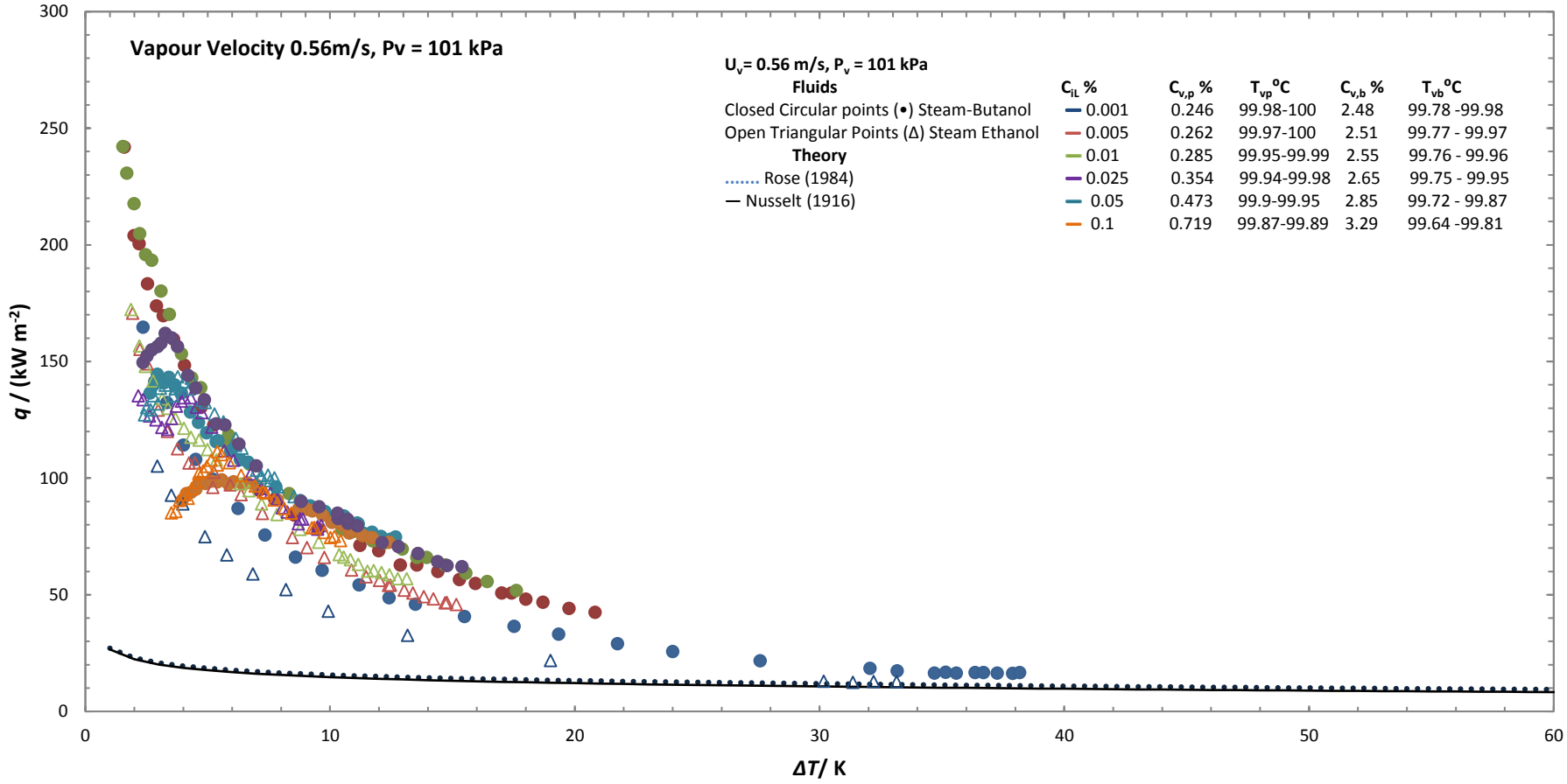

Figure 7.4 (Continued).

(c)

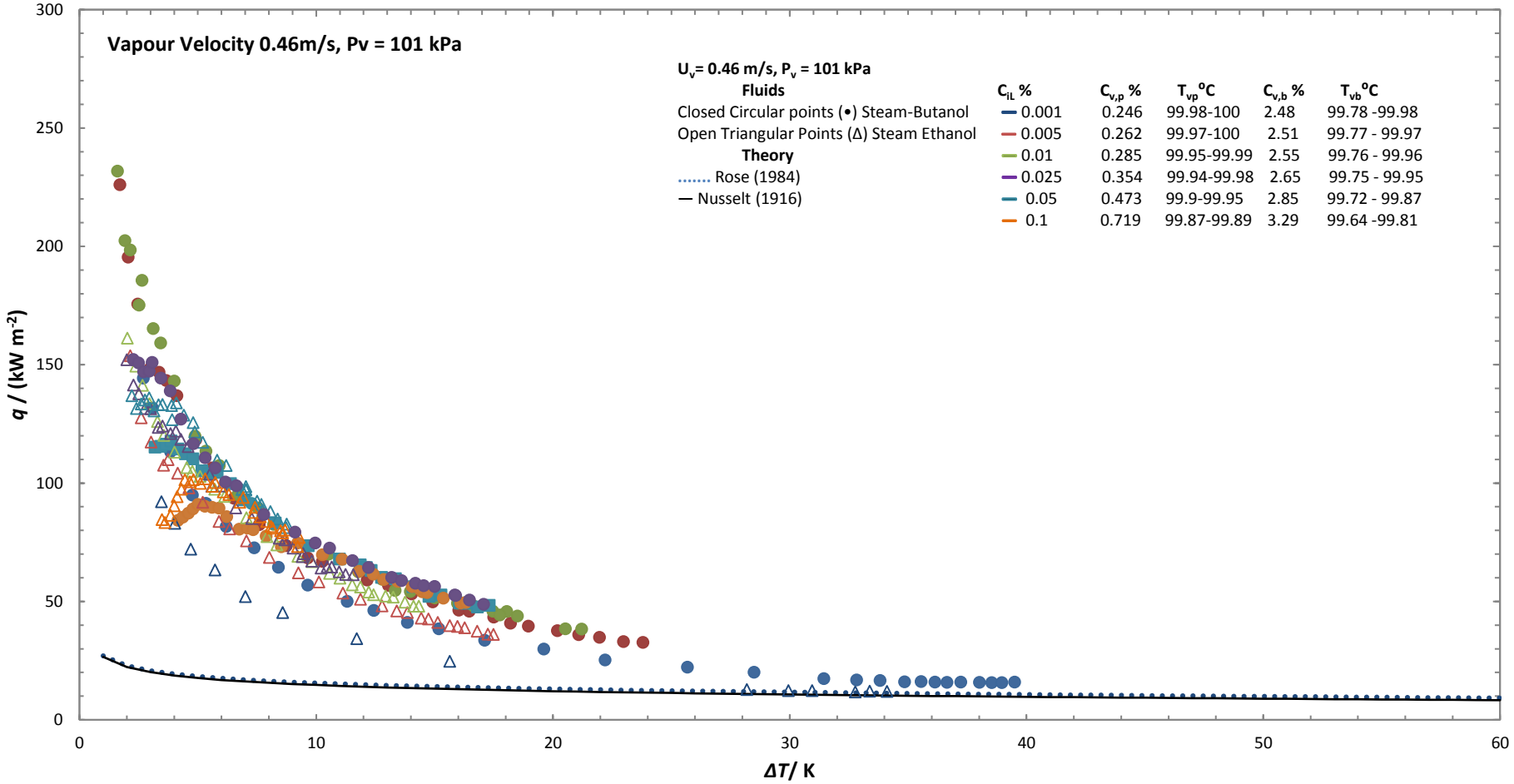

Figure 7.4 (Continued).

(d)

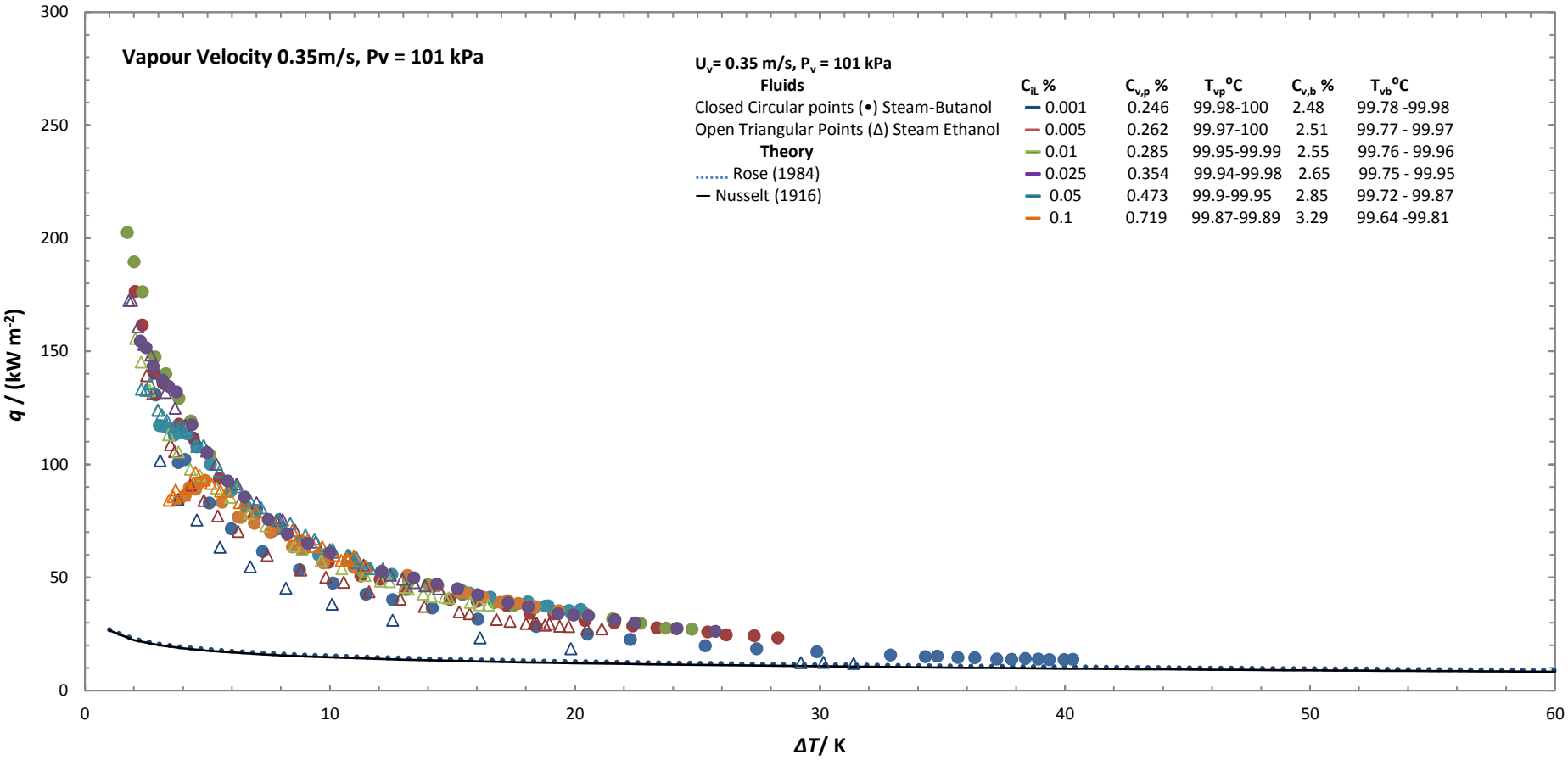

Figure 7.4 (Continued).

(e)

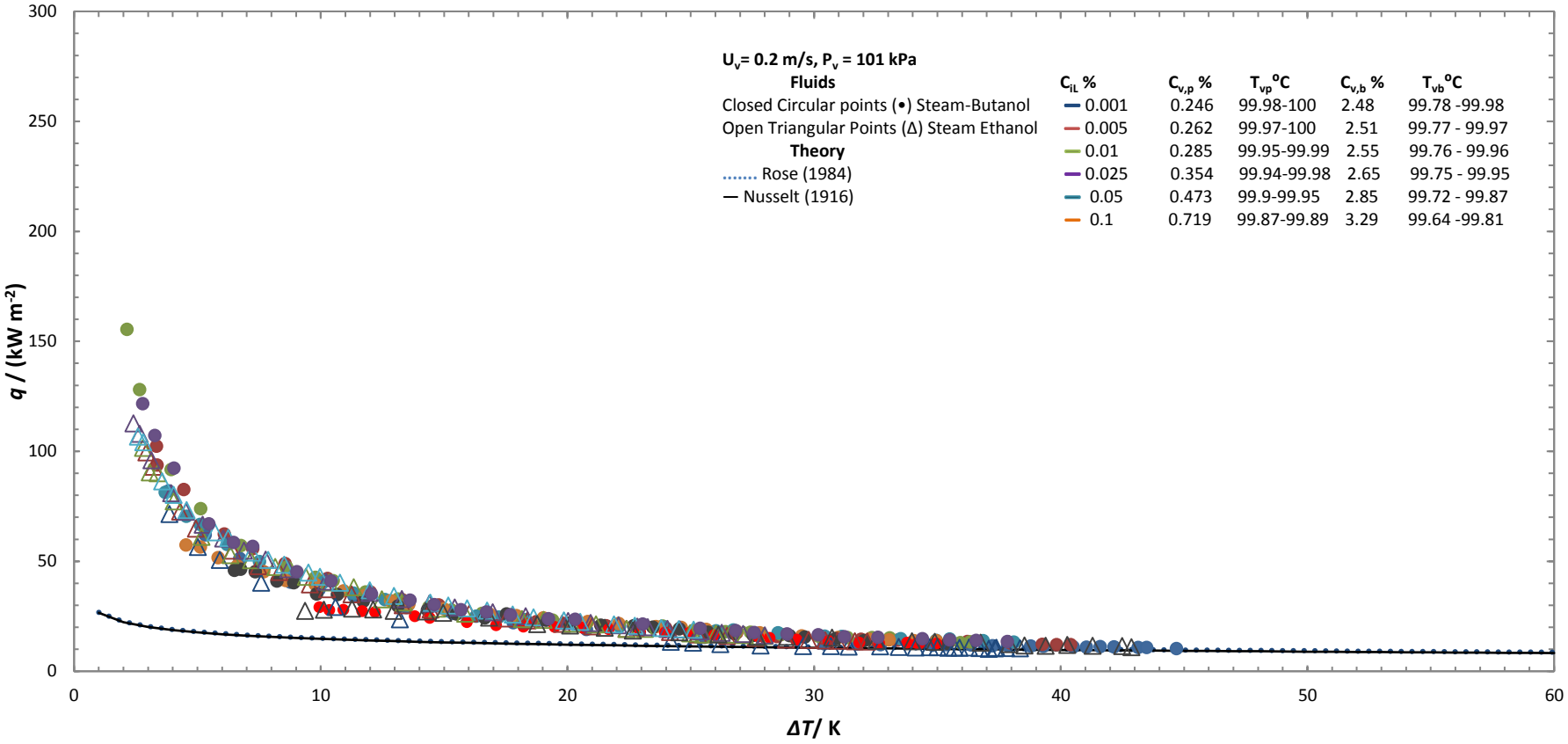

Figure 7.4 (Continued).

7.2.2 Enhancement (comparison with butanol)

Equation 5.3 of enhancement ratio can be modified for steam-propanol mixtures as:

$$\varepsilon_{sp} = \left(\frac{q_{sp}}{q_{Ro,ps}} \right)_{\Delta T, U_v} \tag{7.1}$$

where,

ε_{sp} is the enhancement ratio of the steam-propanol mixture at a given vapour velocity and vapour-to-surface temperature difference.

q_{sp} is observed heat flux for steam-propanol mixtures at a given vapour velocity and vapour-to-surface temperature difference.

$q_{Ro,ps}$ is the theoretical heat flux for pure steam obtained by Rose (1984) theory at a given vapour velocity and vapour-to-surface temperature difference.

For pure steam data, Rose (1984) theory was employed for each vapour velocity as it gives a precise representation of steam experimental data in this investigation (see chapter 5 figures 5.1). Since heat transfer properties are strongly dependent on the vapour-to-surface temperature difference, therefore, the enhancement ratio is also dependent on the vapour-to-surface temperature difference.

Figures 7.5 Shows enhancement ratio for steam-propanol mixtures for various mass compositions and vapour velocities. For all the mass compositions and vapour velocities, the enhancement ratio exceeds unity over the entire range of vapour-to-surface temperature difference. The effect of vapour -to-surface temperature difference is same for steam-propanol mixtures as observed in steam-ethanol and steam-butanol cases. Propanol concentration has a significant effect on the enhancement ratios at lower vapour to surface temperature difference. At lower mass concentrations, the highest enhancement ratio of 7.4 was observed at vapour-to-surface temperature difference (ΔT= 5.23 K) for the mass composition of 0.05%. Figure 7.6 shows the effect of vapour velocity on the enhancement ratio.

Figure 7.7 to 7.12 shows the comparison between enhancement ratios of steam-butanol and steam-ethanol mixtures with stem propanol mixtures respectively. Ethanol shows maximum enhancement ratio of 5.47 at vapour velocity of 0.78m/s for ethanol mass composition of 0.01%, steam-butanol mixture shows an enhancement ratio of 11. And steam-propanol mixture shows an enhancement ratio of 8.4.

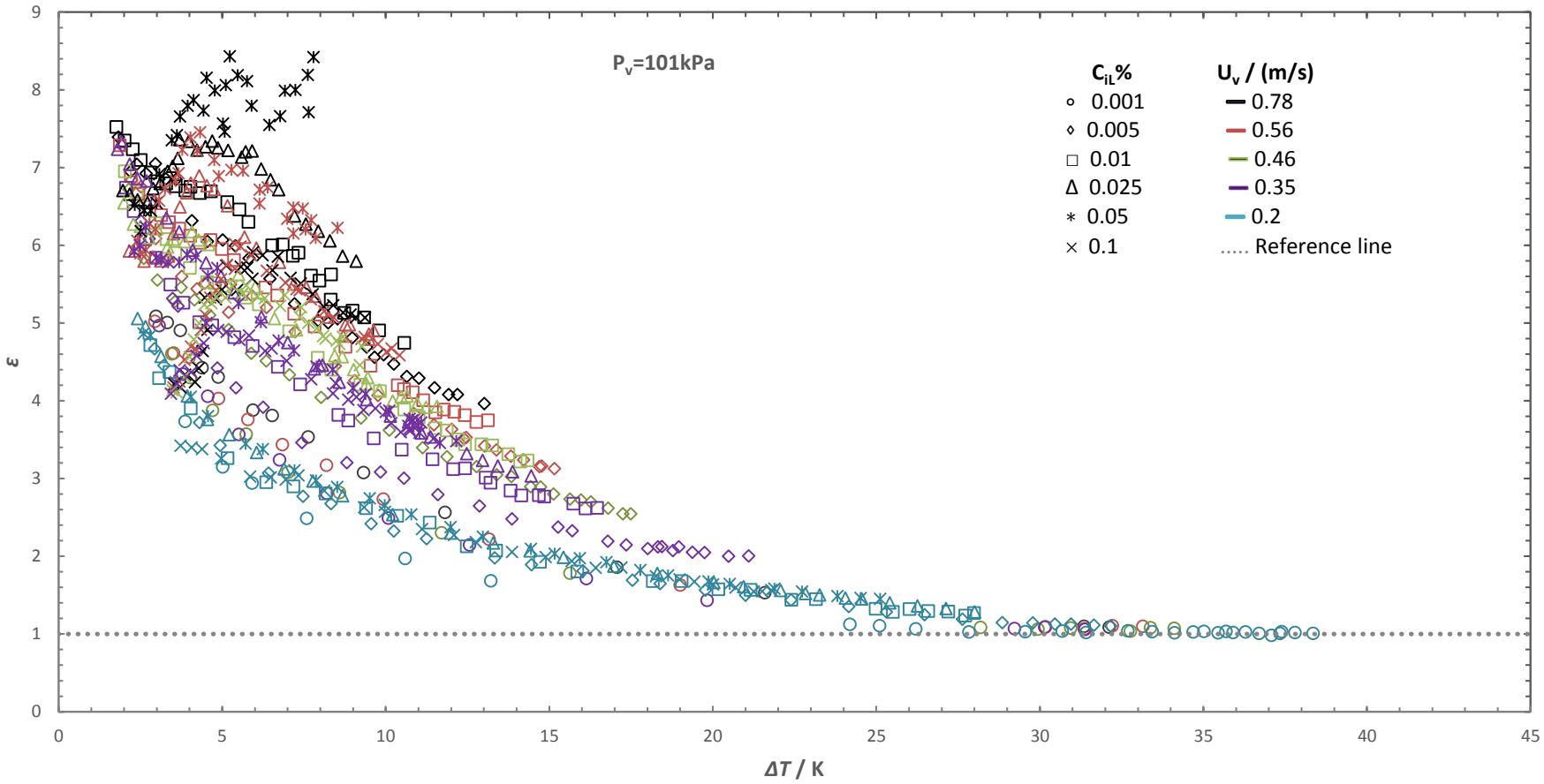

Figure 7-5: Enhancement Ratio of steam-propanol mixtures of various compositions and vapour velocities. The grey dotted line is the pure steam line used as a reference.

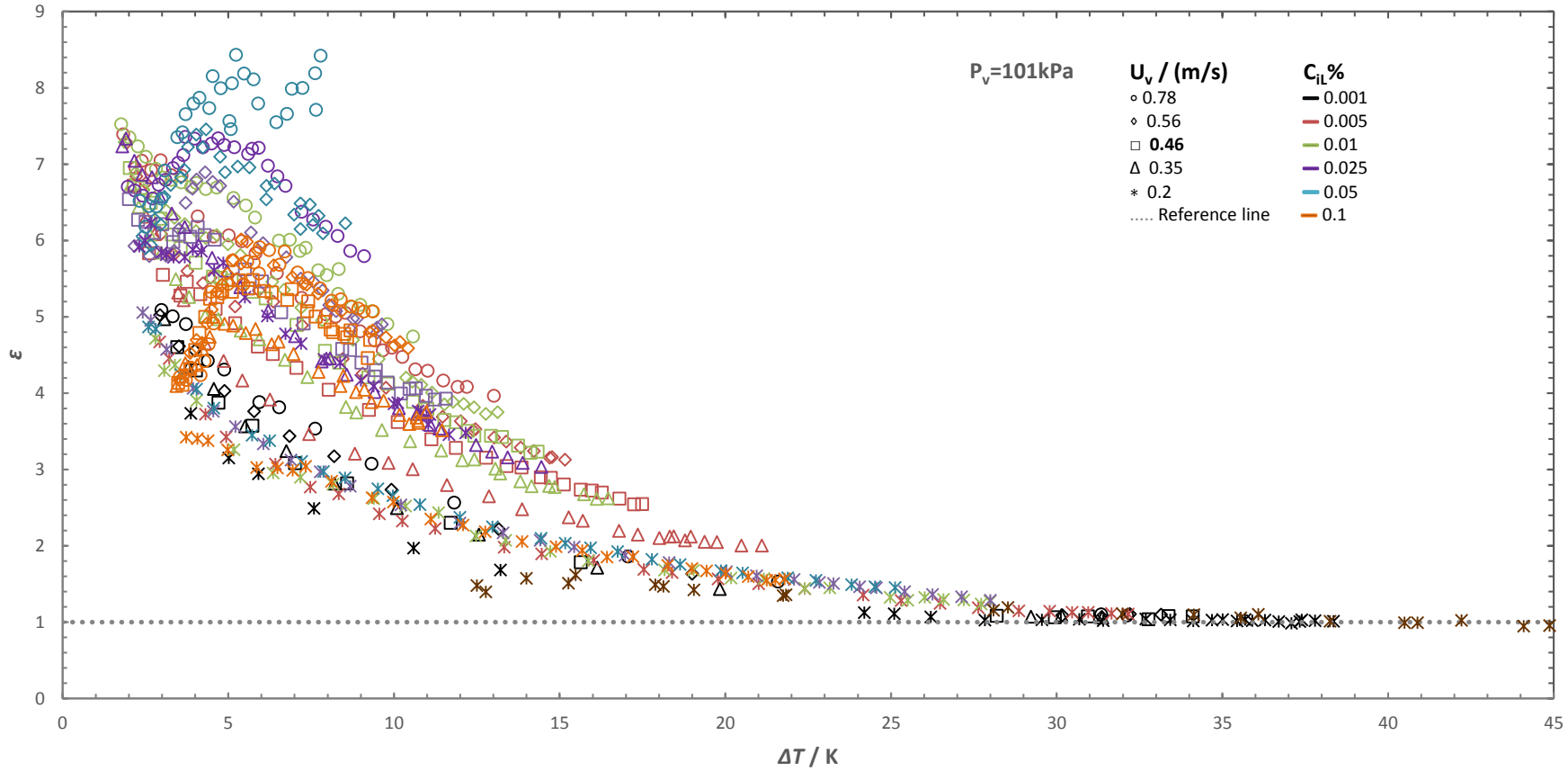

Figure 7-6: Enhancement Ratio of steam-propanol mixtures of various compositions and vapour velocities. The grey dotted line is the pure steam line used as a reference.

(a)

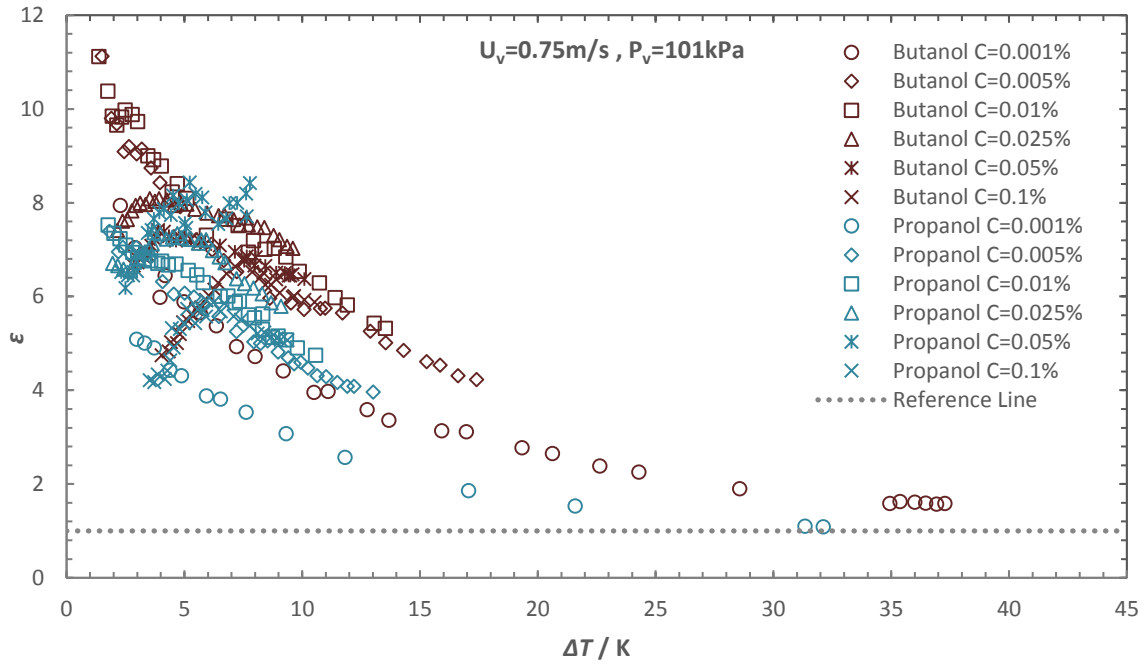

(b)

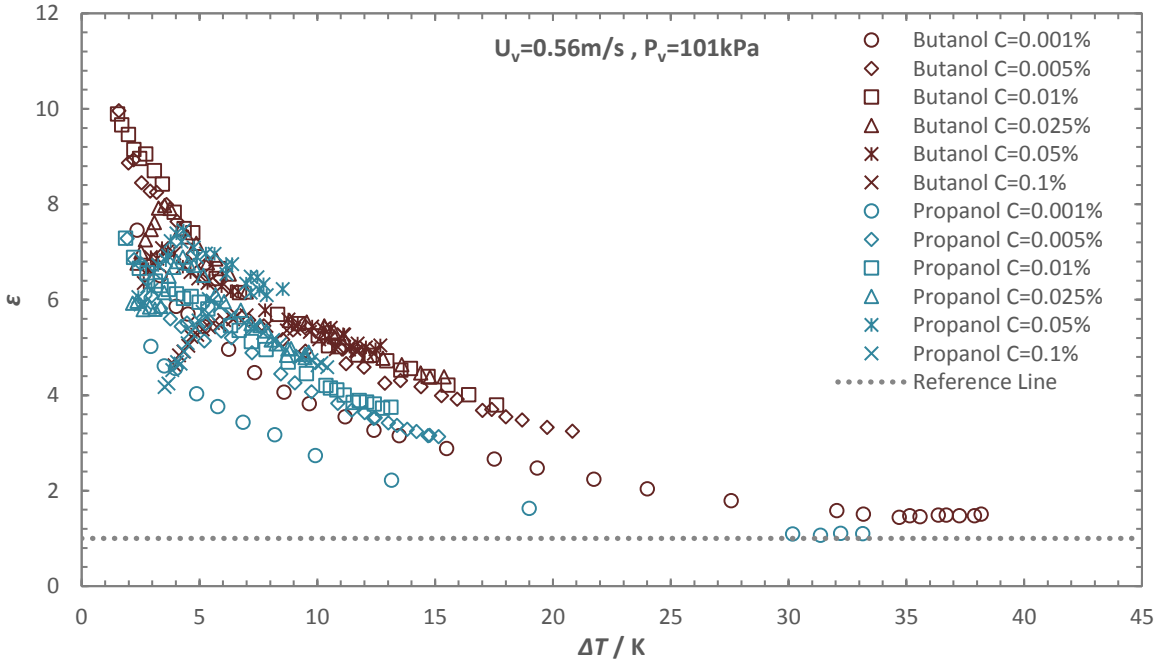

Figure 7-7: Comparison between the enhancement ratio of steam-butanol with steam-propanol for various mass compositions at each vapour velocity. Steam-butanol results are in dark red colour and steam-propanol results in cyan colour.

(c)

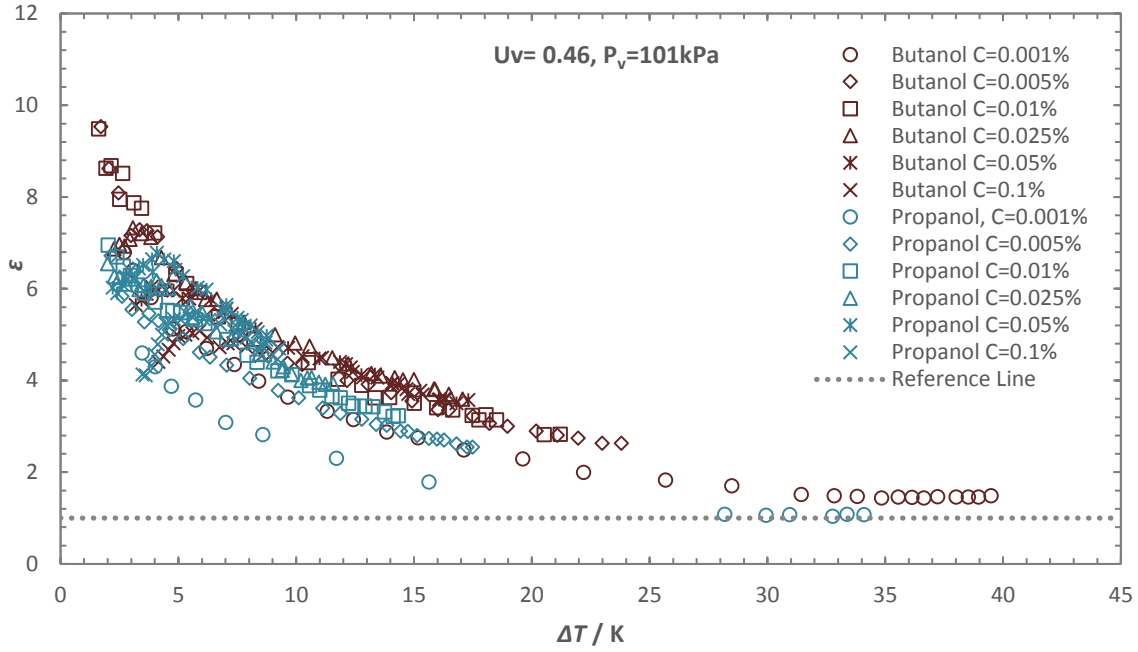

(d)

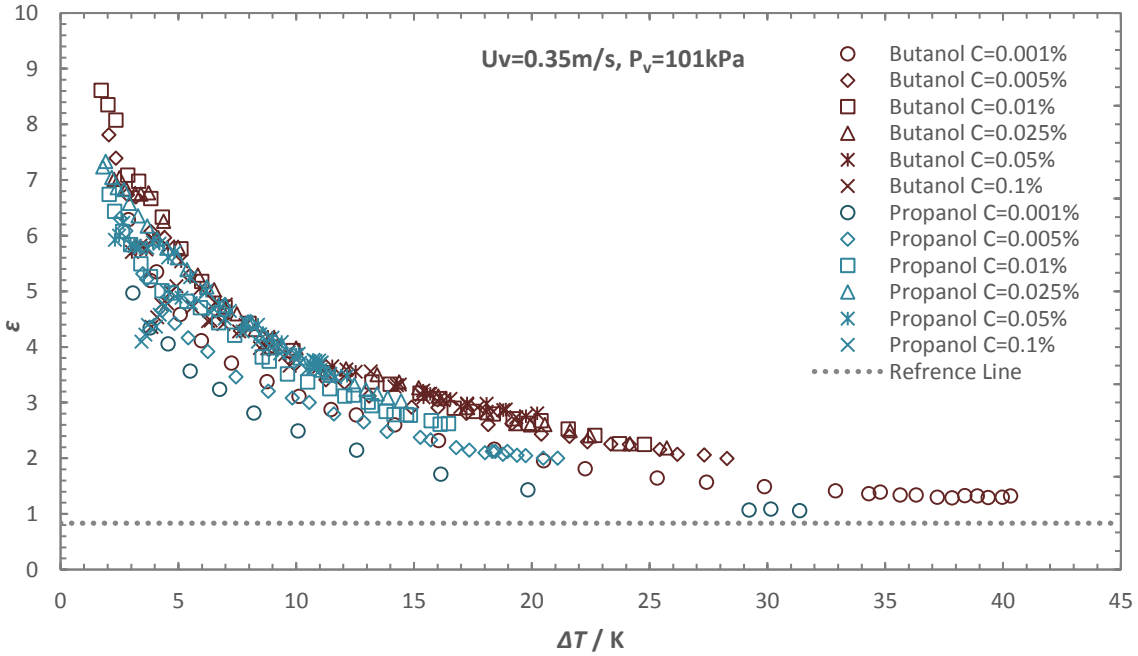

Figure 7.7 (Continued).

(e)

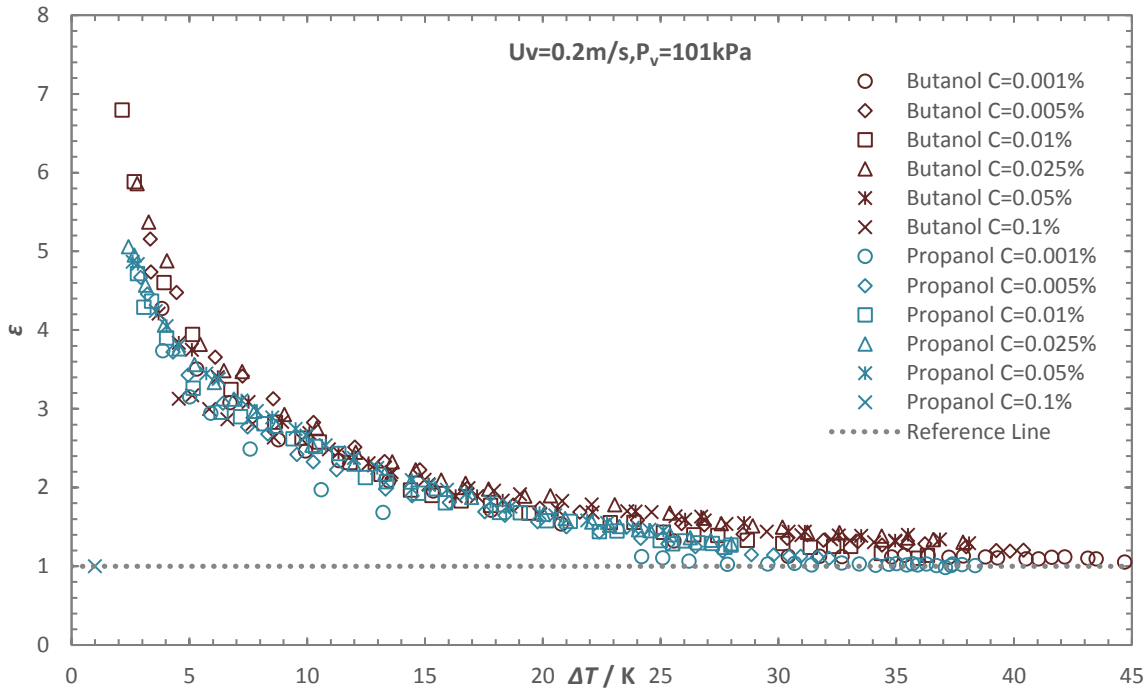

Figure 7.7 (Continued).

7.2.3 Comparison between steam-ethanol and the steam-propanol mixtures

(a)

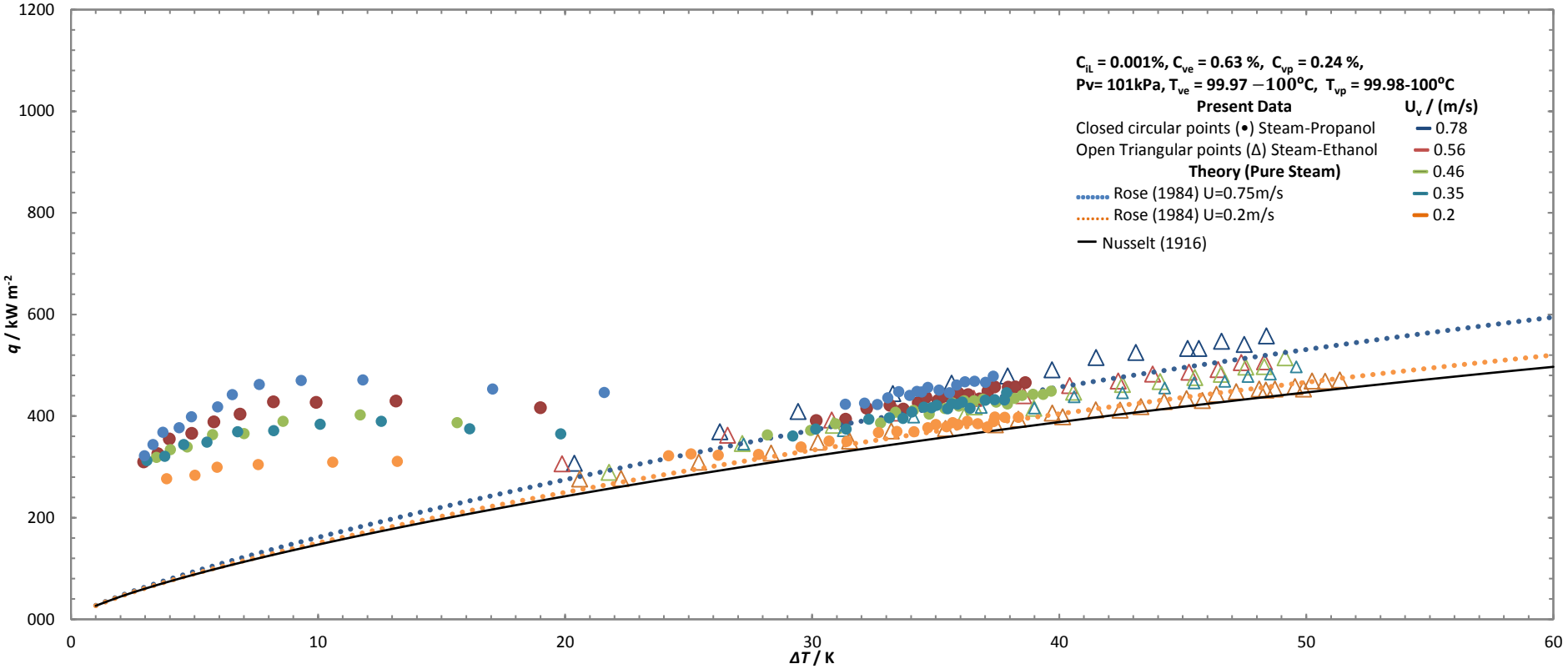

Figure 7-8: (a)-(f) shows variation of heat flux against vapour-to-surface temperature difference for varying vapour velocities at each propanol mass concentration. (a) CiL = 0.001%, (b) CiL = 0.005%, (c) CiL = 0.01%, (d) CiL = 0.025%, (e) CiL = 0.05% and (f) CiL = 0.1%. Steam-propanol data is presented with closed points and steam-ethanol data with open points. Test section vapour pressure is 101 kPa.

(b)

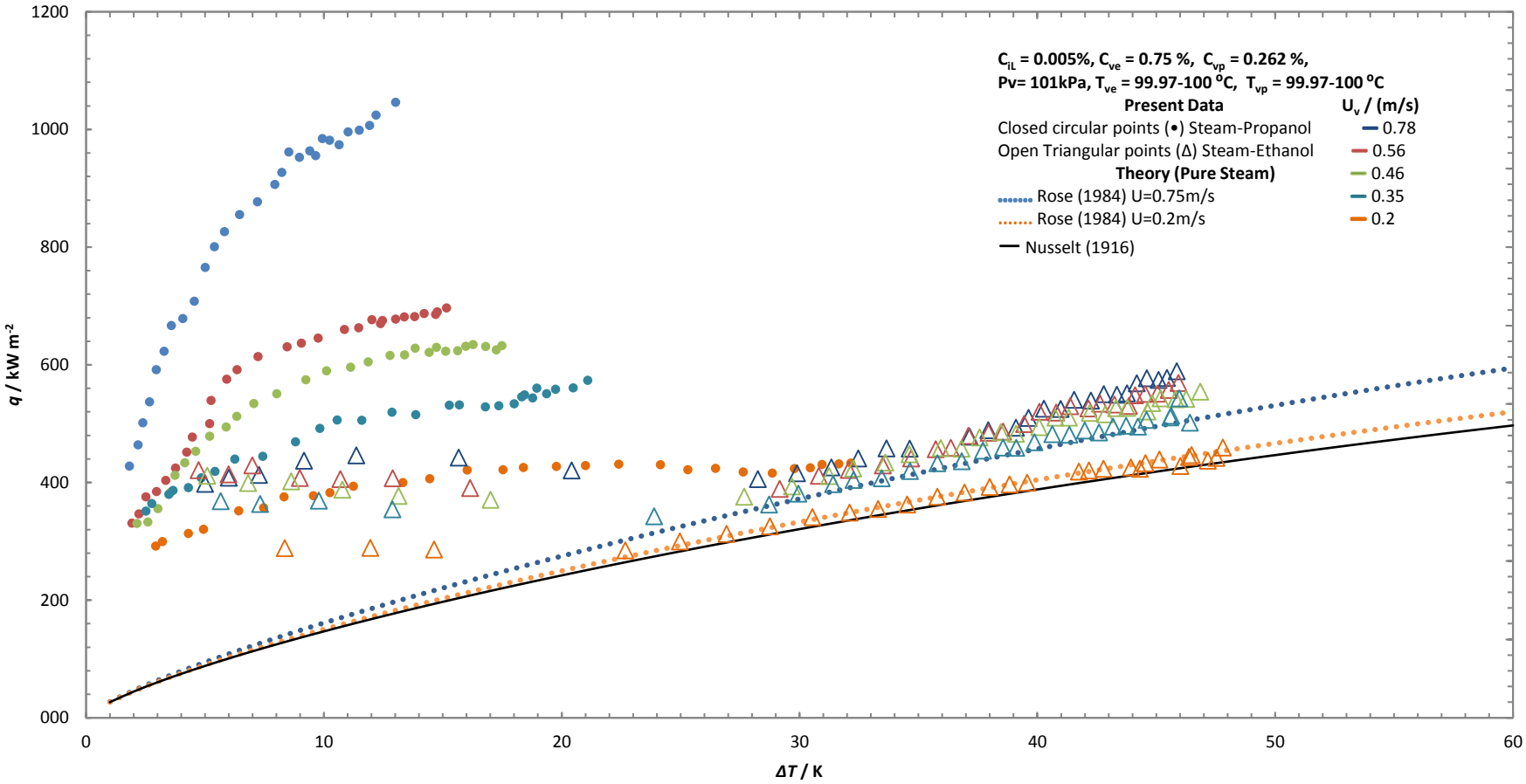

Figure 7.8 (Continued).

(c)

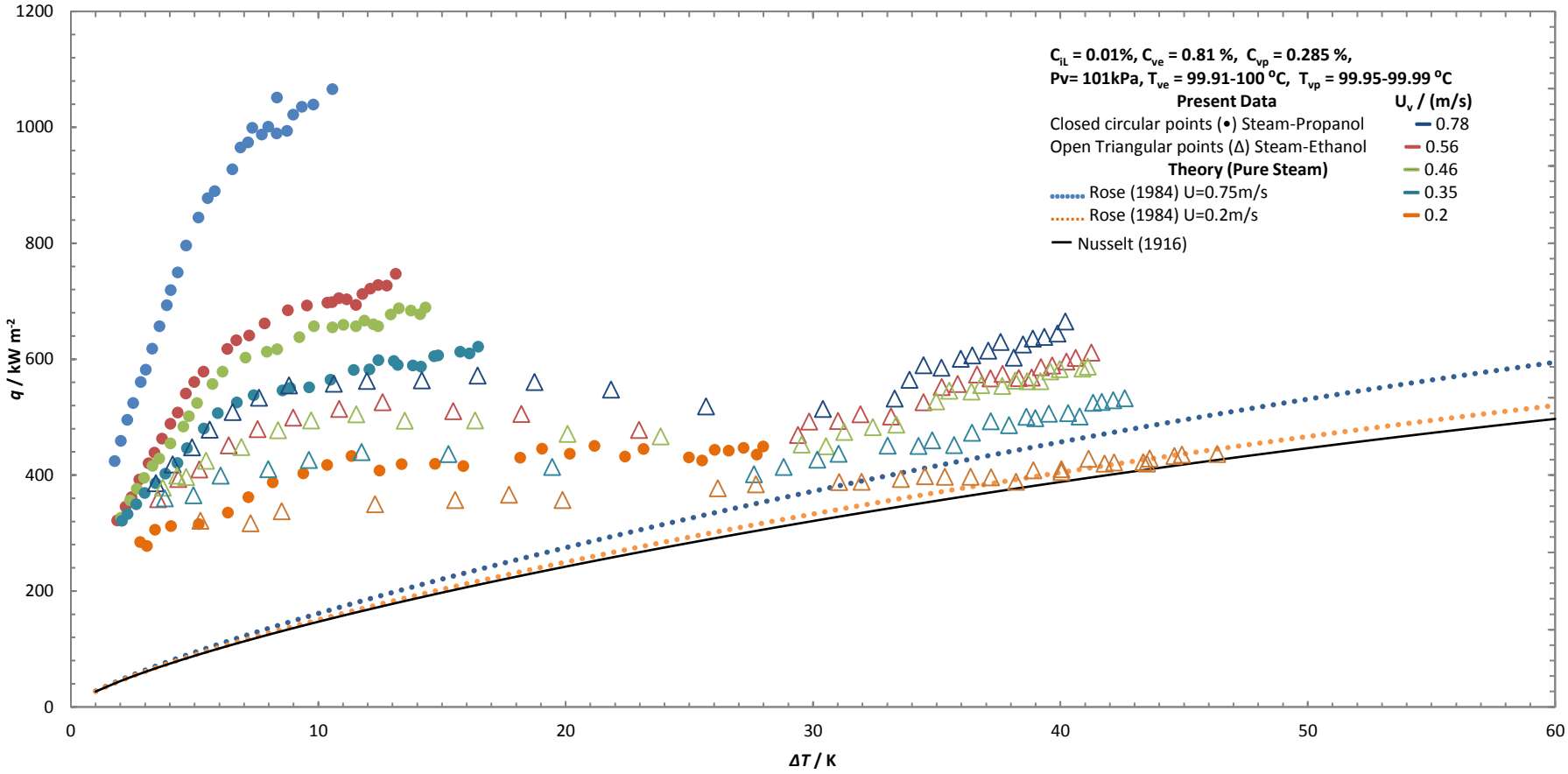

Figure 7.8 (Continued).

(d)

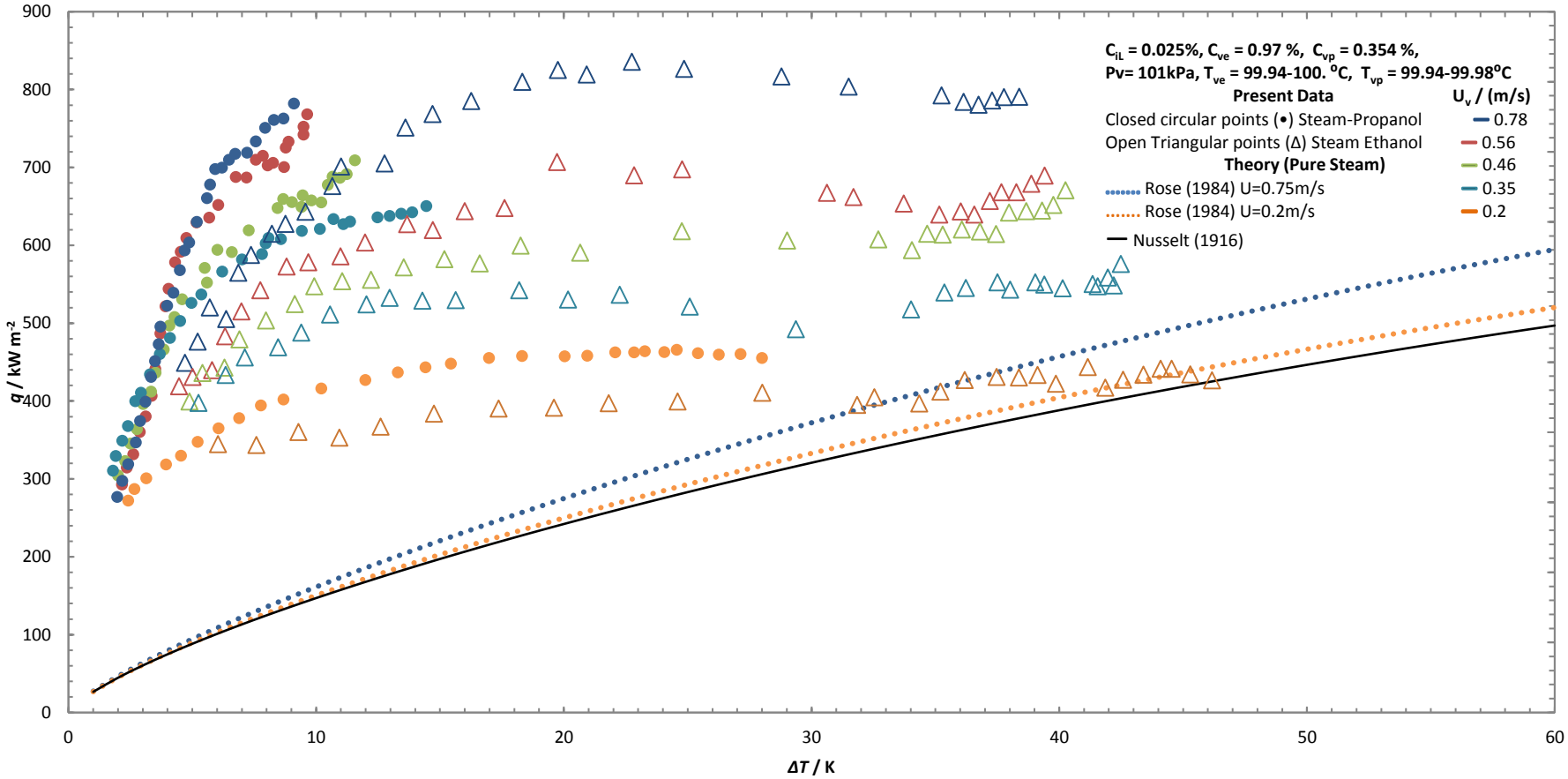

Figure 7.8 (Continued).

(e)

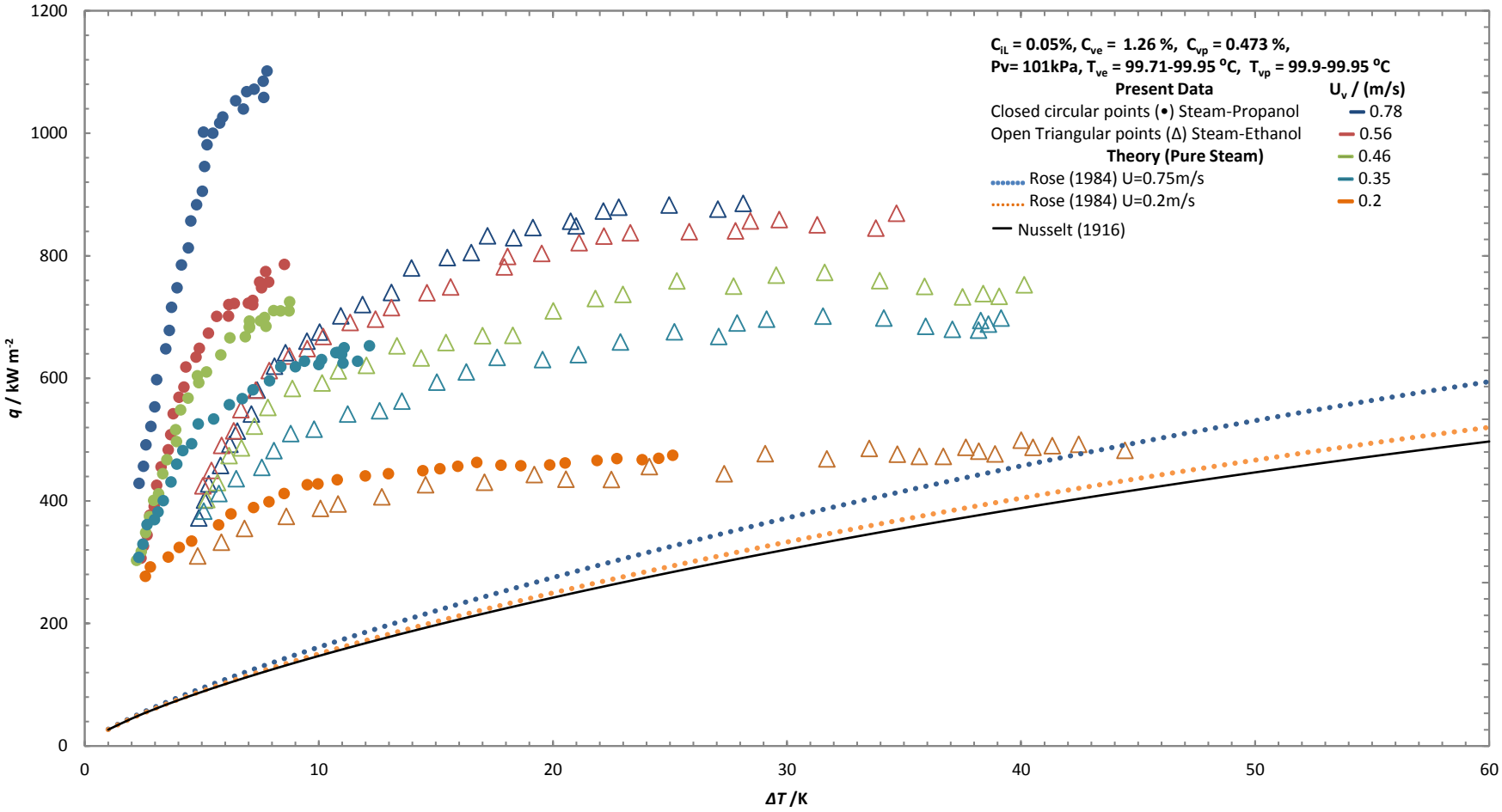

Figure 7.8 (Continued).

(f)

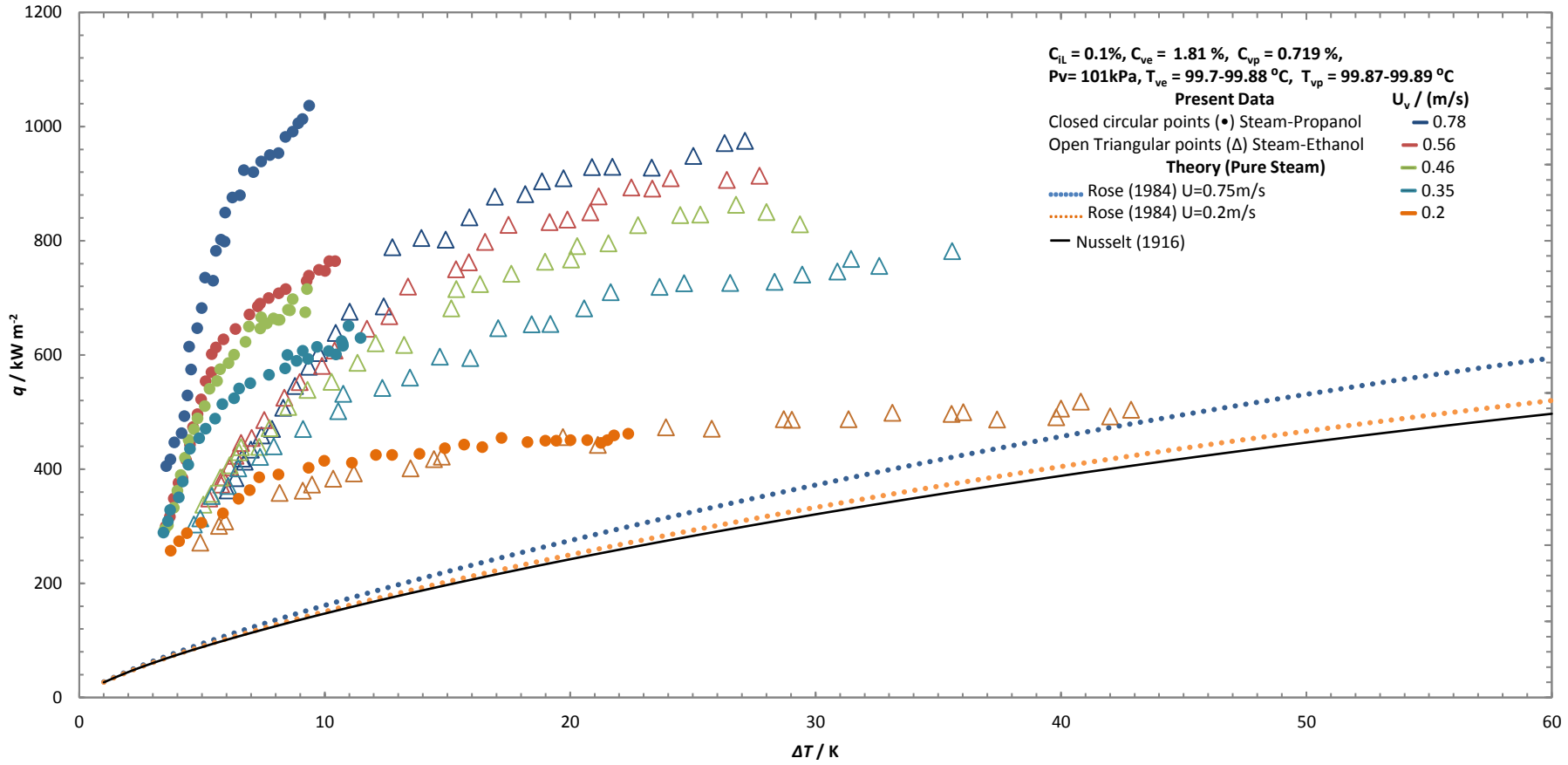

Figure 7.8 (Continued).

(a)

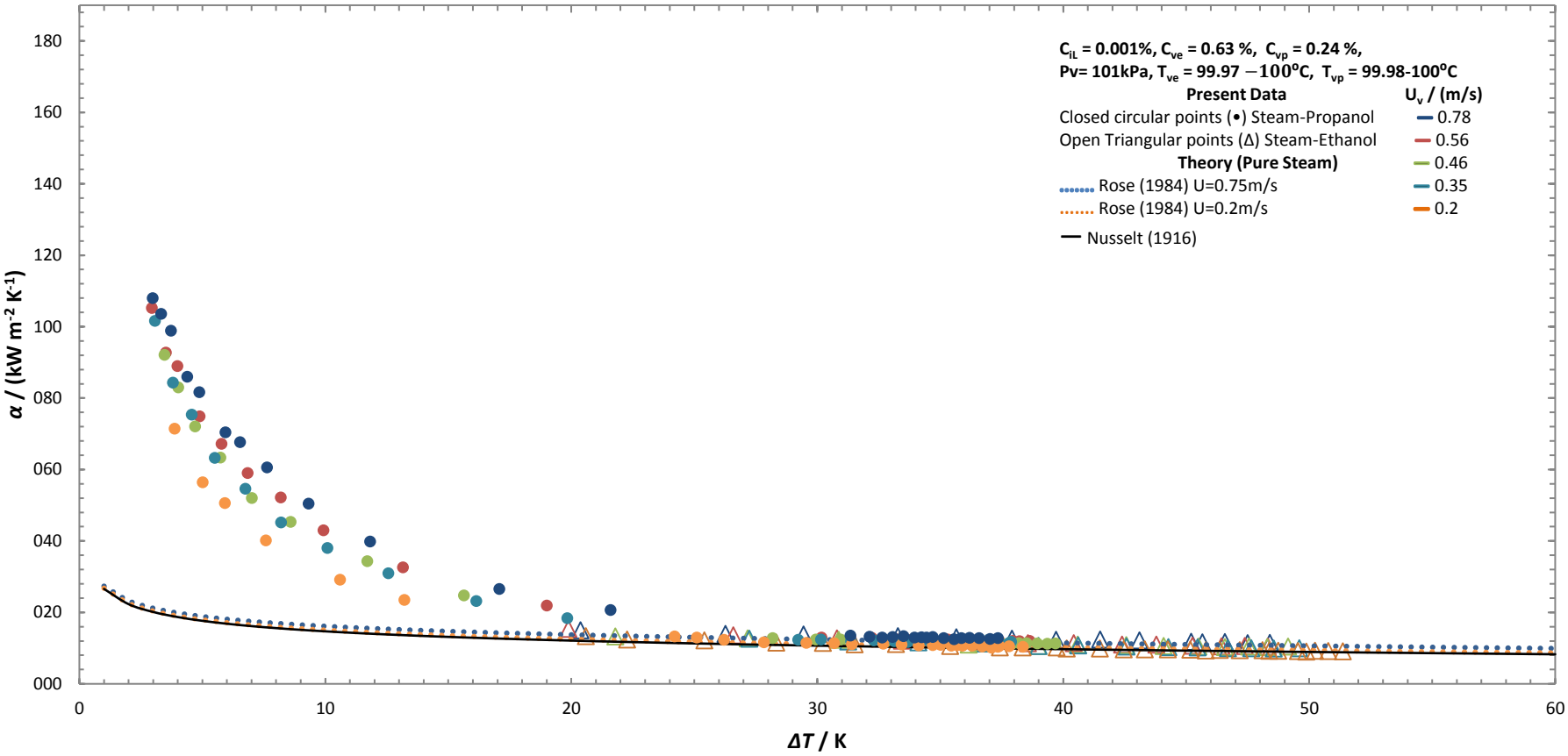

Figure 7-9: (a)-(f) shows variation of heat transfer coefficient against vapour-to-surface temperature difference for varying vapour velocities at each butanol mass concentration. (a) C_{iL} = 0.001%, (b) C_{iL} = 0.005%, (c) C_{iL} = 0.01%, (d) C_{iL} = 0.025%, (e) C_{iL} = 0.05% and (f) C_{iL} = 0.1%. Steam-propanol data is presented with closed points and steam-propanol data with open points. Test section vapour pressure is 101 kPa.

(b)

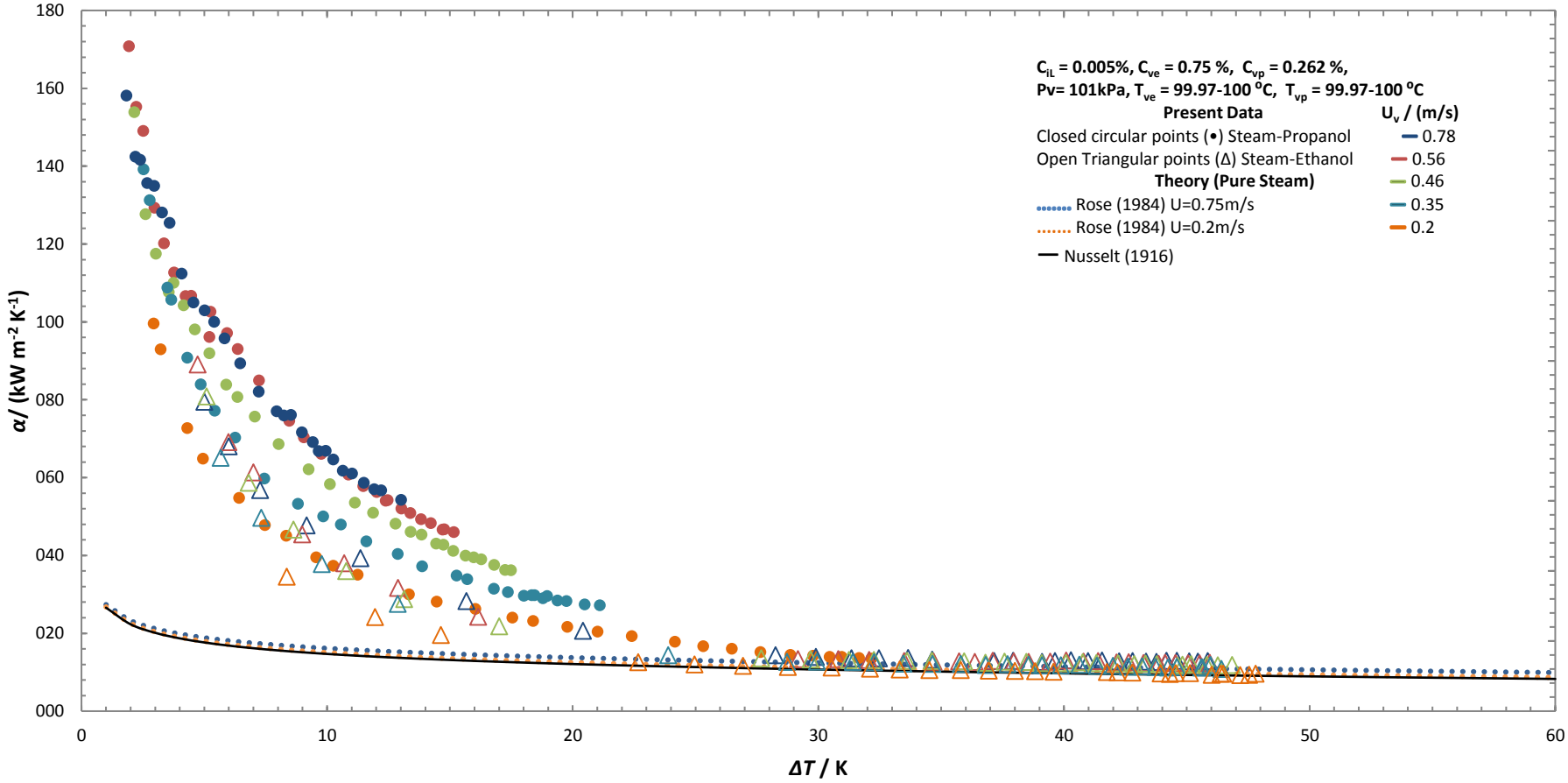

Figure 7.9 (Continued).

(c)

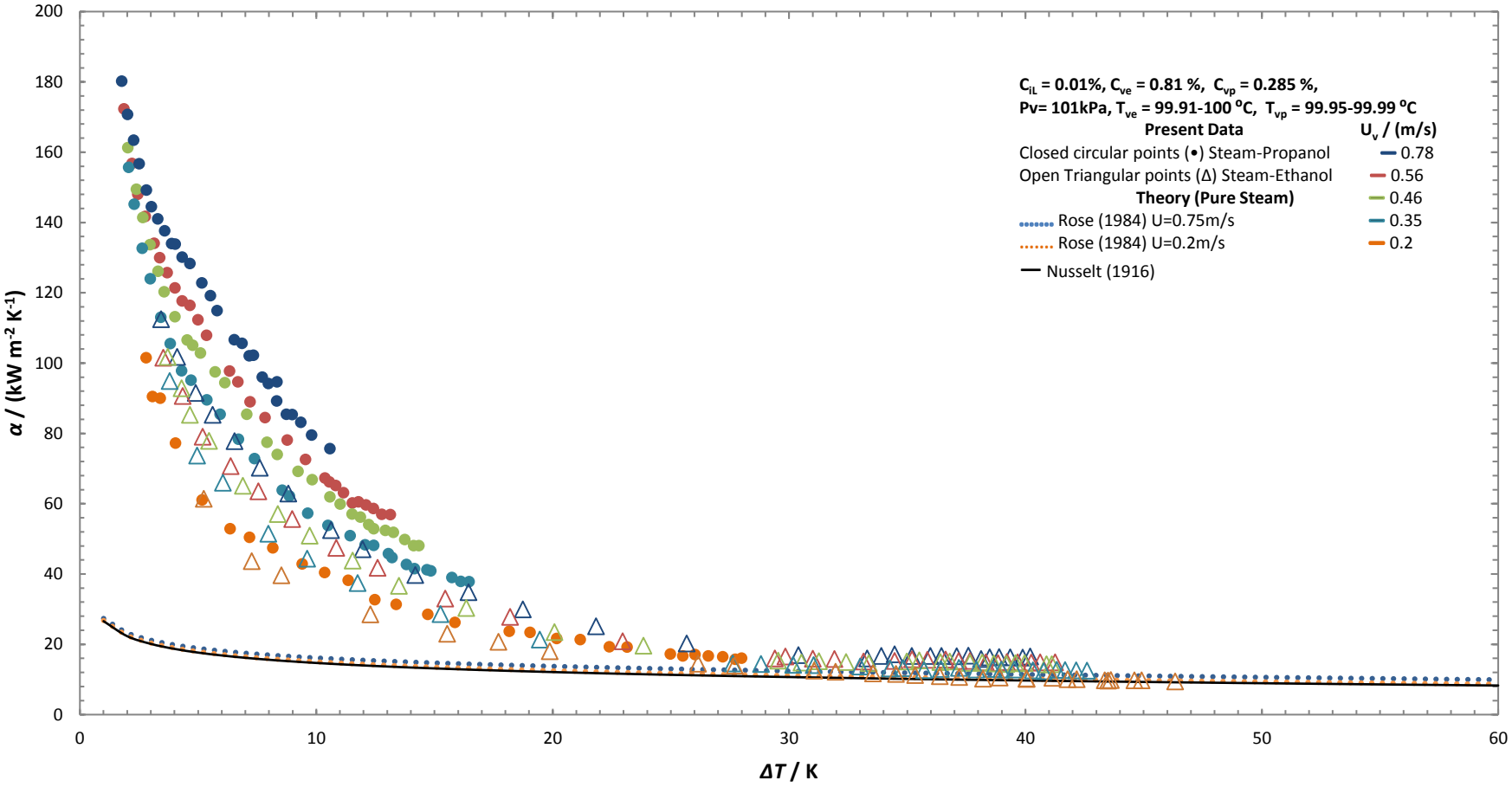

Figure 7.9 (Continued).

(d)

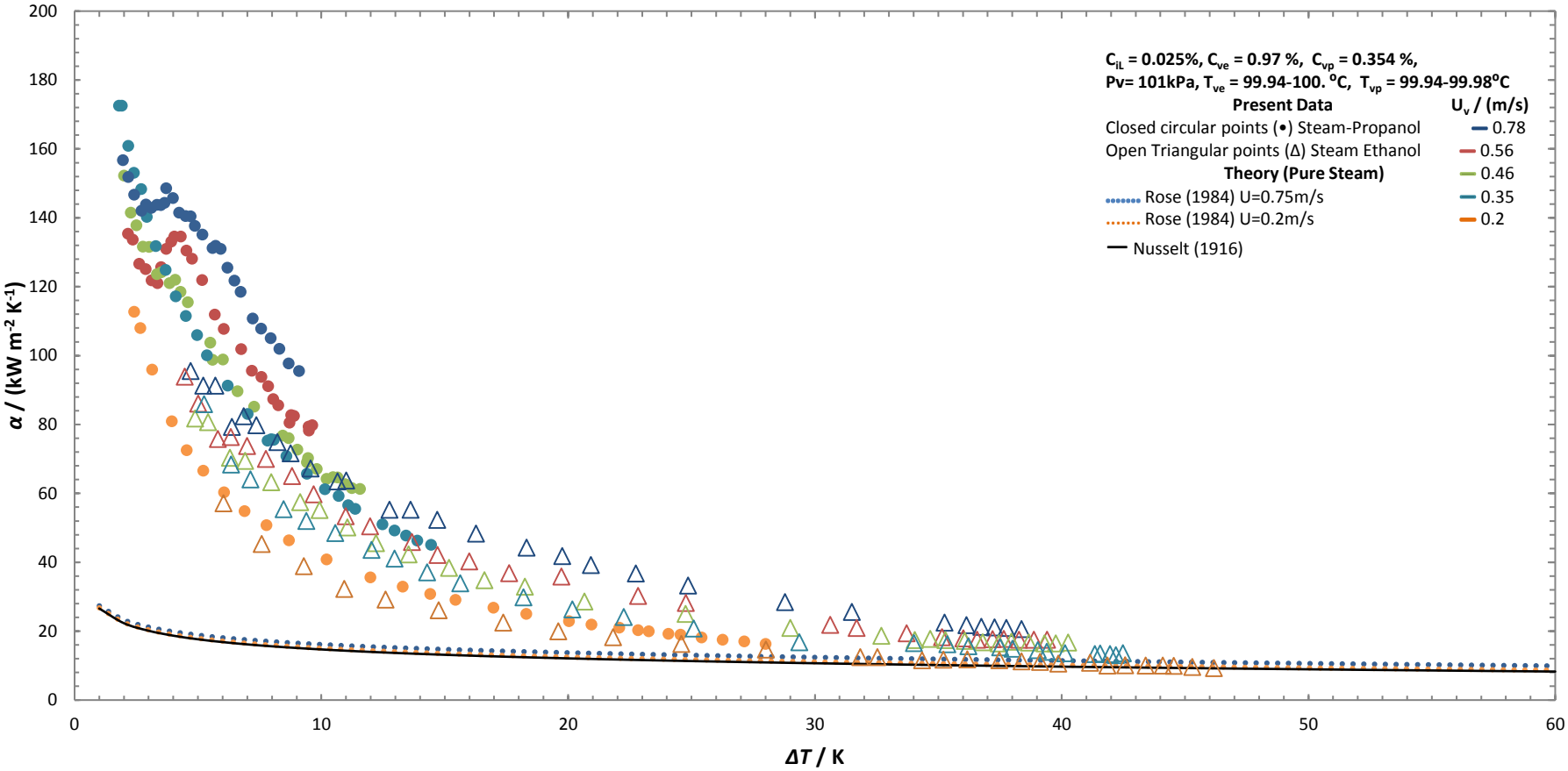

Figure 7.9 (Continued).

(e)

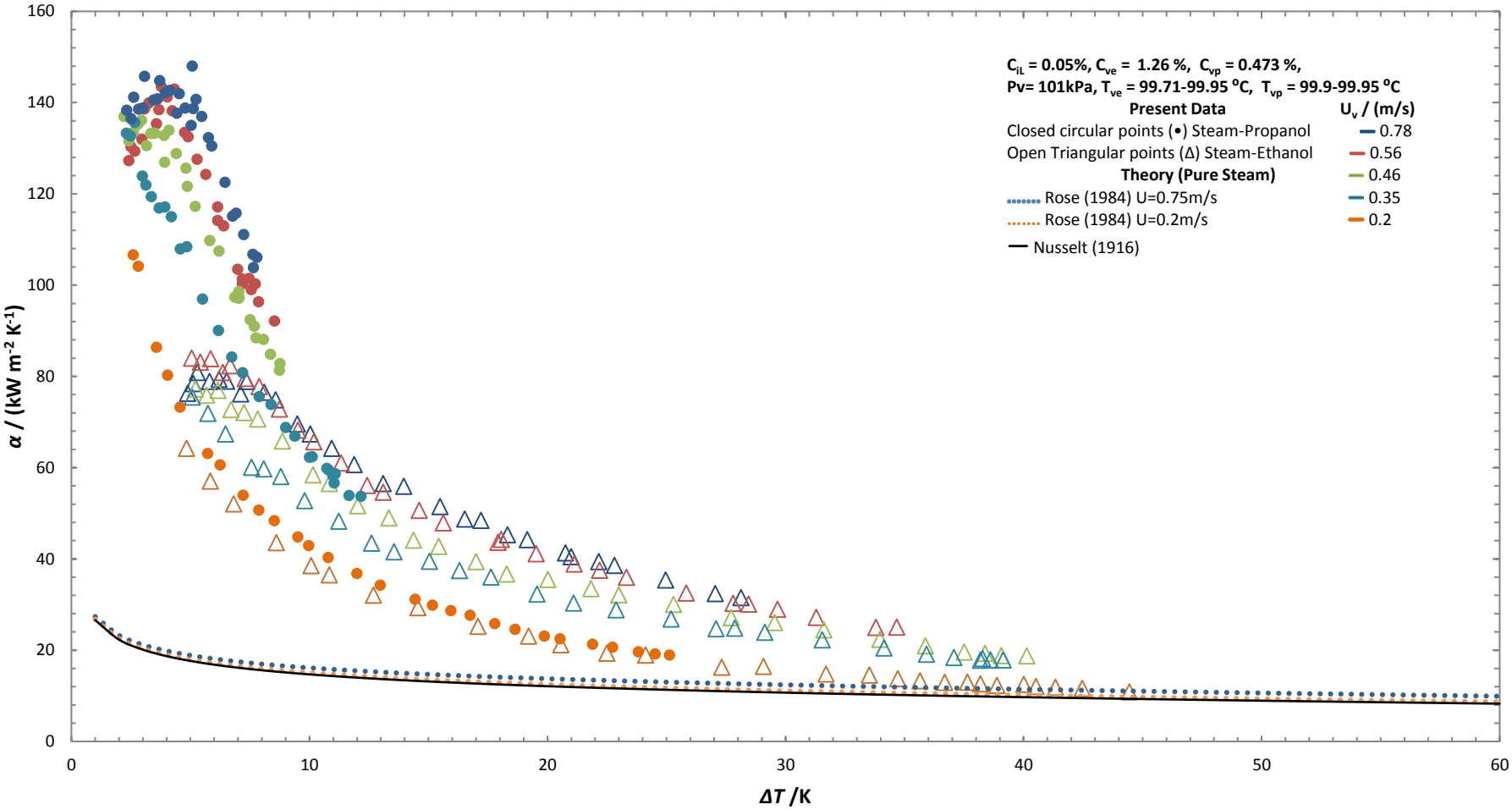

Figure 7.9 (Continued).

(f)

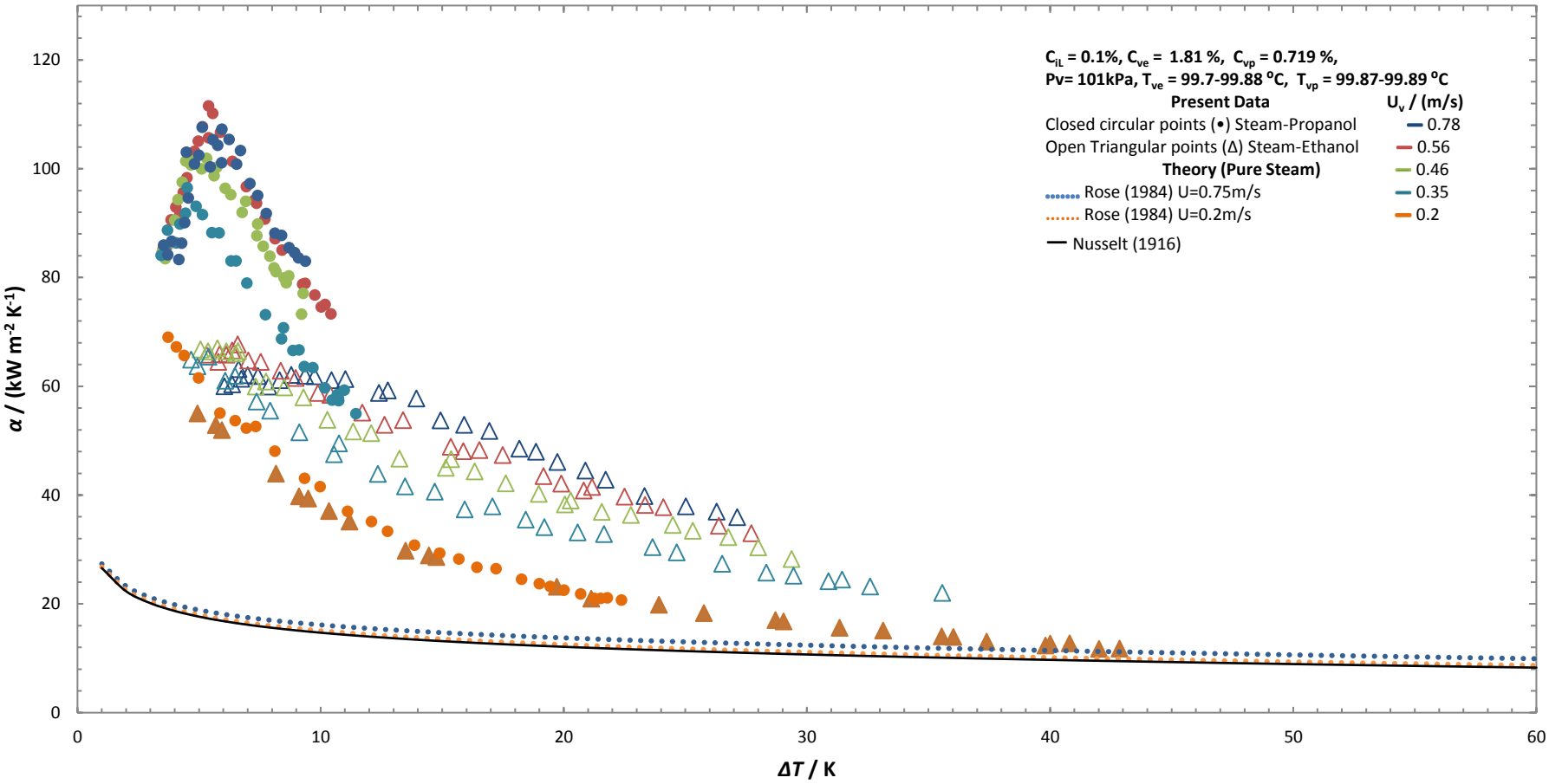

Figure 7.9 (Continued).

(a)

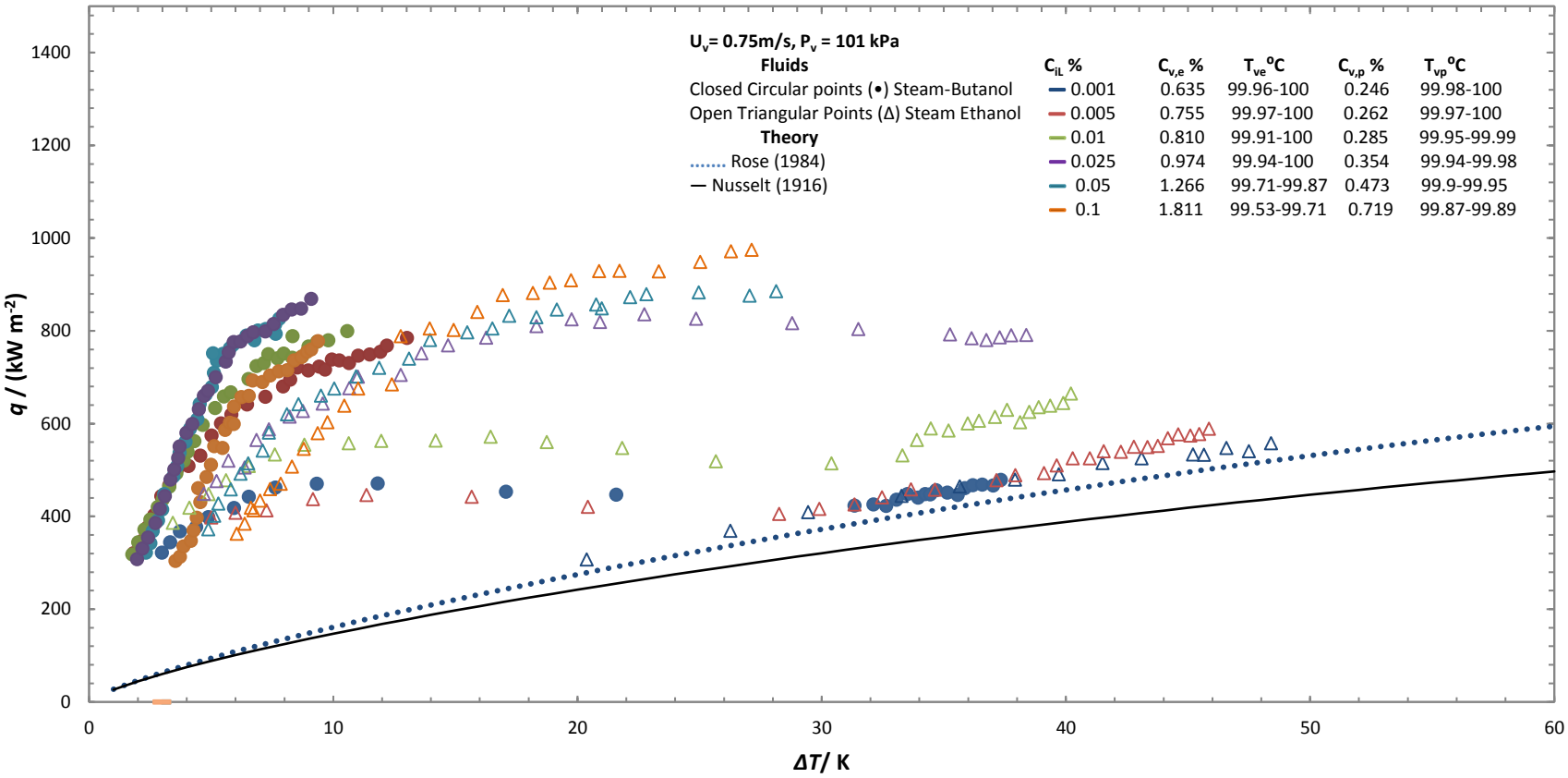

Figure 7-10: (a)-(e) shows variation of heat flux against vapour-to-surface temperature difference for varying mass concentrations at each vapour velocity. (a) Uv = 0.75 m/s, (b) Uv = 0.56 m/s, (c) Uv = 0.46 m/s, (d) Uv = 0.35 m/s, (e) Uv = 0.20 m/s. Steam-propanol data is presented with closed points and steam-ethanol data with open points. Test section vapour pressure is 101 kPa.

(b)

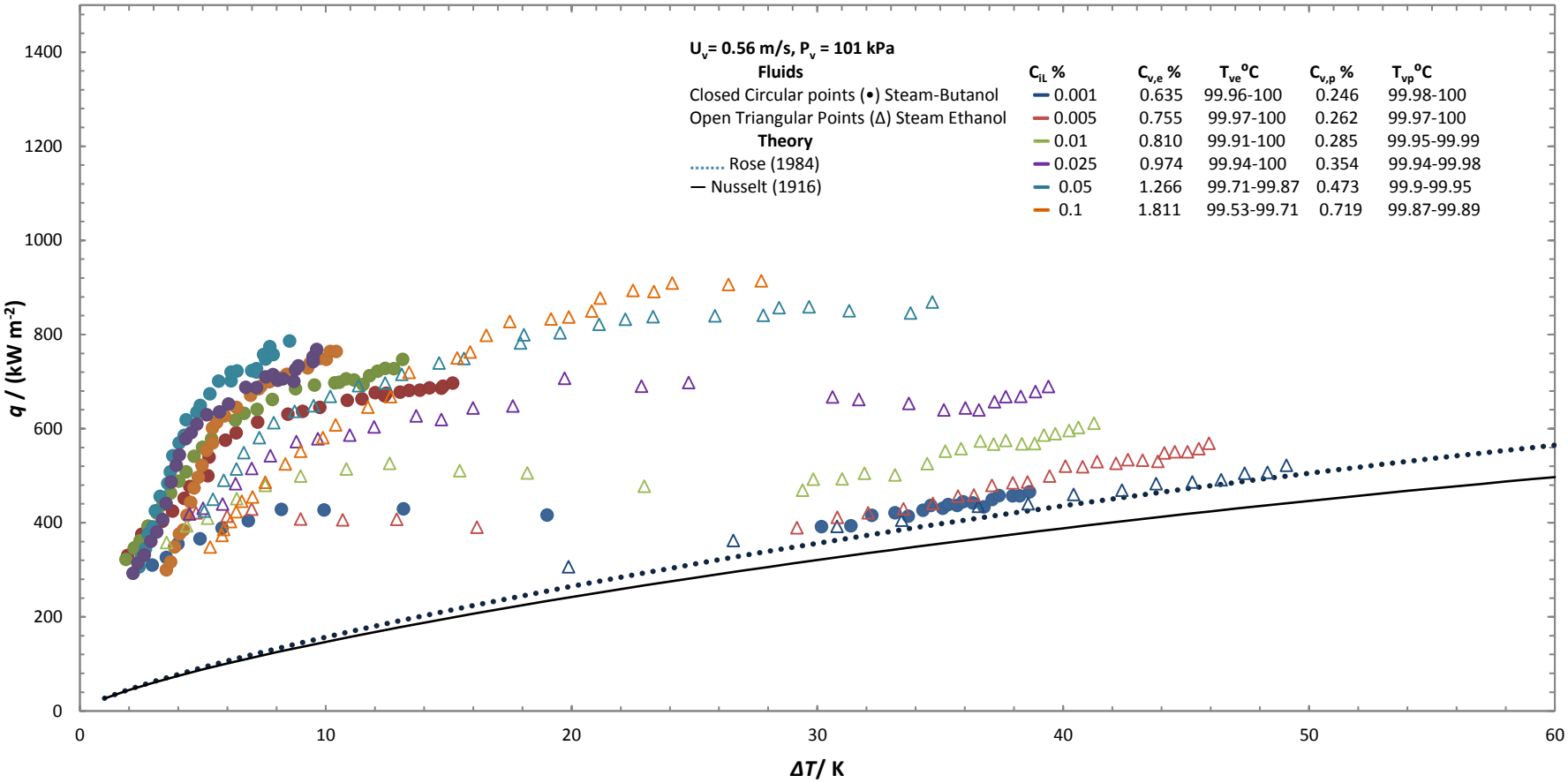

Figure 7.10 (Continued).

(c)

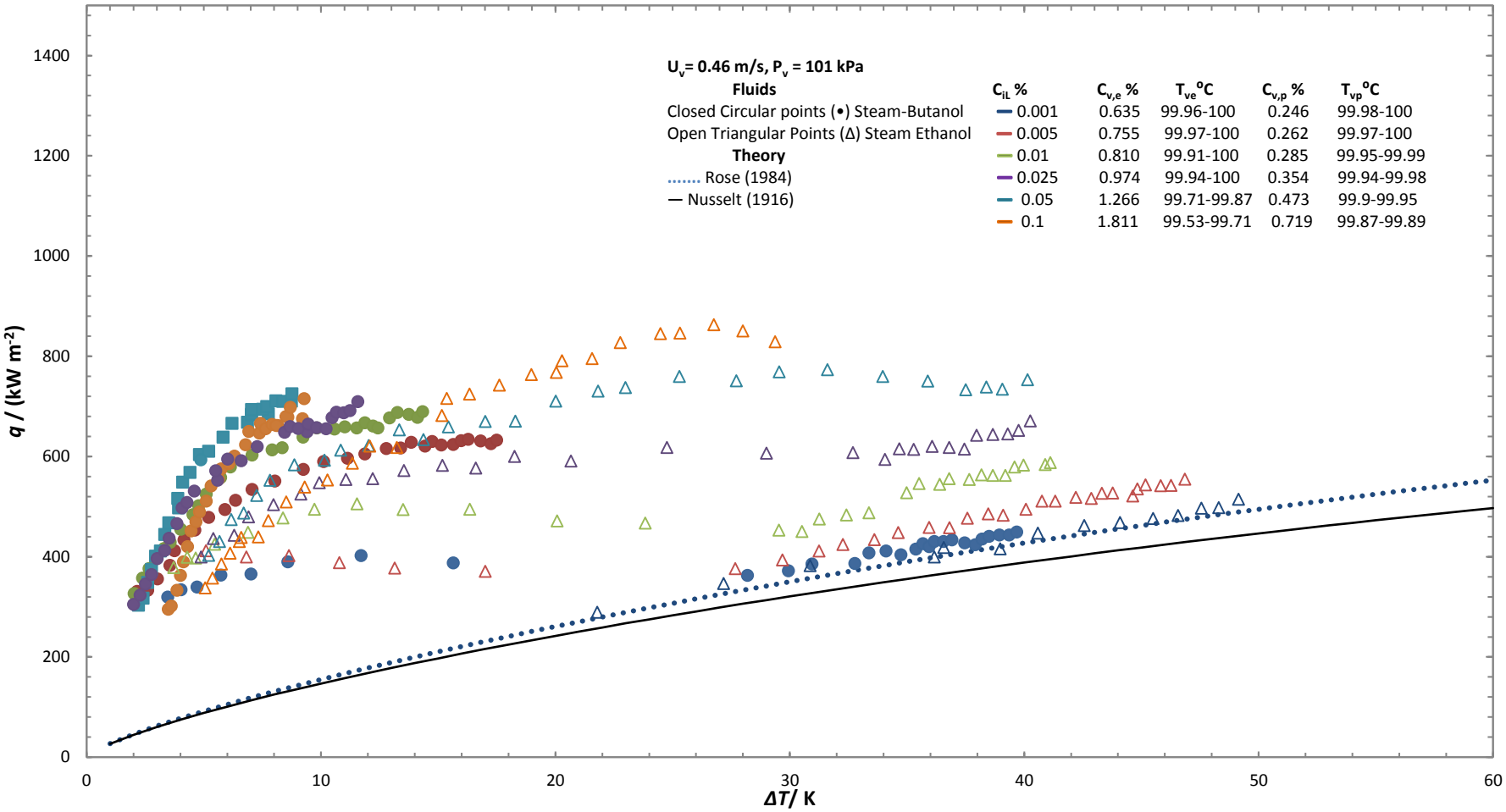

Figure 7.10 (Continued).

(d)

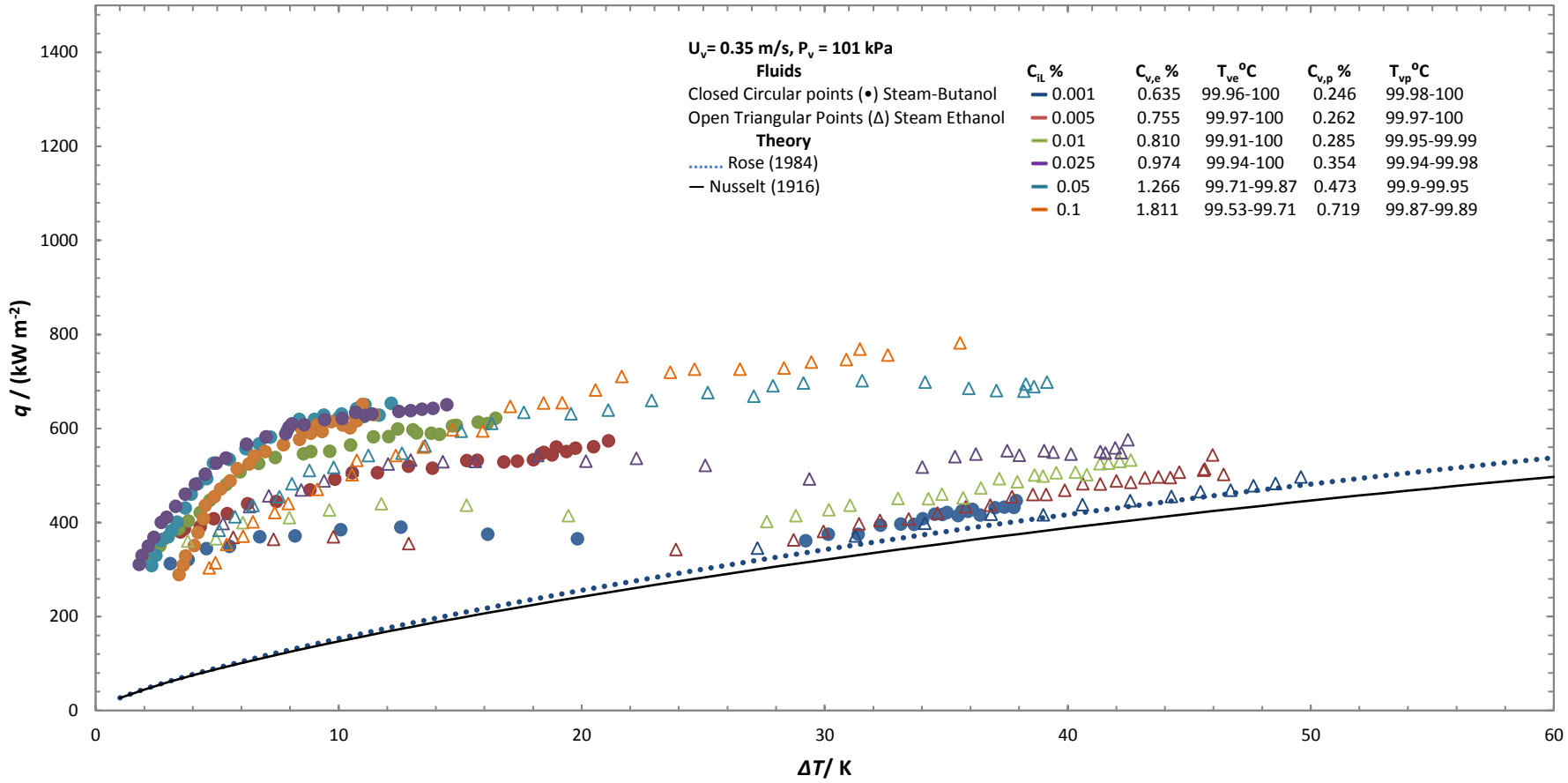

Figure 7.10 (Continued).

(e)

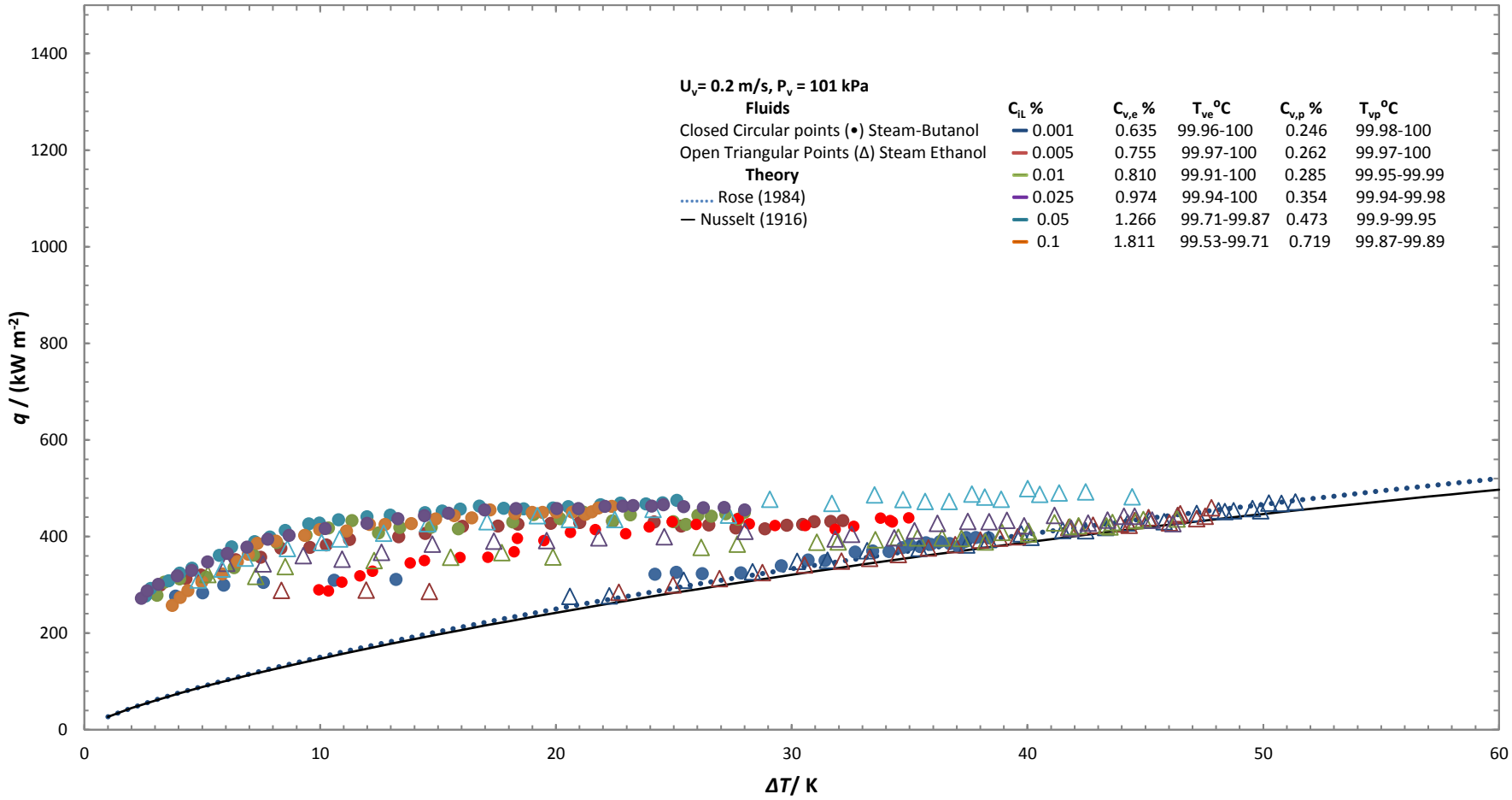

Figure 7.10 (Continued).

(a)

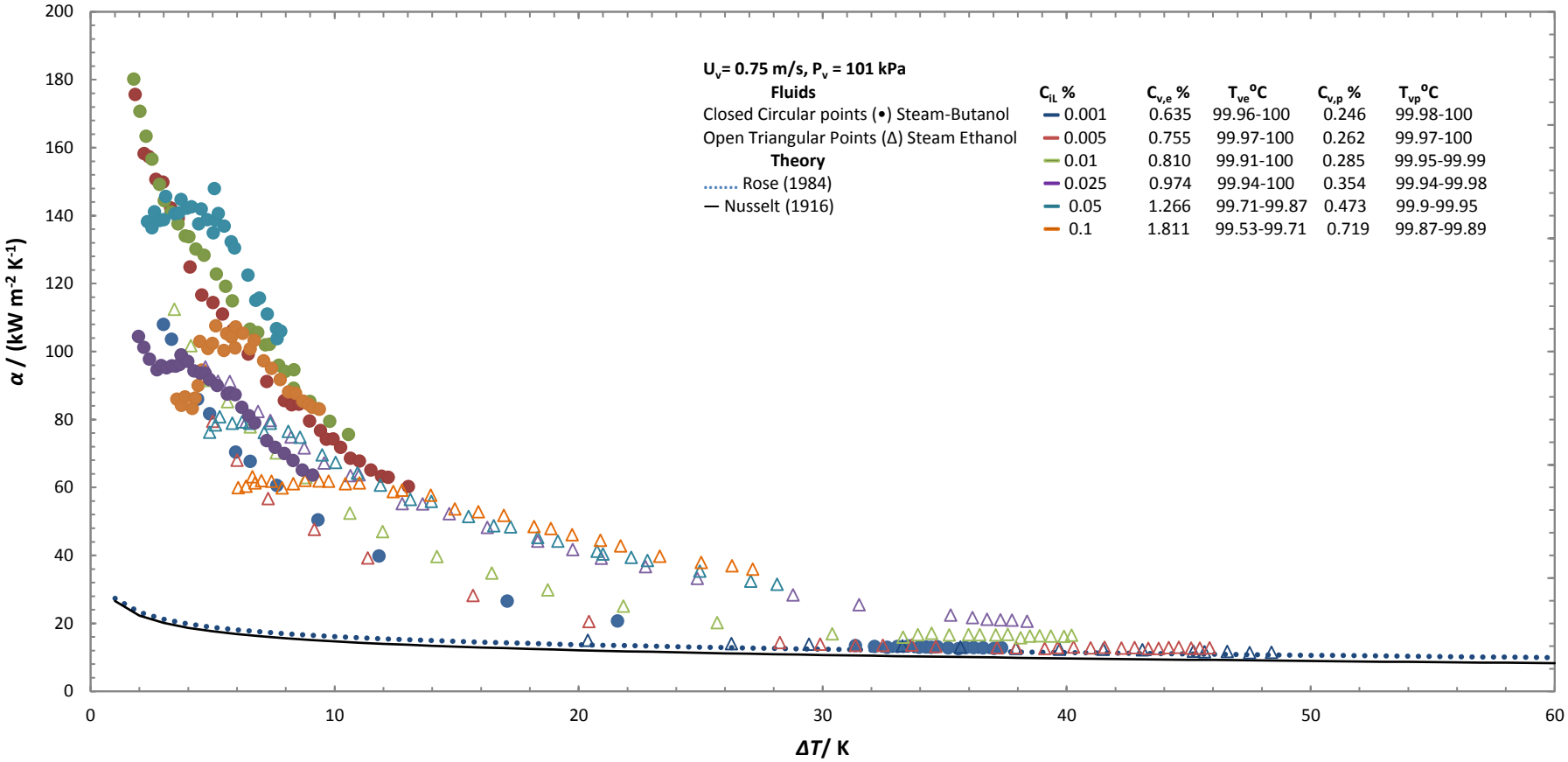

Figure 7-11: (a)-(e) shows variation of heat transfer coefficient against vapour-to-surface temperature difference for varying mass concentrations at each vapour velocity. (a) Uv = 0.75 m/s, (b) Uv = 0.56 m/s, (c) Uv = 0.46 m/s, (d) Uv = 0.35 m/s, (e) Uv = 0.20 m/s. Steam-propanol data is presented with closed points and steam-ethanol data with open points. Test section vapour pressure is 101 kPa.

(b)

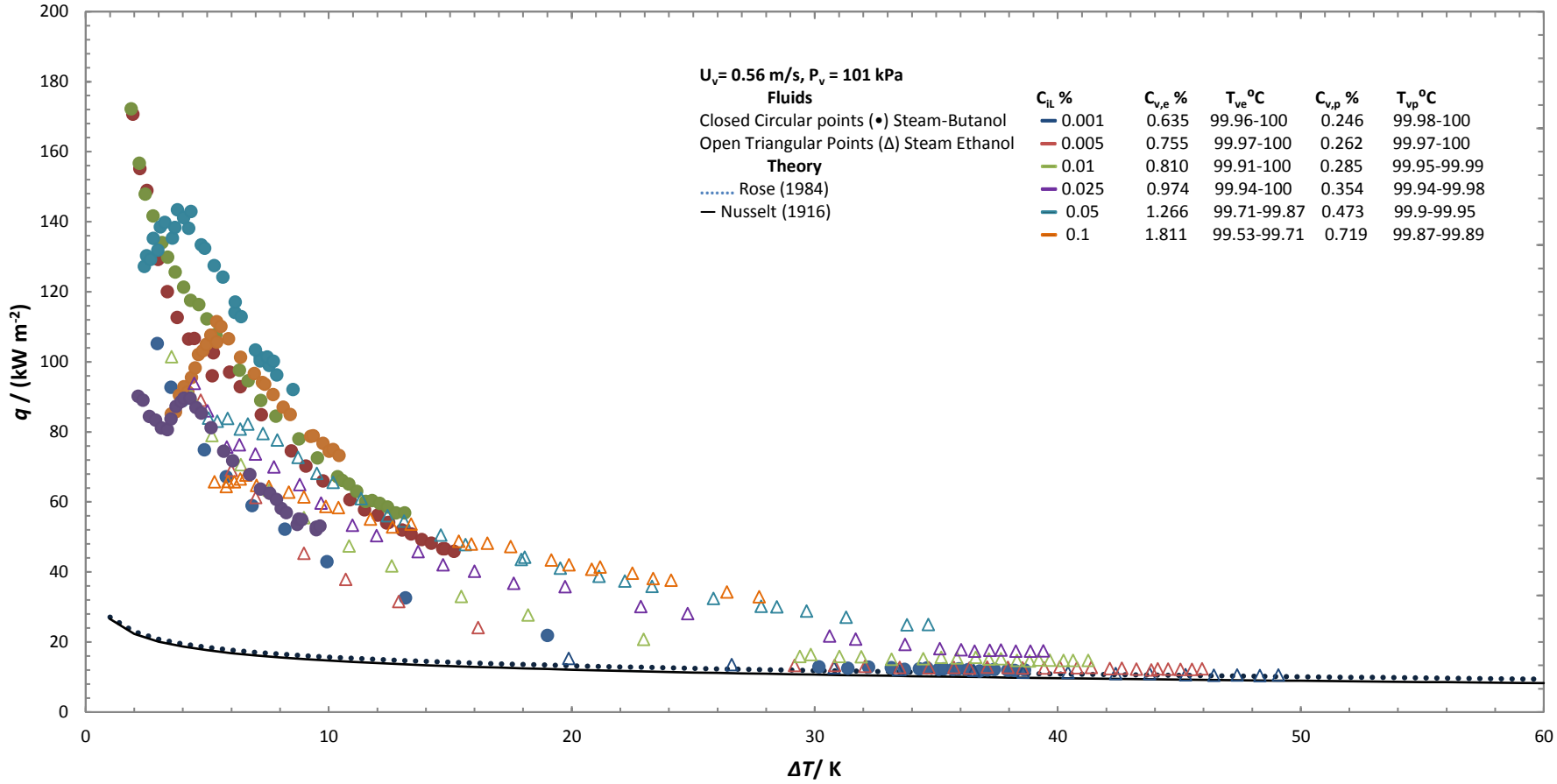

Figure 7.11 (Continued).

(c)

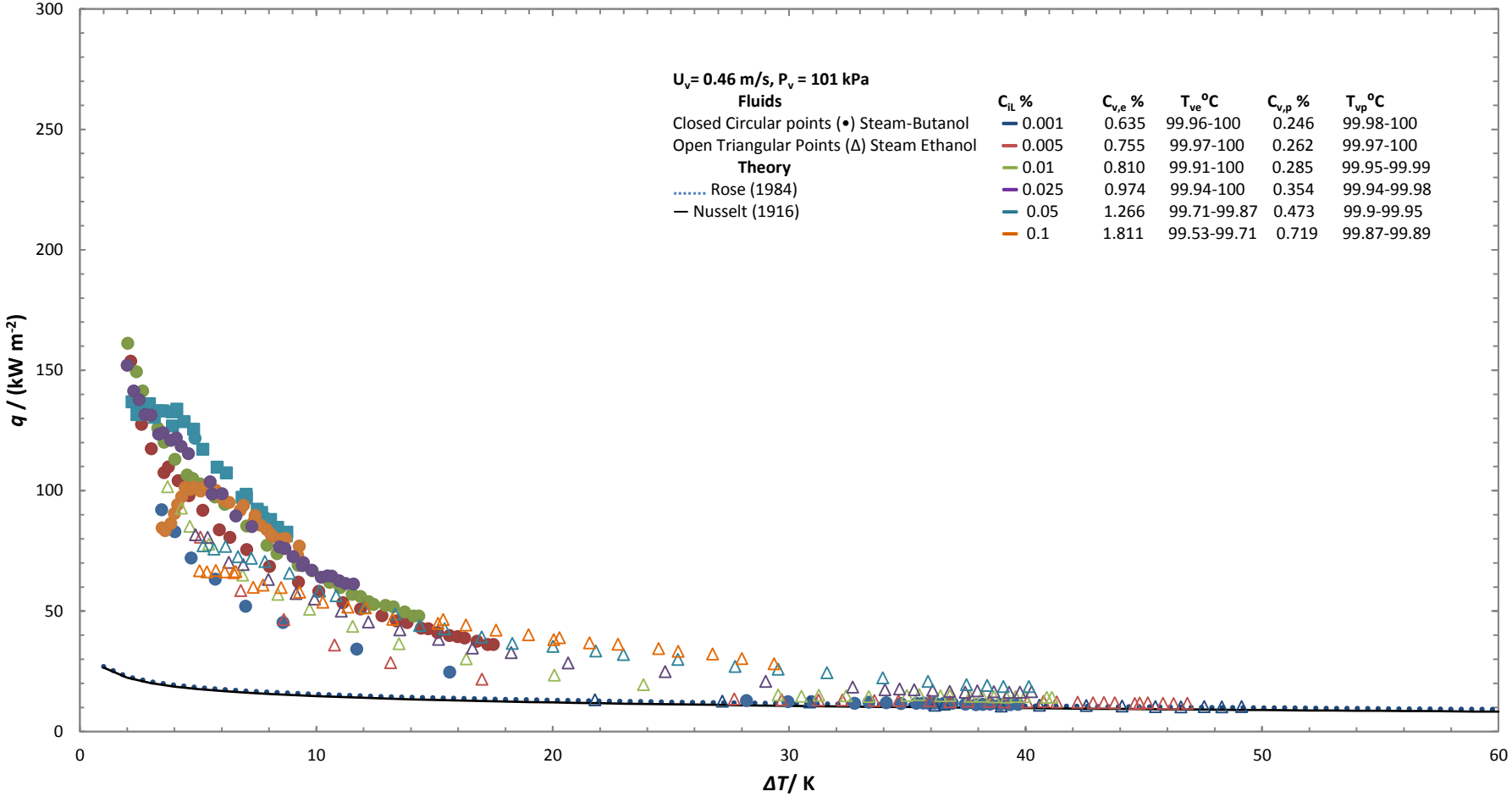

Figure 7.11 (Continued).

(d)

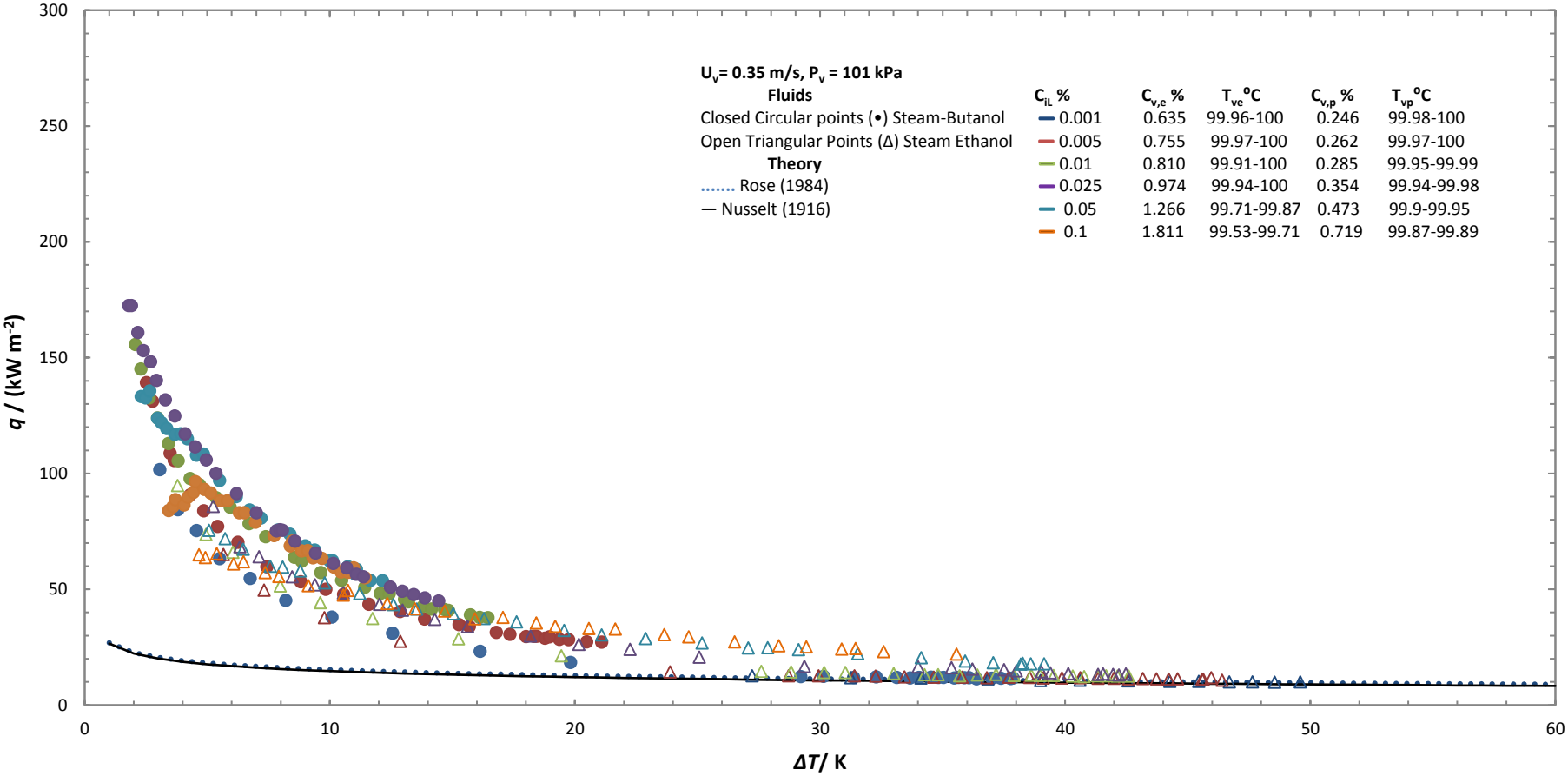

Figure 7.11 (Continued).

(e)

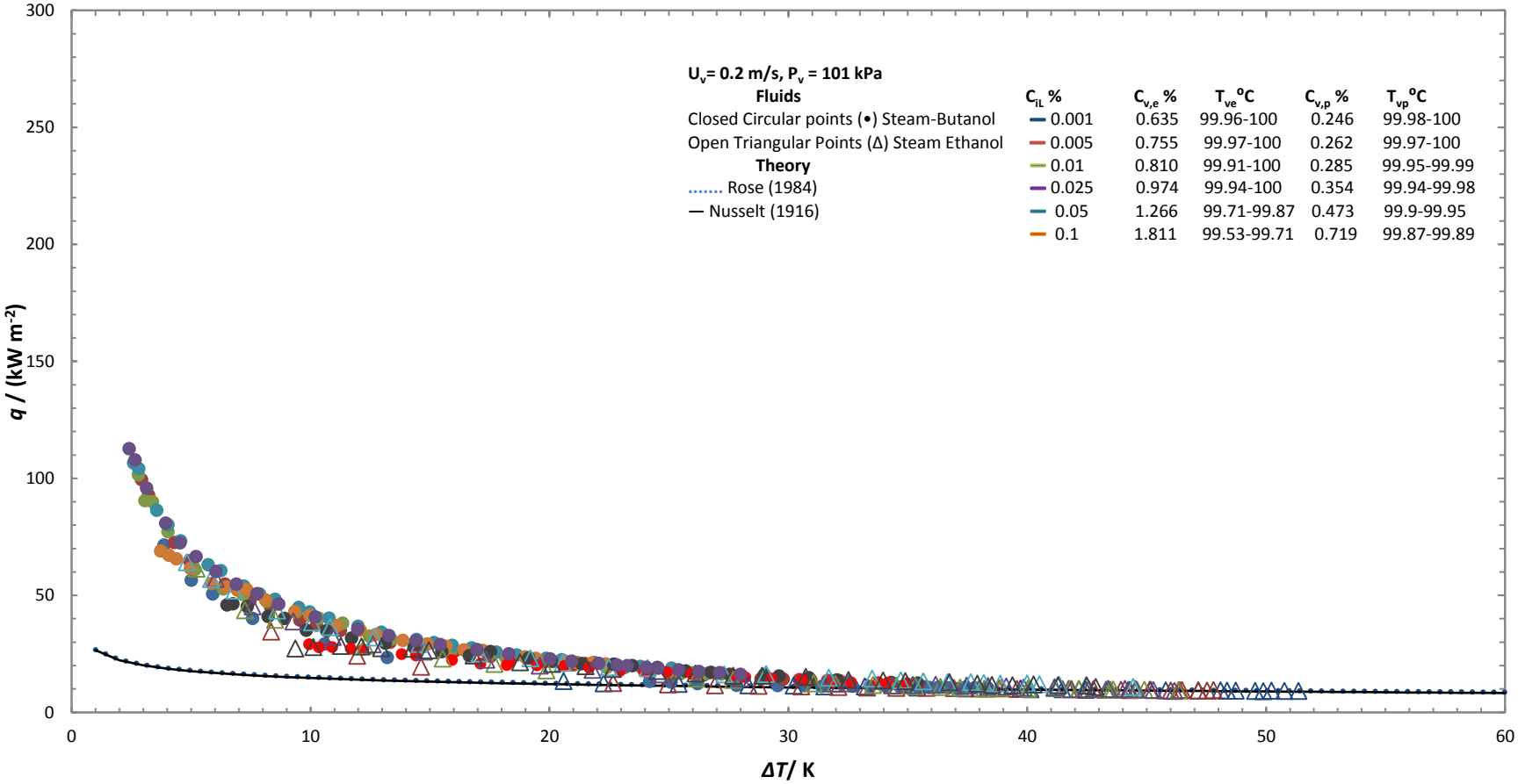

Figure 7.11 (Continued).

7.2.4 Enhancement (comparison with steam-ethanol mixtures)

(a)

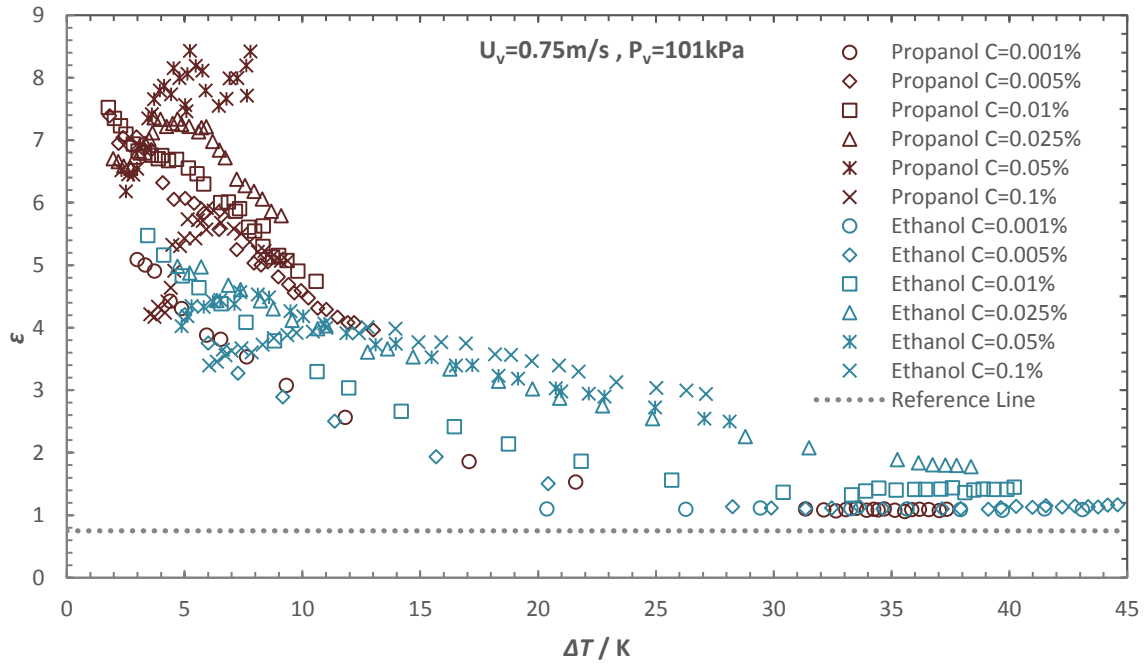

(b)

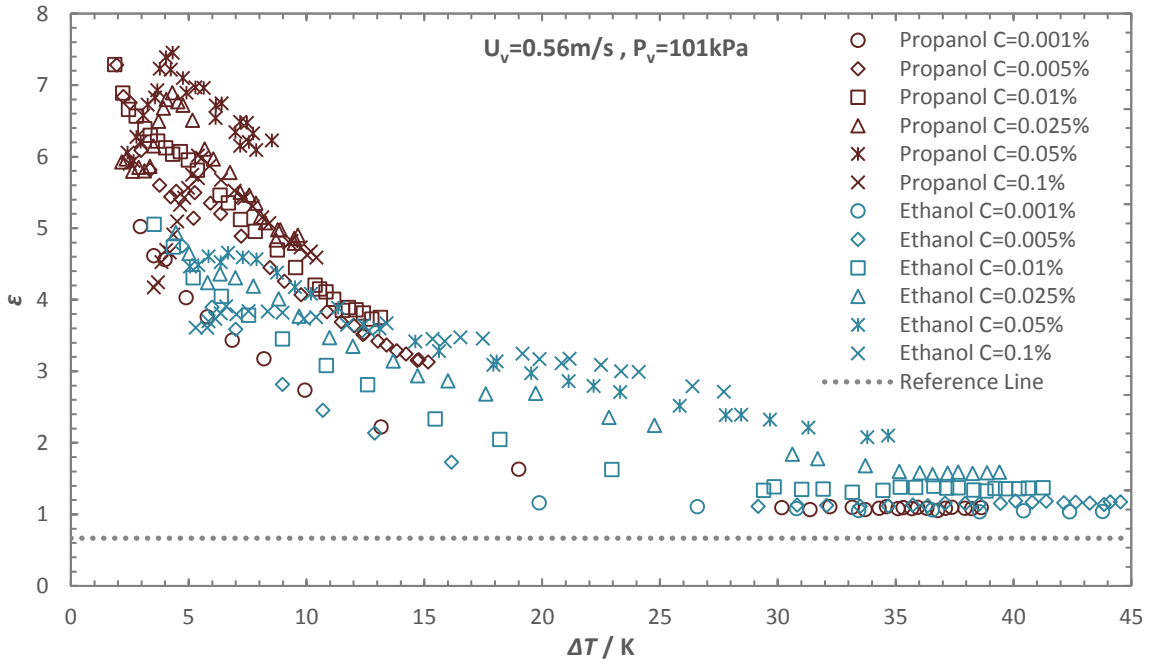

Figure 7-12: Comparison between the enhancement ratio of steam-ethanol with steam-propanol for various mass compositions at each vapour velocity. Steam-butanol results are in dark red colour and steam-propanol results in cyan colour.

(c)

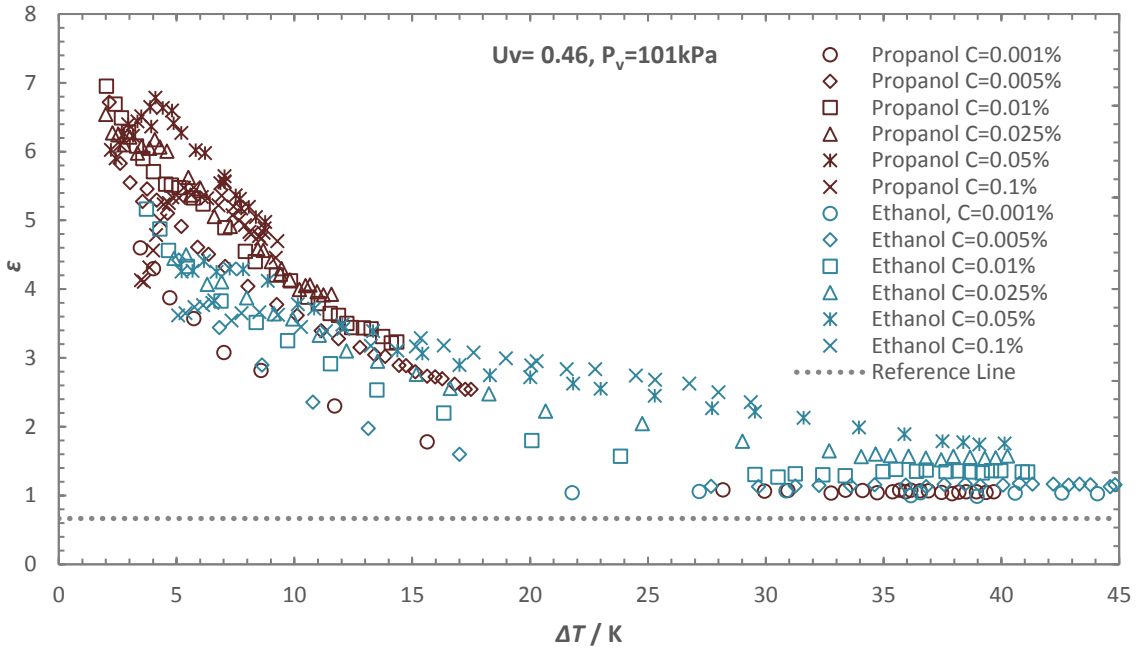

(d)

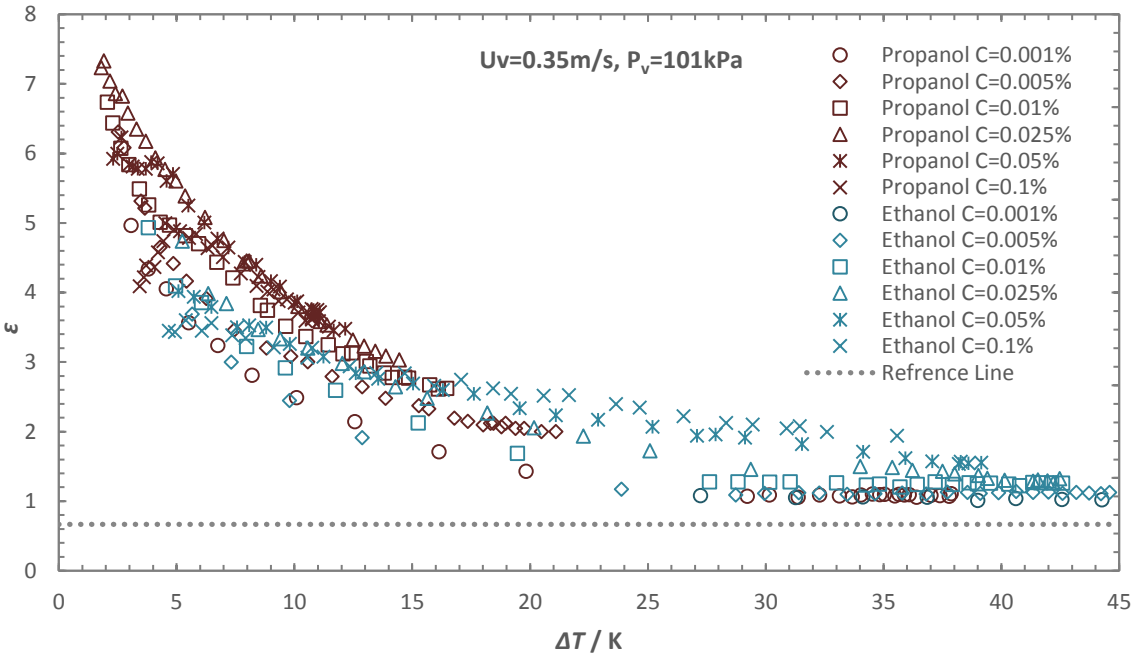

Figure 7.12 (continued)

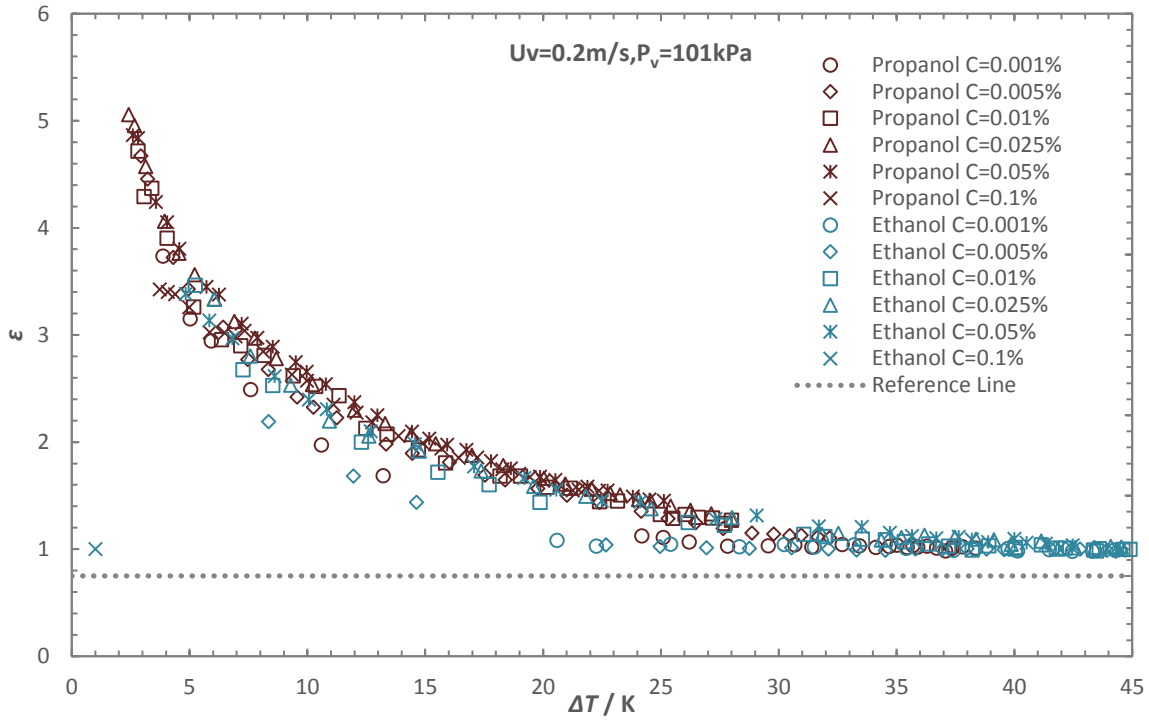

Figure 7.12 (continued)

7.2.5 Visual observation

Visual observation of steam-propanol mixture was similar to steam-butanol mixtures. All condensate appearances; wavy films, droplets, a mixture of wavy and droplets and dropwise were seen throughout the experiments. The trend and behaviour were the same as the steam-butanol case.

7.3 Summary

Measurements of heat transfer during Marangoni condensation of steam-propanol mixtures were conducted successfully and the results were compared with the condensation of steam-ethanol and steam-butanol mixtures. Heat flux and heat transfer coefficients for steam-propanol mixtures were s higher compared to steam-ethanol mixtures but lower than the steam-butanol case, for a given mass concentration and vapour-to-surface temperature difference. Secondly, the effect of diffusion resistance in steam-propanol mixtures is found to be lower compared to steam-ethanol mixtures for the given mass concentrations.

Enhancement ratio was found to be strongly dependant on propanol concentrations at lower vapour to surface temperature difference. Enhancement also depends significantly on the vapour velocity for all mass concentrations. The effect of velocity is more prominent at lower concentrations. Maximum enhancements were achieved at higher velocities and lower mass concentrations at lower vapour-to-surface temperature difference. The peak enhancement value was generally found around 6.5 at a vapour-to-surface temperature difference of 3 K and mass concentrations of 0.005% and 0.01%.

Chapter 8

8 Semi empirical modelling of Marangoni condensation.

In this chapter, an attempt has been made to model Marangoni condensation of steam ethanol mixtures. In the first section, the diffusion theory of Sparrow and Marschall (1969) has been used to obtain interface temperature for given concentration of ethanol in the binary mixture of steam-ethanol. Later using the interface temperature obtained from diffusion theory and Rose (2002) dropwise theory empirical model is generated to predict the heat flux of Marangoni condensation of steam-ethanol mixtures.

8.1 Finding interface temperature by solving the diffusion problem

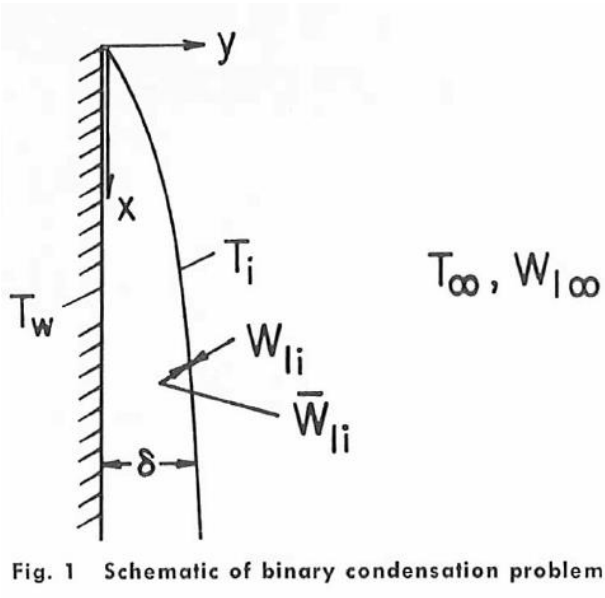

Fig. 1 Schematic of binary condensation problem

Figure 8-1: Schematic of a binary condensation problem

To find interface Temperature Ti, it is necessary to analyse the transport process in the vapour

Vapour Boundary Layer. Four conservation equations are required to fully describe flow, heat transfer and the diffusion process. The conservation equations are as follows:

Momentum conservation equation:

$$u\frac{\partial u}{\partial x}+v\frac{\partial u}{\partial y}=\mathrm{g}\left(1-\frac{\rho_\infty}{\rho}\right)+\nu\frac{\partial^2 u}{\partial y^2} \tag{8.1}$$

Energy conservation equation:

$$u\frac{\partial T}{\partial x}+v\frac{\partial T}{\partial y}=\alpha+\nu\frac{\partial^2 u}{\partial y^2} \tag{8.2}$$

Mass conservation equation:

$$\frac{\partial u}{\partial x}+\frac{\partial \mathrm{u}}{\partial y}=0 \tag{8.3}$$

Species conservation equation:

$$u\frac{\partial W_1}{\partial x}+v\frac{\partial W_1}{\partial y}=D\frac{\partial^2 W_1}{\partial y^2} \tag{8.4}$$

where,

$\mathrm{g}\left(1-\frac{\rho_\infty}{\rho}\right)$ is the buoyancy force which sets up a free convection motion in the vapour. Apart from density ratio $\frac{\rho_\infty}{\rho}$ all other property terms are constant. To process buoyancy force must be rephrased in terms of other dependent variables of the problem (W_1 and T).

$$p=Z\left[\rho\left(\frac{\bar{R}}{M}\right)T\right] \tag{8.5}$$

where,

Z is compressibility factor

$\bar{R}$ is the universal gas constant

M is the mixture molecular weight

Employing equation 8.5, density ration can be written as:

$$\frac{\rho_\infty}{\rho} = \frac{Z}{Z_\infty}\frac{M_\infty}{M}\frac{T}{T_\infty} \tag{8.6}$$

The pressure P is cancelled out since it is essentially constant across the boundary layer

Condensation process occurs at low pressure so $\frac{Z}{Z_\infty}$ =1

M= $X_1M_1 + X_2M_2$ (Where X1 and X2 are mole fractions)

Mole fraction can be written in form of a mass fraction as:

$$w_1 = \frac{X_1}{X_1 + (1 - X_1)(M_2/M_1)} \tag{8.7}$$

where,

W is the mass fraction in the vapour.

Equation 8.6 then becomes:

$$\frac{\rho_\infty}{\rho} = \frac{T}{T_\infty}\left[1 - \frac{M_1 - M_2}{M_1 - W_{1\infty}(M_1 - M_2)}(W_1 - W_{1\infty})\right] \tag{8.8}$$

Rearranging equation 8.8 gives:

$$1 - \frac{\rho_\infty}{\rho} = \frac{W_1 - W_{1\infty}}{W_i - W_{1\infty}} + \Omega_T\frac{T - T_\infty}{T_i - T_\infty} - \Omega_w\Omega_T\frac{W_1 - W_{1\infty}}{W_i - W_{1\infty}}\frac{T - T_\infty}{T_i - T_\infty} \tag{8.9}$$

where,

$$\Omega_w = \frac{(M_1 - M_2)(W_{1i} - W_{1\infty})}{M_1 - W_{1\infty}(M_1 - M_2)} \tag{8.9a}$$

And

$$\Omega_T = \frac{T_\infty - T_i}{T_\infty} \tag{8.9b}$$

The boundary layer equations 8.1 to 8.4 with equation 8.9 admits similarity transformation. The new independent variable is defined as:

$$\eta = c(y - \delta)/x^{1/4} \tag{8.10}$$

where,

$$c = (g\Omega_w/4v^2)^{1/4} \tag{8.11}$$

Along with dependent variables

$$f_{(\eta)} = \frac{\psi}{4vcx^{3/4}} \tag{8.12}$$

$$\varphi_{(\eta)} = \frac{W_1 - W_{1\infty}}{W_{1i} - W_{1\infty}} \tag{8.13}$$

$$\vartheta_{(\eta)} = \frac{T_\infty - T}{T_\infty - T_i} \tag{8.14}$$

where,

ψ is a stream function $\left(u = \frac{\partial \psi}{\partial y}, v = -\frac{\partial \psi}{\partial x}\right)$

The execution of similarity transformation yields:

$$f''' + 3ff'' - 2(f')^2 + \varphi + \vartheta\left(\frac{\Omega_T}{\Omega_w}\right) - \varphi\vartheta\Omega_T = 0 \tag{8.15}$$

$$\varphi'' + 3Scf\varphi' = 0 \tag{8.16}$$

$$\vartheta'' + 3Prf\vartheta' = 0 \tag{8.17}$$

In many binary condensation problems of practical interest, temperature changes across the boundary layer are very small compared to the temperature level (temperatures must be expressed in absolute units). That is, the numerical value of the parameter Ω_T is very much less than unity. In such instances, terms involving ϑ can be deleted from the

momentum equation. In the condensation problem convective heat transfer play role of a small superheating of the vapour which has a negligible effect on wall heat transfer. Therefore, the energy equation (8.17) is discarded.

Then the reduced set of boundary layer equations with negligible temperature effect in the vapour is as follows:

$$f''' + 3ff'' - 2(f')^2 + \varphi = 0 \tag{8.18}$$

$$\varphi'' + 3Scf\varphi' = 0 \tag{8.19}$$

Using the Runge Kutta technique the differential equations were solved to obtain interface temperature. Figure 8-2 shows the plot of interface temperature against vapour-to-surface temperature difference. Interface temperature decreases initially at low vapour to surface temperature difference due to diffusion resistance. It reaches a minimum value at critical vapour-to-surface temperature difference and then stays constant. This is where the diffusion effect is dominated by surface tension effect and a significant increase in heat transfer coefficients are observed.

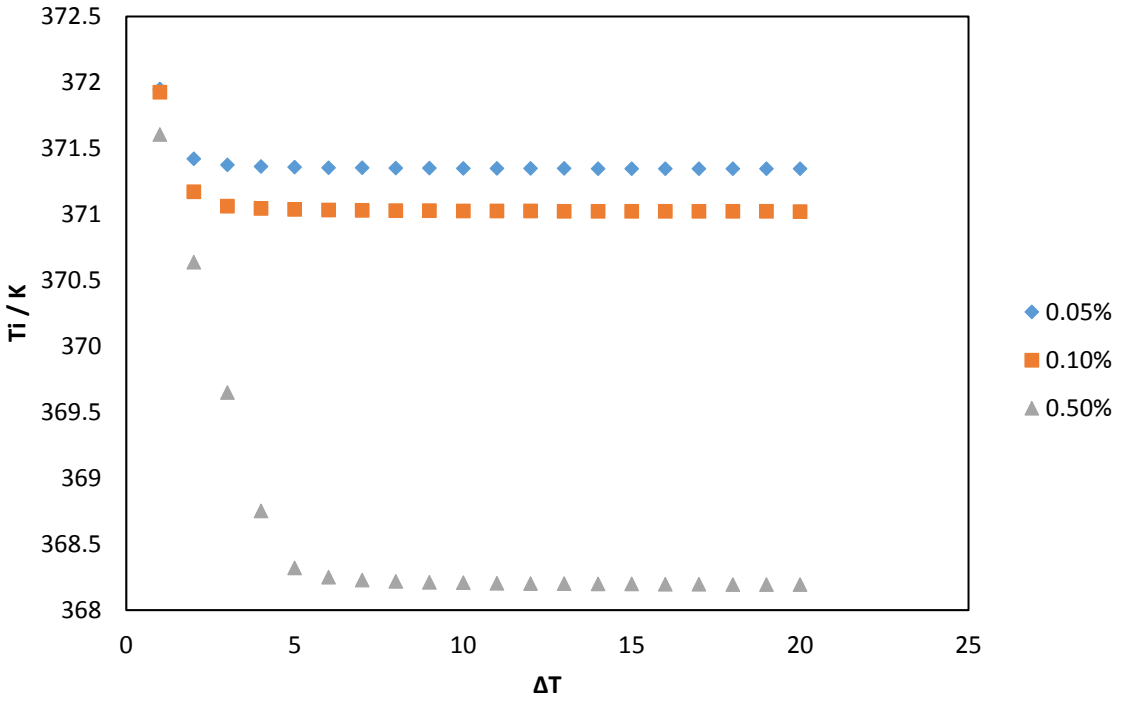

Figure 8-2: Interface temperature (T_i) for different concentrations of ethanol (C_{iL}= 0.05%, 0.1% and 0.5%).

8.2 Empirically modelling of steam-ethanol mixtures

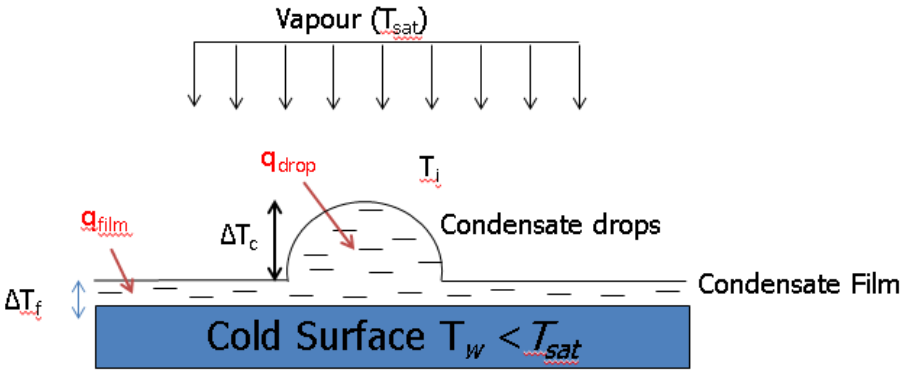

T_i : Interface temperature

T_{sat} : Saturation Temperature

ΔT_f : Temeprature difference across film

ΔT_c : Temeprature difference across drop due to conduction

Figure 8-3: Schematic of condensate on cooling surface of psuedo-dropwise mode.

Distribution of drop sizes

- **Mean size distribution function**

$$f\left(\frac{r}{r_{\max}}\right)=\left(\frac{r}{r_{\max}}\right)^{\frac{1}{n}} \tag{8.20}$$

- **The fraction of surface area covered by drops**

$$A(r)dr=\frac{1}{nr_{\max}}\left(\frac{r}{r_{\max}}\right)^{\frac{1}{n}-1}dr \tag{8.21}$$

(Le Fevre & Rose (1964))

- **Number of drops per unit area**

$$N(r)dr = \frac{1}{\pi r^2 n r_{\max}} \left(\frac{r}{r_{\max}} \right)^{\frac{1}{n}-1} dr \tag{8.22}$$

(Le Fevre & Rose (1964))

Heat transfer through of a given size

- **Conduction in a drop**

$$\Delta T_c = \frac{K_1 q_b r}{k} \tag{8.23}$$

(Le Fevre & Rose (1964))

where,

q_b is the heat flux at the base of the drop.

r is the base radius of the drop.

k is the thermal conductivity of the drop.

- **Surface curvature effect**

$$\Delta T_\sigma = \frac{2\sigma T_{sat}}{r_c \rho h_{fg}} \tag{8.24}$$

(Le Fevre & Rose (1964))

where,

σ is the surface tension.

T_{sat} is the saturated vapour temperature.

h_{fg} is the specific latent heat of vaporization.

ρ is the density of condensate.

r_c is the radius of curvature of the liquid surface.

If the drop is a segment of a sphere, r would be defined as follows:

$$r = r_c \sin\beta \tag{8.25}$$

where,

β is the contact angle, which is taken to be as $\frac{\pi}{2}$.

- **Interface temperature drop**

$$\Delta T_i = \frac{3}{8}\left(\frac{\gamma+1}{\gamma-1}\right)\frac{q_i v_{fg}\left(RT_{sat}\right)^{\frac{1}{2}}}{h_{fg}{}^2} \tag{8.26}$$

(Le Fevre & Rose1964)

where,

q_i is the heat flux at the liquid-vapour interface, which is defined as $K_{20}q_b$.

K_{20} is the ratio of the base area to the curved surface area of the drop, defined as $\frac{1}{2}\left(1+\cos\beta\right)$ (K_{20}= 0.5 for hemisphere).

v_{fg} is the difference between the vapour and liquid specific volumes.

R is the specific ideal-gas constant of the fluid.

γ is the ratio of the principal specific heat capacities of the vapour, taken to be as $\frac{5}{3}$.

- **Heat flux at a base of a drop**

$$q_b = \frac{\Delta T - \frac{2\sigma T_{sat}\sin\beta}{r\rho h_{fg}}}{\frac{K_1 r}{k} + \frac{3K_{20}v_{fg}T_{sat}\left(RT_{sat}\right)^{\frac{1}{2}}}{8h_{fg}{}^2}\left(\frac{\gamma+1}{\gamma-1}\right)} \tag{8.27}$$

- **Heat flux through the area covered by drops**

The heat flux through the drops for the whole surface, q_d, is given:

$$q_d = \frac{Q_d}{A_d} = \frac{1}{A_d}\int_0^{Q_d} dQ = \frac{1}{A_d}\int_{r_{\min}}^{r_{\max}} N(r) A_t \pi r^2 q_b dr \tag{8.28}$$

$$q_d = \frac{A_t}{A_d}\int_{r_{\min}}^{r_{\max}} \frac{1}{n r_{\max}}\left(\frac{r}{r_{\max}}\right)^{\frac{1}{n}-1} A_t q_b dr = \frac{A_t}{n r_{\max} A_d}\int_{r_{\min}}^{r_{\max}} q_b \left(\frac{r}{r_{\max}}\right)^{\frac{1}{n}-1} dr$$

where,

A_t is a total surface area of the tube

A_d is the total surface area covered by drops

r_{min} is the base radius of the smallest viable drop given by the following equation,

$$r_{\min} = \frac{2\sigma T_{sat} \sin\beta}{\rho h_{fg} \Delta T} \tag{8.29}$$

$r_{\max}$ is the base radius of the largest viable drop given by the following equation,

$$r_{\max} = K_3 L_3 = K_3\left(\frac{\sigma}{g(\rho_f - \rho_v)}\right)^{\frac{1}{2}} \tag{8.30}$$

where,

K_3 is constant, which is taken to be as 0.4 (Le Fevre & Rose (1964)).

Rose (1984) film model

The heat flux through the film is determined by the following equation:

$$Nu = \frac{0.9 + 0.728F^{\frac{1}{2}}}{\left(1 + 3.44F^{\frac{1}{2}} + F\right)^{\frac{1}{4}}} \tilde{\mathrm{Re}}^{\frac{1}{2}} \tag{8.31}$$

where,

$$F = \frac{\mu h_{fg} g d}{k \Delta T U_{\infty}^{2}} \tag{8.32}$$

$$\tilde{\mathrm{Re}} = \frac{\rho U_{\infty} d}{\mu} \tag{8.33}$$

$$Nu = \frac{\alpha d}{k} = \frac{q_f d}{k \Delta T} \tag{8.34}$$

- **<u>Heat flux through the whole surface area of the tube</u>**

  The expression of entire heat flux due to the Marangoni condensation effect is given as follows:

$$q_e = q_f f_f + q_d f_d \tag{8.35}$$

where,

q_d is the heat flux through the condensate film.

f_d is the fraction covered by drops, which is defined as $\left(\frac{r_{\min}}{r_{\max}} \right)^{\frac{1}{n}}$

q_f is the heat flux through the drops.

f_f is the fraction covered by condensate film.

The fraction of area covered by the drops and the film are related by the following equation:

$$f_d + f_f = 1 \tag{8.36}$$

Using the above relationship, equation (1) can be expressed by the following equation:

$$q_e = q_d f_d + q_f (1 - f_d) \tag{8.37}$$

Equation (3) can also be written as follows:

$$(q_f - q_d) f_d - q_f + q_e = 0 \tag{8.38}$$

By substituting 0 with y from the above equation, the following equation would be:

$$y = (q_f - q_d) f_d - q_f + q_e \tag{8.39}$$

For a givenΔT, the value of n from equation (1) can be determined using Newton's Raphson Method , based on the experimental data, which is shown as follows:

$$n_{new} = n_{old} - \frac{y_{old}}{(\frac{dy}{dn})_{old}} \tag{8.40}$$

where,

$$y_{old} = (q_f - q_d) f_d - q_f + q_e \tag{8.41}$$

$$\frac{y_{old}}{\left(\frac{dy}{dn}\right)_{old}} = -(q_f - q_d)\left(\frac{1}{n^2}\right)\left(\frac{r_{max}}{r_{min}}\right)^{\frac{1}{n}} ln\left(\frac{r_{min}}{r_{max}}\right) - \left(\frac{r_{max}}{r_{min}}\right)^{\frac{1}{n}}\left(\frac{q_{d2} - q_{d1}}{n_2 - n_1}\right) \tag{8.42}$$

The recommended correlation for n is expressed as follows:

$$n = A(H)^B(F)^C(X)^D \tag{8.43}$$

where,

H,$F$and X are the dimensionless numbers, which are defined as follows:

$$H = \frac{C_p \Delta T}{h_{fg}} \tag{8.44}$$

$X = Concentration\ of\ ethanol\ within\ the\ bolier$

Where A, B, C, D are the best-curve coefficients that can be obtained using the computational data of n, based on the experimental (by taking the natural logarithms of equation (7)), which is shown below:

$$\ln(n) = a + Bln(H) + Cln(F) + Dln(X) \tag{8.45}$$

where,

$$a = \ln(A)$$

The following equation represents the sum of the residual between the theoretical n (equation 8.45) and experimental n.

$$R = \sum_{1}^{N} \left(ln(n_{exp}) - ln(n_{theo}) \right)^2 \tag{8.46}$$

$$R = \sum_{1}^{N} \left(ln(n_{exp}) - a - Bln(H) - Cln(F) - Dln(X) \right)^2 \tag{8.47}$$

The minimization of the residual R takes place by the following conditions:

$$\frac{\partial R}{\partial a} = \frac{\partial R}{\partial B} = \frac{\partial R}{\partial C} = \frac{\partial R}{\partial D} = 0 \tag{8.48}$$

This will lead to the following matrix relationship

$$\frac{\partial R}{\partial a} = 2\sum_{1}^{N}\left(ln\left(n_{exp}\right) - a - Bln(H) - Cln(F) - Dln(X)\right)(-1) = 0$$

$$\frac{\partial R}{\partial b} = 2\sum_{1}^{N}\left(ln\left(n_{exp}\right) - a - Bln(H) - Cln(F) - Dln(X)\right)\left(-ln(H)\right) = 0$$

$$\frac{\partial R}{\partial c} = 2\sum_{1}^{N}\left(ln\left(n_{exp}\right) - a - Bln(H) - Cln(F) - Dln(X)\right)\left(-ln(F)\right) = 0$$

$$\frac{\partial R}{\partial d} = 2\sum_{1}^{N}\left(ln\left(n_{exp}\right) - a - Bln(H) - Cln(F) - Dln(X)\right)(-ln(X)) = 0$$

$$\begin{bmatrix} N & \sum_{1}^{N}\ln(H) & \sum_{1}^{N}\ln(F) & \sum_{1}^{N}\ln(X) \\ \sum_{1}^{N}\ln(H) & \sum_{1}^{N}(\ln(H))^2 & \sum_{1}^{N}(\ln(H))(\ln(F)) & \sum_{1}^{N}(\ln(H))(\ln(X)) \\ \sum_{1}^{N}\ln(F) & \sum_{1}^{N}(\ln(F))(\ln(H)) & \sum_{1}^{N}(\ln(F))^2 & \sum_{1}^{N}(\ln(F))(\ln(X)) \\ \sum_{1}^{N}\ln(X) & \sum_{1}^{N}(\ln(X))(\ln(H)) & \sum_{1}^{N}(\ln(X))(\ln(F)) & \sum_{1}^{N}(\ln(X))^2 \end{bmatrix} \begin{bmatrix} a \\ B \\ C \\ D \end{bmatrix} = \begin{bmatrix} \sum_{1}^{N}\ln(n_{\exp}) \\ \sum_{1}^{N}(\ln(H))(\ln(n_{\exp})) \\ \sum_{1}^{N}(\ln(F))(\ln(n_{\exp})) \\ \sum_{1}^{N}(\ln(X))(\ln(n_{\exp})) \end{bmatrix}$$

From the above matrix relationship, the coefficients of a, B, C and D are determined by the following matrix relationship:

$$\begin{bmatrix} a \\ B \\ C \\ D \end{bmatrix} = \begin{bmatrix} N & \sum_1^N \ln(H) & \sum_1^N \ln(F) & \sum_1^N \ln(X) \\ \sum_1^N \ln(H) & \sum_1^N (\ln(H))^2 & \sum_1^N (\ln(H))(\ln(F)) & \sum_1^N (\ln(H))(\ln(X)) \\ \sum_1^N \ln(F) & \sum_1^N (\ln(F))(\ln(H)) & \sum_1^N (\ln(F))^2 & \sum_1^N (\ln(F))(\ln(X)) \\ \sum_1^N \ln(X) & \sum_1^N (\ln(X))(\ln(H)) & \sum_1^N (\ln(X))(\ln(F)) & \sum_1^N (\ln(X))^2 \end{bmatrix}^{-1} \begin{bmatrix} \sum_1^N \ln(n_{\exp}) \\ \sum_1^N (\ln(H))(\ln(n_{\exp})) \\ \sum_1^N (\ln(F))(\ln(n_{\exp})) \\ \sum_1^N (\ln(X))(\ln(n_{\exp})) \end{bmatrix}$$

The range of the experimental data of H is divided into three regions, where each of these regions has its own coefficients of a, B, C and D. H_{1crit} denotes the critical value of H that separates region1 from region2, while H_{2crit} illustrates the critical value of H that separates region2 from region3. The overall product moment correlation coefficient (coefficient used to measure the strength of the relationship between the input and the output variables) of the data is obtained from the following equation:

$$r^2 = 1 - \frac{R_{overall}}{V_{overall}} \tag{8.49}$$

where,

$R_{overall}$ = Overall residual between the theoretical and the experimental data for all regions, which is defined as:

$$R_{overall} = R_1 + R_2 + R_3$$

R_1 = The residual between theoretical and the experimental data in region 1, based on coefficients a1, B1, C1 and D1.

R_2 = The residual between theoretical and the experimental data in region 2, based on coefficients a2, B2, C2 and D2.

R_3 = The residual between theoretical and the experimental data in region 3, based on coefficients a3, B3, C3 and D3.

$V_{overall}$ = The variance of the experimental data, which is defined as follows:

$$V_{overall} = \sum_{1}^{N} (\ln(n_{\exp}) - Y)^2$$

where,

$$Y = \frac{\sum_{1}^{N} \ln(n_{\exp})}{N} \tag{8.50}$$

The following table represents the values of the overall product-moment correlation coefficients for the given values of H_{1crit} and H_{2crit}.

Table 8-1: Optimising values of $H_{critical}$

	H-2crit	0	0.005	0.01	0.015	0.02	0.025	0.03	0.035	0.04	0.045	0.05
H-1crit												
0		0.604	0.608	0.622	0.656	0.678	0.703	0.706	0.712	0.700	0.683	0.668
0.005			0.608	0.623	0.657	0.679	0.703	0.706	0.713	0.700	0.683	0.669
0.01				0.622	0.661	0.679	0.705	0.710	0.717	0.707	0.691	0.678
0.015					0.656	0.683	0.710	0.719	0.728	0.722	0.710	0.700
0.02						0.678	0.708	0.720	0.731	0.728	0.720	0.712
0.025							0.703	0.718	0.731	0.732	0.728	0.723
0.03								0.706	0.718	0.721	0.719	0.716
0.035									0.712	0.718	0.718	0.717
0.04										0.700	0.702	0.702
0.045											0.683	0.683
0.05												0.668

The values of H_{1crit} and H_{2crit} where the overall maximum product-moment correlation coefficient occurs are 0.025 and 0.04. The following table represents the coefficients of a, B, C and D for each of the three regions, which correspond the overall maximum product-moment correlation coefficient:

	a	B	C	D
Region 1	-0.1950	0.0069	-0.2172	-0.0797
Region 2	0.3150	-0.1085	-0.0798	-0.0968
Region 3	-0.6791	-0.6158	0.0232	-0.1031

Therefore, the expression of n for each of the three regions would be:

$$n = 0.8228(H)^{0.0069}(F)^{-0.2172}(X)^{-0.0797} \qquad H < 0.025 \tag{8.51a}$$

$$n = 1.3702(H)^{-0.1085}(F)^{-0.0798}(X)^{-0.0968} \qquad 0.025 \leq H < 0.04 \tag{8.51b}$$

$$n = 0.5071(H)^{-0.6158}(F)^{0.0232}(X)^{-0.1031} \qquad 0.04 \leq H \tag{8.51c}$$

Using the above expressions for n, their corresponding heat flux through the drops for each region was found. Later all three regions were coupled altogether to give one smooth function.

Smoothing of region 1and region 2:

$$q_{d12} = q_{d1} + \frac{(1 + \tanh(k \times H - i_{12}))}{2}(q_{d2} - q_{d1}) \tag{8.52}$$

where,

$q_{d1} = heat\ flux\ through\ drop\ from\ region\ 1$

$q_{d2} = heat\ flux\ through\ drop\ from\ region\ 2$

$q_{d12} = heat\ flux\ through\ drop\ after\ smoothing\ region\ 1\ and\ 2$

$k = smoothnes\ factor\ higher\ the\ value\ of\ k\ closerthe\ function\ is\ to\ \exp\ data$

$i = intersection\ point\ between\ two\ regions$

Similarly, smoothing of region 3 with the above smooth region will give:

$$q_{d123} = q_{d12} + \frac{(1 + \tanh(k \times H - i_{123}))}{2}(q_{d3} - q_{d12}) \tag{8.53}$$

where,

$q_{d123} = heat\ flux\ through\ drop\ after\ smoothing\ all\ regions$

$q_{d3} = heat\ flux\ through\ drop\ from\ region\ 3$

Figure 8-4 shows the results of the empirical model and experimental results obtained from Murase (2007) and Hassan (2012). The results are in good agreement with previous experimental data.

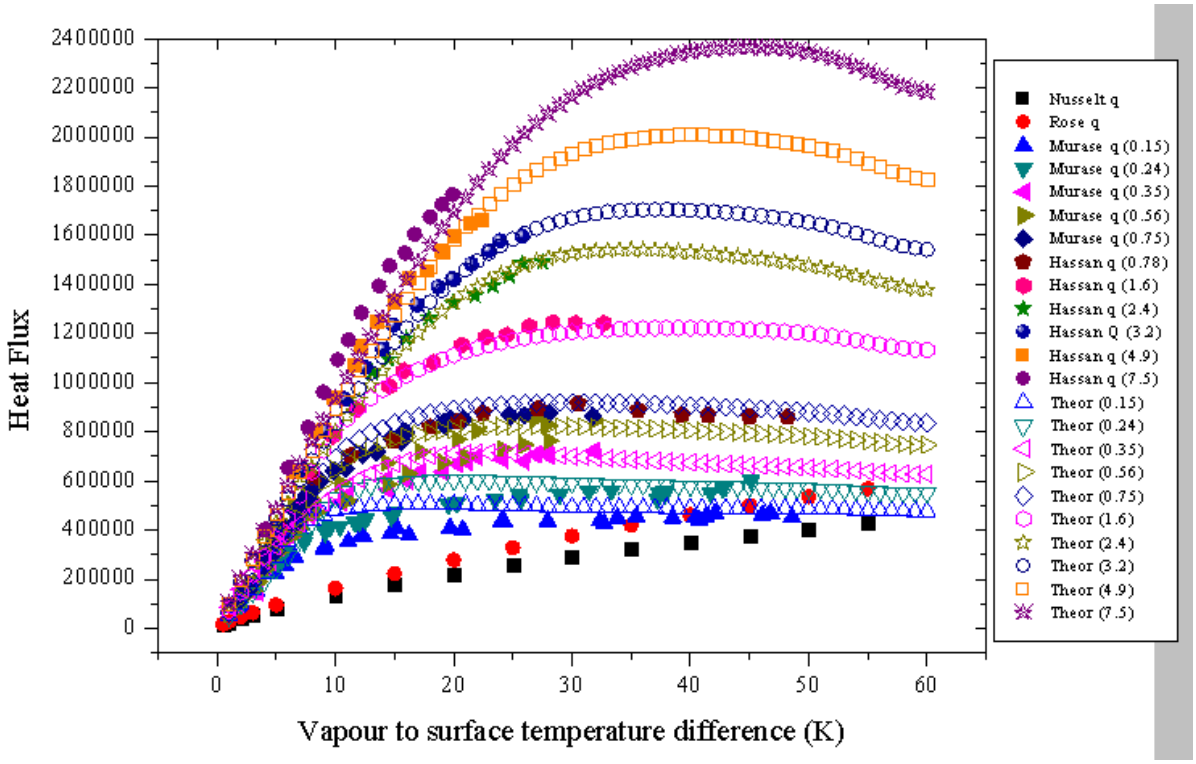

Figure 8-4: Results of the empirical model with previous experimental data. Theor represents current empirical model results.

8.3 Summary

So far, no theoretical model for Marangoni condensation is available and there is no empirical model that is applicable to a wide range of steam-ethanol data. Here an attempt was made to develop a semi-empirical model to predict heat transfer characteristics of steam ethanol mixture in Marangoni condensation. The model incorporates the diffusion theory of Sparrow and Marschall (1969) to predict the interface temperature drop due to diffusion and then using dropwise theory of Rose (1984) modified the model to predict heat transfer rate and heat transfer coefficients. The model predicts the heat transfer rate with up to 5% of uncertainty.

Chapter 10

9 Overall conclusion and summary of further work

So far Marangoni condensation of steam-ethanol mixtures of various compositions and vapour velocities have been widely investigated in earlier experimental studies. Almost all studies have concluded that steam-ethanol mixtures perform 5-8 times better than pure steam condensation. However, mixtures of steam-with other alcohols have never been investigated. Here, Experimental investigations on Marangoni condensation of binary mixtures of steam with different alcohols, such as steam-ethanol, steam-butanol and steam-propanol, on a horizontal smooth tube have been carried out. Alcohols concentrations, vapour velocity and vapour-to-surface temperature difference have been systematically varied and heat flux and heat-transfer coefficients are calculated. Good agreement with pure-steam theories and earlier steam-ethanol data have been found. Significant enhancements are reported for steam-butanol and steam-propanol mixtures.

9.1 Marangoni condensation of steam-ethanol mixtures

The aim of using steam-ethanol mixtures was to fill the gap in the data already available for Marangoni condensation of steam-ethanol mixtures. A large number of data was useful in developing an empirical model for a wide range of parameters. while the sole purpose of this part of the research was to gather data, nonetheless, it indeed helped in understanding the heat transfer characteristics and its relation to condensation mode.

Higher heat transfer coefficients and heat flux were obtained compared to pure steam data. Enhancements of up to 5 were recorded. Enhancement ratio was found to be dependent on the mode of condensation. Dropwise mode of condensation gave higher enhancements than wavy film and pure films. Mode of condensation varies with vapour-to-surface temperature difference and ethanol concentration. Enhancements were higher at low concentrations and lower vapour-to-surface temperature difference. At higher vapour-to-surface temperature difference and lower concentration transition from

pseudo-dropwise mode to filmwise mode was observed, and enhancement reduces to unity. At higher concentrations of 0.5% and 1%, the graphs seem to drift away from origin due to diffusion resistance of more volatile component (i.e. ethanol). At lower vapour-to-surface temperature difference and higher concentrations due to diffusion enhancements trend would lead to unity or even less.

9.2 Marangoni condensation of steam-butanol mixtures

Steam-butanol mixture was chosen because of its vapour liquid equilibrium behaviour. It was expected to give higher heat transfer coefficients by reducing diffusion at lower vapour to surface temperature difference. Steam-butanol mixtures have already proved their potential in boiling investigation, however, in condensation studies, it was still to be tested.

The present investigation has obtained significantly higher heat transfer coefficients and heat fluxes for steam-butanol mixtures compared to pure steam and steam-ethanol data. The maximum enhancement of up to 11 was recorded. Enhancement ratio, similar to the steam-ethanol case, was found to be dependent on the mode of condensation. Mode of condensation varies with vapour-to-surface temperature difference and so does the enhancement ratio. Enhancement ratio was also significantly affected by butanol concentrations. The enhancement was higher at low concentrations and lower vapour-to-surface temperature difference. At higher vapour-to-surface temperature difference and lower concentration transition from pseudo-dropwise mode to filmwise mode was observed, and enhancement reduces to unity. The diffusion effect was lesser in the steam-butanol case compared to steam ethanol case and relatively higher heat fluxes were obtained at higher concentrations and lower vapour-to-surface temperature difference.

9.3 Marangoni condensation of steam-propanol mixtures

Steam-propanol mixtures were used as a secondary fluid to understand the surface tension effect and diffusion resistance. It was expected to have higher diffusion resistance than steam-butanol but lower diffusion resistance then steam-ethanol. It indeed proved

the hypothesis right. Heat transfer coefficients and heat flux obtained for steam-propanol case lie in between the steam-butanol and steam-ethanol cases. Enhancement of up to 8 was recorded. Again, the enhancement ratio was found to be dependent on the mode of condensation. Dropwise mode of condensation gave higher enhancements than wavy film and pure films. Mode of condensation varies with vapour-to-surface temperature difference and ethanol concentration. The enhancement was higher at low concentrations and lower vapour-to-surface temperature difference. At higher vapour-to-surface temperature difference and lower concentration transition from pseudo-dropwise mode to filmwise mode was observed, and enhancement reduces to unity. Similar to steam-butanol case diffusion has the lesser effect compared to steam-ethanol cases.

9.4 Semi-empirical modelling of steam-ethanol mixtures

Modelling Marangoni condensation on the basis of the purely analytical solution is not only difficult but near to impossible job. As it involves an overlapping of the very complicated phenomenon. Firstly, it is affected by diffusion resistance and then surface tension plays its role in the instability of condensate film. Instability causes different modes of condensation and the transition from one mode to other is very difficult to analyse. However, the semi-empirical model is developed. Using Sparrow and Marshall (1969) diffusion model and Rose (1984) dropwise model. Combining these models for different regions and using previous experimental data a model was developed that predicts heat transfer characteristics with up to 5% uncertainty.

9.5 Future work

Steam-butanol and steam-propanol have shown real potential in Marangoni Condensation of binary mixtures. These were the first ever results produced showing 11 times higher heat transfer coefficients. For these results to acknowledged by the industry more experiments of a similar kind are required. All the experiments conducted were at higher pressure and low vapour velocities compared to practical industrial conditions.

Therefore, to understand the actual effectiveness of such fluid they need to be tested at realistic conditions such as the pressure of 14kPa and vapour velocity of up to 7.5 m/s.

There is still no theoretical model for Marangoni condensation. To understand the phenomenon of film instability, advanced experimental equipment with laser beam technology and infrared cameras are required to measure the change in film thickness with time. dropwise theory of Rose (1984) is a good start but its only applicable to dropwise region in Marangoni condensation. When the mode of condensation changes, the transition part is still not understood fully and, in the film-wise region Nusselt film theory is not applicable and film behaves differently under surface tension effect. Therefore, there is a need to carry out a set of experiments to break down the problem into four parts; diffusion region, transition region, dropwise region and film-wise region, and analyse them separately.

10 References

Abe, Y., 2006. Self-rewetting fluids beneficial aqueous solutions. *Space technology,* pp. 650-667.

Ali, H., 2012. Marangoni condensation of steam-ethanol mixtures on horizontal smooth, low finned tubes and a bank of tubes. *Journal of Heat transfer,* pp. 1-296.

Ali, H., Wang, H., Briggs, A. & Rose, J., 2013. Effects of vapour velocity and pressure on Marangoni condensation of steam-ethanol mixtures on a horizontal tube. *Journal of heat transfer,* pp. 1502-1510.

Avramenko, A., Shevchuk, I., Souad Harmand, S. & Tyrinov, A., 2015. Thermocapillary instability in an evaporating two-dimensional thin layer film. *International Journal of Heat and Mass Transfer,* pp. 77-88.

Bochkarev, A. & Pukhovoy, M., 1997. *Condensation of zinc and butanol vapours on a cryogenic surface.* s.l.:Pergamon.

Buffonea, C., Sefianeb, K. & Minetti, C., 2015. The effect of wall thickness and material on Marangoni driven convection in capillaries. *Colloids and Surfaces A: Physicochem. Eng. Aspects,* pp. 384-392.

Burr, K., Akylas, T. & Mei, C., 2016. Two-dimensional laminar boundary layers. In: *School-wide Program on Fluid Mechanics Modules on High Reynolds Number Flows.* s.l.:I-campus project, pp. 1-33.

Celli, M., Barletta, A. & Alves, L., 2015. Marangoni instability of a liquid film flow with viscous dissipation. *Physical Review,* pp. 1-9.

Chen, X. et al., 2015. Experimental Study on Condensation Heat Transfer of Ethanol-Water Vapor Mixtures on Vertical Micro-tubes. *Int J Thermophys,* pp. 1598-1617.

Chen, Z. & Utaka, Y., 2012. Condensate drop: Movement by surface temperature gradient on the heat transfer surface in Marangoni dropwise condensation. In: *Condensate Drop Movement by Surface Temperature Gradient on Heat Transfer Surface in Marangoni Dropwise Condensation.* Yokohama: Intech, pp. 219-246.

Christy, J., Sefiane, K. & Munro, E., 2010. A Study of the Velocity Field during Evaporation of Sessile Water and Water/Ethanol Drops. *Journal of Bionic Engineering,* p. 321–328.

Denga, H., Fernandinoa, M. & Doraoa, C., 2015. *Numerical study of the condensation length of binary zeotropic mixtures.* Norway, Cross mark, pp. 43-50.

Deng, H., Fernandino, M. & DoraoV, C., 2014. Numerical study of heat and mass transfer of binary mixtures Numerical study of heat and mass transfer of binary mixtures. *International Communications in Heat and Mass Transfer,* pp. 45-53.

Duffy, D., Wilson, K. & Holland, D., 2009. *Quasi-steady spreading of a thin ridge of fluid with temperature-dependent surface tension on a heated or cooled substrate.* Glasgow: Oxford university press.

Dunn, G. et al., 2009. The strong influence of substrate conductivity on droplet evaporation. *J.Fluid Mech,* pp. 329-351.

Fan, L. et al., 2010. Contact Angle of Ethanol and n-Propanol Aqueous Solutions on Metal Surfaces. *Chemical engineering technology,* p. 1535–1542.

Ford, J. & McAleer, J., 1971. Non-Filmwise Condensation of Binary Vapors: Mechanism and Droplet Sizes. *Canadian J. Chem. Eng,* pp. 157-158.

Ford, J. & Missen, R., 1968. On the Conditions of Stability of Falling Films Subject to Surface Tension Disturbances; the Condensation of Binary Vapours. *Canadian J. Chem*, pp. 309-312.

Fronk, B. & Garimella, S., 2013. In-tube condensation of zeotropic fluid mixtures: A review. *International journal of refrigeration,* pp. 534-561.

Fujii, T., 1991. *Theory of Laminar Film Condensation.* s.l.: Springer.

Fujii, T., Osa, N. & Koyama, S., 1993. *Free Convection Condensation of Binary Mixtures on a Smooth Tube: Condensing Mode and Heat Transfer Coefficient of Condensate.* Florida, Augustine, pp. 171-182.

Golobic, I. & Sitar, A., 2014. Heat transfer enhancement of self-rewetting aqueous n-butanol solutions boiling in microchannels. *International Journal of Heat and Mass Transfer,* pp. 198-206.

Grooten, M. & Geld, C., 2011. Dropwise condensation from flowing air-steam mixtures: Diffusion resistance assessed by controlled drainage. *International Journal of Heat and Mass Transfer,* pp. 4507-4517.

Hijakata, K., Fukasaku, Y. & Nakabeppu, O., 1996. Theoretical and Experimental Studies on the Pseudo-Dropwise Condensation of a Binary Vapor Mixture. *J. Heat Transfer,* p. 140–147.

Hijikata, K., Fukasaku, Y. & Nakabeppu, O., 1996. Theoretical and Experimental studies on the Pseudo-Dropwise condensation of a binary vapour mixture. *Journal of heat transfer,* pp. 140-147.

Hua, Y., Zhang, S., Li, X. & Wang, S., 2015. Heat transfer enhancement of subcooled pool boiling with self-rewetting fluid. *International Journal of Heat and Mass Transfer,* pp. 64-68.

Hu, Y., Liu, T., Li, X. & Wang, S., 2014. Heat transfer enhancement of micro-oscillating heat pipes with self-rewetting fluid. *International Journal of Heat and Mass Transfer,* p. 496–503.

Jiang, R. et al., 2015. Visualization study of condensation of ethanol-water mixtures in trapezoidal microchannels. *International Journal of Heat and Mass Transfer,* pp. 339-349.

Jun-Jie Yan, S. & Ji-Ping Liu, J., 2007. Effect of temperature gradient on Marangoni condensation heat transfer for ethanol-water mixtures. *Journal of multiphase flow,* pp. 935-947.

JunJie Yan, W. & JiPing Liu, S., 2009. Marangoni condensation heat transfer of water-ethanol mixtures on a vertical surface with temperature gradients. *International Journal of Heat and Mass Transfer,* pp. 2324-2334.

Kanatani, K., 2015. On the critical thickness and wavelength of a condensing thin liquid film in a binary vapour mixture system. *International Journal of Heat and Mass Transfer,* pp. 199-205.

Kanatani, K. & Oron, A., 2016. Nonlinear effect of surface disturbances on mass flux and its modelling in Marangoni dropwise condensation. *International Journal of Heat and Mass Transfer,* pp. 419-425.

Li, Y. et al., 2015. Heat transfer characteristics of Marangoni condensation for ethanol-water mixtures on a horizontal plate. *International Journal of Heat and Mass Transfer,* p. 561–567.

Li, Y., Yan, J., QiaO, L. & Hu, S., 2008. Experimental study on the condensation of ethanol-water mixtures on vertical tube. *Heat mass transfer,* pp. 607-616.

Li, Y., Yan, J., Wang & J, 2011. A semi-empirical model for condensation heat transfer coefficient of mixed ethanol-water vapours. *Journal of heat transfer,* pp. 1501-1511.

Ma Xuehu, L., Sifang, W., Mingzhe, W. & Xiaonan, L., 2010. Effects of surface free energy and nanostructures on dropwise condensation. *Chemical engineering journal,* pp. 546-552.

Ma, X. et al., 2012. Effects of surface free energy difference on steam-ethanol mixture condensation heat transfer. *International Journal of Heat and Mass Transfer,* pp. 531-537.

Miljkovic, N., Enright, R. & Wang, E., 2016. Modelling and Optimization of Superhydrophobic condensation. *Journal of heat transfer,* pp. 1-37.

Mirkovich, V. & Missen, R., 1961. Non-filmwise condensation of binary vapours of miscible liquids. *Canadian J. Chem. Eng,* pp. 86-87.

Morrison, J. & Deans, J., 1997. Augmentation of Steam Condensation Heat Transfer by Addition of Ammonia. *Int. J. Heat and Mass Transfer,* pp. 765-772.

Morrison, J., Philpott, C. & Deans, J., 1998. Augmentation of Steam Condensation Heat Transfer by Addition of Methylamine. *Int. J. Heat Mass Transfer,* pp. 3683-3697.

Murase, T., Wang, H. & Rose, J., 2007. Marangoni condensation of steam–ethanol mixtures on a horizontal tube. *International Journal of Heat and Mass Transfer,* pp. 3774-3779.

Nusselt, W., 1916. "Die Oberflachenkodensation Des Wasserdampfes. *Z. Vereines Deutsch. Ing,* pp. 569-575.

Orozco, D., 2016. Thermal Marangoni instability of a thin film flowing down a thick wall deformed in the backside. *Physics of fluids,* pp. 1-13.

Paterson, C., Wilson, S. & Duffy, B., 2015. The strongly coupled interaction between a ridge of fluid and an inviscid airflow. *Physics of fluids,* pp. 1-25.

Peng, B. et al., 2015. Experimental investigation on steam condensation heat transfer enhancement with vertically patterned hydrophobic–hydrophilic hybrid surfaces. *International Journal of Heat and Mass Transfer,* pp. 27-38.

Philpott, C. & Deans, J., 2004. The Enhancement of Steam Condensation Heat Transfer in a Horizontal Shell and Tube Condenser by Addition of Ammonia. *Int. J. Heat Mass Transfer,* pp. 3683-3693.

Prokudina, I., 2016. Non-linear development of the Marangoni instability in liquid films. *Journal of Engineering Physics and Thermophysics,* pp. 921-928.

Prokudina, L., 2014. *Marangoni instability and nonlinear development of perturbations in fluid films.* s.l., s.n., pp. 1-8.

Rose, J., 1984. Effect of Pressure Gradient in Forced Convection Film Condensation on a Horizontal Tube. *Int. J. Heat Mass Transfer,* pp. 39-47.

Rose, J., 1998. Condensation heat transfer fundamentals condensation. *Chemical engineering research and design,* pp. 143-152.

Rose, J., 2016. Theory of dropwise condensation. *Journal of heat transfer,* pp. 1-16.

S´aenza, P., Valluria, P., Sefianea, K. & Matarb, O., 2014. Stability and two-phase dynamics of evaporating Marangoni-driven flows in laterally-heated liquid layers and sessile droplets. *Procedia IUTAM,* pp. 116-123.

Savinoa, R., Abeb, Y. & Fortezza, R., 2008. Comparative study of heat pipes with different working fluids under normal gravity and microgravity conditions. *Acta Astronautica,* pp. 24-34.

Savinoa, R. et al., 2009. Marangoni heatpipe:Anexperimentonboard MIOsat Italian microsatellite. *Acta Astronautica,* pp. 1582-1592.

Savinoa, R., Francescantonioa, N., Fortezzab, R. & Abec, Y., 2007. Heat pipes with binary mixtures and inverse Marangoni effects for microgravity applications. *Acta Astronautica,* pp. 16-26.

Savino, R., Abe, Y. & Fortezza, R., 2008. Comparative study of heat pipes with different working fluids under normal gravity and microgravity conditions. *Acta Astronautica,* pp. 24-34.

Savino, R., Cecere, A. & Paola, R., 2009. Surface tension-driven flow in wickless heat pipes with self-rewetting fluids. *International Journal of Heat and Fluid Flow,* pp. 380-388.

Savino, R., Paola, R., Cecere, A. & Fortezza, R., 2010. Self-rewetting heat transfer fluids and nano brine for space heat pipes. *Acta Astronautica,* pp. 1030-1037.

Shekriladze, I. G. & Gomelauri, V., 1966. Theoretical Study of Laminar Film Condensation of a Flowing vapour. *Int. J. Heat Mass Transfer,* p. 581–591.

Sitar, A. & Golobic, I., 2015. Heat transfer enhancement of self-rewetting aqueous n-butanol solutions boiling in microchannels. *International Journal of Heat and Mass Transfer,* p. 198–206.

Smyrnaios, D., Pelekasis, N. & Tsamopoulosc, J., 2002. Laminar boundary layer flow of saturated vapour and its condensate over a horizontal tube. *Physics of Fluids,* pp. 1945-1957.

Sparrow, E. & Marschall, E., 1969. Binary, Gravity-Flow Film Condensation. *Journal of Heat Transfer,* pp. 205-211.

Stauber, J., Wilson, S. & Duffy, B., 2015. Evaporation of Droplets on Strongly Hydrophobic Substrates. *American Chemical Society,* pp. 3653-3660.

Stauber, J., Wilson, S., Duffy, B. & Sefiane, K., 2015. On the lifetimes of evaporating droplets with related initial and receding contact angles. *Physics of fluids,* pp. 1-14.

Stauber, K., Wilson, S., Duffy, B. & Sefiane, K., 2014. On the lifetimes of evaporating droplets. *J. Fluid Mech,* pp. 744-756.

Stephan, K., 1992. *Heat Transfer in Condensation and Boiling.* Berlin: Springer.

Stephan, K., 2006. Interface temperature and heat transfer in forced convection laminar film condensation of binary mixtures. *International Journal of Heat and Mass Transfer,* pp. 805-809.

Stephan, K., 2010. Total and partial condensation of binary mixtures under gravity-driven film flow. *International Journal of Thermal Sciences,* pp. 2242-2249.

transfer, S. t. e. a. e. o. c. h., 2004. Rose, J, W. *Chemical engineering research and design,* pp. 419-429.

Utaka, Y. & Chen, Z., 2011. Characteristics of condensate drop movement with the application of a bulk surface temperature gradient in Marangoni dropwise condensation. *Journal of heat and mass transfer,* pp. 5049-5059.

Utaka, Y. & Kamiyama, T., 2008. Condensate Drop Movement in Marangoni Condensation by Applying Bulk Temperature Gradient on Heat Transfer Surface. *Heat transfer,* pp. 388-397.

Utaka, Y., Kashiwabara, Y. & Ozaki, M., 2013. Microlayer structure in nucleate boiling of water and ethanol at atmospheric pressure. *International Journal of Heat and Mass Transfer,* pp. 222-230.

Utaka, Y., Kashiwabara, Y., Ozaki, M. & Chen, Z., 2014. Heat transfer characteristics based on microlayer structure in nucleate pool boiling for water and ethanol. *International Journal of Heat and Mass Transfer,* pp. 479-488.

Utaka, Y. & Nishikawa, T., 2003. Measurement of Condensate Film Thickness for Solutal Marangoni Condensation Applying Laser Extinction Method. *J. of Enhanced Heat Transfer,* p. 119–129.

Utaka, Y. & Shixue, W., 2004. Characteristic curves and the promotion effect of ethanol addition on steam condensation heat transfer. *International Journal of Heat and Mass Transfer,* p. 4507–4516.

Utaka, Y. & Terachi, N., 1995. Measurements of Condensation Characteristic Curves for Binary Mixture of Steam and Ethanol Vapour. *Heat Transfer,* pp. 57-67.

Utaka, Y. & Wang, S., 2004. Characteristic Curves and Promotion Effect of Ethanol Addition on Steam Condensation Heat Transfer. *Int. J. Heat Mass Transfer,* p. 4507–4516.

Utaka, Y. & Wang, S., 2004. Characteristic Curves and Promotion Effect of Ethanol Addition on Steam Condensation Heat Transfer. *Int. J. Heat Mass Transfer,* p. 4507–4516.

VanHook S, et al., 1997. Long-wavelength surface-tension-driven Benard convection: experiment and theory. *J.Fluid Mech,* pp. 45-78.

Wang, J. et al., 2015. The correlation for Marangoni condensation heat transfer of water-ethanol mixture vapours. *Heat Transfer Engineering,* pp. 1-35.

Wang, S., Yan, J., Li, Y. & Hu, H., 2009. Experimental Investigation of Marangoni Condensation of Ethanol-Water Mixture Vapors on Vertical Tube. *Int. J. Heat Mass Transfer,* p. 1533–1541.

Yan, J. et al., 2009. Research on Marangoni Condensation Modes for Water-Ethanol Mixture Vapors. *Microgravity Science and Technology,* pp. 77-85.

Yan, J. et al., 2007. Effect of Vapor Pressure/Velocity and Concentration on Condensation Heat Transfer for Steam-Ethanol Vapor Mixture. *Int. J. Heat Mass Transfer,* p. 51–60.

Yoshiyuki, A., Akira, I. & Tanaka, K., 2005. Thermal Management with self-Rewetting fluids. *Microgravity,* pp. 149-152.

Zhao, J., Dong, B. & Wang, S., 2016. Study on the Droplet Size Distribution of Marangoni Condensation. *Advances in Control and Communication,* p. 187–194.

Zheng, Z. et al., 2015. Numerical investigation on Marangoni convection of binary fluids in a closed microcavity. *Applied Thermal Engineering,* pp. 462-472.

Zhou, L. et al., 2014. Multi-jet flows and bubble emission during subcooled nucleate boiling of the aqueous n-butanol solution on a thin wire. *Experimental Thermal and Fluid Science,* pp. 1-8.

Zhou, L., Wang, Z., Du, X. & Yang, Y., 2015. Boiling characteristics of water and self-rewetting fluids in a packed bed of spherical glass beads. *Experimental Thermal and Fluid Science,* p. 537–544.

11 Appendix

11.1 Appendix A: Thermo-physical properties of test fluids

11.1.1 Nomenclature and units

C_{pf} specific isobaric heat capacity of saturated liquid, J/kg.K

C_{pg} specific isobaric heat capacity of saturated vapour, J/kg.K

h_{fg} specific enthalpy of evaporation, J/kg

k_f thermal conductivity of the saturated liquid, W/m.K

k_c thermal conductivity of copper tube, W/m.K

M molecular mass, g/mol

P pressure, Pa

P_{sat} saturation pressure, Pa

R ideal gas constant, J/kg K

T thermodynamic temperature, K

T_{sat} thermodynamic temperature at saturation, K

x vapour mole fraction

W_L liquid mass fraction of mixture

W_v vapour mass fraction of mixture

v_f specific volume of saturated liquid, m^3/kg

v_g specific volume of superheated vapour, m^3/kg

μ_L dynamic viscosity of the saturated liquid, kg/m.s

μ_v dynamic viscosity of saturated vapour, kg/m.s

σ surface tension, N/m

Subscripts

e ethanol

mix mixture

w water

11.1.2 Properties of water

The specific volume of saturated liquid (Lee (1982))

$$v_{\mathrm{f}} = 0.0012674 - T\left(2.02915\times10^{-6} - 3.8333\times10^{-9}T\right) \tag{A.1}$$

Specific volume of saturated vapour (LeFerve et al. (1975))

$$v_{\mathrm{g}} = \frac{\left[1+\left(1+T_{\mathrm{c}}T_{\mathrm{d}}\right)^{1/2}\right]}{T_{\mathrm{d}}} \tag{A.2}$$

where,

$$T_{\mathrm{a}} = \frac{1500}{T} \tag{A.3}$$

$$T_{\mathrm{B}} = 2.5\ln\left(1-\exp^{-Ta}\right) \tag{A.4}$$

$$T_{\mathrm{c}} = \frac{0.0015}{1+0.001T} - 0.000942\left(\frac{1}{T_{\mathrm{a}}}\right)^{1/2}\exp^{\left(Ta+Tb\right)} - 0.0004882T_{\mathrm{a}} \tag{A.5}$$

$$T_{\mathrm{d}} = \frac{P}{230.755T} \tag{A.6}$$

Saturation pressure of liquid (Lee (1982))

$$P_{\mathrm{sat}} = 10^{6}\,exp^{\mathrm{A}} \tag{A.7}$$

where,

$$A = A_1 + \frac{A_2}{T_{\mathrm{f}}} + A_3\ln\left(T_{\mathrm{f}}\right) + A_4T_{\mathrm{f}} + A_5{T_{\mathrm{f}}}^2 + A_6{T_{\mathrm{f}}}^3 + A_7{T_{\mathrm{f}}}^4 + A_8{T_{\mathrm{f}}}^5 + A_9{T_{\mathrm{f}}}^6 + A_{10}{T_{\mathrm{f}}}^7 + A_{11}{T_{\mathrm{f}}}^8 \tag{A.8}$$

where,

$$T_{\mathrm{f}} = \frac{T}{1000} \tag{A.9}$$

A_1 = A_6 = 123.568834637

15.49217901

A_2 = A_7 = −188.31212064

−5.6783717693

A_3 = A_8 = 660.91763485

1.4597584637

A_4 = A_9 = −1382.4740091

13.877000608

A_5 = A_{10} = 1300.1040184

−80.887673591

A_{11} = −449.39571976

The specific isobaric heat capacity of saturated liquid (Nobbs (1975))

$$C_{\mathrm{pf}} = 10768.539 - T\left(57.216 - T\left(0.16359 - 1.536\times10^{-4}T\right)\right) \tag{A.10}$$

The specific isobaric heat capacity of saturated vapour (Nobbs (1975))

$$C_{\mathrm{pg}} = 1000\left(1.86238 + 5.1713\times10^{-4}\theta + 2.9015\times10^{-6}\theta^2 + 9.106027\times10^{-8}\theta^3\right) \tag{A.11}$$

where,

$$\theta = T - 273.15$$

Specific enthalpy of evaporation (Lee (1982))

$$h_{\mathrm{fg}} = 3468920 - T\left(5707.4 - T\left(11.5562 - 0.0133103T\right)\right) \tag{A.12}$$

The thermal conductivity of saturated liquid (Lee (1982))

$$k_{\mathrm{f}} = -0.92407 + T_{\mathrm{g}}\left(2.8395 - T_{\mathrm{g}}\left(1.8007 - T_{\mathrm{g}}\left(0.52577 - T_{\mathrm{g}}\,0.07344\right)\right)\right) \tag{A.13}$$

where,

$$T_g = \frac{T}{273.15}$$

Dynamic viscosity of saturated liquid (Lee (1982))

$$\mu_{\mathrm{f}} = 0.0002414 \times 10^{\mathrm{A}} \tag{A.14}$$

Where,

$$A = \left(\frac{247.8}{T - 140}\right) \tag{A.15}$$

Surface tension (Masuda (1985))

$$\sigma_{\mathrm{f}} = \frac{75.6 - 0.138\left(T - 273.15\right) - 0.0003\left(T - 273.15\right)^2}{1000} \tag{A.16}$$

11.1.3 Properties of ethanol

The specific volume of saturated liquid (Fujii et al. (1983))

$$v_{\mathrm{f}} = \frac{1}{-0.90055T + 807.44} \tag{A.17}$$

The specific volume of saturated vapour (Fujii et al. (1983))

$$v_g = \frac{ZRT}{P} \tag{A.18}$$

$$R = 197.63 \tag{A.19}$$

$$\frac{1}{z} = 1 + 0.09\left(\frac{P}{T}\right)$$

(A.20)

Saturation pressure of liquid (Fujii et al. (1983))

$$log\ P_{\text{sat}} = 8.21337 - \frac{1652.05}{(T - 273.15) + 231.48} + \log\left(0.1333\right) \tag{A.21}$$

Equation (A.21) can be simplified as

$$P_{\text{sat}} = 0.1333 \times 10^{8.21337 - \frac{1652.06}{T - 41.67}} \tag{A.22}$$

Saturation temperature

$$T_{\text{sat}} = 41.67 + \frac{1652.05}{8.21337 - \log \frac{P_{\text{sat}}}{0.1333}} \tag{A.23}$$

The specific isobaric heat capacity of saturated liquid (Fujii et al. (1983))

$$C_{\text{pf}} = 2.262 \times 10^3 + 6.53\left(T - 273.15\right) + 0.094\left(T - 273.15\right)^{1.79} \tag{A.24}$$

The specific isobaric heat capacity of saturated vapour (Fujii et al. (1983))

$$C_{\text{pg}} = 1.52 \times 10^3 + 2.9\left(T - 273.15\right)^{1.011} \tag{A.25}$$

Specific enthalpy of evaporation (Fujii et al. (1983))

$$h_{\text{fg}} = 920 - 0.5\left(T - 273.15\right) - 5.8 \times 10^{-6}\left(T - 273.15\right)^{3.5} \tag{A.26}$$

The thermal conductivity of saturated liquid (Fujii et al. (1983))

$$k_{\text{f}} = 0.17256 - 2.3412 \times 10^{-4}\left(T - 273.15\right) \tag{A.27}$$

Dynamic viscosity of saturated liquid (Fujii et al. (1983))

$$\mu_{\text{f}} = 1.545 \times 10^{-7} \times 10^{A} \tag{A.28}$$

Where,

(A.29)

$$A = \frac{1817}{(T - 273.15) + 447.22}$$

Dynamic viscosity of saturated vapour (Fujii et al. (1983))

$$\mu_g = (76.33 + 0.33425(T - 273.15)) \times 10^{-7} \tag{A.30}$$

The surface tension of the saturated liquid (Faghri and Zhang (2006))

$$\sigma_e = 24.419 - 8.1477 \times 10^{-2} T - 1.145 \times 10^{-4} T^2 + 8.65 \times 10^{-7} T^3 - 7.6432 \times 10^{-9} T^4 + 1.9148 \times 10^{-11} T^5 \tag{A.31}$$

11.1.4 Properties of water-ethanol mixture

The specific volume of saturated vapour (Fujii et al. (1983))

$$v_{g_{mix}} = W_{ve} v_{ge} + W_{vw} v_{gw} \tag{A.32}$$

The specific isobaric heat capacity of saturated liquid (Fujii et al. (1983))

$$C_{pf\,mix} = W_{Le} C_{pf\,e} + W_{Lw} C_{pf\,w} \tag{A.33}$$

Specific enthalpy of evaporation (Utaka and Wang (2002))

$$h_{fg_{mix}} = W_{Le} h_{fge} + W_{Lw} h_{fgw} \tag{A.34}$$

Surface tension of saturated liquid (Tamura et al. 1995), see appendix F.

$$\sigma_m^{1/4} = \psi_w^{\sigma} \sigma_w^{1/4} + \psi_e^{\sigma} \sigma_e^{1/4} \tag{A.35}$$

Dynamic viscosity of vapour mixture (Wilke (1950))

$$\theta_{we} = \frac{\left[1 + \left(\frac{\mu_{vw}}{\mu_{ve}}\right)^{1/2} + \left(\frac{M_e}{M_w}\right)^{1/4}\right]^2}{\frac{4}{\sqrt{2}}\left[1 + \left(\frac{M_w}{M_e}\right)\right]^{1/2}} \tag{A.36}$$

$$\theta_{ew} = \frac{\left[1+\left(\frac{\mu_{ve}}{\mu_{vw}}\right)^{1/2}+\left(\frac{M_w}{M_e}\right)^{1/4}\right]^2}{\frac{4}{\sqrt{2}}\left[1+\left(\frac{M_e}{M_w}\right)\right]^{1/2}} \tag{A.37}$$

$$\mu_{vm} = \frac{\mu_{vm}}{1+\left(\frac{x_{vm}}{x}\right)\theta_{we}} + \frac{\mu_{vw}}{1+\left(\frac{x_{vm}}{x}\right)\theta_{ew}} \tag{A.38}$$

where μ_w and μ_e were calculated using A.14 and A.28 respectively.

11.1.5 Property of test tube

The thermal conductivity of copper tube (Niknejad (1979))

$$k_c = 438.643 - 0.130692T + 4.540943\times10^{-5}T^2 \tag{A.39}$$

11.2 Appendix B: Calibration of thermocouples

Thermocouples were calibrated against the platinum resistance thermometer. The bath contained water and was heated to the desired temperature selected by a thermostat. The fluid was continuously circulated around the bath so that temperature was kept uniform in the range of 0.005 K.

The temperature in the isothermal bath was measured using a platinum resistance thermometer calibrated by Universal calibration laboratories Ltd. Measurements were taken twice, at 20 K intervals over a range of 273 K to 373 K. The results of two samples agreed within 0.005 K at all points in range. The following equation was thus obtained by the least squares method.

$$T = 273.15 + 0.025091E - 7.56632\times10^{-8}E^2 - 1.73740\times10^{-10}E^3 + 3.66234\times10^{-14}E^4 - 2.1105\times10^{-18}E^5 \quad \text{(B.1)}$$

where E is the e.m.f in μV and T is the temperature in K.

11.3 Appendix C: Correction for a dissipative temperature rise of coolant

To determine the dissipative temperature rise as a function of coolant flow rate, tests were done by running coolant through the tubes at room temperature without condensing any steam on it. Results are shown in Table C.1.

Table C.1.Calibration results.

Coolant flow rate l/min	Voltmeter reading of Thermopile / µV
3	0.5
4	0.8
5	1.2
6	1.6
7	1.9
8	2.3
9	3.1
10	3.8
11	4.5
12	4.9
13	5.6
14	6.1
15	6.5
16	7.1
17	7.9
18	8.3
19	8.5
20	9.2
21	10.2
22	10.7
23	11.1
24	11.6
25	11.9
26	12.7
27	13.3
28	13.7
29	14.3
30	15

11.4 Appendix D: Surface tension calculation of steam-ethanol mixtures

Nomenclature

e	constant used in Eq. (D.6)
q	Constant depending on a number of carbon atoms in alcohol (ethanol *q* = 2), used in Eq. (D.5)
T	temperature/ K
V	molar volume, m^3/mol
w	constant used in Eq. (D.5)
x	bulk mole fraction
β	constant used in Eq. (D.4)
σ	surface tension/ (N/m)
ψ	superficial bulk volume fraction
ψ^{σ}	Superficial surface volume fraction

Subscripts

m	mixture
e	ethanol
w	water

The surface tension of the water-ethanol mixture was calculated according to Tamura et al. (1955).

Superficial volume fraction, ψ, for water and ethanol can be expressed as:

$$\psi_{\mathrm{w}} = \frac{x_{\mathrm{w}} V_{\mathrm{w}}}{x_{\mathrm{w}} V_{\mathrm{w}} + x_{\mathrm{e}} V_{\mathrm{e}}} \tag{D.1}$$

$$\psi_{\mathrm{e}} = \frac{x_{\mathrm{e}} V_{\mathrm{e}}}{x_{\mathrm{w}} V_{\mathrm{w}} + x_{\mathrm{e}} V_{\mathrm{e}}} \tag{D.2}$$

$$\frac{\psi_{\mathrm{w}}}{\psi_{\mathrm{e}}} = \frac{x_{\mathrm{w}} V_{\mathrm{w}}}{x_{\mathrm{e}} V_{\mathrm{e}}} \tag{D.3}$$

To obtain a surface tension of mixture using superficial surface mole fractions of individual components, the following equations can be used

$$\beta = \log \frac{\psi_{\mathrm{w}}}{\psi_{\mathrm{e}}} \tag{D.4}$$

$$w = 0.441 \frac{q}{T} \left(\frac{\sigma_{\mathrm{e}} V_{\mathrm{e}}^{2/3}}{q} - \sigma_{\mathrm{w}} V_{w}^{2/3} \right) \tag{D.5}$$

$$e = \beta + w \tag{D.6}$$

$$e = \log \frac{\psi_{\mathrm{w}}^{\sigma}}{\psi_{\mathrm{e}}^{\sigma}} \tag{D.7}$$

$$\psi_{\mathrm{w}}^{\sigma} + \psi_{\mathrm{e}}^{\sigma} = 1 \tag{D.8}$$

Individual surface tension for water and ethanol can be found from equations A.16 and A.31 from appendix A.

Equation (D.9) is the final correlation to find mixture surface tension.

$$\sigma_{\mathrm{m}}^{1/4} = \psi_{\mathrm{w}}^{\sigma} \sigma_{\mathrm{w}}^{1/4} + \psi_{\mathrm{e}}^{\sigma} \sigma_{\mathrm{e}}^{1/4} \tag{D.9}$$

Variation of surface tension plotted against ethanol concentrations are shown in Figure 11.1 below.

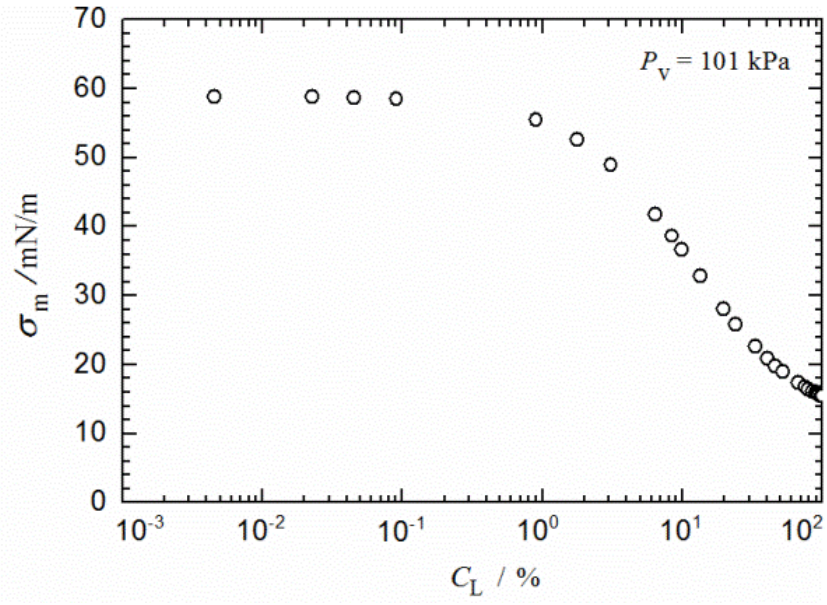

Figure 11-1Variation of the surface tension of the water-ethanol mixture with ethanol concentration based on the method of Tamura et al. (1955).